PHOTON EMISSION FROM ION BOMBARDED SOLIDS

P.J. MARTIN

A THESIS SUBMITTED FOR THE DEGREE OF DOCTOR OF PHILOSOPHY OF THE AUSTRALIAN NATIONAL UNIVERSITY.

NOVEMBER 1976

All measurements and data analysis of work specifically related to ion-induced photon emission are the results of my own efforts.

The work described in Chapter Five concerning correlation of photon emission data with secondary ion measurements was undertaken jointly with Drs Bayly and MacDonald.

.....

P.J. Martin

CONTENTS

ABSTRACT

CHAPTER ONE - PARTICLE INTERACTION WITH SURFACES

1.1	INTRODUCTION	1
1.2	RADIATION EFFECTS	1
1.2.1	APPLICATIONS OF ION BEAMS	3
1.3	PARTICLE-SOLID INTERACTION AND RELATED PHENOMENA	4
1.3.1	ELASTIC PROCESSES	7
1.3.1.1	ION BACKSCATTERING AND REFLECTION	7
1.3.1.2	SPUTTERING	8
1.3.1.2.1.	THE COLLISION-CASCADE SPUTTERING MODEL	9
1.3.1.2.1.1	DEPENDENCE OF THE SPUTTERING YIELD ON ANGLE OF INCIDENCE	11
1.3.1.3	ENERGY DISTRIBUTION OF SPUTTERED PARTICLES	11
1.3.1.4	ANGULAR DISTRIBUTION OF SPUTTERED PARTICLES	13
1.3.1.5	SPUTTERING OF TWO COMPONENT SYSTEMS	14
1.3.2	INELASTIC PROCESSES	15
1.3.2.1	SECONDARY ELECTRON EMISSION	15
1.3.2.1.1	POTENTIAL ELECTRON EJECTION	15
1.3.2.1.2	KINETIC ELECTRON EJECTION	16
1.3.2.1.3	ENERGY DISTRIBUTION OF SECONDARY ELECTRONS	17
1.3.2.2	X-RAY EMISSION	19
1.3.2.3	PHOTON EMISSION IN THE ULTRA-VIOLET AND VISIBLE REGION	20
	REFERENCES	22

CHAPTER TWO - EXCITATION, DE-EXCITATION AND PHOTON EMISSION AT ION BOMBARDED SURFACES.

2.1	INTRODUCTION	27
2.2	THE BASIC THEORETICAL ELECTRON EXCHANGE PROCESSES	27
2.2.1	NEUTRALISATION OF PRIMARY IONS AND PHOTON EMISSION	27
2.2.2	SINGLE AND MULTISTAGE ELECTRON TRANSITIONS	28
2.2.3	THE TRANSITION RATES FOR ELECTRON EXCHANGE PROCESSES	31
2.3	THE EXCITED STATES OF SPUTTERED PARTICLES	33
2.4	THE SHAPE OF SPECTRAL LINES EMITTED BY PRIMARY IONS SCATTERED FROM SOLID TARGETS	33
2.5	SPUTTERED PARTICLES AND PHOTON EMISSION FROM TARGET MATERIAL	38
2.5.1	EARLY RESEARCH	38
2.5.2	GENERAL SURVEY STUDY OF OPTICAL EMISSION	39
2.5.2.1	ION INDUCED PHOTON EMISSION COMPARED WITH ALTERNATIVE EXCITATION PROCESSES	42
2.5.2.1.1	COMPARISON WITH ARC EXCITATION	42
2.5.2.1.2	BEAM FOIL EXCITATION	43
2.5.2.1.3	LASER EXCITATION	44
2.5.2.1.4	ELECTRON INDUCED OPTICAL EMISSION	44
2.5.3	THE VELOCITY DISTRIBUTION AND KINETIC ENERGY OF THE EMITTING PARTICLES	46
2.5.3.1	COMPARISON OF THE ESTIMATED ENERGIES OF EXCITED PARTICLES AND THE ENERGY DISTRIBUTION OF SPUTTERED IONS AND ATOMS	53
2.5.4	THE ENERGY DEPENDENCE OF THE PHOTON YIELD	56
2.5.5	ANGULAR DISTRIBUTION OF THE PHOTON EMISSION	58

2.5.6	SINGLE CRYSTAL EFFECTS	61
2.5.7	THE INFLUENCE OF REACTIVE GASES ON PHOTON EMISSION	63
2.6	APPLICATIONS OF PHOTON EMISSION	71
2.6.1	SPUTTERING	71
2.6.2	SURFACE ANALYSIS USING PHOTON EMISSION	71
2.6.2.1	QUALITATIVE ANALYSIS	71
2.6.2.2	QUANTITATIVE ANALYSIS	73
2.7	SUMMARY OF ION INDUCED PHOTON STUDIES	74
2.8	THEORETICAL MODELS OF SECONDARY ION EMISSION	75
2.8.1	QUANTUM MECHANICAL MODELS	75
2.8.1.1	JOYES IONISATION MODEL	75
2.8.1.2	BLAISE AND SLODZIAN MODEL OF IONISATION	78
2.8.1.3	QUANTUM MECHANICAL MODEL OF SCHROEER AND SROUBEK	79
2.8.2	THERMODYNAMIC MODELS OF SECONDARY ION EMISSION	80
2.8.2.1	ANDERSEN AND HINTHORNE MODEL	80
2.8.2.2	JURELA MODEL	81
2.8.3	MOLECULAR ION EMISSION	82
2.9	CONCLUSION	83
	REFERENCES	84

CHAPTER THREE - EXPERIMENTAL METHOD

3.1	GENERAL DESCRIPTION OF EXPERIMENTAL APPARATUS	89
3.2	EXPERIMENTAL DETAILS	89
3.2.1	ION SOURCE AND SWITCHING MAGNET	89
3.2.2	ION OPTICS	90
3.2.3	ACCELERATOR VACUUM SYSTEM	90
3.2.4	TARGET CHAMBER	91
3.2.4.1	VACUUM SYSTEM	91
3.2.5	DETECTION SYSTEM	92
3.2.5.1	GRATING MONOCHROMATOR	93

3.2.5.2	PHOTON COUNTING SYSTEM	95
3.2.5.2.1	PHOTOMULTIPLIERS	95
3.2.5.2.2	COUNTING CIRCUIT	96
3.3	CALIBRATION OF THE DETECTOR SYSTEM	97
3.4	EXPERIMENTAL TECHNIQUE	99
3.4.1	TARGETS	99
3.4.2	PRIMARY ION CURRENT MEASUREMENT	100
	REFERENCES	101

CHAPTER FOUR - PHOTON EMISSION FROM ION-BOMBARDED METALS, SEMICONDUCTORS AND INSULATORS

4.1	INTRODUCTION	102
4.2	EXPERIMENTAL CONDITIONS	102
4.3	PHOTON EMISSION FROM METALS	103
4.3.1	MAGNESIUM AND ALUMINIUM Mg, Al	103
4.3.2	Sc, Ti, V, Cr, Mn, Fe, Ni, Cu, Zn	105
4.3.3	Zr, Nb, Mo, Hf, Ta, W	109
4.3.4	Ag, Pt, Au, Pb	113
4.4	PHOTON EMISSION FROM SEMI-CONDUCTORS	113
4.4.1	Si	113
4.4.2	Ge	116
4.4.3	III-V SEMICONDUCTORS	116
4.4.3.1	ENERGY BAND AND ATOMIC LEVEL CORRELATIONS	117
4.4.3.2	LINE PROFILES OF GaI EMISSION	119
4.4.3.3	PHOTON EMISSION FROM V ELEMENTS	120
4.5	PHOTON EMISSION FROM INSULATORS	122
4.5.1	ALKALI HALIDES - LiF, NaCl, NaBr, KCl, RbCl, CsI	122
4.5.2	POLYMERS - POLYMETHYL METHACRYLATE (PERSPEX) $CH_2\ C(CH_3)\ COOCH_3$	124
4.6	SUMMARY	125
	REFERENCES	127

CHAPTER FIVE - PHOTON EMISSION FROM NEUTRAL AND CHARGED PARTICLES SPUTTERED FROM LIGHT ELEMENTS

5.1	INTRODUCTION	130
5.2	DE-EXCITATION PROCESSES NEAR THE SURFACE OF ION BOMBARDED SiO_2 AND Si	131
5.2.1	TARGET PREPARATION	132
5.2.2	EXPERIMENTAL MEASUREMENTS	132
5.2.2.1	PHOTON MEASUREMENTS	132
5.2.2.2	SECONDARY ION MEASUREMENTS	133
5.2.3	PHOTON EMISSION RESULTS	134
5.2.4	SECONDARY ION EMISSION RESULTS	135
5.2.5	DISCUSSION OF RESULTS	137
5.2.6	SUMMARY OF THE SiO_2- Si DATA	144
5.3	EMISSION LINE PROFILES FROM SPUTTERED PARTICLES	144
5.3.1	RESULTS	146
5.3.2	DISCUSSION	148
5.3.3	SUMMARY	151
	REFERENCES	154

CHAPTER SIX - SINGLE CRYSTAL EFFECTS IN THE PHOTON AND SECONDARY ION YIELDS FROM ION BOMBARDED ALUMINIUM

6.1	INTRODUCTION	155
6.2	EXPERIMENTAL	156
6.3	RESULTS	159
6.3.1	PHOTON DATA	159
6.3.2	SECONDARY ION DATA	161
6.4	DATA ANALYSIS AND DISCUSSION	162
6.5	CONCLUSION	168
	REFERENCES	170

CHAPTER SEVEN - THE SPECTROSCOPY OF ION-INDUCED PHOTON EMISSION AND ITS APPLICATION TO QUANTITATIVE SURFACE ANALYSIS

7.1	INTRODUCTION	171
7.2	LOCAL THERMODYNAMIC EQUILIBRIUM IN A PLASMA	172
7.3	L.T.E. AND SECONDARY ION ANALYSIS	173
7.4	L.T.E. AND ION INDUCED PHOTON EMISSION	174
7.5	THE CALCULATION OF TEMPERATURES USING SPECTROCHEMICAL METHODS	174
7.6	EXPERIMENTAL	177
7.6.1	TARGETS SUITABLE FOR TEMPERATURE DETERMINATION	177
7.6.2	EXPERIMENTAL METHOD	178
7.7	RESULTS	178
7.8	DISCUSSION	179
7.8.1	QUANTITATIVE ANALYSIS USING PHOTON EMISSION	179
7.8.2	PHYSICAL INTERPRETATION OF L.T.E. TEMPERATURES	184
7.8.3	THE EFFECT OF OXYGEN ON PHOTON EMISSION	188
7.9	CONCLUSION	191
	REFERENCES	193

CHAPTER EIGHT - CONCLUSION 195

ACKNOWLEDGEMENTS 198

ABSTRACT

A study has been made of the photon emission produced by excited particles sputtered from the surface of solid targets subjected to ionic bombardment.

A detailed systematic study of the emission from a large number of elements and compounds has enabled many characteristics of the emission to be recognised. The influence of the electronic band structure of the target on the photon emission has been examined in the case of III-V semiconducting compounds and the light elements Mg, Al and Si.

Correlation of secondary ion and photon emission data taken during the bombardment of an SiO_2 layer thermally grown on a Si substrate has enabled the principal mode of de-excitation of sputtered particles to be identified. The influence of single crystal structure on the photon and ion emission from aluminium bombarded under channeling conditions has also been examined.

The correspondence between arc-excited and ion-induced photon spectra and the possibility of describing the emission using the concept of local thermodynamic equilibrium has been investigated.

The results have indicated that the excited states of certain targets can be described by a Boltzmann distribution function, and enabled effective excitation temperatures to be estimated. These temperatures have been found to be typical of those encountered in the ion microprobe analysis technique which is based on the L.T.E. model. Furthermore, the behaviour of the photon yield from Cr,Fe and Cu has been investigated under conditions of reduced primary ion current and oxygen background pressure.

CHAPTER ONE

PARTICLE INTERACTION WITH SURFACES

1.1 INTRODUCTION

Although the study of charge particle interaction with solids and solid surfaces, both theoretical and experimental, has been extensive in recent years, its origin can be traced back at least to 1852 when *Grove* studied the sputtering process using a glow discharge. Interest in the field has intensified and all effects of particle-surface interaction both elastic and inelastic are now being studied. There have been many comprehensive reviews of the ion-solid interaction process and related phenomena, the most frequently cited being those of *Carter and Colligon (1968), Kaminsky (1965), Arifov (1969) and McCracken (1975).*

1.2 RADIATION EFFECTS

The impetus for the comparatively recent growth of interest in particle solid interaction was prompted by the development of nuclear reactors. Before the first reactors were in operation *Wigner (1946),* realised that intense bombardment of structural materials would lead to substantial radiation damage. Metals bombarded at high temperatures and large doses of fast particles develop microporosity.

Radiation damage at room temperature is generally of the form of single atomic vacancies, self interstitials and small vacancy clusters, resulting from atoms being knocked out of their lattice positions by the radiation cascade. As the temperature is raised the defects mobilise and agglomerate into large defect clusters. Under sufficiently large dosage the vacancy clusters develop into small cavities or voids of submacroscopic size leading to a swelling of the

irradiated material. Such phenomena create major problems concerning the mechanical stability of any reactor vessel. These problems have been the concern of several international conferences. Radiation damage processes have been discussed by *Seitz (1956), Kelly (1966) and Thompson (1969). Kaminsky (1974),* has further suggested that the bombardment of the first wall of a potential fusion reactor by MeV neutrons may result in wall erosion and plasma contamination.

Plasma radiation striking the vacuum walls of any potential fusion reactor will produce two major effects. First there is the problem of wall erosion through the sputtering process, the same problem encountered in fission reactors. Secondly, major quantities of gas may be liberated from the walls and seriously contaminate the plasma such that its temperature falls below the minimum requirement. The vacuum walls in a typical fusion reactor using the D-T reaction are estimated to reach values of 600°C to 1000°C. The reactor power loss increases rapidly with the atomic number of the contaminant Z_2. For a hydrogen-isotope plasma ($Z_1 = 1$) the ratio R of the power losses with and without the contaminant is given by -

$R = 1 + f\ (Z_2 + Z_2^2) + f^2\ Z_2^3$, where f is the fractional concentration of the impurity (*Kaminsky 1971*). Typical values for an upper value of f are $4.9\ 10^{-3}$ for Be, $1.8\ 10^{-4}$ for V, $5.8\ 10^{-5}$ for Nb, and $5.5\ 10^{-5}$ for Mo.

The problems of wall erosion through neutron sputtering and plasma particles have been discussed by *Behrisch (1972, 1975).* It has been calculated that the erosion due to fast neutron sputtering is $\sim 10^{10}$ atoms cm^{-2} s^{-1} or 320 Å/year so that fast neutrons are not considered to be a major cause of first wall erosion. However, the sputtering yields of deuterons and helium ions are considerably higher and *Summers (1971)* has estimated a lifetime of only 1.7 years

for a 1 cm Nb wall in a 5000 MW controlled thermonucleur reactor with a particle flux of 2 x 10^{16} particles cm^{-2} s^{-1} (deuterium, tritium, and helium).

There exists therefore a need to simulate the first wall erosion process in a future fusion reactor to obtain data on the sputtering effects of plasma particles on possible reactor wall materials and to estimate erosion and contamination rates.

1.2.1 APPLICATIONS OF ION BEAMS

The study of ionic bombardment of solids has led to the development of several specialised fields, prominent among them being ion implantation, which has been extensively reviewed by many authors (*Dearnaley 1969 and Schultz 1974* for example). Basically the technique involves bombarding a semiconducting substrate with primary ions of energies ranging from KeV to MeV. Using this method small controlled amounts of foreign atoms or dopants can be selectively introduced into the substrate. A particular advantage of ion implantation is the ease in fabricating steep doping profiles close to the surface.

The last decade has seen the introduction of many new sophisticated surface analysis techniques. The developments in ion beam technology has added several more potentially powerful weapons to the arsenal of the surface scientist. The surface is a dominant characteristic of any solid since it results from an abrupt end to the periodic array of closely spaced atoms and in a region in which electrical and mechanical properties differ from the bulk. Its study is therefore of great importance to solid state science. The techniques involving the use of ion beams are particularly applicable to surface analysis where monolayer resolution is required. This degree of sensitivity is necessary in semiconductor device fabrication where

most of the device physics occurs within nanometers of the semiconductor surface. *Lieberman (1976)*, has edited the proceedings of the IV N.B.S. workshop held in Washington in April 1975 which was devoted entirely to the surface analytical techniques for silicon devices. The techniques offered by ion beam technology include secondary ion mass spectrometry (SIMS), Rutherford backscattering, proton induced X-ray emission, ion neutralisation spectroscopy and surface composition by analysis of neutral and ion induced radiation (SCANIIR). Some of these techniques can identify with monolayer precision, trace impurity elements and provide information on chemical bonding and densities of states.

Each analytical technique has its own specialised application and all are complementary to the extent that no individual method can be regarded as the ultimate weapon.

Ionic bombardment has numerous other applications such as the possibility of 'ion milling' with the total elimination of tool wear, the inhibition of metal corrosion and the alteration of the properties of optical components. These topics have been described by *Dearnaley (1973)*.

The study of particle-solid interaction has therefore many applications extending from the erosion of nuclear reactor vessels to the fabrication of microelectronic semiconductor devices. The following section will consider the physical processes accompanying ionic bombardment of solids.

1.3 PARTICLE-SOLID INTERACTION AND RELATED PHENOMENA

This section will be concerned with the general physical picture of the bombardment of a solid or solid surface with energetic ions, neutral atoms or molecules. For the purpose of this outline review, low energy will generally refer to particles of energy less

than 10 KeV, medium energy 10 to 100 KeV and high energy to particles with energies extending from 100 KeV to the MeV region. It is further general practice to divide the phenomena into two categories, that is, those due to elastic collisions (ion scattering and sputtering) and those that result from inelastic processes (electron emission, ionisation, UV and X-ray photon emission). Fig 1.0 illustrates the basic processes resulting from ionic bombardment of a solid and related analysis techniques.

The interaction of an energetic beam of particles with a solid surface leads to a complex variety of phenomena simultaneously taking place. Calculations by *Oen and Robinson (1975)* indicate that these processes take place in a time less than 10^{-12} seconds, that is less than the vibration time of the atoms in the host lattice. With typical beam densities of the order of $\mu A\ cm^{-2}$ there will be no interference of processes caused by different primary ions. The interaction can then in essence be regarded as the collision between a single primary particle and the surface layer of atoms.

The primary particle considered in this review will be an ion although the same processes are applicable to neutral atoms and molecules.

The primary ion on impact of the solid surface may be reflected or backscattered from the surface atomic rows in the form of a neutral or ion in various stages of excitation. Alternatively the ion may penetrate the surface region before being trapped through the ion implantation process. The primary ion will transfer energy to the solid during the slowing down process and the energy loss is generally divided into two parts, that due to electronic collisions and that due to nuclear collisions. Detailed descriptions of these mechanisms have been given by *Lindhard and Scharff (1961), Chadderton (1965) and Thompson (1969)*. The essential distinction between these

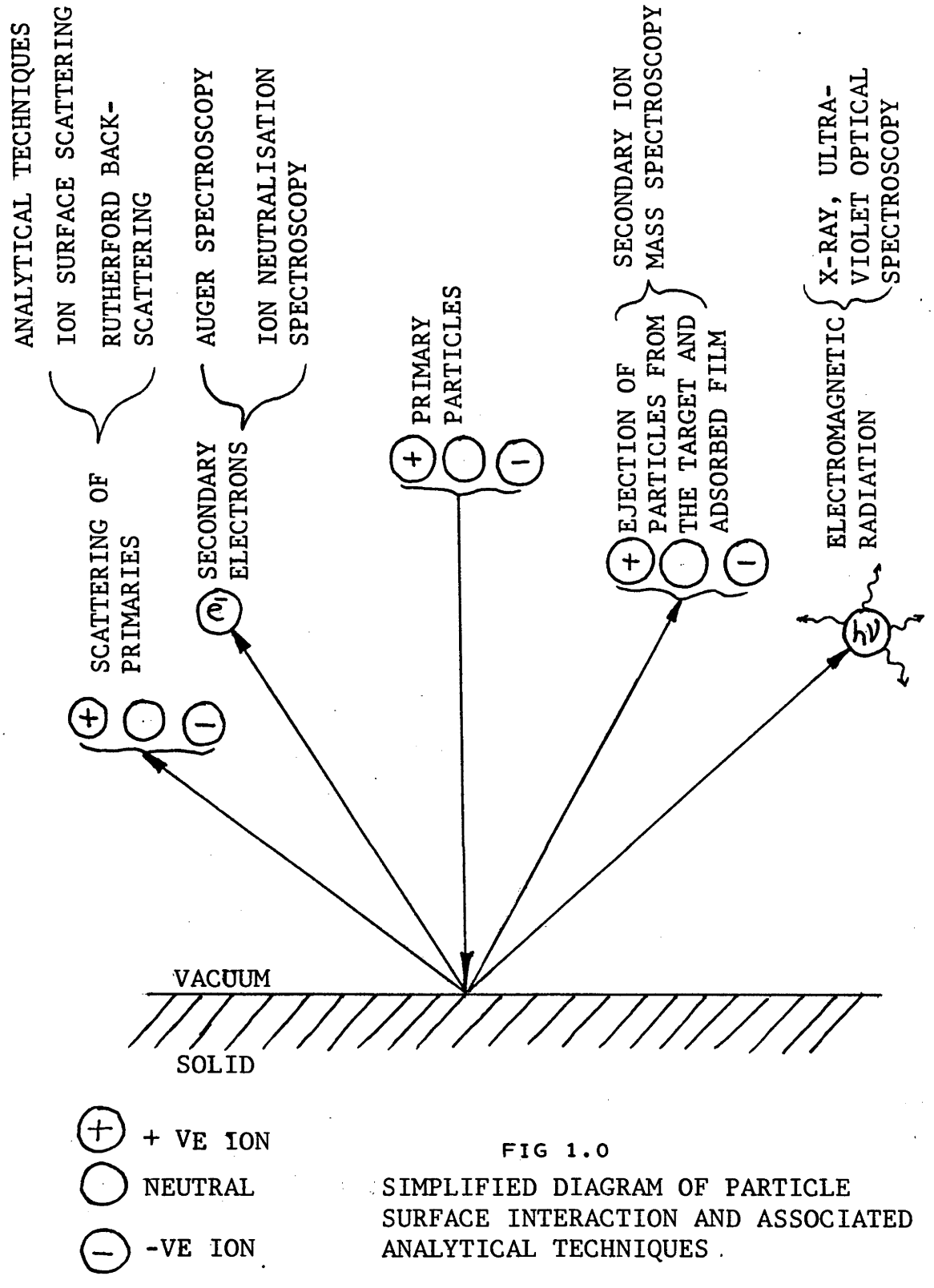

FIG 1.0

SIMPLIFIED DIAGRAM OF PARTICLE SURFACE INTERACTION AND ASSOCIATED ANALYTICAL TECHNIQUES.

mechanisms is that excitation of bound and valence electrons is an inelastic process whereas the nuclear loss mechanism involves much lower collision frequencies enabling the interaction to be described by two-body elastic collisions. In the latter case energy and momentum is conserved. The 'rule of thumb' for these loss mechanisms is that energy lost to the lattice is predominant at energies less than A KeV, where A is the atomic weight of the incident ion.

The energetic primary ion then will transfer energy to the lattice initiating a collision cascade of atoms in the solid. When energy sufficient to overcome the binding energy of the solid is transferred to the surface atoms these atoms will be ejected or sputtered. (The term sputtering was originally defined as the removal of atoms from a surface by the impact of an ion but the definition has been generalised to include the impact of neutral atoms, neutrons and also electrons). The detailed process of sputtering will be considered in section 1.3.1.2. The sputtered particles may be neutral atoms or molecules or ionised species in various stages of excitation. The detection and analysis of ionised particles is termed secondary ion mass spectrometry and is a technique of great sensitivity for the study of solid surfaces. Recent developments in SIMS have been reviewed by *Benninghoven (1975) and Liebl (1975)*.

The secondary particles if in excited states, can de-excite by the emission of characteristic electrons (Auger electrons) by the emission of ultra violet or visible light or by X-ray emission. Each de-excitation provides a possible means of identification of the secondary particle and illustrates the degree to which all of these mechanisms are complementary.

Subsequent sections will consider each process individually in more detail, although strict categorisation of each aspect of ion

solid interaction is not particularly desirable to gain an overall view of the process. It is however more practical for the purposes of this brief review. Emphasis will be placed on those secondary processes which are related to the emission of electromagnetic radiation.

1.3.1 ELASTIC PROCESSES

1.3.1.1 ION BACKSCATTERING AND REFLECTION

Low energy ion scattering as an analytical tool has the advantage that the outermost atomic layer can be studied. There have been many studies of this technique and reviews by *Harrington (1973), Smith (1971) and McCracken (1975)* are some of the more recent articles. At the low energy region 0.5 to 2 KeV the process is termed ion scattering spectroscopy (ISS) while at the high energy from 0.5 to 3 MeV the technique is called Rutherford backscattering (RBS). Both spectroscopies measure the energy loss of the primary ion after it experiences an elastic binary collision with a target atom. The energy loss serves to identify the struck atom.

Heiland and Taglauer (1976) have discussed the elastic and inelastic effects of ISS. The energy loss of the primary ion can be calculated from the conservation of energy and momentum to be -

$\Delta E = (1 - f(\frac{M1}{M2}, \Phi))$ where M1 is the mass of the projectile, M2 the mass of the target Φ the laboratory scattering angle and E the primary energy. $f(\frac{M1}{M2}, \Phi)$ is given by -

$$\frac{M1^2}{(M1 + M2)^2} \left(\cos \Phi \pm \left[\left(\frac{M2}{M1}\right)^2 - \sin^2 \Phi \right]^{\frac{1}{2}} \right)^2$$

The differential cross section for scattering can be written in terms of the impact parameter ρ and the scattering angle in the centre of mass coordinates Φ cm

$$\Phi \text{ cm} = \pi - 2 \int_{r \text{ min}}^{\infty} \frac{\rho \, d \, r}{r^2 \left(\left(1 - \frac{\rho}{r}\right)^2 - \frac{V(r)}{E} \right)^{\frac{1}{2}}}$$

here r min is the distance of closest approach and V is the ion-atom potential. This last factor poses a problem in that its choice for a specific case cannot be predicted theoretically. The problems associated with the choice of correct interatomic potentials have been discussed by *Wedepohl (1969)*. Computer simulations can also take into account the effects of lattice-atom thermal vibrations on the reflection of ions from single crystals (*Karpuzov 1974)*, Auger neutralisation (*Heiland and Taglauer)* and other surface effects.

1.3.1.2 SPUTTERING

This is perhaps the better known of all ion surface interaction phenomena and has been reviewed extensively (*Kaminsky 1965, Carter and Colligon 1968, MacDonald 1970, Sigmund 1972, and Anderson 1974)*. The process of sputtering, that is the erosion of surfaces during bombardment by energetic particles, is fundamentally important to any discussion of secondary emission processes and some of the more important aspects will be outlined.

Experimental evidence indicates that the sputtering effect arises as a consequence of the cascade of atomic collisions produced inside the target by the impact of the primary ion. It was at one time considered to be an evaporation mechanism. Early experiments by *Wehner (1955)*, on the emission patterns of atoms sputtered from single crystal Fe, Cu, Ag and W showed that the patterns had concentrations in emission intensity along close

packed directions of the target crystal. The concept of focused collision sequences was subsequently introduced by *Silsbee (1957)*. Here at a low energy called the focusing energy Ef, momentum is focussed along a row of atoms. However, later measurements by *Musket (1969) and Hofer (1972)* indicated that the spots contained only 20 per cent of the total sputtered intensity indicating that focused collision phenomena were of limited importance.

Sputtering is strongly affected by the channeling mechanism, an effect which causes the sputtering yield of single crystals to vary in a non-monotonous way with the angle of incidence. The effect is a correlated scattering of incident projectiles along atomic rows and planes of the target crystal. Many authors have studied this phenomena (*Rol 1959, Almén and Bruce 1961, Onderdelinden 1966, Zwangobani and MacDonald 1973)*. In polycrystals the channeling effects are integrated over the randomly orientated crystallites and amorphous materials do not exhibit the channeling effect since they have no ordered structure.

1.3.1.2.1 THE COLLISION-CASCADE SPUTTERING MODEL

The most successful sputtering model to date applicable to random targets has been that due to *Sigmund (1969, 1972)*. An incident projectile scatters several times on target atoms creating a generation of primary recoil or knock-on atoms. The P.K.A. sequences scatter on other target atoms and a collision cascade is created, spreading out in space and developing until all the atoms within it have slowed down to energies of a few eV. Where the target surface intercepts the cascade, target atoms receiving energies in excess of the binding energy will be ejected.

The model is based on random collision processes and uses the Boltzmann transport equation. The sputtering yield is derived by

calculating the amount of energy given to the lattice near the surface of the target. For isotropic cascades the sputtering yield is obtained from the deposited energy distribution F_D (X, E, η) *(Sigmund 1969, Weissmann and Sigmund 1973)*. F_D is determined from the transport equation -

$$(1) \quad -\eta \frac{\partial F}{\partial x} = NS_e \frac{\partial F}{\partial x} + \int d\sigma_n \, [F(x,E,\eta) - F(x,E-T,\eta') - F(x,T,\eta'')]$$

where S_e is the energy loss to the electrons and $d\sigma_n$ is the differential cross section for energy loss (T,dT) in an elastic collision.

The number of low energy atoms with an energy ($E_o dE_o$) in the layer (x,dx) is given by -

$$(2) \quad \frac{6}{\pi^2} \quad \frac{F(x,E,\eta)}{E_o^2} \quad d\,E_o\, dx \text{ for } E_o \ll E \text{ (E = primary energy)}$$

the number of atoms S with sufficient energy to overcome the surface barrier is found on integrating equation (2) to be -

$$S = \frac{3}{4\pi^2} \frac{F(0,E,)}{N\, U_o C_o}$$ Here N is the target atom density and C_o a constant. There are however several factors which affect the calculation of absolute sputtering yields such as the surface binding energy function and the low energy cross-sections.

The two main solutions to the theory that have practical application are the expressions for (A) the low energy (<] KeV) sputtering yield and (B) the sputtering yield for KeV energies and heavy to medium-mass ions -

$$(A) \quad S(E) = \frac{3}{4\pi^2} \alpha \frac{4\, M1\, M2}{(M1 + M2)^2} \frac{E}{U_o}$$

$$(B) \quad S(E) = 0.0420 \; \alpha \; 4\pi \; Z_1 Z_2 \; \frac{e^2 a}{U_o} \left(\frac{M1}{M1 + M2} \right) S\eta \, (\varepsilon)$$

where $\varepsilon = [M2 \; E/(M1 + M2)] \; / \; (Z_1 \; Z_2 \; e^2/a)$

$$a = 0.885 \; a_o \; (Z_1^{2/3} + Z_2^{2/3}) - 1/2$$

where a_o is the Bohr radius, α is a dimensionless quantity dependent upon M2/M1 and $S\eta(\varepsilon)$ is a univeral function tabulated by *Lindhard(1968)*.

1.3.1.2.1.1. DEPENDENCE OF THE SPUTTERING YIELD ON ANGLE OF INCIDENCE

The angular dependence of the sputtering yield has been calculated by *Sigmund* and an approximation is given by -

$$\frac{S(E,\eta)}{S(E,1)} = (\cos \theta)^{-f}$$

where the factor f is a function of M2/M1. This result is substantiated by experimental evidence (*Betz et al 1970*).

The situation is of course very different for single crystals because of channeling which leads to transparency effects in the sputtering yield.

1.3.1.3 ENERGY DISTRIBUTION OF SPUTTERED PARTICLES

The variation of sputtering yield can be calculated from the collision-cascade theory and the procedure has been outlined by *McCracken (1975) (page 268)* and detailed by *Thompson (1968)*, *Robinson (1965) and Sigmund (1972)*. An approximate calculation indicates that the atom flux is proportional to E^{-2}, the approximation being more accurate in the case of heavy targets. For lighter elements the spectra vary more slowly with energy. Account must also

be taken of the surface binding energy. The model described by *Thompson* assumes that the binding energy force is normal to the surface reducing the normal velocity component and not the parallel component. This assumption then predicts a peak in the energy spectrum at ~ Eb/2 where Eb is the surface binding energy.

The energy spectra of sputtered atoms are from the experimental point of view most difficult to obtain and much work has been published on the subject. Fig 1.1A shows the experimental results obtained by *Thompson (1968)* from polycrystalline and single crystal Au using Ar^+ and Xe^+ bombardment. The results are compared with the E^{-2} approximation. The technique used was based on time-of-flight measurements the apparatus for which is described by *Thompson, Farmery and Newson (1968) and Thompson (1969) page 227*. The results shown in Fig 1.1A indicate a low energy peak around 1eV and approximate E^{-2} dependence from 10 eV to 10^3 eV.

There have been a number of publications on the energy spectra of the positively charged component of the sputtered particle yield. The study of the secondary ion spectrum eliminates the difficulty of the cluster contribution encountered in time-of-flight measurements. Among the more recent publications of secondary ion spectra are those of *Jurela 1973, Dennis and MacDonald 1972, Blaise and Slodzian 1973, Sroubek 1974*. Fig 1.1B is an example of type of energy distribution obtained using secondary ion mass spectrometry. These particular results were obtained by *Blaise and Slodzian* and indicate the variation in energy spectra to be expected from copper clusters (Cu^+, Cu_2^+, Cu_3^+). Again there is a characteristic low energy peak (1 to 5eV) and a high energy tail.

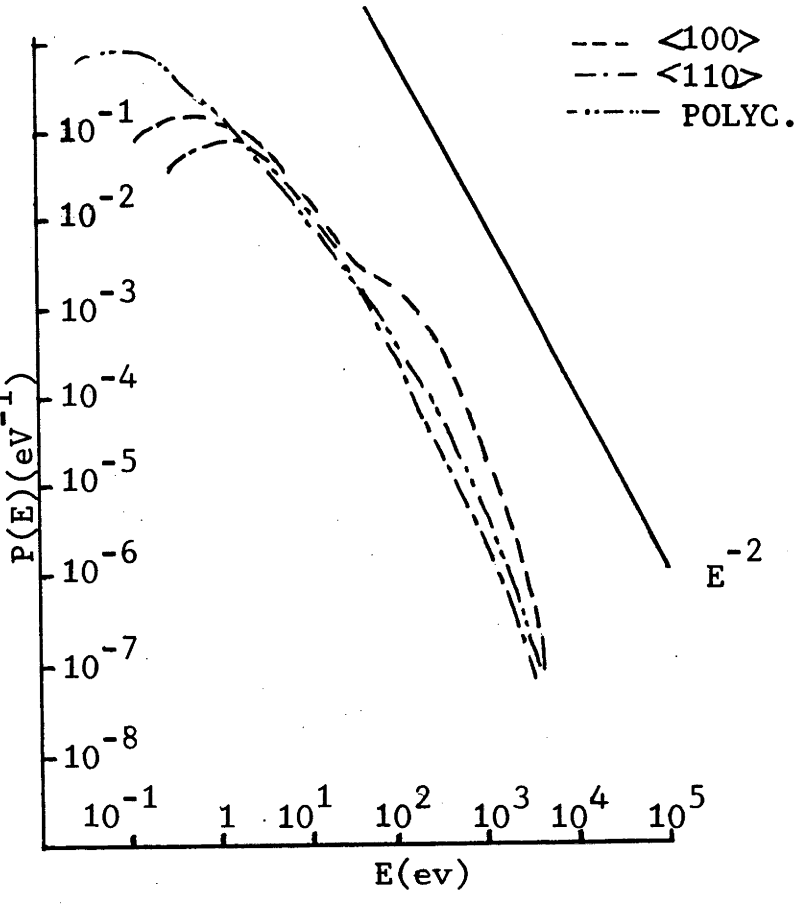

FIG 1.1A ENERGY DISTRIBUTION OF NEUTRALS SPUTTERED FROM Au (THOMPSON 1963)

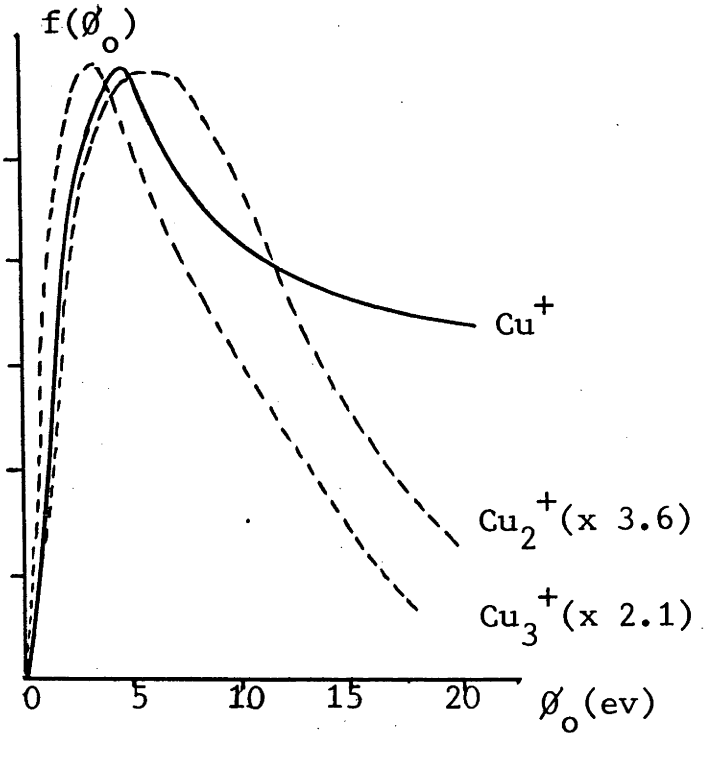

FIG 1.1B ENERGY DISTRIBUTION OF SECONDARY IONS FROM Cu (SLODZIAN 1975)

Expressions for the energy distribution of sputtered dimers have been developed by *Konnen (1974)* who obtained favourable agreement with the energy distribution of K_2 dimers sputtered from a polycrystalline K target.

Post-ionisation techniques have also been used to study energy spectra of sputtered neutrals (*Stuart and Wehner 1964, Oechsner 1970, Oechsner and Gerhard 1974).*

1.3.1.4. ANGULAR DISTRIBUTION OF SPUTTERED PARTICLES

The determination of the angular distribution of sputtered atoms provided some evidence against the thermal evaporation model of particle emission (*Kaminsky 1965)* but there has been little consistent data accumulated about the angular distribution and the variation of its shape with the primary beam type and energy. For the low energy range below 1 KeV *Wehner (1960)* found an 'under cosine' distribution changing to 'cosine' at 1 KeV. It has been suggested by some that the variation in the distribution from one group to another is due to the difficulty in obtaining a truly amorphous material. One of the most recent attempts to measure the angular distribution of sputtered copper atoms has been made by *Rodelsperger et al (1974)* using an experimental arrangement based on a micro-photometer system. Using this technique experimental results were obtained for the angular distribution of copper atoms sputtered by noble gas ions of energy 0.1 to 1 MeV. The higher energy range was chosen to eliminate pure surface effects. The results indicated that the angle of maximum emission varied with ion energy and angle of incidence. (Typical results are shown in Fig 1.2). It was found that $\Phi_{max} = \frac{\pi}{4} + \frac{\Theta}{4}$ where Φ and Θ are as indicated.

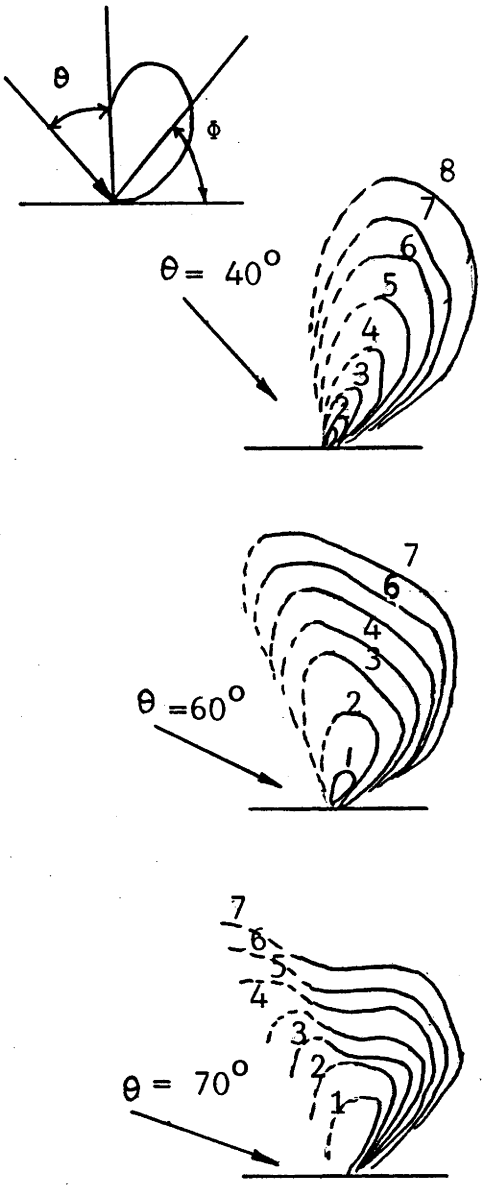

FIG 1.2 ANGULAR DISTRIBUTIONS OF COPPER ATOMS SPUTTERED BY 500 KeV Ar^+ IONS WITH INCREASING ION DOSE AT ANGLES OF INCIDENCE OF 40°, 60°, 70°.

(RODELSPERGER et al 1974)

1.3.1.5 SPUTTERING OF TWO COMPONENT-SYSTEMS

The collision cascade model has been extended by *Anderson and Sigmund (1974)* to calculate the sputtering of homogenous multi-component systems. The flux ratio was found to be -

$$\frac{V_o G_1 (E,E_o)}{V_o G_2 (E,E_o)} \sim \frac{\alpha_1}{\alpha_2} \frac{S_{21}}{S_{12}} \frac{(E_o)}{(E_o)}$$

where $\alpha_1 + \alpha_2 = 1$ and $\left(\begin{matrix} N_1 = \alpha_1 N \\ N_2 = \alpha_2 N \end{matrix} \right)$ atoms of type 1 and 2 per unit volume.

$G_1 (E,E_o)$ and $G_2 (E,E_o)$ represent the average number of atoms moving per energy interval (E_o, dE_o) started by atoms of energy E. The flux of atoms is given by $V_o G (E,E_o)$ and S_{21}, S_{12} is the partial nuclear-stopping power of two atoms moving in the target.

Experimental verification of this ratio is complicated by the binding energies of the component constituents. Some study has been made of III - V and II - VI semiconductors but the most studied two component systems have been oxides (*Kelly and Lam 1973, Edwin 1973, Turos 1974, Naguib and Kelly 1975*). In some systems, oxygen is sputtered preferentially (Ag_2O, CuO, TiO_2, V_2O_5), whereas others (SiO_2, MgO) show little departure from stoichiometry.

Energetic ion bombardment of non-metallic materials has been shown to produce amorphisation for a large variety of materials (*Naguib and Kelly 1975*) for both intermediate doses ($\sim 10^{13} - 10^{16}$ ions cm^{-2}) and high doses ($\simeq 10^{17}$ ions cm^{-2}).

In summary of the preceding sub-sections it can be stated that the flux of sputtered atoms is determined by the slowing down density, the spatial distribution of deposited energy and the surface binding energy for random targets. In the case of compound targets if any deviation from stoichiometry during sputtering occurs, the cascade

theory of *Anderson and Sigmund (1974)* is not applicable. The bombardment of a large number of materials (tabulated by *Naguib and Kelly)* results in a crystalline-amorphous transition, e.g. GaAs, InAs, GaSb, GeO_2 and Si.

1.3.2. INELASTIC PROCESSES

1.3.2.1 SECONDARY ELECTRON EMISSION

As with most other secondary processes accompanying the ionic bombardment of solids there have been many specialised reviews of secondary electron emission (*Kaminsky 1965, Medved and Strausser 1965, Carter and Colligon, 1968, McCracken 1974)* and only a brief outline will be given here.

There are two distinct forms of secondary electron emission from solids under ionic bombardment, potential and kinetic electron ejection. Potential ejection arises as a consequence of the relative energy level structure of the interacting systems whereas kinetic ejection results from an inelastic collision of the incident particle with the atoms of the solid. The simplified diagrams in Fig 1.3 illustrate the two electron ejection processes.

1.3.2.1.1. POTENTIAL ELECTRON EJECTION

The principle of potential electron ejection is shown in the simplified diagram of Fig 1.3A (*Medved and Strausser 1965)*. The diagram shows an atom of ionisation potential E_i at the exterior of the target surface. Electron 1 in the metal target may tunnel through the potential barrier to the empty ground state of the in-coming atom. If $E_i > 2q$, where q is the work function of the metal, energy will be transferred to electron 2 which may subsequently be ejected from the solid. The one step process (A) is the Auger neutralisation

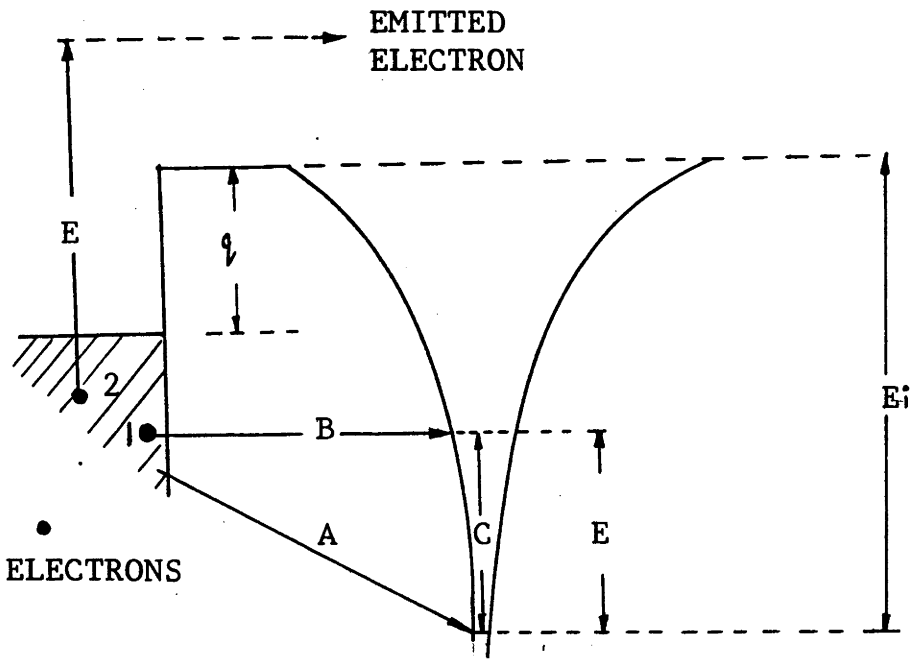

FIG 1.3A POTENTIAL ELECTRON EMISSION

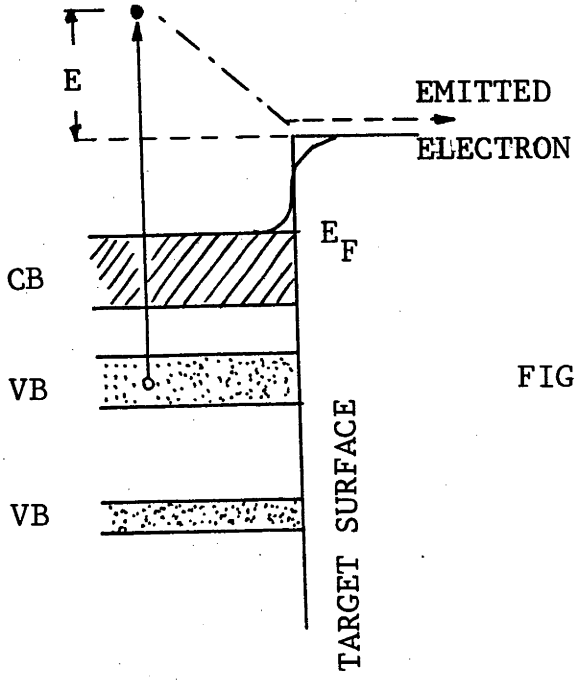

FIG 1.3B KINETIC ELECTRON EMISSION

process. The alternative process is a resonance transition (B) followed by the transition (C) (Auger de-excitation). Analogous processes take place when a secondary ion leaves the solid surface. This situation will be discussed in Chapter Two.

Potential emission has been studied for some years, extensively by *Hagstrum 1954*, and has led to the development of a new electron-emission spectroscopy termed ion-neutralisation spectroscopy (I.N.S.). The basic electronic transition process on which ion-neutralisation spectroscopy is based is the two-electron Auger-type process that occurs when a slow ion with a large neutralisation energy is neutralised at a solid surface. The in-coming ion provides a vacant low-lying level for the Auger process to occur. The Auger neutralisation mechanism is shown in Fig 1.3A. The energy analysis of the emitted electrons enables information on the density of states in the surface region to be obtained.

Potential electron emission is an important aspect of the de-excitation of excited atoms and neutralisation of ions and is considered in detail in Chapter Two.

1.3.2.1.2 KINETIC ELECTRON EJECTION

Fig 1.3B shows a simple view of kinetic electron ejection in which an electron is promoted from a filled band by phonons excited by the collision cascade or directly excited. If the energy loss is less than ΔE the electron will be emitted.

There have been numerous theoretical studies of secondary electron emission both at high and low energies (*Parilis and Kishinevskii 1960, Sternglass 1957, Firsov 1959, Kanaya 1973*). The theory of Parilis and Kishinevskii (1960) concerning kinetic

emission at low energies is based on the Auger recombination of a conduction electron with a hole. The hole is created through the collision of an incident fast particle and a lattice atom raising an electron from the valence to the conduction band. The higher energy problem studied by *Sternglass (1957)*, is simplified in that the incident ions have a constant energy when passing through the region of the target from which secondary electrons are produced.

Sternglass based his treatment on the formation of secondaries according to the Bohr-Bethe theory of ionisation which essentially is the diffusion of slow secondaries to the surface and their subsequent escape to the vacuum. The yield was found to be proportional to the rate of energy loss of the incident particles independent of work function and other bulk properties.

More recently, *Kanaya and Ono (1973)* have improved agreement between theoretical and experimental reduced yield-energy curves using a power potential law between incident ions and lattice electrons.

1.3.2.1.3. ENERGY DISTRIBUTION OF SECONDARY ELECTRONS

The experimental electron energy distributions are similar to those of sputtered atoms with a low energy peak around 1-10 eV. Fig 1.4 shows the distributions obtained from molybdenum under He^+ and Ar^+ bombardment at 2 KeV, 5 KeV, 10 KeV and 15 KeV, (*Wehner 1966*). It can be seen that the peak in the distribution changes by only a fraction of an eV over the range of primary ion energies used. *McCracken (1975)* has suggested that the peak position is primarily determined by the surface workfunction.

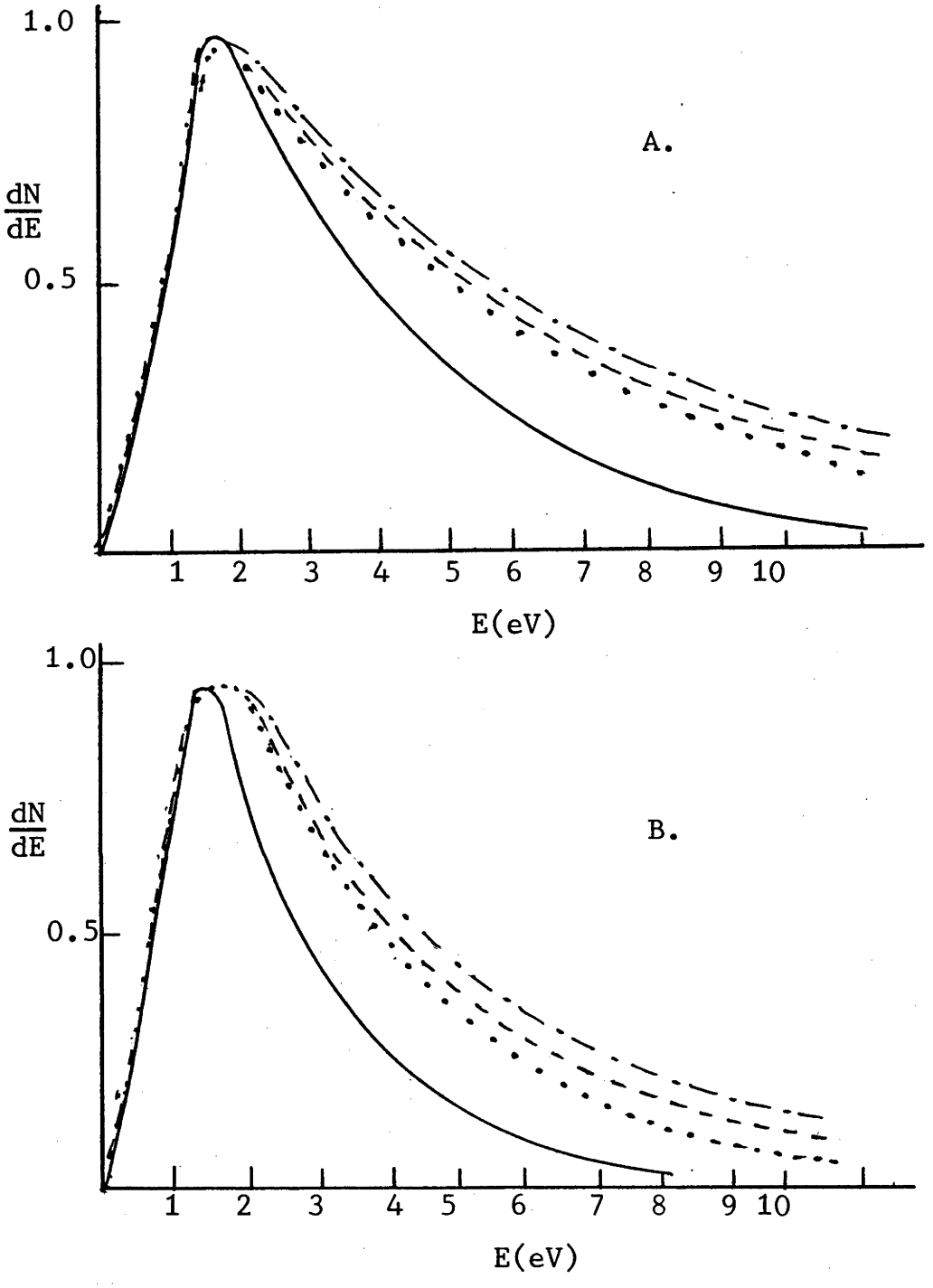

FIG 1.4 SECONDARY ELECTRON DISTRIBUTIONS (WEHNER 1966)

A. $He^{+} \rightarrow$ Mo B. $Ar^{+} \rightarrow$ Mo

2 KeV —— 10 KeV ----
5 KeV ····· 15 KeV —·—·

Higher resolution measurements on the energy distribution of secondary electrons reveals the existence of structure which can be attributed to characteristic Auger transitions. Electron induced Auger emission has received much attention in recent years because of its importance as an experimental technique for the study of solid surfaces. *(Tracy 1973, Matthew 1974, Riviere 1973, Hercules 1970, Chang 1974).* This has led to a development in high resolution electron analysers which are now being used in ion-induced electron experiments. One of the earliest experiments on ion-induced Auger electron emission was made by *Snoek et al (1965)*, who studied secondary electron emission from Au and Cu using Ar^+ primary ions. They detected peaks at 191-193 eV from Au and 181-182 eV from Cu using 60, 80, 90 KeV primary ions and interpreted the results using the molecular orbital model of *Fano and Lichten (1963).*

The field of ion-induced Auger electron emission has since developed and numerous groups have studied the process *(Louchet et al 1972, Benazeth et al 1972, Soszka 1971, Soszka and Lipiec 1972, Mischler et al 1973, 1974, Colombie 1973, Viaris De Lesegno and Hennequin 1974, Arifov 1973, Cook and Burtt 1975, Viel et al 1976, Kruger et al 1976).*

Fig 1.5B shows typical electron energy spectra obtained by *Hennequin and Viaris De Lesegno (1974)* by 10 KeV Ar^+ bombardment of Na, Mg, Al and Si.

Comparisons between electron and ion induced Auger emission have been made by *Haas, Springer, Hooker and Grant (1974).* They obtained results from aluminium using 2 KeV, 2 μA, Ar^+ bombardment and a 2 KeV, 45 μA electron beam and found the argon excited spectrum to be much less intense than that excited by electrons, the relative intensity being 10^{-3}. An interesting aspect of their

work however was that the electron excitation gave a broad asymmetrical $L_{2,3}$ MM peak which they attributed to the band structure of the M levels. In the case of ion excitation the peak was symmetrical and narrower which indicated that the electrons were emitted from essentially free atoms and due to atomic M orbitals. *Musket and Bauer (1972)* have also used proton bombardment at energies of 350 KeV and produced Auger yields comparable to 3 KeV electron bombardment.

1.3.2.2. X-RAY EMISSION

The alternative de-excitation process to Auger electron emission in the case of inner electron shell excitation is the emission of X-rays. Fig 1.5A indicates relative probability of the two competing processes as a function of atomic number. It can be seen that the probability of Auger electron emission is high for light atoms being nearly unity for atomic numbers below 11. X-ray fluorescence is virtually zero for light elements but increases as the Auger yield decreases until a 50 per cent probability point is reached for arsenic. Auger electron emission therefore is dominant over the first four rows of the periodic table.

In terms of cross sections, the probability of X-ray production (fluorescence yield) w,is the ratio of the X-ray emission cross section σx to the inner shell ionisation cross section σ_1

$$w = \frac{\sigma x}{\sigma_1} = \frac{\cdot \sigma x}{\sigma x + \sigma_A}$$

(σ_A is the cross section for Auger emission).

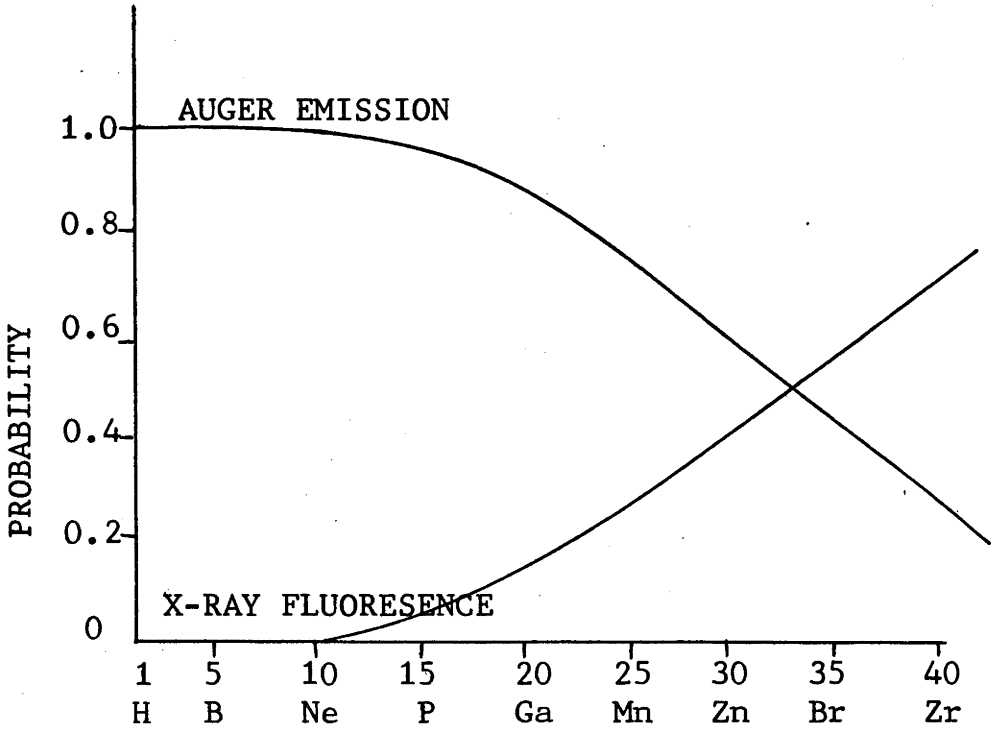

FIG 1.5A PROBABILITY OF AUGER ELECTRON EMISSION AND X-RAY PRODUCTION AS FUNCTIONS OF ATOMIC NUMBER

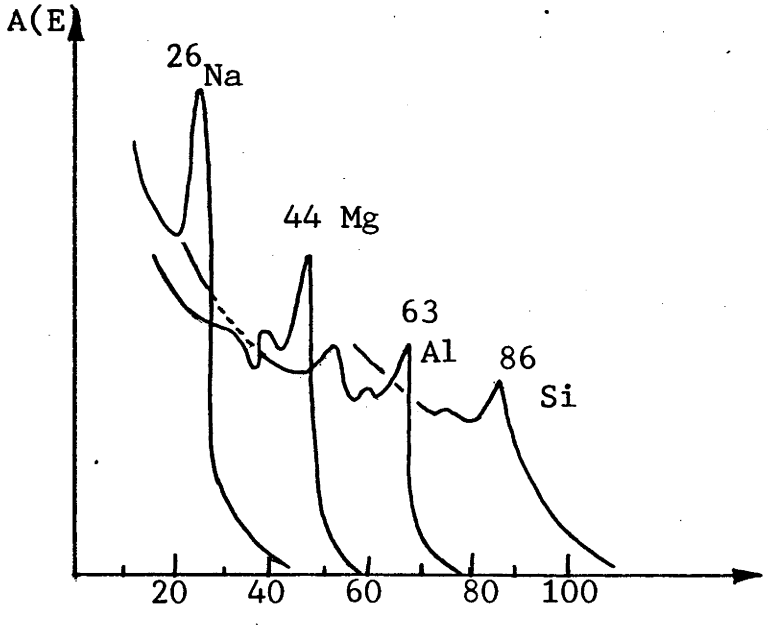

FIG 1.5B ION-INDUCED AUGER SPECTRA (HENNEQUIN AND VIARIS DE LESEGNO 1974)

The production mechanism for inner shell vacancy formation is different for heavy and light primary ions incident on the target. In the case of light ions a direct Coulomb interaction of the primary ion with the bound electron is thought to be responsible whereas the *Fano and Lichten (1972)* molecular orbital model has been proposed for the case of heavy ions. In the M O model the electron shells overlap forming a quasi molecule which gives rise to the promotion of specific molecular levels as the distance between projectile and target is reduced. After the collision a vacancy is formed in the inner shell. A prominent feature of heavy ion X-ray production is the cyclic variation of σx with atomic number of the projectile and target atom (*Specht 1965*). The effect is produced whenever the binding energy of the projectile is equal to the binding energy of one of the inner shells of the target. The most recent review article on the production of X-rays under ion bombardment is that of *McCracken (1974)*.

1.3.2.3. PHOTON EMISSION IN THE ULTRA-VIOLET AND VISIBLE REGION

Photon emission has received very little attention in the literature until recently when its potential as another surface analytical tool was realised. The preceding sections have briefly discussed the major aspects of ionic bombardment of solid surfaces and the secondary processes that result. The primary ion can be scattered elastically or inelastically off the target surface in an ionised state or a neutral state and in various stages of excitation. The reflected particle may then de-excite by emission of a photon.

In addition to binary collisions between incident ions and surface atoms taking place the primary ion may initiate a collision cascade in the solid and cause surface particles to be sputtered from the target. These particles may also be neutral or ionised, atomic or molecular and excited to various levels from which they may decay by photon emission. The three principal modes of photon emission from solid surfaces are shown in Fig 1.6. Electronic excitation in the target, particularly insulators, will also lead to the emission of radiation in the visible region of the spectrum. As with X-ray fluorescence there are alternative de-excitation modes such as Auger type electron transitions, competing with the radiative process.

Photon emission is then a common feature to all secondary processes occuring when an ion beam interacts with a solid surface. It may be regarded as a useful property of secondary emission processes since it enables one to characterise the radiating particle. A comprehensive review of the experimental data available to date on the emission of ultra-violet and optical radiation during ionic bombardment of solids will be presented in the following chapter.

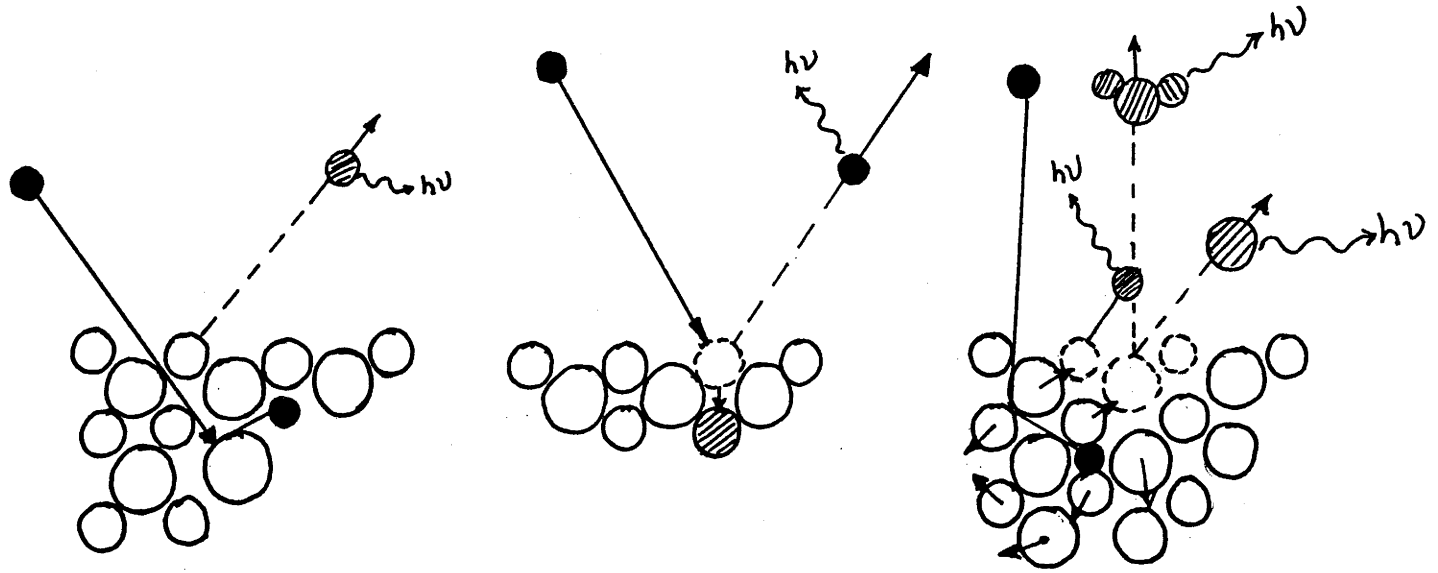

FIG 1.6 THE BASIC PROCESSES OF ION-INDUCED PHOTON EMISSION

REFERENCES

ALMEN, O and BRUCE G, Nucl. Instr. Methods 11, 257 (1961).

ARIFOV, U A, GAIPOV, S and RAKHIMOV, R R, Rad. Effects, 19, 151,(1973).

ANDERSON, C A, Microprobe Analysis, John Wiley, N.Y. (1973).

ANDERSON, H H, Proceedings of 7th Yugoslav Symposium and Summer School on the Physics of Ionised Gases. Edited by Viynovic, V, p. 361 (1974).

ANDERSON, N and SIGMUND, P, Atomic Collisions in Solids, Plenum N.Y., (1974).

ARIFOV, A, Interactions of Atomic Particles with a Solid Surface, Translated from Russian by G.D. Archard, Consultants Bureau, N.Y., London 1969.

BEHRISCH, R, Nuclear Fusion, 12, 695 (1972).

BEHRISCH, R, Nucl. Instr. Methods 132, 293 (1975).

BENAZETH, C, VIEL, L and COLOMBIE, N, Surface Science 32, 618 (1972).

BENNINGHOVEN, A, Surface Science 53, 596 (1975).

BETZ, G, DOBROZEMSKY, R and VIEHBÖCH, F P, Nederlands Tijdscrift voor Vacuumtechniek 8, 203 (1965).

BLAISE, G and SLODZIAN, G, Rev. Phys. Appl. (Paris) 8, 105 (1973).

CARTER, G and COLLIGON, J A, Ion Bombardment of Solids, Heineman, London, 1968.

CHADDERTON, L T, Radiation Damage in Crystals, Methuen, London, 1965.

CHANG, C C, Characterisation of Solid Surfaces, Edited by Kane, P.F. and Larrabee, G.B., Plenum N.Y., 509 (1974).

CHANG, C C, Surface Science 48, 9 (1975).

COLOMBIE, N, BENAZETH, C, MISCHLER, J AND VIEL, L., Rad. Effects. 8, 251 (1973).

COOK, N and BURTT, R B., J. Phys. D: Appl. Phys., 8, 800 (1975) A.

COOK, N and BURTT, R B., J. Phys. D: Appl. Phys., 8, 812 (1975) B.

DEARNALEY, G, FREEMAN, J H, NELSON, R S and STEPHEN J, Ion Implantation (Amsterdam: North-Holland). (1973).

DENNIS, E and MACDONALD, R J, Rad. Effects, 13, 243 (1972).

EDWIN, R P, J. Physics. D, Appl. Phys. 6, 233 (1973).

FANO, U and LICHTEN, W, Phys. Rev. Lett., 14, 627 (1965).

FIRSOV, O B, Sov. Phys. J.E.T.P., 9, 1076 (1959).

GROVE, W R, Philosophical Trans. Roy. Soc., 142, 87 (1852).

HAAS, T W, SPRINGER, R W, HOOKER, M P and GRANT J T, Phys. Lett. 47A, 317 (1974).

HAGSTRUM, H D, Phys. Rev., 96, 336 (1954).

HAGSTRUM, H D, Science, 178, 275 (1972).

HEILAND, W and TAGLAUER, E, Nucl. Instr. Methods, 132, 535 (1976).

HENNEQUIN, J F and VIARIS DE LESEGNO, P, Surface Science, 42, 50 (1974).

HERCULES, D M, Analytical Chem. 42, 20A (1970).

HOFER, W O, Rad. Effects, 19, 263 (1973).

JURELA, Z, Int. J. Mass. Spectrom. Ion Phys., 12, 33 (1973).

KAMINSKY, M, Atomic and Ionic Impact on Metal Surfaces, Springer-Verlag, Berlin (1965).

KAMINSKY, M, IEEE Trans. Nucl. Sci., NS-18, 208 (1971).

KAMINSKY, M, IEEE Trans. Nucl. Sci., NS-21, 37 (1974).

KANAYA, K, HOJOU, K, KOGA, K and TOKI, K, Jap. J. Appl. Phys., 12, 1297 (1973).

KANAYA, K and ONO, O., Jap. J. Appl. Phys., 13, 944 (1974).

KANE, P F and LARRABEE, G R, Characterisation of Solid Surfaces Plenum, N.Y., (1974).

KARPUZOV, D S, Phys. Stat. Sol. (b), 64, 351 (1974).

KARPUZOV, D S, Surface Science, 45, 342 (1974).

KELLY, B T, Irradiation Damage to Solids, Pergamon (1966).

KELLY, R and LAM, N, Rad. Effects, 19, 39 (1973).

KONNEN, G P, TIP, A and DEVRIES, A E, Rad. Effects, 21, 269 (1974).

KRÜGER, W, SCHARMANN, A, and STILLER, N., Nucl. Instr. Methods, 132, 483 (1976).

LIEBERMAN, G, N.B.S. Special Publication (1976).

LIEBL, H., J.Appl. Phys. 38, 5277 (1967).

LIEBL, H., J. Phys. E., 8, 797 (1975).

LINDHARD,J and SCHARFF, M., Phys. Rev. 124, 128 (1961).

LOUCHET, F, VIEL, L, BENAZETH, C, FAGOT, B and COLOMBIE, N., Rad. Effects 14, 123 (1972).

MACDONALD, R J, Adv. in Physics 19, 457 (1970).

MATTHEW, J A D , Endeavour, XXXIII, 19, 86 (1974).

MCCRACKEN, G M, Rep. Prog. Phys., 38, 241 (1975).

MEDVED, D B and STRAUSSER, Y E, Adv. Electron. Electron Phys. 21, 1071 (1965).

MISCHLER, J, COLOMBIE, N and FERRE, J, C.R. Acad. Sc. Paris, 276 , 381 (1973 A).

MISCHLER, J and COLOMBIE, N., Surface Science, 40, 311 (1973B).

MISCHLER, J and COLOMBIE, N., C.R. Acad. Sc. Paris, 278, 897 (1974).

MUSKET, R G and SMITH, H P Jr., J. Appl. Phys. 38, 3579 (1968).

MUSKET, R G and BAUER, E., Appl. Phys. Lett., 20, 455 (1972).

NAGUIB, H M and KELLY R, Rad. Effects, 25, 1 (1975).

OECHSNER, H, Phys. Rev. Lett. 24, 583 (1970).

OECHSNER, H, Z.Physik. 238, 433 (1970).

OECHSNER, H and GERHARD, W., Surface Science, 44, 480 (1974).

OEN, O S, and ROBINSON, M T, J.A.P., 46, 5069 (1975).

ONDERDELINDEN, D, Appl. Phys. Lett., 8, 189 (1966).

PARILIS, E S and KISHINEVSKII, L M, Sov. Phys. Solid State, 3, 885 (1960).

RIVIERE, J C, Contemp. Phys., 14, 513 (1973).

ROBINSON, M T, Phil. Mag., 12, 145 (1965).

RODELSPERGER, K, KRÜGER, W, and SCHARMANN, A, Z. Physik. 269, 83, (1974).

ROL, P K, FLUIT, J M, and KISTEMAKER, J, Physica, 26, 1000 (1960).

SEITZ, F and KOEHLER, J S., Solid State Physics, 2, 305 (1956).

SCHULTZ, M., Appl. Phys., 4, 91 (1974).

SIGMUND, P., Phys. Rev. 184, 383 (1969).

SIGMUND, P., Rev. Roumaine Phys. 17, 1079 (1972).

SILSBEE, R H., J. Appl. Phys., 28, 1246 (1957).

SMITH, D P., J. Appl. Phys., 38, 340 (1967).

SNOEK, C, GEBATH, R, VANDER WEG, W F, ROL, P K and BIERMAN, D J., Physica, 31, 1553 (1965)

SOSZKA, W., Physica, 60, 257 (1972).

SOSZKA, W and LIPIEC, J., Surface Science, 36, 714 (1972).

SPECHT, H J, Z. Physik, 185, 301 (1965).

SROUBEK, Z., Surface Science, 44, 47 (1974).

STERNGLASS, E J., Phys. Rev. 108, 1, (1957).

STUART, R V and WEHNER, G K., J.Appl. Phys., 35, 1819 (1964).

SUMMERS, A, FREEMAN, N and DALY, N., IEEE Trans. Nucl.Sci., NS-18, 347 (1971).

THOMPSON, M W, Phil. Mag., 18, 377 (1968).

THOMPSON, M W, FARMERY, B W and NEWSON, P A., Phil. Mag, 18, 361, (1968).

THOMPSON, M W., Defects and Radiation Damage in Metals, Cambridge University Press, 1969.

TRACY, J C., Electron Emission Spectroscopy, Reidel Holland, 295, 1973.

TSONG, I S T., and MCLAREN, A C, Spect. Act. 30 B, 343 (1975).

TUROS, A, VAN DER WEG, W F, SIGURD, D and MAYER, J M, J. Appl. Phys., 45, 2777 (1974).

VIARIS DE LESEGNO, P and HENNEQUIN, J F., J. de Phys. 35, 759 (1974A).

VIARIS DE LESEGNO, P and HENNEQUIN, J F., Phys. Lett. 49A, 265(1974B).

VIEL, L, BENAZETH, C and BENAZETH, N., Surface Science, 54, 635 (1976).

WEDEPOHL, P T, Rad. Effects, 1, 77, (1969).

WEHNER, G K, J. Appl. Phys. 26, 1056 (1955).

WEHNER, G K, Phys. Rev., 102, 690 (1956).

WEHNER, G K, J. Appl. Phys. 31, 1392 (1960).

WEHNER, G K, Z. Physik, 193, 439 (1966).

WEISSMAN, R and SIGMUND, P, Rad. Effects, 19, 7 (1973).

WIGNER, E P., J. Appl. Phys. 17, 857 (1946).

ZWANGOBANI, E and MACDONALD, R J, Rad. Effects, 20, 81 (1973).

CHAPTER TWO

EXCITATION, DE-EXCITATION AND PHOTON EMISSION AT ION BOMBARDED SURFACES

2.1 INTRODUCTION

In this chapter the theoretical and experimental aspects of photon emission from solid targets bombarded with ion beams will be reviewed. First the theoretical aspects of electron exchange processes occuring between excited atoms and ions in the immediate vicinity of the target are examined. These processes, which have a significant effect on radiative de-excitation of scattered primaries and sputtered target atoms are then used in a discussion of the available experimental data on photon emission. Correlations have been made where appropriate with secondary ion emission data and the current theories of secondary ionisation. No attempt is made to exhaustively review secondary ion emission but rather to present in a logical manner the published work on ion-induced photon emission, drawing analogies with representative secondary ion results. The current theories of secondary ion emission are reviewed briefly and possible areas open for study by photon emission are discussed.

2.2 THE BASIC THEORETICAL ELECTRON EXCHANGE PROCESSES

2.2.1 NEUTRALISATION OF PRIMARY IONS AND PHOTON EMISSION

When a positive ion approaches a metal surface the ion may capture a metallic electron becoming a neutral atom possibly in an excited or metastable state. The atom may subsequently decay by secondary electron emission or alternatively by the emission of a photon. The process of electron ejection from metal surfaces by

positive ions has been considered by several authors. Historically the first attempt was made by *Oliphant and Moon (1930)*. The process was considered as the transition through the potential barrier separating the ion and metal surface, of an electron of given energy from the metal to a state of equal energy in the atom.

A quantum mechanical approach to the problem was first made by *Massey (1930)*, and later in a more correct manner (according to *Janev 1970)*, by *Shekhter (1937)*. The process considered was the impact of H and H^+ on Mo, and of direct interest here, the probability of ion neutralisation occuring accompanied by the emission of photons. A numerical calculation yielded a value of one quantum emission for each 10^7 to 10^8 incident ions. A similar calculation by *Sternberg (1957)* gave a somewhat higher yield of one photon per 10^4, 10 eV He^+ ions colliding with a metal surface.

A number of experimental studies have been made of the light emission characteristic of the primary ion when impacting a metal target. *Mayer (1933)* detected characteristic line emission which was attributed to the neutralisation of alkali positive ions striking a metal surface. *Böhmer and Lüscher (1963)* studied optical emission from low energy (20 eV to 100 eV) He^+ and Ne^+ ions bombarding a tungsten surface. Spectral analysis was not possible with the apparatus used and therefore little information on the actual transitions involved could be obtained. However, an estimate by the authors of the photon yield gave a value of one quantum emitted per 10^3 to 10^4 incident ions, somewhat higher than the theoretical estimates of Shekhter and Sternberg.

2.2.2 SINGLE AND MULTISTAGE ELECTRON TRANSITIONS

The theoretical studies of Oliphant and Moon, Shekhter, Massey and others were later extended by *Hagstrum (1954)*.

Hagstrum distinguished between four basic electronic transitions involving an ion or excited atom and a metal surface -

1. Resonance neutralisation of an ion
2. Resonance ionisation of an atom
3. Auger neutralisation of an ion
4. Auger de-excitation of an excited atom

These four basic processes are illustrated in Fig 2.1. The one electron resonance transitions are shown in Fig 2.1A. The diagram represents an atom or ion of ionisation potential Ei, at a distance S from a metal surface of work function Φ which is represented by a Sommerfield potential well of depth ε_o filled to the fermi level E_F. The atom of ionisation potential Ei is in an excited state Ee. When the energy level of the electron in the metal coincides within narrow limits with that in the atom, transition (1) takes place. The two states are in resonance and a tunneling transition of an electron through the potential barrier may occur through the resonance neutralisation process. From energy consideration the resonance neutralisation process can only occur when -

$$\varepsilon_o > Ei - Ee > \Phi$$

The reverse process, transition (2) is termed resonance ionisation and is energetically possible whenever -

$$\Phi > Vi - Ve$$

The alternative to the one electron resonance electron exchange transitions are the two electron or *Auger (1975)* transitions of Fig 2.1BC. Auger neutralisation of an ion, Fig 2.1B, involves the downward transition of electron (1) from the conduction band of the metal to the ground state of the atom. An excited electron (2)

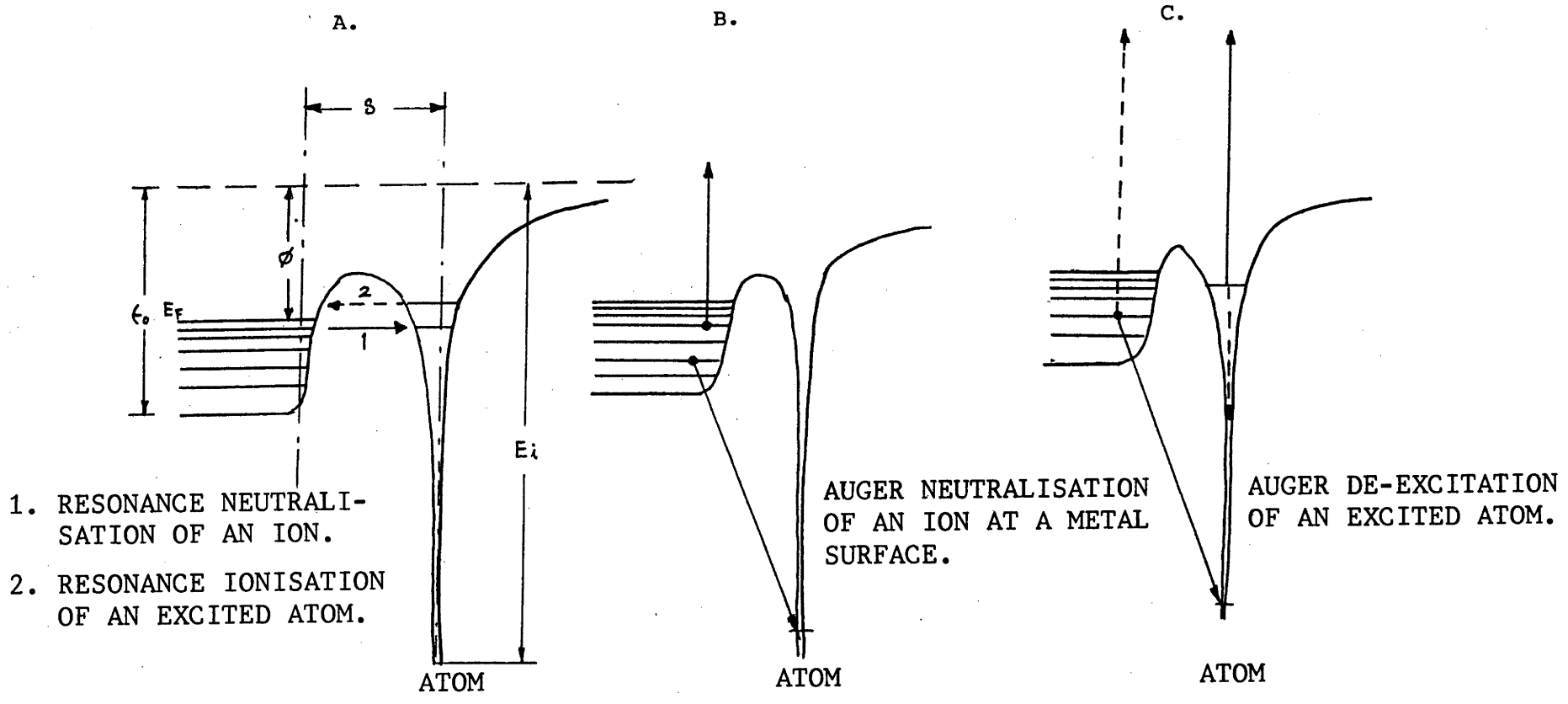

FIG 2.1 BASIC ELECTRON EXCHANGE PROCESSES OCCURRING BETWEEN AN ATOM OR ION NEAR A METAL SURFACE.

is ejected from the conduction band to the vacuum whenever Ei> 2 Φ. The Auger neutralisation process can occur whenever Ei > Φ.

Auger de-excitation of a metastable atom at a metal surface is shown in Fig 2.1C. The process may proceed by an exchange of electrons (full lines) or a non exchange (dashed lines). The process is energetically possible whenever $E_e > \Phi$.

The four basic electronic exchange processes described above can be represented by the equations of *Hagstrum and Becker (1973)*, given in Table 2.1.

TABLE 2.1

A. Resonance neutralisation (R N) and Resonance Ionisation (R I) Transitions.

1. $X^{+} + e^{-}s \quad (-E_i^{o}) \rightleftarrows X^{o}$
2. $X^{+} + e^{-}s \quad (-E_i^{o*}) \rightleftarrows X^{o*}$
3. $X^{+*} + e^{-}s \quad (-E_i^{o**}) \rightleftarrows X^{o**}$
4. $X^{++} + e^{-}s \quad (-E_i^{+}) \rightleftarrows X^{+}$
5. $X^{++} + e^{-}s \quad (-E_i^{+*}) \rightleftarrows X^{+*}$

B. Two-electron Auger de-excitation (A D) Transitions.

1. $X^{o*} + e^{-}s(-\alpha) \rightarrow X^{o} + e^{-} \quad (E_e^{o*} - \alpha)$
2. $X^{o**} + e^{-}s(-\alpha) \rightarrow X^{o*} + e^{-} \quad (E_e^{o**} - E_e^{o*} - \alpha)$
3. $X^{+*} + e^{-}s(-\alpha) \rightarrow X^{+} + e^{-} \quad (E_e^{+*} - \alpha)$

C. Two-electron Auger neutralisation (A N) Transitions.

1. $X^{+} + e^{-}S(-\alpha) + e^{-}s(-\beta) \rightarrow X^{o} + e^{-} \quad (E_i^{o} - \alpha - \beta)$
2. $X^{+*} + e^{-}s(-\alpha) + e^{-}s(-\beta) \rightarrow X^{o*} + e^{-} \quad (E_i^{o} + E_e^{+*} - \alpha - \beta)$
3. $X^{+*} + e^{-}s(-\alpha) + e^{-}s(-\beta) \rightarrow X^{o} + e^{-} \quad (E_i^{o} + E_e^{+*} - \alpha - \beta)$

Notation for the formulae of Hagstrum and Becker given in Table 2.1.

X	atomic particle
o	neutral atom
+	singly charged ion
++	doubly charged ion
e^-_s	conduction band electron
e^-	ejected Auger electron
E_e	excitation energy
*	excitation of single electron
**	excitation of two electrons
E_i	ionisation energy
α β	variable energy values appropriate to the band structure of the solid.

Multistage processes were also considered by Hagstrum, the simplest being the following (from Table 2.1) -

1. R N (A2 →) + A D (B1)

2. R I (A2 ←) + A N (C1)

2.2.3 THE TRANSITION RATES FOR ELECTRON EXCHANGE PROCESSES

Both *Shekhter (1937) and Cobas and Lamb (1944)* have derived an expression for Rt (S), the probability per unit of time for a process to occur at a distance S between an atom and metal surface, to be of the form -

(i) Rt (S) = A exp (- aS) where A and a are constants for a given process.

The probability Po (S, vo) that an incident particle starting at an infinite distance toward the metal will reach a distance S without undergoing a transition is -

(ii) $Po(S, vo) = \exp\left[- \int_s^\infty Rt\ (S)\ ds/vo \right]$ (Hagstrum 1954).

The probability that it will undergo a transition in ds at S is -

$$\text{(iii)} \quad Pt\ (S,vo)\ ds = [Rt\ (S)\ ds/vo\ ]\ \exp\ [\ -\ \int_s^{\infty} Rt(S)\ ds/vo\ ]$$

assuming vo is constant and substituting (i)

$$\text{(iv)} \quad Po\ (S,vo) = \exp\ [\ -\ (A/a\ vo)\ \exp\ (-\ as)\ ]$$

and

$$\text{(v)} \quad Pt\ (S,vo) = \frac{A}{vo}\ \exp\ [-\ (A/a\ vo)\ \exp\ (-\ as)\ -\ as\ ]$$

Theoretical values for A and a for resonance and Auger transitions are given in Table 2.2

TABLE 2.2

Published theoretical transition rate parameters

	AUGER PROCESSES					
	Neutralisation		De-excitation		Resonance processes	
	$A(sec^{-1})$	$a(cm^{-1})$	$A(sec^{-1})$	$a(cm^{-1})$	$A(sec^{-1})$	$a(cm^{-1})$
Shekhter	6.35×10^{14}	3.9×10^{8}			5.74×10^{19}	3.2×10^{8}
Cobas & Lamb			9.6×10^{16}	7.3×10^{8}	9.1×10^{18}	1.9×10^{8}

The calculations of Shekhter and Cobas and Lamb indicate that the transition rates for resonance processes are much greater than for Auger processes. The two stage process of resonance neutralisation followed by Auger de-excitation was considered by *Hagstrum (1954)* to be less probable than single transitions, due to the variation of energy levels near the metal restricting the resonance process.

When atomic energy level shifts with S were taken into account, a three stage process was postulated by Hagstrum for an incoming ion. The ion when inside a critical distance Sc for resonance processes may be neutralised at $S < S_c$, resonance ionised at S > Sc and finally Auger neutralised. The deformation of the ionic potential was also considered by *Varnerin (1953)*, who studied the $He^+ \rightarrow He\ (^3S_1)$ transition at a Mo surface. It was found that in this case Auger type processes were responsible for most of the secondary electrons.

2.3 THE EXCITED STATES OF SPUTTERED PARTICLES

The preceeding sections have exclusively dealt with the electronic transitions occuring between a primary ion and a metal surface. *Van der Weg and Rol (1965)* have considered the processes occuring when a sputtered excited particle leaves the surface of the target. The probability for a particle of velocity v to escape without undergoing a transition was given as -

$P(\infty, v) = \exp(-A/av)$. This equation, similar to that of Hagstrum's, expressed the fact that only atoms with relatively high energies leave a metal surface in an excited state and are de-excited at larger distances by photon emission. The situation is analogous to the model considered by Hagstrum to describe an ion approaching a metal surface and may be used to describe an ion leaving a surface through the sputtering mechanism.

2.4 THE SHAPE OF SPECTRAL LINES EMITTED BY PRIMARY IONS SCATTERED FROM SOLID TARGETS

The strongest emission that occurs from proton bombardment of solid targets is the 1216 Å Lyman α transition. *Dunn, Geballe*

and Pretzer (1962) detected Lyman α photons produced by 2.5 KeV protons on tungsten at normal incidence and measured an efficiency of 5.10^{-3} photons per proton. The work was extended by *Sterk, Marks and Saylor (1966)* who studied Lyman α emission from protons on aluminium and by *Khan et al (1967)* who studied Lyman α from protons on copper. However, it was not until 1970 that the first line profiles of Lyman α emission were measured by *McCracken and Erents*. Measurements of the Doppler shift of the emission showed that the Lyman α was emitted by the decay of excited protons backscattered from molybdenum. A blue shift (towards short wavelengths) was interpreted as backscattering of atoms, and a red shift also evident in the profiles was thought to result from backscattered atom radiation reflected off the target into the spectrometer.

Several more detailed studies of radiation from incident ions impacting metal surfaces have been made by *Parilis (1965, 1969), Kerkdijk and Thomas (1973), Olander et al (1974), Kerkdijk et al (1974), Baird et al (1974) and Warczak et al (1975).*

Kerkdijk et al (1974), studied the Balmer-β line at 4861 Å emitted by protons of energy 10 to 40 KeV incident on a copper single crystal. Experimental results were compared with the model of *Olander et al (1974)* for predicting the line shapes of Doppler-broadened spectral lines. The model assumed that the primary ions enter the solid as a collimated beam at a predetermined angle with respect to the surface normal. Energy is then lost through electronic interaction with the solid and occasionally Coulombic collisions cause particles to be scattered back towards the surface. These particles may eventually emerge in an excited state and subsequently

emit Doppler broadened lines. The initial slowing down process was described by the electronic stopping power law of *Lindhard et al (1963)*.

$$S = K E^n$$

The Rutherford differential cross section was used to describe the Coulombic collisions -

$$\sigma (E,\theta) = \frac{K}{E^2 \, Sin^4(\theta/2)}$$ where E is the particle energy at collision and θ the scattering angle. Also included in the calculations was the excitation probability, the radiationless de-excitation probability of Van der Weg, the energy and angular distribution of backscattered particles and the Doppler effect. No allowance was made for the reflection of light emitted from the backscattered particles by the surface and subsequent collection by the detector. The Doppler shift as a function of target orientation and also primary beam energy as well as the maximum photon intensity as a function of these parameters was found to agree reasonably well with the experimental data when a value of 1.5×10^8 cm/sec was used for the non-radiative decay rate. This value was found to be consistent with the theoretical value of *Cobas and Lamb (1944)*. It was concluded that only high velocity hydrogen atoms could escape from the surface and radiate.

Baird et al (1975) have studied the Doppler broadening of emission lines produced by 20-30 KeV He^+ ions backscattered from polycrystalline niobium and copper surfaces in a neutral excited state. For He^+ on copper and niobium the 5876 Å, 4472 Å, 3889 Å and 6678 Å HeI lines were detected. The results were also compared with a model to predict the measured line shape. The model took into account the projectile penetration into the target, which according to *McCracken and Freeman (1969) and Lindhard and Scharff*

(1961) loses energy to the target electrons at a rate given by -

$$\frac{dE}{d\xi} = - Z_1^{1/6} \frac{Z_1 Z_2}{(Z_1^{2/3} + Z_2^{2/3})^{3/2}} 8\pi n e^2 a_o \left(\frac{E}{E^1} \right)^{1/2}$$

$$= - K E^{1/2}$$

where $Z_1 Z_2$ are the atomic numbers of the ion and target atom respectively n is the density of nuclei in the target, a_o is the Bohr radius, E, E^1 the primary energy and energy at which the ion velocity equals the electron velocity in the first Bohr orbit.

As with the model of *Kerkdijk et al (1974)*, allowance was also made for the possibility of radiationless de-excitation of the excited atoms by including a term given by *Hagstrum (1954)*. The probability of radiationless decay at a distance S from the surface is given by -

$P(S) = A e^{-as}$ where A and a are constants related to the wave functions of the electrons and the potential barrier. The probability of a particle escaping without undergoing radiationless decay is given by -

$R(V \perp) = \exp(-A/a\ V \perp)$ (Section 2.3). The ratio of A/a is regarded as a survival coefficient. From the results a value of A/a of 0.8 to 1.2 x 10^8 cm sec^{-1} was determined from the 5876 Å emission induced by He^+ on niobium. An example of the effect of different values of survival coefficient on the line shape is given in Fig 2.2A. Some uncertainty in the shape of the predicted line profile was caused by excited atoms emitting photons towards the target which then reflects towards the observer, an effect not considered by Kerkdijk et al. Consequently a value for the surface reflectance had to be estimated. The results did however agree favourably with the model for a survival coefficient of 1.2 x 10^8 cm sec^{-1} and surface

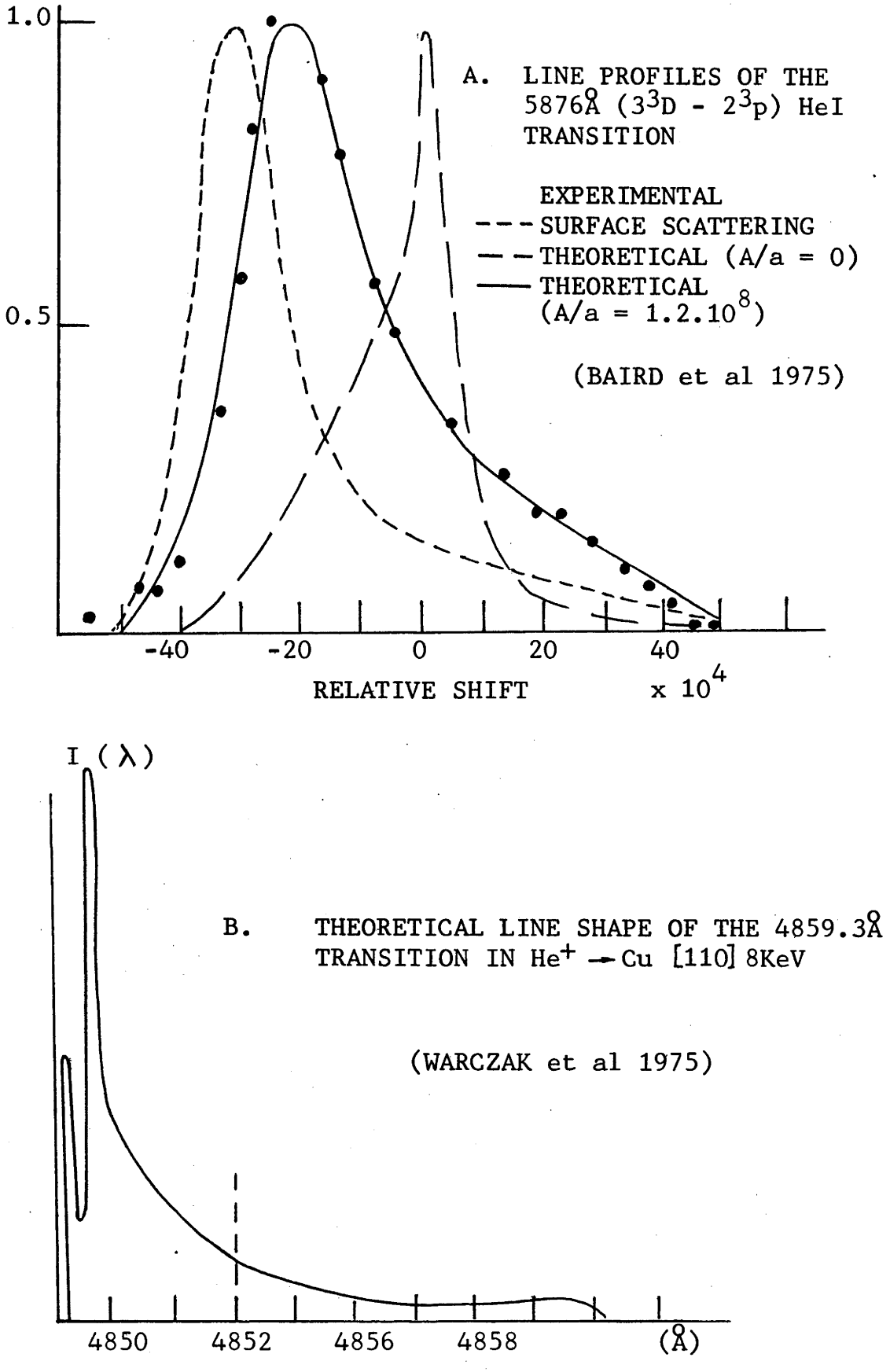

FIG 2.2 EXAMPLES OF THEORETICAL LINE PROFILES FROM BACKSCATTERED PRIMARY PARTICLES

reflectance of 0.28 in the case of 30 KeV He^+ ions incident on niobium at an angle of 45^o. This value for the coefficient of 1.2×10^8 cm sec^{-1} is not too dissimilar to that of Kerkdijk's of 1.5×10^8 cm sec^{-1};

One of the most recent attempts to predict the Doppler shape of spectral lines emitted by He^+, Ne^+ and Ar^+ ions scattered on a Cu target has been by *Warczak et al (1975) and Warczak (1975)*. The shape of the spectral line inducated by single scattering of ions on a single crystal can be written as -

$$I_1(\lambda) = 2 \int_{\phi(\lambda)}^{\phi(\lambda)} K(\phi) . W(\phi) . P(\phi) . \frac{\partial \phi}{\partial \lambda} \sin \phi \, d\phi$$

(Parylis 1965), where $I_1(\lambda)$ is the number of photons of wavelength between λ and $\lambda + d\lambda$ emitted per unit time by ions in the direction of observation. The function $K(\phi)$ takes into account the crystal transparency for incident and scattered beams. $W(\phi)$ includes the excitation probability dependence on angle ϕ and $P(\phi)$ is the radiationless de-excitation probability. The function K also describes the angular distribution of the scattered particles and the differential cross-section was calculated with the screened Coulombic-Thomas-Fermi-Firsov potential as opposed to the Rutherford cross section used by Kerkdijk (1974).

Using the equation of *Parylis (1969), Warczak et al (1975)* calculated the line shape of the 4682.3 Å transition of Ar^+ on Cu [110] at an energy of 20 KeV and 8 KeV, the 4569 Å transition of Ne^+ on Cu at 20 KeV, and 4859.3 Å transition of He^+ on Cu at 8 KeV. Account was also taken of double scattering of ions off the metal surface. An example of the theoretical line profile is given in Fig 2.2B for the 4859.3 Å transition of He^+ on Cu [110] for a primary

energy of 8 KeV at an angle of 20^{o}. *Warczak et al (1975)* have also considered the influence of thermal vibrations of the lattice on the line shape. Their results indicated a characteristic peak originating from double scattered ions and that thermal vibration of the target atoms influenced only the relative intensity of the single and double scattered peaks. The value of the survival coefficient used in the calculations was that of *Hagstrum (1954)* of 1.63×10^{6} cm sec^{-1}.

The prediction of a double peak structure in the line profile and its temperature dependence are interesting features of the theory of Warczak et al which have yet to be confirmed experimentally.

2.5 SPUTTERED PARTICLES AND PHOTON EMISSION FROM TARGET MATERIAL

2.5.1 EARLY RESEARCH

One of the earliest observations reported on the optical emission of solids during ionic bombardment was by *Arnold (1897)* who detected the Na D lines emitted from Na compounds irradiated with Canal rays. *Carlheim-Gyllensköld (1908)* studied a range of targets and identified prominent atomic emission lines of the target atoms. A more thorough investigation of the phenomenon was later made by *Stark and Wendt (1912)*, who measured the width of the 3967 Å calcium line produced under ionic bombardment. The dispersion of the instrument was 10 Å mm^{-1} and the shift in the emission line was measured to be 0.05 mm, corresponding to 0.5 Å. Using the Doppler relationship for the non-relativistic case -

$\frac{\Delta\lambda}{\lambda} = \frac{u}{C}$ where $\Delta\lambda$ is the Doppler shift

λ the wavelength

u the velocity of the emitters

C the speed of light

a value of $u = 4 \times 10^6$ cm sec^{-1} was calculated. They concluded from their results that the emission came from excited particles sputtered from the target by the ion beam rather than particles excited in the gas phase by the primary ions.

Chaudhri et al (1961, 1963, 1964, 1967) studied the ultraviolet and visible radiation from metals under bombardment of high energy protons and positive ions (1961) and alkali ions (1967). Their results were interpreted in terms of plasma radiation of the metal electrons induced by approaching incident ions. However, the detection system that was used employed "narrow" band ultraviolet filters having a band pass of ~150 Å, insufficient to resolve any atomic line emission. A continuous distribution in spectral radiation was therefore detected.

2.5.2 GENERAL SURVEY STUDIES OF OPTICAL EMISSION

A wide range of materials have been studied by *Tsong (1971)* under the bombardment of 5 to 8 KeV Ar^+. The emission was registered photographically in a quartz prism spectrograph of aperture f = 12. In the case of polycrystalline metals no photon emission was detected for a large number of targets with the exception of Mg. Semiconducting Si and Ge gave only low intensity lines. A variety of ionic crystals were studied and found to give emission lines of the metallic components but not of F, O, Cl and C. Ionised line emission was detected in the case of Ca and Mg in CaF_2, $CaCO_3$, $CaWO_4$ and MgO. The results were interpreted in terms of resonance electron exchange, depopulating the

excited levels of certain atoms through resonance ionisation. This process was used to explain the lack of photon emission detected for the metals Ag, Al, Ca, Cu, Mo, Nb, Ni and Zn for which $\Phi > (E_1 - E_e)$. However, strong emission has been observed by many authors from these metal targets since the work of Tsong indicating the lack of sensitivity of the photographic detection system used.

Terzic and Perovic (1970) have analysed, photoelectrically, the optical emission from polycrystalline targets of Al, Mo and Ag with Ar^+ ions of 40 KeV. A current density of 100 $\mu A\ cm^{-2}$ was used and the background gas pressure was $\sim 3 \times 10^{-6}$ Torr. The spectral range of 3800-6600 Å was covered using a glass prism spectrograph. Line spectra of atoms and ions of the target material were detected in all cases, the most intense being the resonance lines AlI (3961 Å, 3944 Å) and MoI (3864 Å, 3902 Å). ArII emission lines were detected from Ar^+ on Ag but no ArI lines were observed. These results were again interpreted in terms of the resonance and Auger electron transfer processes occuring between an atom and a metal target surface.

White, Simms and Tolk (1972) have also investigated a wide range and variety of targets using both low-energy ion and neutral bombardment. The energy range covered was 10 eV to 10 KeV and the wavelength range 2000 Å to 8500 Å in a vacuum of 1×10^{-7} Torr. The results obtained will be discussed in section 2.6 in connection with surface analysis techniques using photon emission.

Braun, Emmoth and Martinson(1974) used 100-300 KeV Xe^+ ions to bombard targets of Be, Mg, Al, Si, Fe, Cu, Ge, In, Ag, Tm, Ta, Ir, Pb, SiO_2 and GaAs. Characteristic line spectra was observed in most cases, although the authors do not comment on the results from semiconducting Ge and GaAs. Impurity lines of hydrogen at 4861 Å (Hβ), and 4339 Å (Hγ) were detected as well as the CH $A^2\Delta - X^2\pi$

band whose edge is at 4312 Å and the origin of which can be traced to diffusion pump oil contamination on the target surface. The background gas pressure was only 1 x 10^{-6} Torr.and a primary ion current of 30-50 $\mu A cm^{-2}$ was almost certainly insufficient to produce 'clean' spectra. This report was however the first to discuss optical emission in the vacuum ultraviolet region (less than ~1500 Å). In particular a host of oxygen lines from 83 KeV 0^{+} backscattered from Ta were detected.

Medium energy Xe^{+} bombardment of 40 KeV to 50 KeV was used by *Jensen and Veje (1974)* to study Li, Be, B, C, Mg, Al, Ti, Zn, Cu, Sn, Ag, Cd, Tl, Au and Bi. The wavelength region covered was 2000 Å to 6000 Å under a vacuum of 10^{-6} Torr.and a primary ion current of 10 $\mu A\ cm^{-2}$. These conditions were also insufficient to ensure a clean surface during bombardment and CH band emission was evident in their spectra. The authors also detected molecular radiation from Mg at 4900 Å to 5200 Å attributable to the MgO Green System (*Pearce and Gaydon 1965)*. BeH molecular emission was also detected.

Certain metallic targets emit a broad band continuum extending from 2000 to 8000 Å, the origin of which is not fully understood as yet. It has been studied by several researchers, *(White et al 1976, Kerkdijk and Kelly 1976, Kiyan et al 1976)* and a popular theory is that the radiation arises from the radiative decay of sputtered excited clusters which are created as a result of collision processes occuring in the near surface region.

In addition to radiation from excited states of sputtered surface atoms, continuum radiation from ion bombarded insulators can be produced by another mechanism. In the case of low-Z projectiles incident on an insulator, 5 KeV He on Ca F_2 for example, *(White et al)*, a strong continuum is produced from inside the target from radiative

recombination of electrons with the self-trapped ν_K centre (the F_2^- molecule) of the CaF_2 crystal. The ν_K centre is produced by inelastic energy transfer of the projectile energy to bound electrons in the solid. Radiative recombination of the self-trapped hole and mobile electrons then gives rise to a strong broad band continuum. The continuum is reduced significantly when high Z particle bombardment of the same energy is used. This, the authors suggest, is evidence in favour of the model since the dominant energy-loss mechanism for a high Z projectile is due to elastic or nuclear collisions and not inelastic collisions.

2.5.2.1 ION INDUCED PHOTON EMISSION COMPARED WITH ALTERNATIVE EXCITATION PROCESSES

The previous section has discussed the general characteristics of ion-induced photon emission. It is the purpose of this section to briefly compare ion induced photon emission with alternative methods of exciting optical emission.

2.5.2.1.1 COMPARISON WITH ARC EXCITATION

The degree to which the photon emission from ion bombarded Zn and Cu corresponds to an arc excitation has been discussed by *Gabla, Szymónski and Szulkin (1974, 1976)*. Both polarisation and intensity ratio measurements were made on a number of emission lines from single and polycrystalline targets. Crystal structure was found to have a negligible effect on the polarisation measurements and the emission was found to be unpolarised within the limits of experimental error. Emission from the primary ion has also been found to be unpolarised (*Kerkdijk and Thomas 1973)*. Measurements on the intensity ratios of the ZnI triplet ($^3S_1$ - $^3P_{012}$) indicated that the intensities

of long-wave components of the triplet were damped more strongly than short-wave components compared to the arc-excitation data. The emission is also free from self-absorption because of the low vapour density of the sputtered atoms ~ 10^{-7} Torr. and can also be considered to correspond to the low energy region of beam foil spectroscopy.

2.5.2.1.2 BEAM FOIL EXCITATION

Beam foil spectroscopy has gradually developed into a standard technique for measuring lifetimes of excited states and a method of producing lines not previously observed in the laboratory (*Martinson 1973*). The basic technique is to bombard a thin foil (10 μg cm^{-2}) with ions of energies of several hundred kilovolts. Decay from the excited levels then occurs downstream from the foil according to -

$I(x) = I(o) \exp(-x/v\tau)$ where I(o) is the initial intensity of the particle transition, I(x) the intensity at a distance x from the foil, v the particle velocity and τ the mean lifetime of the decaying level. Corrections must be made for transitions influenced by cascade repopulation (population of the level under study from high excited states decaying to that level). If a velocity filter is used to measure the velocity of the emitters the lifetime can be estimated by measuring the intensity of an emission line as a function of the distance x from the foil. *Anderson, Jensen and Sorensen (1969)* have studied beam foil excited AlI, II and III spectra using 100 and 300 KeV Al^{+} beams and 2-4 μg cm^{-2} carbon exciter foils. It was found that at 100 KeV strong emission from the neutral atoms could be detected much the same as in beam solid studies. However, at 300 KeV the neutral emission virtually disappeared leaving only the AlII and III spectra in the

wavelength region investigated (1700 - 5000 Å). The main difference between beam foil and beam solid interaction is the velocity distribution of the emitters which, as discussed in section 2.5.3, is not well defined for the latter case.

2.5.2.1.3 LASER EXCITATION

Ion induced optical emission has been compared to that produced by high energy laser impact on solid targets (*Jensen and Veje 1974*). When a strong (~ 5J) laser beam is fired onto a solid surface a plume of luminous plasma is formed. The luminous plume expands away from the target surface with velocities up to 10^7 cm sec^{-1}. Spectral analysis of the laser produced plume has revealed continuum and line radiation, (*Boland, Irons and McWhirter 1968*). The electron temperature of the plasma produced by a 5J laser on a polyethylene target has also been estimated to be ~2 to 12 eV. The major part of the excitation has been demonstrated by *Boland et al* to take place in the plasma and not when the particles are emitted from the solid. There is very little information in the literature of the optical emission from laser impact on metal targets to compare with ion bombardment results. The laser microprobe has however, developed into a sensitive microprobe technique when used in conjunction with spark excitation (*Andersen 1973, page 423*).

2.5.2.1.4 ELECTRON INDUCED OPTICAL EMISSION

Charge particle interaction with a metal surface can give rise to photon emission through the so called plasmon excitation mechanism first predicted theoretically by *Ferrell (1958)*. The electron 'gas' in a metal is able to undergo plasma oscillations. All the conduction electrons participate collectively in these oscillations which arise from the inertia of the electrons and their

repulsive Coulomb interaction. The oscillations manifest themselves as discrete energy losses in fast electron beams (20 KeV) which pass through thin metal foils. Ferrell considered the possibility that these oscillations might give off detectable radiation with a wavelength characteristic of the plasma frequency -

$\lambda_p = 2\pi c/\omega_p$ where λ_p is the plasma wavelength and ω_p the plasma frequency. Plasma radiation was detected by *Steinmann (1960)* from Ag films bombarded with 25 KeV electrons at a wavelength of 3300 Å or in energy terms 3.75 eV. Since the first measurements of plasmon radiation were made by Steinmann both surface and volume plasmon radiation has been reported in the literature (*Braundmeir and Arakawa, 1970)*.

A second type of radiation produced by electrons at a metal surface is the transition radiation reported by *Boersch, Radeloff and Sauerbrey (1961)*. The radiation is produced when an electron approaches the boundary between vacuo and metal surface. A changing dipole field due to the electron and image charge is produced which results in the emission of electromagnetic radiation. The radiation is found to be a continuum extending from 2500 Å to 6000 Å for Ta, W, Mo and Ti. The essential difference between transition and plasma radiation is that the former only appears on foils with two boundary surfaces and the latter is observed on metals with a single boundary surface.

Plasma and transition radiation are examples of two other possible sources of electromagnetic radiation occuring in the ultraviolet to visible region of the spectrum which arises as a consequence of charge particle-solid interaction. The radiation comes from the solid whereas the ion-induced optical emission comes from particles de-exciting in front of the solid surface free from its influence

and therefore comprised of sharp emission lines. The following sections will discuss the characteristics of the ion induced emission and where appropriate correlation will be made with other secondary emission processes.

2.5.3. THE VELOCITY DISTRIBUTION AND KINETIC ENERGY OF THE EMITTING PARTICLES

A study of the production of excited atoms sputtered from polycrystalline and monocrystalline Cu targets was made by *Fluit, Friedman, Vaneck, Snoek and Kistemaker (1961)*. The targets were bombarded by Ne^+, Ar^+ and Cu^+ ions of 15 KeV energy and the wavelength region of 2000-6000 Å was investigated. The authors attempted to measure secondary metastable particles by recording electron emission from a copper collector plate. The yield of photons from the copper resonance line (λ = 3257 Å, $4^2S_{1/2} - 5^2P_{3/2}$), was measured to be 4×10^{-7} per sputtered atom in 0.1 steradian. The total photon yield was estimated to be 7×10^{-5} photons per sputtered copper atom and the secondary metastable particle yield was measured to be 3×10^{-2}. A rough energy measurement gave a value of 11 eV for the energy peak of the Cu metastable atoms, that is a velocity of 10^6 cm sec^{-1}. The metastable Cu $^4F^o_{4/2}$ level of 5.0 eV was assumed to be responsible for 3 per cent of the metastables among the total number of sputtered Cu atoms. These results are however in doubt since the experiment was repeated by *Kistemaker and Snoek (1962)* using an improved secondary metastable particle detector. The metastable energy value was re-measured and found to be of the order of several KeV.

Estimates of the velocity of the emitters ejected from a Cu target by a 60 KeV Ar^+ beam were also made by *Snoek, Van der Weg*

and Rol (1964). Snoek et al measured the velocity of the particles by two techniques -

(1) The line profile of the CuI resonance line was measured and the velocity estimated from the line broadening due to Doppler shift. The experimental arrangement used is shown in Fig 2.3A. The high frequency side of the spectral line was found to be broadened by several angstroms corresponding to a velocity towards the monochromator of a few times 10^7 cm sec^{-1}, that is, an energy of approximately 10 KeV.

(2) The second method used to measure the mean velocity in the direction perpendicular to the target surface, was to determine the thickness of the light emitting layer. The target position was kept constant with respect to the beam and the monochromator was rotated close to the plane of the target surface. The result obtained by moving the monochromator from just in front of the plane through the target surface to just behind it (between ϕ_1 and ϕ_2 of Fig 2.3A) is shown in Fig 2.3B. The distance from the surface at which the intensity had dropped to e^{-1} of the intensity in front of the target was estimated to be 0.25 to 0.35 mm. Assuming a mean lifetime of a Cu atom in the resonance level to be 0.5×10^{-8} sec the authors arrived at a value of 0.6×10^7 cm sec^{-1} for the mean velocity of Cu atoms in a direction normal to the target surface. The results of Snoek et al indicate that the emitting Cu atoms have velocities of the order of 10^7 cm sec^{-1} corresponding to energies in the kilovolt region.

The fact that the greatest part of the line emission originates from particles with an energy in excess of 100 eV was later confirmed by *Van der Weg and Bierman (1969)* who again studied

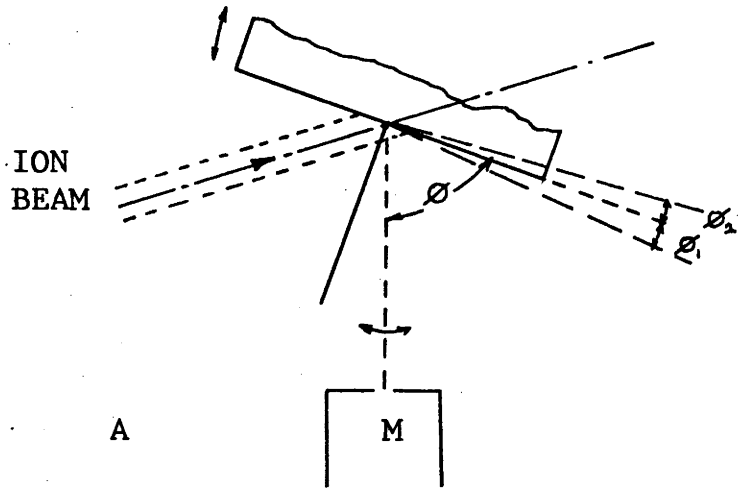

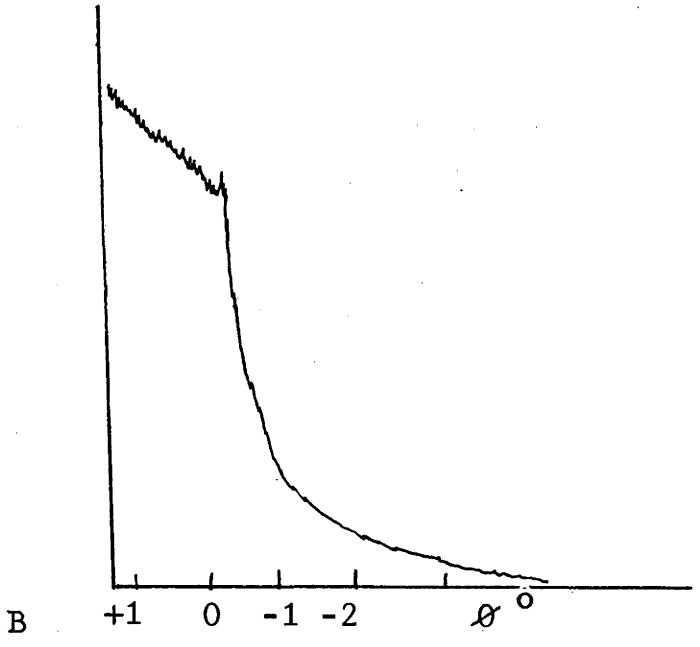

FIG 2.3 THE VELOCITY OF LIGHT EMITTING PARTICLES FROM Cu (SNOEK et al 1964)

A. GEOMETRICAL ARRANGEMENT

B. INTENSITY OF THE 3247 CuI LINE AS A FUNCTION OF Ø FOR SMALL VALUES OF Ø (ONE DEGREE IN Ø CORRESPONDS TO A DISTANCE OF 0.52 MM FROM THE SURFACE)

the Ar^+ - Cu system. The Doppler shift of the 3247 Å CuI resonance line and its full width at half maximum (F.W.H.M.) were measured as a function of the target orientation α. The results obtained for 80 KeV Ar^+ and a detection angle of $\beta = 60^o$ are shown in Fig 2.4A. These results were interpreted in terms of singly scattered particles. For a small value of α, more Cu particles were assumed to be scattered with a sufficient energy to leave the target. These particles were thought to contribute to the low wavelength part of the emission line causing the centre of gravity of the line profile to shift to lower wavelengths. A similar interpretation was put on the increase in width with decreasing α.

Terzic and Perovic (1970) proposed a model of excited particle generation based on the approximation of binary collisions of energetic ions and surface atoms. The total probability of excited particle emission per incident ion was assumed to depend on the excitation cross section, the transition rate of non-radiative processes and also the surface concentration of the target atoms. The expression that was obtained was not evaluated because of the difficulty in assessing the differential cross section and the transition rate. However, a similar approach was used by *Van der Weg and Bierman (1969)*, to calculate the line profile arising from the velocity distribution of light emitting scattered particles. The expression obtained for the number of particles contributing to the radiation with a wavelength $\lambda + \Delta\lambda$ was given as -

$$N(\lambda + \Delta\lambda)\, d\lambda = \iiint [P_{exc}(\phi)\,]\,[\sigma(\phi)\,]\,[R(\phi,\alpha)\,]\left[\delta\left(\frac{V\beta}{C} - \frac{\Delta\lambda}{\lambda}\right)\right] \times 2\pi \sin\phi\, d\phi\, d\gamma\, d\lambda$$

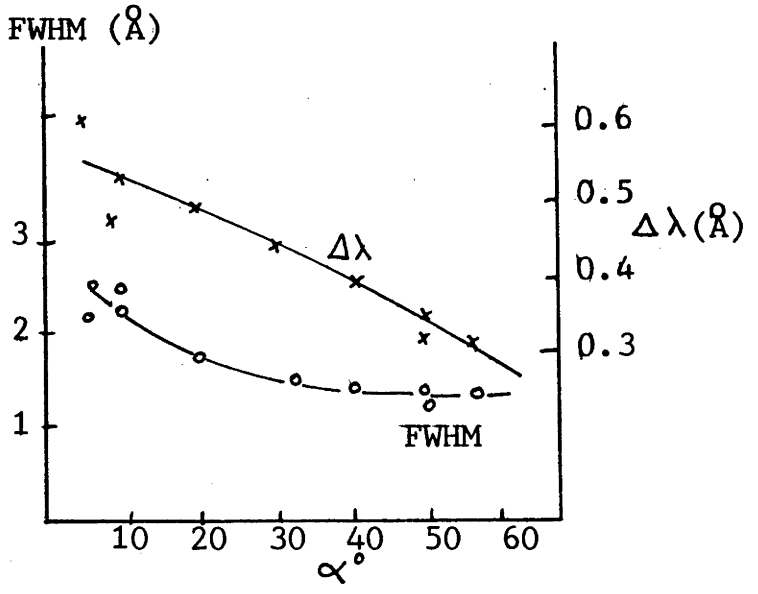

FIG 2.4A WAVELENGTH SHIFT OF THE TOP (Δλ) AND FWHM OF THE LINE PROFILE OF Cu 3247 Å

(VAN DER WEG et al 1965)

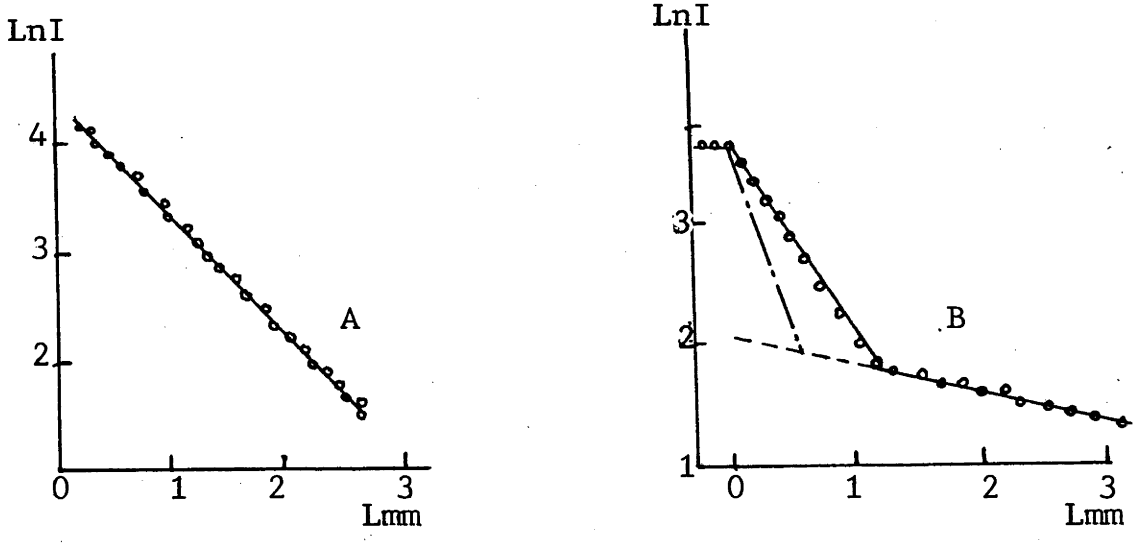

FIG 2.4B LOG I VS l PLOTS FOR A. Cu AND B. Al

(GRITSYNA et al)

where $P_{exc}(\phi)$ is the probability for excitation to a particular level. $\sigma(\phi)$ is the differential cross section and $R(\phi,\alpha)$ the transition rate for radiationless de-excitation. The original wavelength is λ and the δ function denotes the condition for Doppler shift over $\Delta\lambda$. The authors assumed that P_{exc} was a function of $\cos\phi$ and $\sigma(\phi) \propto \cos^{-2}\phi$. The survival coefficient which appears in the expression for $R(\phi,\alpha)$ was varied, and reasonable agreement between the measured and calculated line profiles was obtained by setting $A/a = 2.10^4$ m sec^{-1}.

The model of *Van der Weg and Bierman* has also been used by *Hippler, Krüger, Scharmann and Schartner (1976)*, to predict the line shape of atomic transitions of excited Cu, Zn and Al atoms sputtered from polycrystalline metal and surface coated Zn and Al by the bombardment of 300 KeV Ar^+ ions. The large widths of the measured profiles indicated high velocity emitters, with energies as high as 6 KeV in the case of Al. Only a limited agreement between the measured and calculated line profiles was found in the case of the Cu and Zn targets but a somewhat better agreement for the surface coated Zn. The survival coefficient was found to be 3.10^6 for Cu, 5.10^6 for Zn, 5.10^4 for ZnO and 5.10^5 cm sec^{-1} for Al. These values were found for emission lines above the Fermi level. For those measured below, the coefficient was found to be one order of magnitude smaller. The lack of agreement between these results and those of Van der Weg and Bierman was attributed to the different position of the monochromator in both experiments. In the experiments of *Hippler et al* there was thought to be a greater contribution to the line profile from multiple (rather than single collisions), to the tail of the distribution of excited particles.

A slightly different technique has been used by the Russian group led by Gritsyna to measure the velocity distribution of the excited particles (*Gritsyna et al 1968, 1971, 1972, 1976*). The emission from the ion bombarded solid was focussed into a three prism spectrograph and the analysed light photographically recorded in the region 4000 to 7500 Å. The velocity of the excited particles was obtained by positioning the target so that the radiation from the excited particles entered the spectrograph in a direction perpendicular to the plane formed by the axis of the primary beam and target normal. The height L of the spectral line then characterises the distance travelled by the emitting particles. The authors considered that if the excited particles had a particular velocity, the maximum velocity V max was given by -

$L = V_{max} \tau$ where τ is the lifetime of the excited state of the transition. When two velocity groups are present (fast and slow) the spectral line is photometrically scanned along its height to determine the intensity as a function of l. This function I(l) is proportional to the number of excited atoms N emitting photons at a distance l above the target surface. Also N decreases through spontaneous emission of the excited particles according to -

$N = N_o \exp(-l/V\tau)$, therefore $I = K \exp(-l/\bar{V}\tau)$ where $\bar{V}$ is the effective velocity. A plot of In(I) versus l should then yield a straight line of slope proportional to $\bar{V}$. If two velocity groups are present two straight line segments of different slopes result.

Using this method the authors have studied the velocity distributions of the excited particles emitted from a wide variety of

targets. Typical results for 20 KeV Ar^+ on Cu and Al_2O_3 are shown in Fig 2.4B. The effective velocity of copper atoms was found to be 10^7 cm sec^{-1} (~3 KeV). In the case of the Al_2O_3 target (sapphire), the plots gave a value of 3×10^7 cm sec^{-1} (12 KeV) for λ = 6696 Å. In the case of λ = 3961 Å the ^2S energy level of the transition lies opposite the forbidden band of the target thereby allowing slower particles to escape and decay by photon emission. A value was obtained for both the fast and slow atoms of $2.4.10^7$ cm sec^{-1} (7.8 KeV) and 2.10^6 cm sec^{-1} (54 eV) respectively.

The authors have used this technique to determine the position of energy levels in the solid target by observing the radiation of particles ejected by the ion beam. In the case of Ti the value of the work function was estimated to lie between 3.8 and 4.15 eV, within the range of values obtained by other methods. The conduction band width of NaCl and LiF was estimated to be $\chi \geq 1.019$ eV and $\chi \leq 0.381$ eV respectively (*Gritsyna, Kijan, Koval, Fogel, 1972*).

The method employed by Gritsyna et al has received some attention from *Braun, Emmoth and Martinson (1974)*. The authors measured decay curves (photon intensity as a function of distance away from the target surface) for the 3962 Å (AlI), 3092 Å (AlI), 3587 Å (AlII) and 3602 Å (AlIII) lines emitted from Al under 300 KeV Xe^+ bombardment. These were compared with beam foil measurements using 200 KeV Al^+ ions. The results are shown in Fig 2.5. The curves from the beam foil experiment were fitted to one or two exponentials and values of the 3962Å (AlI), 3092 Å (AlI) and 3587 Å (AlII) lifetimes were extracted. In the "backsputtered" decay curves however, the exponential fitting method did not yield straight lines. The decay curves were simulated by assuming an E^{-2} dependence for the velocity

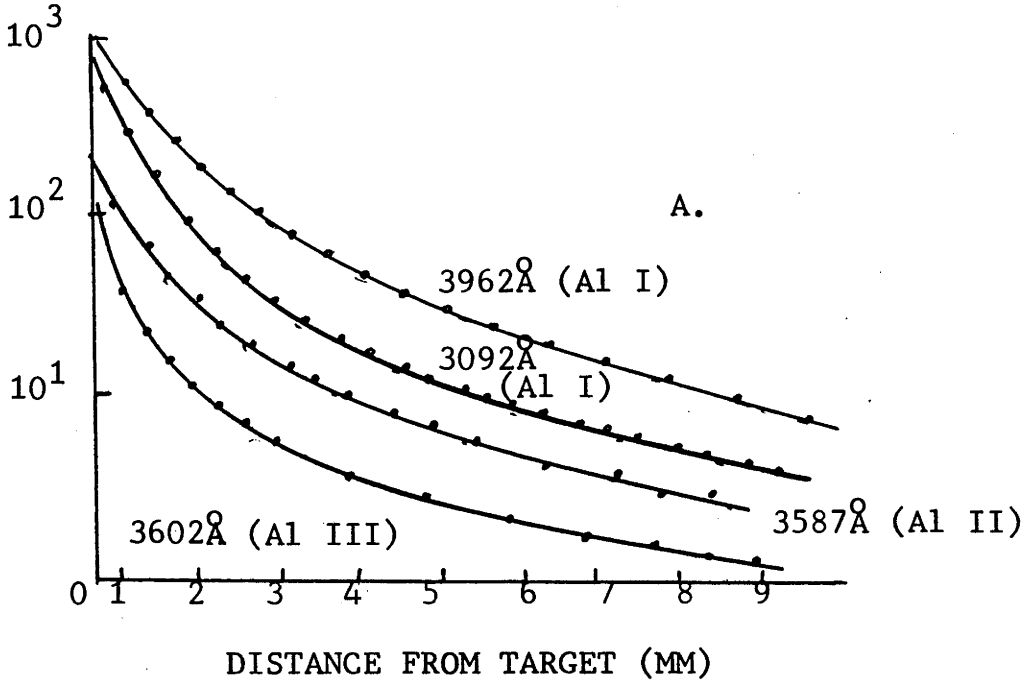

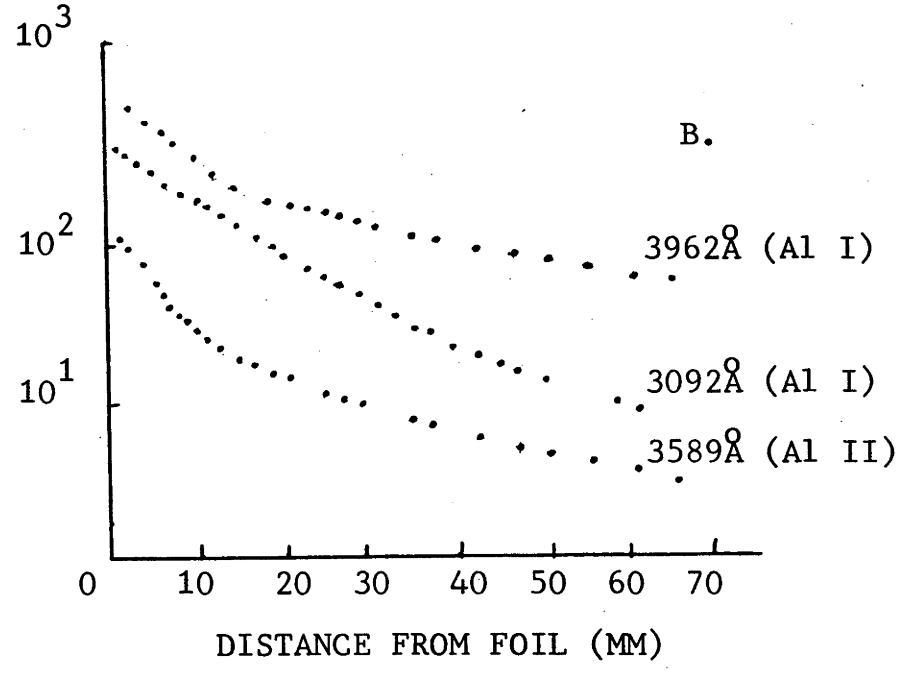

FIG 2.5 DECAY CURVES FOR AlI - AlIII TRANSITIONS.

A. BACKSPUTTERED

B. FOIL EXCITED

(BRAUN et al 1974)

distribution as found for Au by *Thompson et al (1968)*.(Fig 1.1A). The values obtained for the lifetimes in the beam foil measurements were used to estimate a mean velocity for the sputtered particles. The results are given in Table 2.3.

TABLE 2.3

	λÅ	τns	Level	v(x 10^6 cm sec^{-1})
Al I	3092	13.7	$3d^2D$	5.0
Al I	3962	6.4	$4s^2S$	9.0
Al II	3587	4.6	$4f^3F^o$	15.0
Al III	3602	4.6	$4p^2P^o$	16.0

These results are slightly different from those obtained by others but the authors stress that the tails of the distributions correspond to values 5 - 10 times those given in Table 2.3. Factors which the authors considered might influence the measurement of the velocity distribution of sputtered radiating atoms were the excitation probabilities, radiative lifetimes, cascade processes, radiationless de-excitation, velocity and angular distributions of the excited particles and geometry of the detection system.

The Gritsyna technique has been criticised by *Jensen and Veje (1974)*, in that the velocity spectrum of sputtered species does not exhibit distinct velocity groups and that the effect of cascades on the emission intensity changes the log I versus 1 plot quite markedly. However, *Kiyan et al (1976)* have studied Ca under 30 KeV Ar^+ bombardment under an oxygen partial pressure of 2 x 10^7 Torr. and again under 10^{-3} Torr. of nitrogen using the Gritsyna technique, correcting for populations of excited levels by cascade transitions. The one electron and two electron excited levels of Ca were investigated and interpreted in terms of the

electron exchange mechanism. A value of several KeV and ~ 100 eV was obtained for the effective energy of calcium atoms in a residual gas environment using emission of the lines singlet and triplet system of the one electron excited calcium atom. A value as high as 16 KeV was reported for the 4108 CaI emission line. In the case of two-electron excitation from an oxygenated and clean surface, values of KeV energy were obtained in all cases and no contribution from slow sputtered particles was detected as in the one electron excitation. This was explained as being due to the sputtering process transferring insufficient energy to the ejected calcium atoms to excite them to a state of two electron excitation. This degree of excitation was considered to be only energetically possible through binary collisions between incident ions and target atoms. The values obtained from the two electron excitation measurements are given in Table 2.4.

TABLE 2.4

λ (Å)	Transition	Energy of Ca atoms (KeV)	
		Oxygenated	Clean
5349	$3d4p\,^1F_3^o - 4s3d\,^1D_2$	1.4	1.5
5857	$4p^2\,^1D_2 - 4s4p\,^1P^o_1$	1.4	15.0
4318	$4p^2\,^3P_1 - 4s4p\,^3P^o_2$	3.6	16.0
4289	$4p^2\,^3P_1 - 4s4p\,^3P^o_o$	3.8	20.0
4283	$4p^2\,^3P_2 - 4s4p\,^3P^o_1$	2.6	20.0

2.5.3.1 COMPARISON OF THE ESTIMATED ENERGIES OF EXCITED PARTICLES AND THE ENERGY DISTRIBUTION OF SPUTTERED IONS AND ATOMS

The results of most of the studies reviewed in section 2.5.3 have indicated that the excited atoms which give rise to photon emission have energies greater than about 100 eV. According to theoretical

models of the ion induced atomic collision cascades in a sputtering target, the energy distributions Na(E) of sputtered atoms measured in a direction perpendicular to the target surface have been found to obey the relation -

$$\frac{Na(E)}{Na(Ew)} = \frac{27}{4} \frac{E/Uo}{(1 + E/Uo)^3}$$ *(Bernhardt, Oechsner and Stumpe 1976).*

where Ew is the most probable ejection energy and Uo the surface binding energy. The peak of the distribution occurs where Ew = Uo/2. A typical value for the sublimation energy is 3.1 eV (Ag) and the experimental distribution has been found to peak around 2.5 eV for 1 KeV Ar^+ ion bombardment (*Bernhardt et al 1976*). The authors used post-ionisation to study the sputtered atom energy distribution. The intrinsic secondary ion yields also peak at low energies and an example of the Cu^+ energy spectrum can be seen in Fig 1.1B.

Doppler shift measurements indicate that the particles have velocities of the order of 10^6 - 10^7 cm sec^{-1} that is energies of about 450 eV (for Cu). The measurements of Gritsyna et al indicate two velocity groups, one corresponding to several KeV and the other to some tens of eV. The presence of the lower velocity particles is dependent upon the relative position of the excited levels of the isolated atom and the band structure of the solid target. The evidence is therefore in reasonable agreement that the excited particles are predominantly of higher energy than the peak of the sputtered atom or ion energy distribution. Sputtered atoms would appear to influence the emission only when the energy level arrangement if favourable. This point is quite clearly shown by the results of *White, Simms, Tolk and McCaughan (1975)*, who measured the line profile of the SiI 2882 Å emission

line from Si and SiO_2 under 80 KeV Ar^+ bombardment. Substantial differences were obtained for the line width from the two different materials. From SiO_2 the line width was found to be of the order of the limit of the monochromator resolution (~ 1Å). Under identical conditions the line width was found to be ~ 5 Å from a clean Si substrate. The relative intensity was also reduced by a factor of ~50. This result suggested that Si atoms radiating from a clean substrate have higher velocities leading to a greater Doppler shift and broadening than the SiO_2 case. The broadened line from Si is a result of the monochromator integrating over the angular distribution of the moving atoms. In the case of SiO_2 the energy conditions are favourable for the blocking of any non-radiative processes, thereby enabling lower velocity Si atoms to radiate.

There is some evidence in the literature that significant numbers of high energy excited particles are produced in biparticle collisions. *Datz and Snoek (1963)* have measured the energy and angular distribution of secondary ions produced by 40-80 KeV Ar^+ ions incident on Cu, Ag and Au. The detected particles were multiple charged species of both the projectile atoms (Ar^+ to Ar^{6+}) and the target atoms (1+ to 5+). *Jurela and Perovic' (1967)* detected secondary ions from polycrystalline Al, Mn, Co and Ta under 40 KeV Ar^+ bombardment and target ions were found to have energies extending to the KeV region. *Reid, Farmery and Thompson (1976)*, have studied the energy spectra of neutrals sputtered from polycrystalline gold samples by 20 KeV Ar^+ ions at 45° incidence. Analysis was performed at various recoil angles using the time-of-flight technique (*Thompson, 1968*). The results are shown in Fig 2.6. The dotted curves are distributions taken at recoil angles $\theta < 90^\circ$

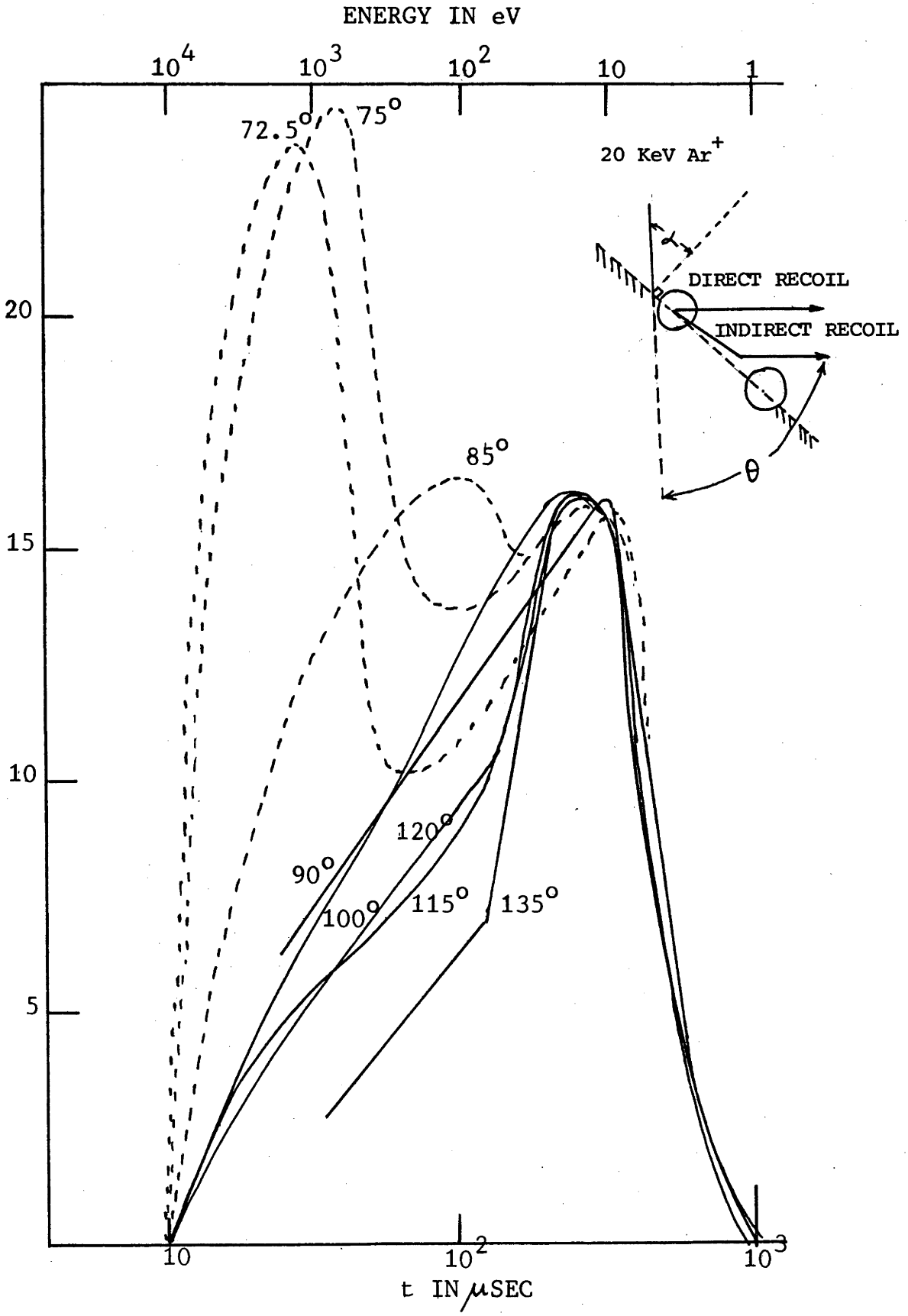

FIG 2.6 THE VARIATION OF THE TIME-OF-FLIGHT NEUTRAL SPECTRUM WITH RECOIL ANGLE FOR 20 KeV Ar^+ ON Au AT 45° INCIDENCE (REID et al 1976)

(where θ is defined in Fig 2.6), and solid lines represent values of $\theta \geq 90^{o}$. The results indicate a transition in the distribution occuring at $\theta = 90^{o}$. The energy distribution for all values of θ shows a low energy peak at 15 ± 5 eV which can be attributed to the random cascade. For $\theta < 90^{o}$ a high energy peak is evident and can be interpreted in terms of direct and deflected recoils.

2.5.4 THE ENERGY DEPENDENCE OF THE PHOTON YIELD

The photon and secondary electron emission dependence upon ion energy has been determined for cesium bombardment of Al, Cu, Ag and stainless steel by *Martel and Olson (1972)*. The energy range 0 to 20 KeV was covered using current densities of 10 to 20 μa cm^{-2} and residual gas pressures of ~ 10^{-8} Torr. The photon and secondary electron emission were found to rise rapidly in intensity over the 0 to 10 KeV range, after which both signals saturated. Their results were interpreted using the *Firsov (1959)* expression for inelastic energy transfer in ion-atom collisions -

$$\xi = \frac{(Za + Zb)^{5/3}.4.3.10^{-8}\ u}{[1 + 3.1(Za + Zb)^{1/3}.10^{7}\ Ro]^{5}}$$

where Za and Zb are the nuclear charges of the colliding particles, Ro the impact parameter and u the velocity of the incident ion. This expression indicates that the inelastic energy loss increases with primary ion energy. The inelastic cross section also given by Firsov is -

$$\frac{\sigma}{\sigma_{o}} = \left[\left(\frac{E}{E_{o}} \right)^{1/10} - 1 \right]^{2}$$

which, combined with the inelastic energy transfer function may account for an initial rise in the photon and secondary electron emission. The eventual saturation of the photon yield, an example

of which is given in Fig 2.7, is explained on a less convincing basis. It was assumed that the optical emission was produced inside the bombarded target by excited atoms. As the primary ion energy increases, the ions penetrate further into the target. It was proposed that the emitted radiation would therefore have further to travel as the primary ion energy was increased and consequently lead to self-absorption of the photon emission at a sufficiently high penetration depth. The preceding section 2.5.3 has shown that the photons are predominantly emitted by high energy particles produced through biparticle collisions, and not from the target itself. A more plausible explanation for the apparent saturation of the optical signals observed by Martel and Olson, is the behaviour of the sputtering ratio S (number of sputtered atoms per incident ion) over the energy range considered. A saturation of S does occur at approximately 10 KeV for Ar^+ on Cu and the variation of S for Xe^+ and Kr^+ over the 0-20 KeV range is also very similar to the photon data (*Almen and Bruce 1961*).

The production of optical radiation over the low energy region 10 to 3000 eV has been investigated by *White and Tolk (1971)* using beams of H_2^+, He^+, Ne^+, N_2^+ and Ar^+ on Cu, Ni, Si, C and Ge. The relative emission functions (photons detected per incident ion) were determined for a number of emission lines. It was found that a completely undefined threshold existed and that the photon yield gradually increased with beam energy. Examples of their data are given in Fig 2.8. In the case of N_2^+ on Ni and Cu an exceptionally conspicuous behaviour was observed. The general emission function for Ar^+ bombardment of Ni, Cu and Si, was approximated by the equation -

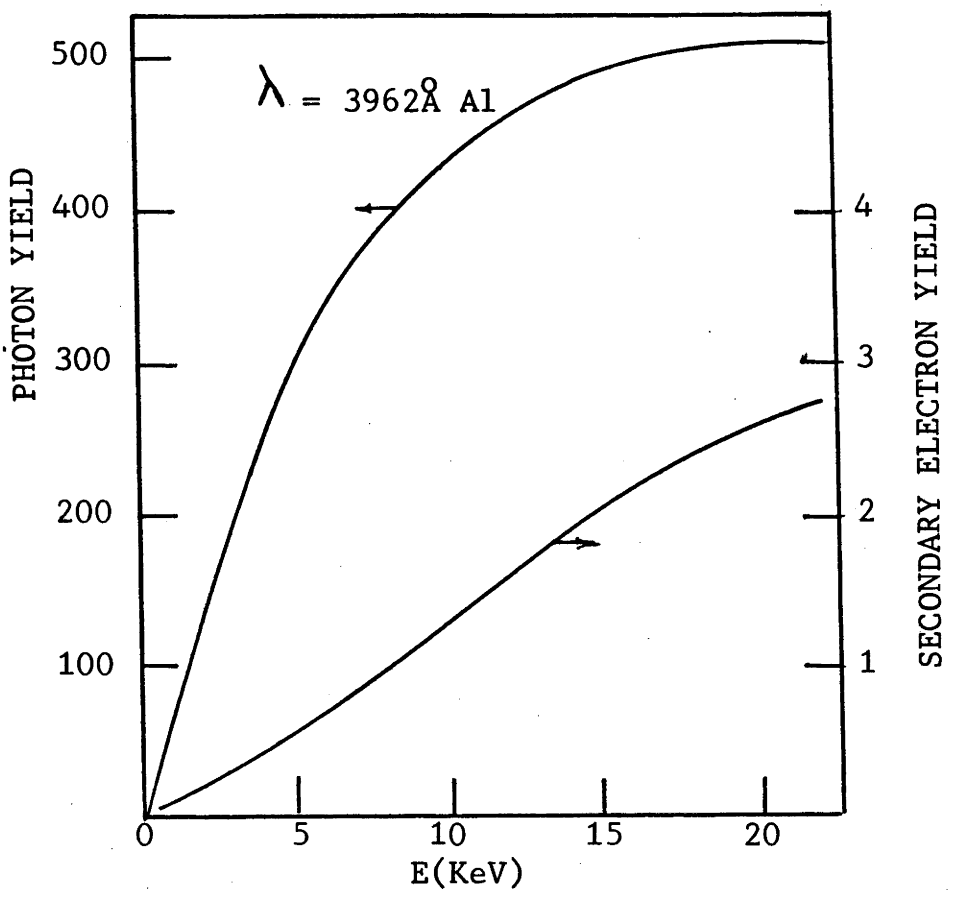

A. Cs BOMBARDMENT OF Al

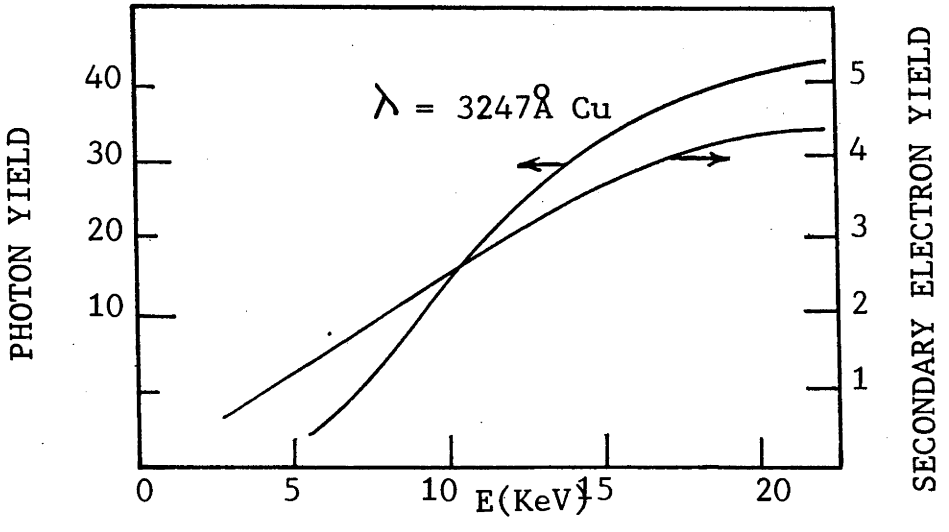

B. Cs BOMBARDMENT OF Cu

FIG 2.7 ENERGY DEPENDENCE OF THE SECONDARY ELECTRON AND PHOTON YIELDS (MARTEL AND OLSON 1972)

$$F(E_o) = k\eta(E_o) \int_0^{v \text{ max } (E_o)} f(v\,1)\, R(v\,1)\, dv\,1$$

where k is a geometrical constant, η (E_o) the excited state excitation efficiency, f(v 1) the perpendicular velocity distribution of excited sputtered atoms and R the survival probability. The latter is given by R = exp - A/a v 1 and has been discussed in section 2.3. The value of f(v 1) was approximated to exp - cv 1, where C is a constant taken from the data of *Stuart, Wehner and Anderson (1969)* to be ~ 2.5. 10^{-6} sec cm^{-1}. This approximation assumed that sputtered excited neutrals had the same perpendicular velocity distribution as the total of all excited and ground-state neutrals of a given species. Further, the quantity C is also assumed independent of the incident ion energy. The upper limit of the integral v max, was determined from simple biparticle collision theory and is the maximum perpendicular velocity component of the sputtered atoms. Using a value of 2.10^6 cm sec^{-1} for the survival coefficient A/a, a reasonable agreement was found between the calculated and experimental excitation functions. The result for the CuI 3247 Å emission line is shown in Fig 2.8A. The discrepancy in the low energy region was attributed to a non-uniform, excited-state excitation efficiency which was presumed to occur in the region where elastic collisions are no longer valid. No attempt was made to interpret the anomalous behaviour of the N_2^+ emission functions. However, reactive ion bombardment of solids is known to have a marked effect on the secondary ion yield and also the photon yield. These aspects are discussed in section 2.5.7.

2.5.5 ANGULAR DISTRIBUTION OF PHOTON EMISSION

The spatial distribution of photon emission during alkali ion bombardment of chromium has been studied by *Kerkow (1972)*.

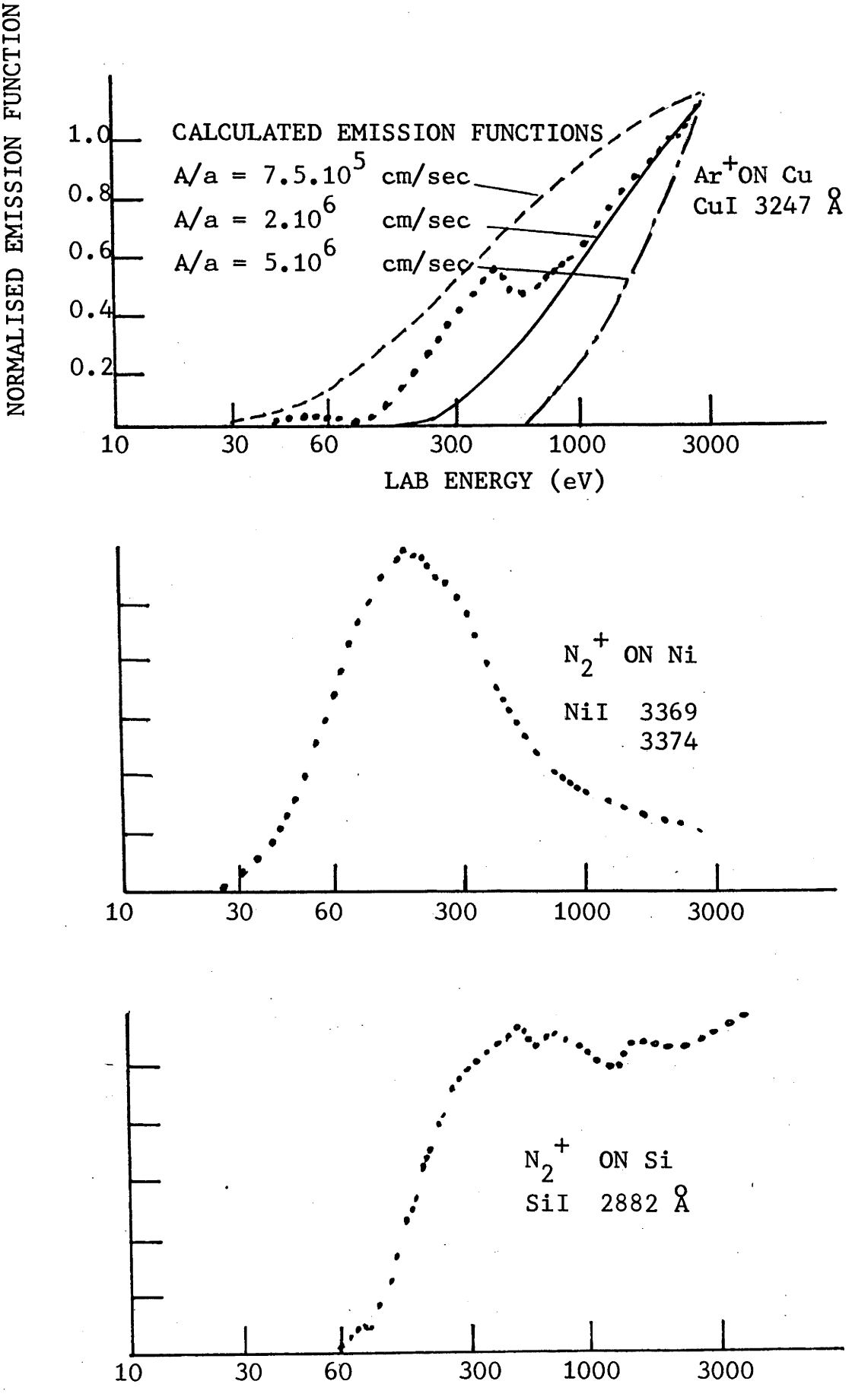

FIG 2.8 EMISSION FUNCTIONS FOR OPTICAL LINES PRODUCED IN ION-SURFACE COLLISIONS (TOLK et al 1973)

The energy range 2 to 10 KeV was covered and the experiments were conducted on polycrystalline materials in a vacuum of 5.10^{-6} Torr. The experimental results were interpreted using a model based on the following approximations. The target atoms were assumed to be excited by the primary ions in the first atomic layers and the energy transfer (inelastic energy loss) was governed by Firsov equation. The excited atoms were assumed to possess impulse components along the target normal and further, that excited and emitted atoms recombine without emitting radiation outside the target surface. Using these assumptions the following model was proposed.

The fraction dN_o^+ of N target atoms subjected to collision which reached the solid angle $d\Omega$ with the angle of deflection θ is given by -

(i) $dN_o^+ = N \cos\theta d\Omega$ where $0 \leqq \theta \leqq 90^0$. With reference to Fig 2.9A, atoms which reach a deflection angleθ within the plane of incidence of more than $90^o-\alpha$ escape to the vacuum. Some of the excited atoms may recombine through radiationless de-excitation processes at the surface according to -

(ii) $\frac{d}{dt}(d N^+) = - R(x)\, d N^+$ where $R(x) = C \exp(- cx)$.

Here, x is the excited atom-target surface distance and C and c are constants which characterise the transitions involved. Integrating equation (ii) over t = o to t = ∞ ,

(iii) $dN = d N_o^+ \exp\left(\frac{-C}{c\, v\, 1}\right)$ and $v\, 1 = 2 \left(\frac{2M1\, E_o}{M1 + M2}\right)^{1/2} \cos\theta \cos\beta$

where the usual notation applies and θ and β are indicated in Fig 2.9A.

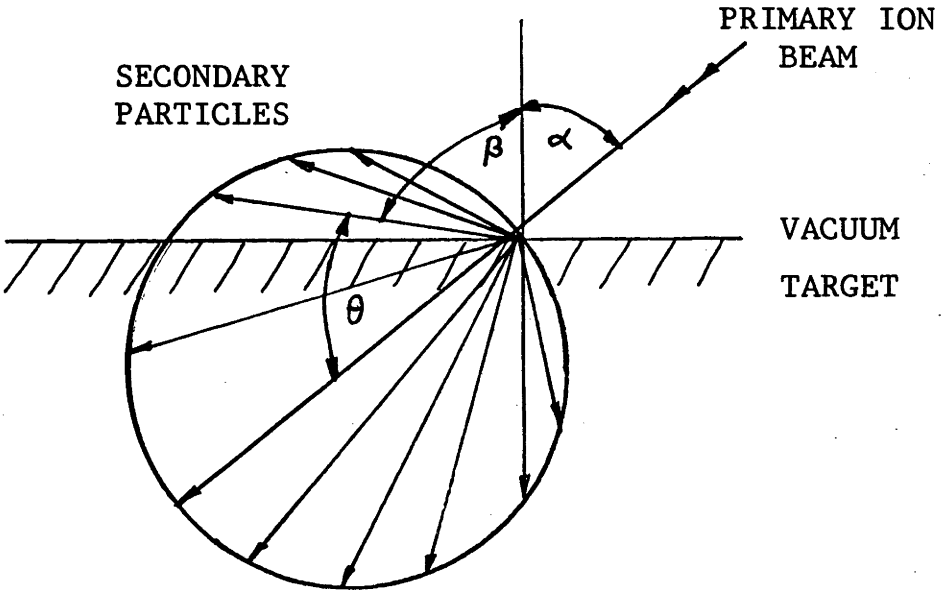

A. INTENSITY DISTRIBUTION OF STRUCK ATOMS AFTER THE FIRST COLLISION

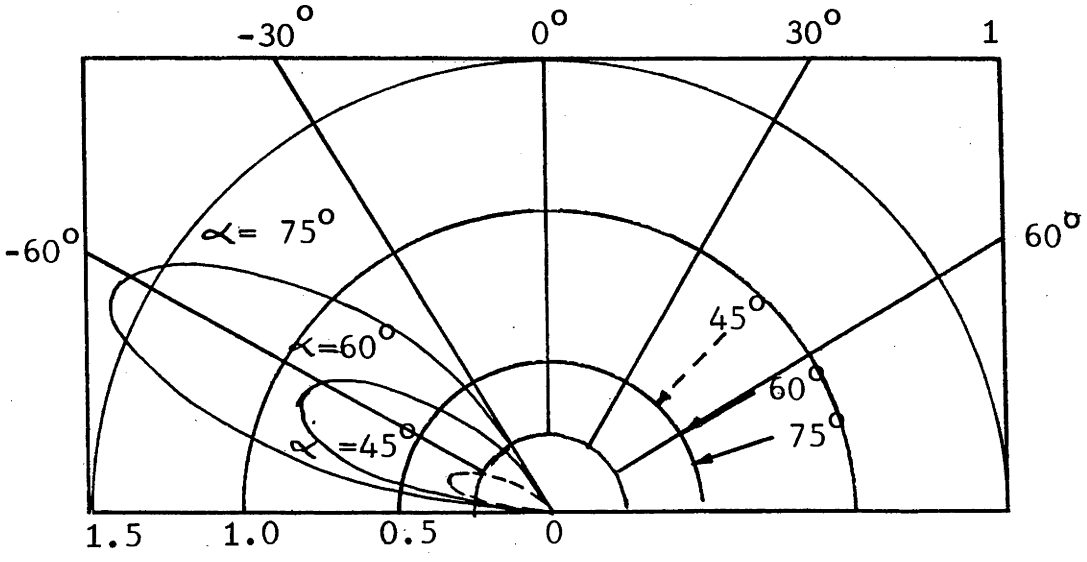

B. ANGULAR DISTRIBUTION OF EXCITED ATOMS

FIG 2.9 ANGULAR DISTRIBUTION OF PHOTON EMISSION (KERKOW 1972)

Substituting equations (i) and (ii) into (iii) -

$$dN = N \cos\theta \exp\left(\frac{-C}{c\, b \cos\theta \cos\beta}\right) \quad (b = (2M_1E_0)^{1/2}/(M1 + M2)\ ).$$

The results of the calculation of the angular distribution of the photon emission for $\alpha = 45^{o}$, 60^{o} and 75^{o} are shown in Fig 2.9B. In agreement with experimental results it was found that the spatial distribution was asymmetric with respect to the target normal. The extension of the emission grew with angle of incidence. The distribution was fairly independent of the projectile energy and mass and the preferred direction of emission was almost independent of the angle of incidence. An estimate of the energy of the emitters was also made by measuring the lateral distribution of photons emitted from 8 KeV Cs^{+} onto Cr (λ = 4348 Å) and found to be ~100 eV.

The angular distribution of the photon emission as determined by *Kerkow (1972)* can be compared to the angular distribution of sputtered neutrals (*Rodelsperger et al, 1974,* see Fig 1.2) and secondary ions. A recent study of the angular distribution of secondary ions has been made by *Kerkow and Trapp (1974)* and a typical result for a polycrystalline Cu target is shown in Fig 2.10. Distribution curves are plotted for 30 eV, 110 eV and Σ(0 - 500) eV secondary ions for incident angles of 45^{o} and 70^{o}. These curves, for 8 KeV Rb^{+} ions on Cu, also indicate that the preferred direction of emission is relatively independent of the angle of incidence; a growth of extension of emission with increasing angle of incidence and asymmetry of the spatial distribution about the target normal. Similar correlations are seen to exist for the case of the neutral particle ejection shown in Fig 1.2. The spatial distribution of photons from excited target particles and the distribution of

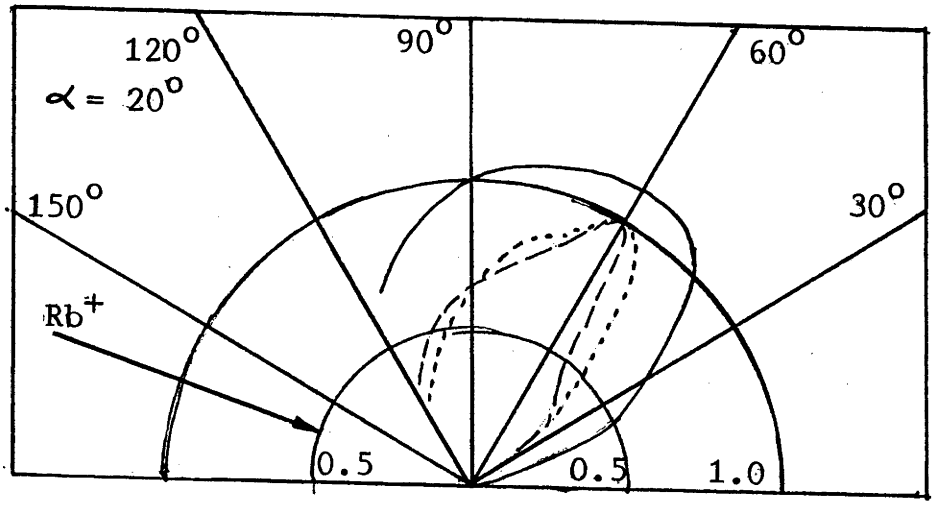

A

KEY

30 eV

110 eV

INTEG.

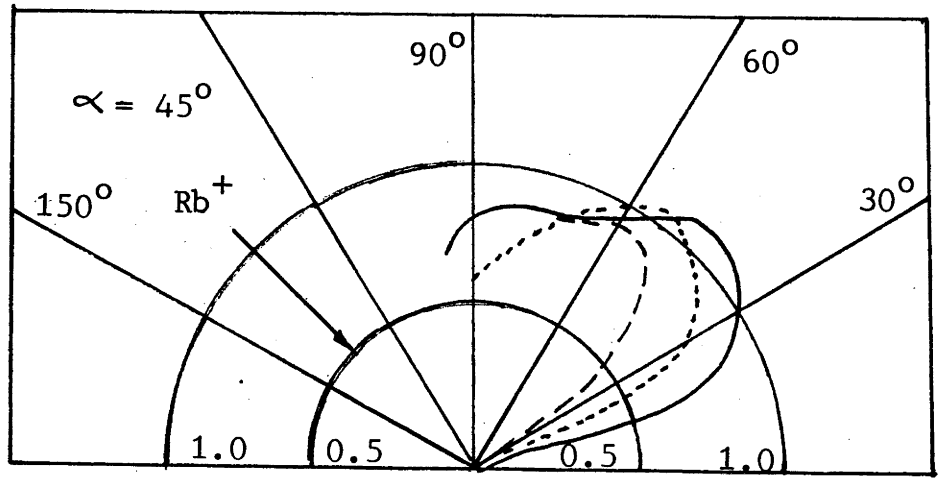

B

FIG 2.10 ANGULAR DISTRIBUTION OF COPPER SECONDARY IONS DURING BOMBARDMENT OF POLYCRYSTALLINE COPPER TARGETS WITH 8 KEV Rb^+ IONS AT A.20° B.45°

(KERKOW 1974)

sputtered neutrals and secondary ions is seen to have similar characteristics.

2.5.6 SINGLE CRYSTAL EFFECTS

The influence of the crystalline nature of a target on the intensity of photons emitted by the sputtered target material was examined by *Snoek, Van der Weg and Rol (1964)*, and *Fluit et al (1961)*. In particular Ar^+ on Cu was studied and the CuI resonance line at 3247 Å monitored as a function of target orientation. In the case of 15 KeV and 10 KeV ions on a (100) Cu surface turning around the <100> direction in the surface, Fluit et al found that structure existed in the resulting intensity distribution (Fig 2.11A) The fine structure was also detected in the sputtering yield. The photon dependence on the angle of rotation was interpreted using the concept of focused collisions. Part of the primary energy is assumed to cause real crystal damage and part is transported through the phonon mechanism. A larger amount of energy leads to impulse transportation along the crystal axes and preferential sputtering of target atoms from the surface. The photon intensity from the polycrystalline Cu target gradually increased with the angle of incidence θ, according to -

$$I\theta = I_o \frac{4 - 3 \cos \theta}{\cos \theta}$$

where θ is the angle between the incident beam and the target normal.

The sputtering yield was found to vary as -

$$I\theta = I_o \frac{2 - \cos \theta}{\cos \theta}$$

The single crystal results however showed a pronounced minimum at 45^o for both the sputtering yield and the photon yield.

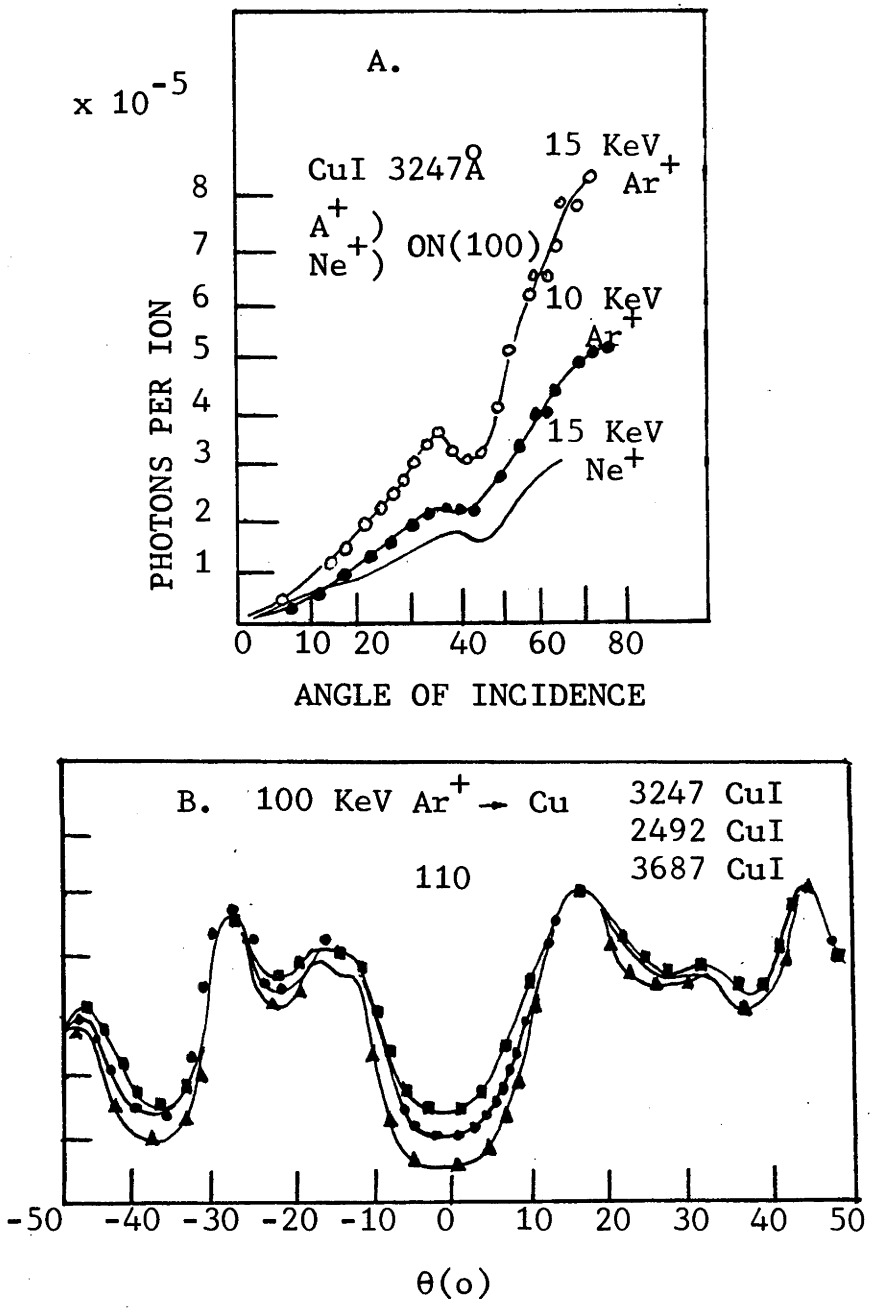

FIG 2.11 SINGLE CRYSTAL EFFECTS ON THE PHOTON YIELDS OF ION BOMBARDED TARGETS

A. FLUIT et al (1961)

B. VAN DER WEG et al (1976)

Optical excitation during ion bombardment of copper under channeling conditions has been studied by *Van der Weg, Tolk, White and Kraus (1976)*. Again, single crystal Cu was studied using Ar^+ of energy 50 and 100 KeV. The 3247 CuI 2492 CuI and 3687 CuII emission lines were studied as a function of the angle of rotation of the target (θ) around its normal, with the ion beam at an incident angle of 60°. The result obtained for the bombardment of a crystal with the <011> axis as its normal is shown in Fig 2.11B. A pronounced minimum occurred when the incoming beam was aligned with the<110> axis. The depth of the minimum was found to vary from line to line. The minimum yield χmin depended upon the excitation energy E exc, of the upper level of the transition considered. The χ min value increased with the excitation energy and the full width at half maximum in the <110> minimum was estimated to be 21.4 to 22.0° in each case. A similar behaviour was observed for HeI and HeII emission from helium ions backscattered from the target, but a shallower minimum and a narrower dip was found for the atomic line as compared to the ionic line. The helium results were interpreted by considering the particles to be excited when inside the solid and experiencing backscatter collisions. It was then thought that the particles subsequently leave the solid in a state of excitation determined by the velocity at the point of exit. Slower particles from deeper regions tend to be neutral whereas faster particles tend to be ionised and come from shallower regions. In the case of copper atoms it was proposed that recoil particles were created in a collision with the argon ions. If in a low degree of excitation the particle travelled in this state and de-excited in the vacuum. Higher excited particles had greater probability of loosing excitation and consequently were produced only near the surface region.

The secondary ion emission also shows well defined directions for minimum and maximum ion yields which are dependent upon the single crystal orientation. A typical result obtained from a (100) surface of Al bombarded along the <110> direction is shown in Fig 2.12A. The variation in Al^+ is plotted as a function of the angular position of the sample relative to the primary beam. An opaque direction is indicated by A and a transparent direction of the primary beam by B (*Slodzian 1976*).

Fig 2.12B shows the secondary ion yields from a two component single crystal as a function of angular rotation (*Zwangobani and MacDonald 1972*). The dependence of In^+, Sb^+ and Sb^{++} is shown for (110) InSb crystal bombarded with 10 KeV Ne^+. The authors estimated the critical angles for channeling, relative reductions in yield and transparency ratios from ion bombarded Ge and InSb crystals. It was concluded that the channeling model of *Onderdelinden (1968)* was capable of predicting the overall features of the variation of the yield with the angle of ion incidence. The half widths of the minima were found to vary with incident ion energy and ion species and also to be independent of the type of particles monitored. Amorphisation of the targets was prevented by maintaining the targets above the transition temperatures. (the temperature above which the annealing of defects is greater than the damage production)

2.5.7 THE INFLUENCE OF REACTIVE GASES ON PHOTON EMISSION

A variety of solid targets bombarded with 40 KeV Ar^+ ions have been studied by *Van der Weg and Lugujjo (1975)*. The authors investigated the behaviour of the photon yield with beam interruption time using the residual gas in the target chamber to contaminate the target surface. The line intensities were recorded as a function of time t whilst bombarding the target with a

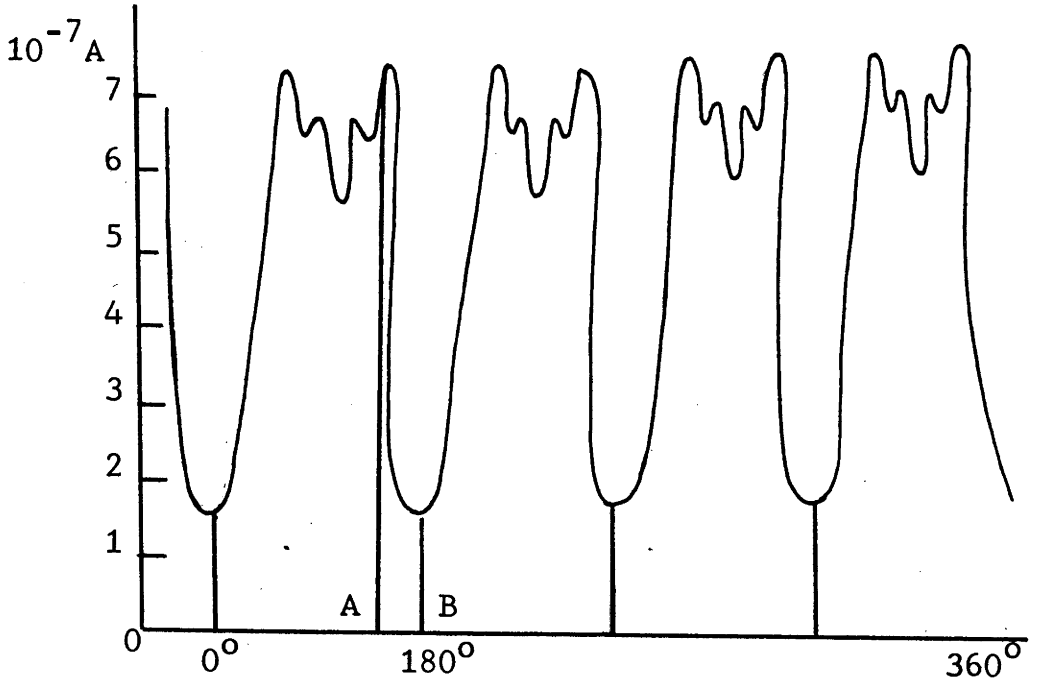

A. Al^+ YIELD FROM Ar^+ BOMBARDED Al DIRECTED ALONG A 110 DIRECTION (SLODZIAN 1975)

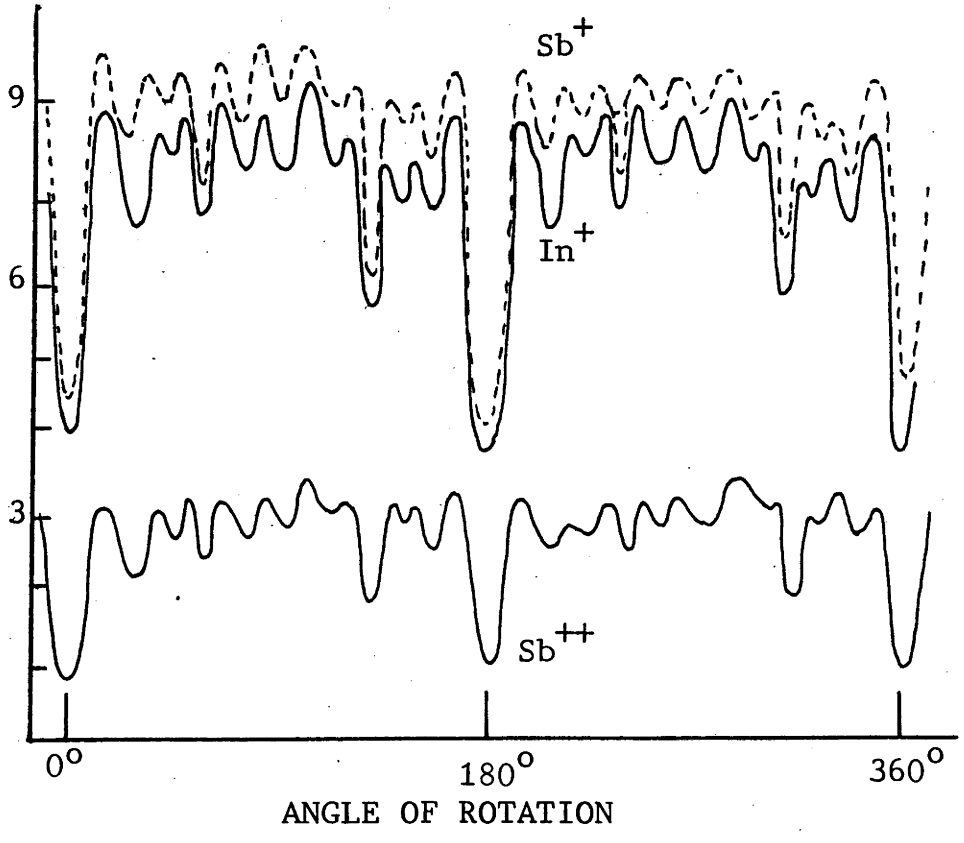

B. CHANNELING EFFECTS IN In Sb (ZWANGOBANIet al 1972)

FIG 2.12 EXAMPLES OF SINGLE CRYSTAL EFFECTS ON SECONDARY ION YIELDS

1μA beam over 0.2 cm^2 in a background gas of 6.10^{-7} Torr. When an equilibrium intensity was reached the beam was switched off for a time τ and the irradiation continued again. It was found that the equilibrium value $R(\infty,\tau)$ was independent of τ and that for CuI emission, the initial value $R(o,\tau)$ was a factor of 6 larger than $R(\infty,\tau)$. The halfwidth of the line intensity above the equilibrium value $t_{1/2}$ was larger for smaller beam currents, and $R(\infty,\tau)$ was strongly affected by the pressure in the target chamber. The transient behaviour was only observed for certain metals.

Introduction of oxygen into the target chamber increased the optical signal of both atomic and ionic lines of Si, but did not alter those from the W spectrum. The results indicated that for certain elements, particularly transition metals, that an oxide was formed on the surface which prevented electrons tunneling from the excited atom to the surface, thus causing an increase in radiative transitions. The transient effect was interpreted as a temporary enhanced probability of radiation due to the accumulation of oxygen on the surface during the time τ. A correlation was found between the transient effect and the number of electrons in the d-shell of the element. Elements with filled or nearly filled d-bands showed strong transient effects but those with only a few d-electrons did not exhibit the effect. This was related to the absorption properties of the elements. For metals such as Ag and Pt an equilibrium fractional coverage of the surface by oxygen atoms is given by -

$f = \frac{P\sigma}{IS}$ where P is the number of oxygen atoms, σ the sticking probability, I the primary beam current and S the sputtering ratio. For systems in which $f < 1$ (Ag, Pt), additional oxygen could

be absorbed during beam interruption and then subsequently removed leading to transient behaviour. For systems in which f > 1 (Fe, Ni, Mo and W) additional absorption was thought to be unlikely and therefore explain the insensitivity of these elements to oxygen.

A more quantitative approach to the effect of oxygen on the photon intensity has been made by *Kelly and Kerkdijk (1974), Kerkdijk and Kelly (1975) and Kerkdijk (1975).* The intensities of a number of AlI emission lines were observed during bombardment of polycrystalline Al with 10 KeV Ne^+ ions. A base pressure of 7.10^{-7} Torr. was used and primary current densities of up to 200 μA cm^{-2}. The intensity of the emission lines was found to be influenced by the presence of oxygen in the target chamber. The intensity of an emission line varied as -

Intensity $\propto I\theta$ where I is the beam current and θ the fractional oxygen coverage of the target surface. The equilibrium between the coverage and oxygen pressure P was expressed as -

$$\frac{d\theta}{dt} = K_1 I\theta + K_2 P(1 - \theta) \text{ where } K_1 \propto S_o/AN_s ,$$
$$\text{and } K_2 \propto \eta/M^{1/2} T^{1/2} Ns$$

The steady state condition is $\theta_\infty = K_2P/(K_2P + K_1I)$, where K_1 is a constant determined by the sputtering coefficient S for adsorbed oxygen, A the beam area and N_s the surface atom density. K_2 is calculated from the sticking coefficient η.

Using these expressions reasonable agreement was obtained between the experimental and calculated behaviour of the photon intensity with primary beam current. It was also found that recoil implantation of adsorbed oxygen atoms influenced the transient behaviour of the Al photon yield.

The most interesting aspect of the work of Kelly and Kerkdijk was the authors' proposition that adsorbed oxygen approximates to an oxide-like band structure on the substrate surface. An atom leaving a solid is influenced by the surface. The electrons are able to transfer from the metal to the atom or atom to the metal through the potential barrier as discussed in section 2.2. When the excited states of the neutral atom and the ion are correlated with the energy band structure of clean and oxide covered aluminium, the oxygen dependence of the photon intensity of particular transitions may be predicted on the basis of simple resonance electron exchange mechanisms. The relevant diagram for Al and Al_2O_3 is given in Fig 2.13A. All the excited states of AlI indicated by Al^* were found to be enhanced by oxidation in keeping with the model. The model also enabled a value of ~0.8 eV to be assigned to the electron affinity of Al_2O_3 since the transition of Al* at -0.8 to -6.0 eV was enhanced by oxidation. This placed the conduction band at an energy less than -1 eV in accordance with the transfer electron model.

The model has also been applied to the case of 10 KeV Ne^+ bombardment of Mg by *Kerkdijk (1975)*. Some 44 discrete lines were detected and assigned to MgI, MgII, NeI, NeII, OII and HI and also possible molecular emission from MgO and MgH was detected. As with the aluminium data reported by Kelly and Kerkdijk, the oxygen dependence of the spectral lines was predicted by the resonant-electron transfer model.

The model also qualitatively predicts the behaviour of secondary ion emission from Al and Mg. Secondary ion emission has been studied by *Guenot (1966)* as a function of oxygen partial pressure. It was found that the singly charged state increased markedly for the light elements. *Brochard and Slodzian (1971)*

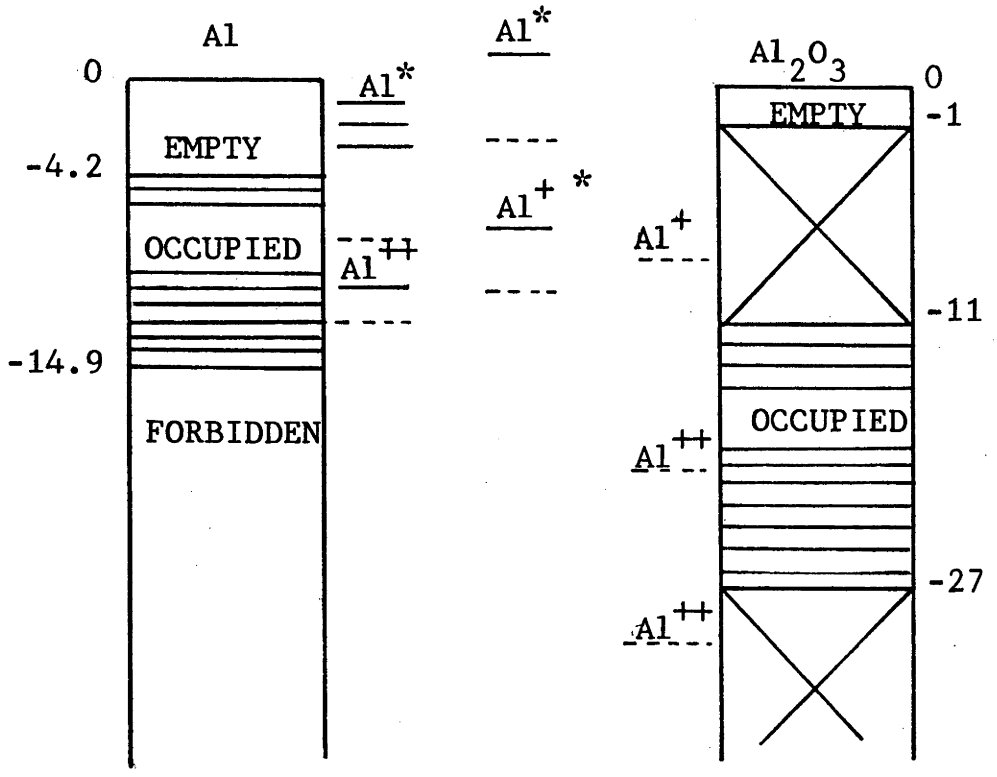

A.

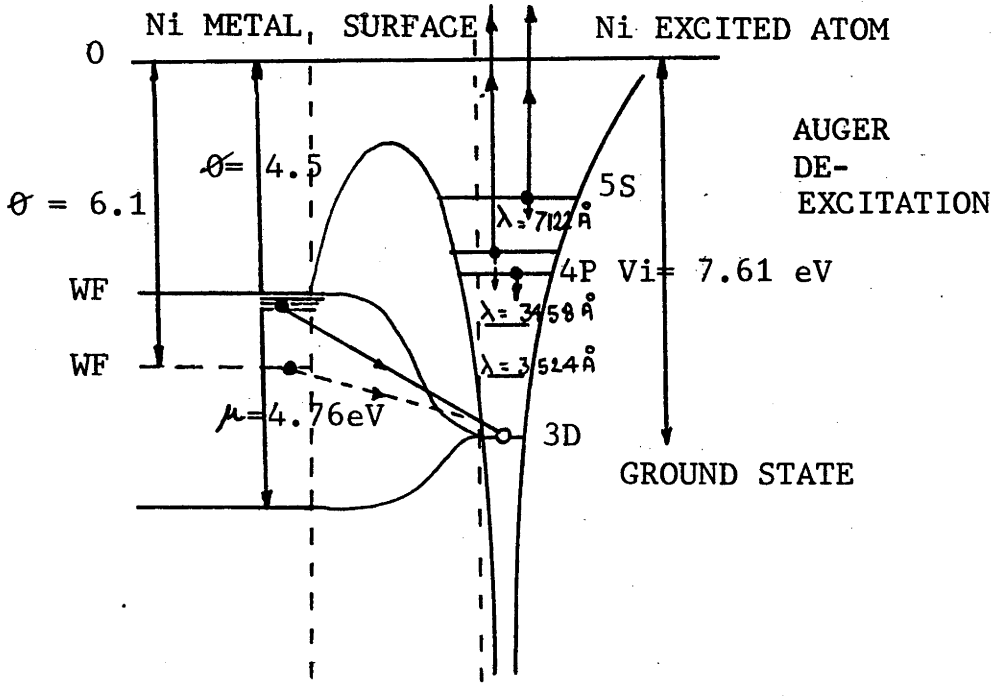

B.

FIG 2.13 ENERGY LEVEL DIAGRAMS OF EXCITED ATOMS NEAR THE SURFACE OF THE TARGET

A. THE BAND STRUCTURE OF Al and Al_2O_3 IN RELATION TO THE ENERGY LEVELS OF Al IONS AND EXCITED NEUTRALS (KERKDIJK AND KELLY 1975).

B. ENERGY LEVEL DIAGRAM OF THE Ni ATOM - Ni SURFACE SYSTEM (MERIAUX et al 1975).

have investigated the behaviour of Al^{+}, Al^{++}, Al^{+++} with oxygen and found Al^{+} to be enhanced, Al^{++} to decrease whereas Al^{+++} was largely unaffected. On a qualitative basis this behaviour of the Al secondary ions may be explained with reference to Fig 2.13A. An example would be that of the Al^{+} ion which can be neutralised by the metal and not the oxide and therefore would be expected to exhibit a positive oxygen dependence.

Further work on the influence of chemically active gas on the photon emission from metallic targets under positive ion bombardment has been reported by *Meriaux, Gouette and Guilland (1975)*. In this particular case polycrystalline Al, Ni and Mo were studied in oxygen, nitrogen and argon atmospheres. Emission lines of the neutral spectrum of aluminium (3944, 3961 Å) and ionised spectra (4529 Å AlIII and 4663 Å AlII) were monitored as a function of oxygen pressure. The intensity of these lines increased by factors of 2.7, 1.8 and 1.8 respectively. It is worth noting the energies of the levels involved in these particular transitions with respect to the band diagrams of Kerkdijk and Kelly (Fig 2.13A). The neutral lines are, according to the model, favoured by oxidation but the ionised emission should be unaffected by the oxidation since the upper levels cannot be de-populated by resonance transfer to the clean surface (occupied region) or to the oxide (forbidden zone). However, an enhancement is reported for all these lines. Meriaux et al also observed an enhancement of all detected lines from NiI with oxygen but not in the case of Mo.

An Auger mechanism was proposed to explain the behaviour of Ni in the presence of oxygen. The diagram used by the authors to explain the 3458 Å and 3524 Å Ni transitions is shown in

Fig 2.13B. For the clean surface an Auger de-excitation mechanism is shown where an electron from the Ni valence band transfers to the vacant hole on the 3D ground state level. The excess energy is transferred to the excited electron in the 4P or 5S level which is subsequently ejected. This transition was considered not energetically possible when the work function Φ was increased by 1.6 eV in the presence of oxygen, therefore increasing the probability for radiative de-excitation and enhancing the photon yield.

The authors interpreted the Mo data using a different approach. It was proposed that a metal oxide under ionic bombardment is reduced according to -

$$MO^{o} \xrightarrow{Ar^{+}} M^{*} + O^{o}$$ where M represents metal components and O the oxygen component.

This reduction process has been found by *Kim and Winograd (1974)* to be related to the free energy of formation of the oxide ΔG_f. For reduction to occur, ΔG_f must be less than 108 K cal/mole, i.e. possible for NiO (ΔG_f = 52 K cal/mole) but not for MoO_2 (119 K cal/mole). A Mo target was therefore thought to be unlikely to produce more excited particles in an oxygen atmosphere. A nitrogen atmosphere produced similar effects to that of oxygen but argon had no influence on the photon emission.

A number of studies of the chemical effect of reactive gases on photon emission have been reported in the literature by *Thomas and Kluizenaar (1974, 1975, 1976)*. Radiation from the molecular species CuO, AlO and AlH was detected as well as atomic emission lines when Cu and Al were bombarded with 10 KeV Kr^{+} ions in atmospheres of O_2 and H_2O. Photon emission from excited molecules sputtered from chemisorbed layers of oxygen, nitric oxide, water,

ammonia, methanol, and methyl mercapatan on silicon was also reported. Excited diatomic molecules were considered to be formed from bombardment-induced fragmentation of the chemisorbed layers.

Some interesting results were reported on the effect of adsorption and coadsorption of Cs and O_2 on photon emission from Cu and Al (*Thomas and Kluizenaar 1976*). Cs was chosen to lower the work function of the target so that photoelectron emission currents could be excited by a He-Ne laser (6328 Å wavelength and 1.96 eV photon energy) to estimate the degree of Cs coverage. Over the range of 0.3 to 0.5 monolayers coverage only a minor effect on the intensity of the ion bombarded targets was observed. The intensity decreased by an estimated 20 per cent. These results were not consistent with the transfer electron model for the following reasons. Cesiation of the target surface resulted in a change in the work function in excess of 2.5 eV. A typical value for a clean surface work function of Cu is 4.3 eV which places the Fermi level at approximately 0.5 eV below the upper level of the excited atomic state of the Cu transition monitored (3247 Å $4s^2S - 4p^2P$ at 3.82 eV). Cesiation then raises the Fermi level to an energy of 2 eV above the atomic level which should then prevent the excited electron from transferring to the metal due to the paucity of available vacant electronic states. The blocking of the radiationless electron transfer should result in an increase in the photon yield contrary to the observed experimental result.

Thomas and Kluizenaar obtained a similar result for cesiated Al. They also observed an increase in the photon yield with oxygen leakage which coincided with an increase in the work function (decay of the photoelectron current). The behaviour with oxygen pressure was however different for the cesiated surface compared

to clean surfaces. In the former case no increase was observed until a pressure of around 2.10^{-5} Torr. was reached whereas in the latter case a rapid rise was observed at much lower pressures. The observations were interpreted using the concept of band formation between substrate atoms and adsorbates. On the cesiated surface Cs atoms were thought to adsorb oxygen preferentially leading to an enhancement of the Cs photon signal and not that of the substrate. At a sufficient oxidation level the oxygen was then thought to attack the substrate and cause an increase in the substrate photon signal.

There have been many studies on the effect of gas adsorption on secondary ion emission. As a general rule it has been found that the first charge state increases with oxygen partial pressure for all elements, particularly so for the transition elements (*Benninghoven and Müller, 1970*). Oxygen exposure has been used to enhance sensitivity in secondary ion mass spectrometry (*Andersen and Hinthorne 1972*) and also to study surface reactions by monitoring specific molecular ions (*Benninghoven and Wiedmann 1974, Müller and Benninghoven 1974; Werner, De Grefte and Van den Berg 1974, Werner 1975*). Reactive gas adsorption would therefore appear to be a useful method of improving not only secondary ion yields but also photon emission and provide information on molecules sputtered from the target surface. The transfer electron model satisfactorily explains in a qualitative manner, the behaviour of certain elements in the presence of oxygen but some studies (Thomas and De Kluizenaar) have indicated that further work is necessary to investigate the applicability of the model to other systems.

2.6 APPLICATIONS OF PHOTON EMISSION

2.6.1 SPUTTERING

The emission of photons characteristic of a given target under ionic bombardment is a very useful phenomenon and has been used by *Kreye (1964)* to determine low-energy sputtering yields for (110) oriented gold single crystals. The method was based upon both emission and absorption of radiation emitted during the sputtering of a gold target. A method for studying sputtered particles based entirely on emission spectroscopy was developed by *Sawatzky and Kay (1966)*. A scanning monochromator monitored the presence of particles sputtered from a target. A low energy electron beam was used to excite the particles sputtered from Cu with 5 KeV Ar^+ ions and the relative excitation function for the CuI resonance lines was determined. Sputtering yields were also determined over the range of 0 to 14 KeV. The effect of temperature on the sputtering yield of Cu has recently been studied by *Windawi (1976)* utilising the spectroscopic emission of sputtered particles. For low energy argon ion bombardment of copper a reasonable agreement was obtained between experimental and analytic yield curves over the temperature range of 500 to 800^{o}K.

2.6.2 SURFACE ANALYSIS USING PHOTON EMISSION

2.6.2.1 QUALITATIVE ANALYSIS

The spectral analysis and identification of characteristic emission lines emitted by sputtered particles is a sensitive and relatively simple method of qualitatively analysing surface layers. The technique was first developed by the research group working at the Bell Telephone Laboratories (*White and Tolk, 1971 , White, Simms and Tolk 1972, White 1975)*, and has been called SCANIIR (surface composition by analysis of neutral and ion impact radiation).

Fig 2.14A illustrates schematically the type of experimental apparatus used in SCANIIR. The apparatus produces both ions and neutrals the latter being used to prevent charge accumulation in insulating materials. The primary particle energy is varied over the range of 50 eV to 8 KeV. A typical background pressure of $3 .10^{-7}$ Torr. is used and spectral analysis is performed over the region of 2000 Å to 8000 Å using a 0.3 metre instrument of aperture f/5. Photon production efficiency has been found to be substantially greater for insulating targets than metal targets. Table 2.5 lists detection sensititives for elements contained in SiO_2. The improvement of photon production from insulators is due to the reduction of non radiative processes as discussed in section 2.5.7.

White et al (1975) have used the SCANIIR technique to measure concentration profiles in thin films. Fig 2.14B shows the result obtained from a SiO_2 (2000 Å)/ Al_2O_3 (500 Å)/SiO_2 (1000 Å) sandwich layer on a Si substrate. The intensities of the 2882 Å SiI and 3961 Å AlI lines were measured as a function of bombardment time using 5 KeV Ar^+ primary ions. The Al signal is seen to rise and fall as a function of sputtering time but does not actually drop to the noise level when the film is effectively sputtered away. The authors have interpreted this as an effect due to cratering from the beam profile, however it does indicate a possible means of monitoring an ion milling process.

Fig 2.14C shows an attempt to measure the range of implanted ions in silicon dioxide. The implant dose was 10^{15} Al ions per square centimetre at an energy of 25 KeV. From the sputtering rate and SiO_2 film thickness, the peak in the distribution of aluminium implanted ions was estimated to be 350 Å.

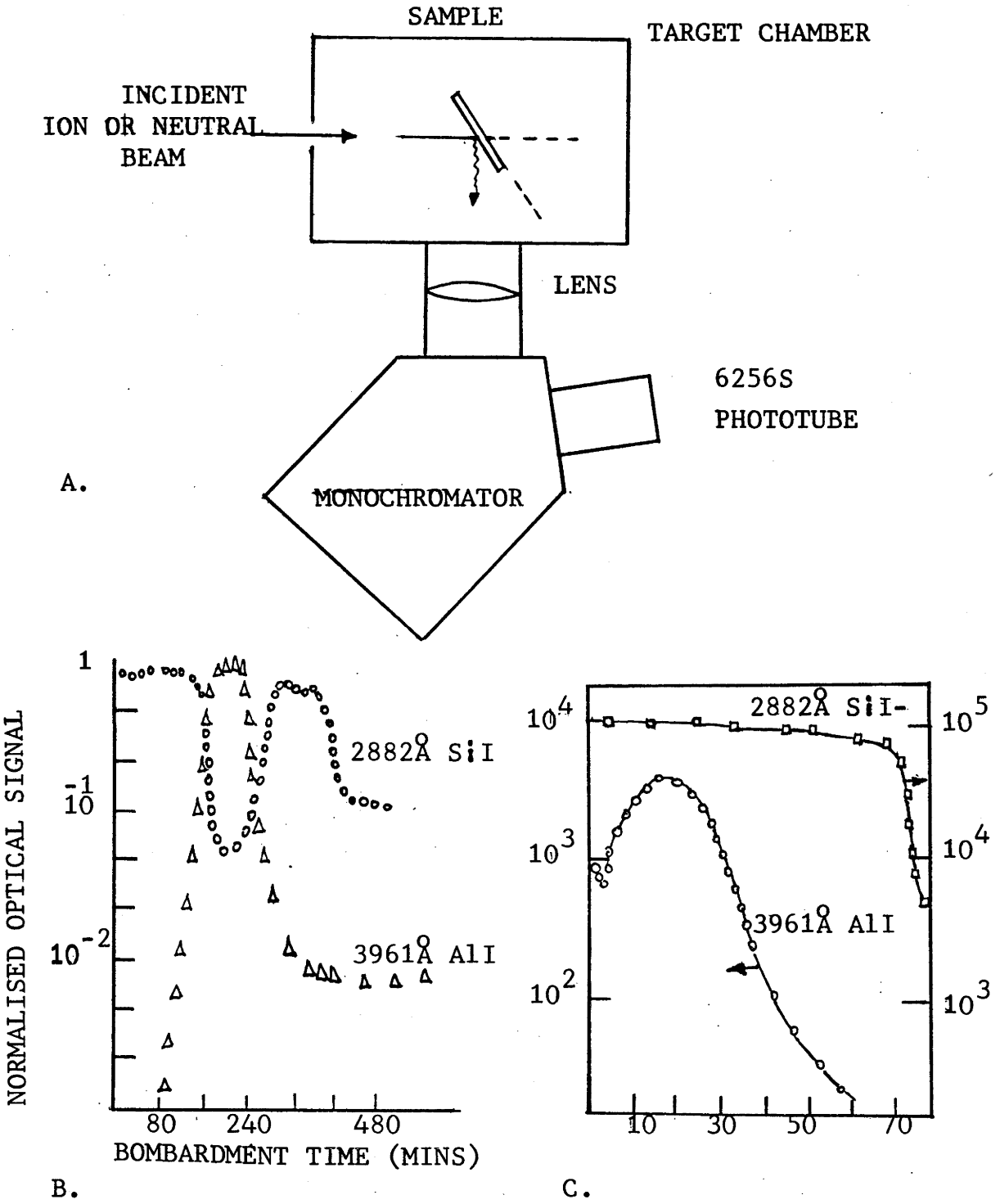

FIG 2.14 SURFACE COMPOSITION BY ANALYSIS OF NEUTRAL AND ION IMPACT RADIATION (WHITE 1975)

A. DETECTION SYSTEM

B. PROFILE OF $SiO_2/Al_2O_3/SiO_2/Si$ USING 5 KeV Ar^+

C. PROFILE OF Al^+ IMPLANTED IN SiO_2 USING 8 KeV Ar^+ BOMBARDMENT.

Several other reports concerning general observations of a qualitative nature on glasses, steels (*Thomas and De Kluizenaar 1975*) and insulators (*Meriaux 1968*), have also appeared in the literature.

TABLE 2.5

SCANIIR Detection Sensitivities in SiO_2

(White, 1975)

(impurity concentration necessary for observation with a S/N ratio of 1:1)

Element	Sensitivity
Al	7.10^{-5}
Fe	8.10^{-4}
Ca	2.10^{-5}
Mg	1.10^{-4}
K	8.10^{-4}
Na	3.10^{-5}
Rb	7.10^{-5}
Li	1.10^{-5}
Sr	7.10^{-5}
Ba	8.10^{-5}
Mn	1.10^{-4}
Ti	1.10^{-3}
Be	4.10^{-5}

2.6.2.2 QUANTITATIVE ANALYSIS

The first reported attempt to use ion-induced photon emission for quantitative analysis was made by *Tsong and McLaren (1974)*. The apparatus used in the technique was called IBSCA (ion beam spectrochemical analyser). The first measurements were made on feldspars (*Tsong and McLaren 1974*).

In the case of feldspar analysis a 'standard' feldspar was first analysed using an electron microprobe. Next, the ratios of Al, Fe, Ca, Na and K lines to the SiI 2882 Å emission line were determined. The ratios of these emission lines were then measured from unknown feldspars and the concentration ratios determined by comparison with the standard. The technique was later

improved and took account of the sputtering yield, the primary ion current and the geometry of the optical system. A linear relationship was found to exist between the intensity of a particular emission line from a given element and the concentration of the element in the sample for feldspars. In the IBSCA system it is assumed that all the sputtered atoms created in excited states decay by photon emission which was shown to be the case for the insulating materials examined. The authors have not examined conducting materials such as standard steels which may be considerably influenced by non-radiative electron exchange mechanisms.

2.7 SUMMARY OF ION-INDUCED PHOTON STUDIES

Photon emission has been detected from a large number of elements and a few isolated reports have appeared on emission from alloys and compounds. There have however, been very few attempts to systematically survey the periodic table and those reports that have been published appear to have been made under mediocre vacuum conditions or with relatively insensitive detection systems. The experimental evidence to date substantiates the theory that the intrinsic emission is predominantly produced as a consequence of biparticle collisions between incident ions and target atoms. The emission is also produced by backscattered primaries and sputtered molecules as well as the fast scattered atoms. Photons have also been observed from excited ionised states of sputtered target atoms (principally light elements), and this does provide a link with the data available on secondary ion emission. Certain correlations between the two can be made concerning angular distributions, single crystal effects and the effect of reactive gases. Correlations also exist concerning the ionisation and

excitation efficiency of particular elements. The halogens have for example, a very low secondary ion yield and have not as yet been detected in photon experiments, whereas light elements such as Na, Al, Mg and Si are all easily ionised and excited. On the basis of the similarities in behaviour between ion and photon emission it would seem reasonable to regard ionisation as an extreme excitation of the atom and to consider the existing ionisation theories from the point of view of photon emission and excitation in general.

2.8 THEORETICAL MODELS OF SECONDARY ION EMISSION

For the purposes of this outline study of secondary ion emission models it is useful to classify the current theories into two categories: quantum mechanical models and thermodynamic models. Some discussion will also be made of the models which are concerned mainly with molecular ion emission.

2.8.1 QUANTUM MECHANICAL MODELS

2.8.1.1 JOYES IONISATION MODEL

A model which describes secondary ion emission as a kinetic process was first developed by *Joyes (1968, 1969, 1973)*. In the process, illustrated in Fig 2.15A , primary ions initiate a collision cascade in the target. During this process target atoms may be sufficiently excited that a bound electron is ejected. Some of the excited particles will reach the surface without losing their excitation and therefore escape in a neutral state but still carrying their 'bound level excitation'. Once outside the target ionisation can occur through an Auger type process, and if sufficient energy is available multiple ionisation is possible. The two major quantities which are needed in this model are, firstly, the probability for a

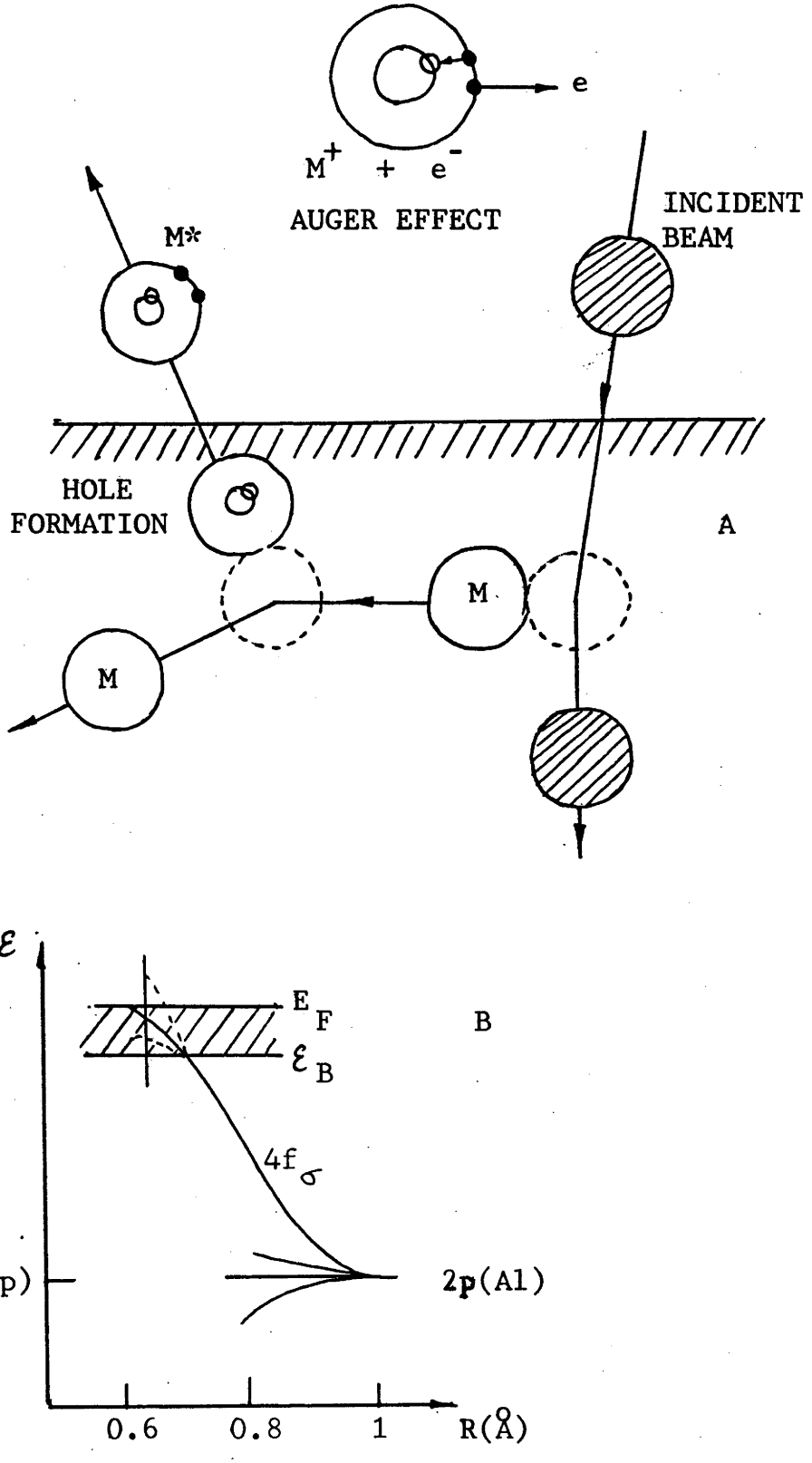

FIG 2.15 THE JOYES KINETIC IONISATION MODEL

A. THE KINETIC MECHANISM

B. 2p HOLE FORMATION IN Al

bound level excitation to be created and secondly, the Auger life-time of such a bound level hole in a metal.

The probability of the creation of a hole on a bound level during the collision of two atoms of a solid was described using the molecular orbital model of *Fano and Lichten (1965)*, first used to describe inelastic collisions in gases. As the distance R between the nuclei of the collision partners is reduced, the electronic levels become molecular levels whose energies vary with R. When two levels cross, exchanges between them occur, and higher levels previously vacant may be partly filled.

In the case of a solid the band structure has to be considered. For the Al → Al collision the initial 2p levels give rise to 4 molecular levels as shown in Fig 2.15B. Of these 4 levels the 4fσ is promoted the quickest and eventually its energy can cross the energies of the conduction band at an internuclear distance of about 0.7 Å. Once this situation is reached the 4fσ level is no longer well defined, but is broadened such that electrons can escape when the upper energies of the broadened level interact with the free states above the Fermi energy.

The Auger life-time of a bound level hole in a metal was calculated by *Joyes (1968)* using one-electron approximation and the results compared favourably with experimental values obtained from X-ray line widths for some metals. In the case of the Al 2p hole an Auger life-time of 10^{-14} sec was calculated and found to be comparable to the time of 8.10^{-14} sec for the slowing of an Al atom from 1 KeV to 20 eV in the cascade. Consequently, it was considered possible for some particles to de-excite outside the target. For the equivalent situation in a transition metal, Cu for example, the 3d level is the relevant level for hole formation and its Auger life-time was found to be ~ 1.10^{-16} sec. In this case it was assumed

that the destruction of the 3d hole would occur almost instantaneously inside the metal thus reducing the external Auger ionisation process for a large number of particles and therefore reducing the number of secondary ions. The secondary ion yield of Al is in fact found to be two orders of magnitude greater than that of Cu.

The Joyes kinetic ionisation model does require knowledge of the promotion of the molecular orbitals of the collisions partners. In the case of light element compounds such as the Al-O compounds, this information may be obtained by drawing correlation diagrams in which the atomic levels at $R = \infty$ are joined by straight lines to the levels of the united atom at $R = 0$. These diagrams only indicate whether the levels have a large or a small total promotion and do not accurately predict the precise evolution of the levels. Nevertheless, for the Al-Al collision, shown in Fig 2.15B, the 2p level gives rise to the $4f\sigma$ level which is rapidly promoted. In a compound such as Al-O (low oxygen content) the molecular level which is most rapidly promoted is of the $3d\sigma$ type and does not reach the free states above the Fermi energy at E_F, thereby reducing the number of kinetic secondary ions.

Qualitative data on the variation of the secondary ion yields from Al in the presence of oxygen does appear to confirm that the Al^{++} kinetic ion yield decreases with oxygen pressure (*Brochard and Slodzian 1971*). The decrease was also observed in the Auger electrons, the existance of which were originally predicted by Joyes, by *Henneguin and Viaris de Lesegno (1971)*.

The Joyes model therefore appears to explain on a qualitative basis at least, the behaviour of multiply charged secondary ion yields from compounds of relatively low oxygen content. The negative oxygen dependence of the Al^{++} ion can however also be explained on the basis

of the simple transfer electron model discussed earlier in section 2.5.7. Observation of the photon emission from excited multiply charged states of Al and other light elements where the molecular level promotion concept is applicable, should also provide information on the ionisation process. If the excited ions are produced by biparticle collisions between the incident ion and the target atoms one would not expect to observe any change in the photon yield for a clean surface and low oxygen coverage of the surface since an $Ar^+ \rightarrow X$ collision would be responsible for hole formation in either case. A change would presumably only occur when the stoichiometry of the surface is substantially altered.

2.8.1.2 BLAISE AND SLODZIAN MODEL OF IONISATION

A similar process to the Joyes kinetic ionisation mechanism has been considered by *Blaise and Slodzian (1970 and 1973)*. The model, generally applied to transition metals and alloys, considers an atom to be ejected in a super-excited state. The atom subsequently ionises through the auto-ionisation process in vacuum immediately in front of the target surface.

The model is largely based on evidence obtained from the optical spectroscopy of Cu in an arc discharge and the phenomenon of autoionisation (*Shenstone 1938, Allen 1932*).

During ionic bombardment it is proposed that excited states of energies less than the ionisation potential, and also greater than the ionisation potential are produced. The latter are referred to as 'super excited' states which may be of a radiative or non-radiative (autoionising) nature. The study of ionic emission on the basis of this model is then reduced to the study of the autoionising states.

These processes have been studied in detail by the authors but the results do not easily lend themselves to predicting on a quantitative basis, the ionic yield from bombarded metals. Data on the electronic structure of the elements is required in the calculations which is not accurately known, particularly under the conditions of ionic bombardment.

2.8.1.3 QUANTUM MECHANICAL MODELS OF SCHROEER AND SROUBEK

In the model of *Schroeer (1972)*, it is assumed that sputtered atoms leave the surface in a neutral unexcited state and are subsequently ionised by a quantum-mechanical transition of the atoms' valence electrons to the top of the conduction band of the metal. The ionisation probability is calculated using the adiabatic approximation giving -

$$R^{+} = \left[\frac{A}{I - \Phi} \right]^{2} \left[\frac{\hbar V}{a (I - \Phi} \right]^{n}$$

where A is the surface binding energy of the sputtered atom, $\hbar$ is a constant, V the velocity, a is one-half the surface layer thickness (~ 1.5 Å), I the ionisation energy, Φ the work function and n a fitting parameter. The model has been reasonably successful in the analysis of alloys and the bombardment of pure metals with argon ions.

A similar result was obtained by *Sroubek (1974)* using the theory of molecular orbitals to calculate the quantum-mechanical probabilities but experimental tests have been limited so far.

The use of the adiabatic perturbation theory in the model of Schroeer has been criticised by *Cini (1976)* who proposed that a

quasiadiabatic method was physically more justifiable. However, the theory developed using the quasiadiabatic method was not compared with experimental data and eventually indicated that further theoretical work and experimental study was required before any quantitative estimates of the ionisation probability could be made.

A more simplified quantum mechanical model was proposed by *Antal (1976)* but only limited agreement was obtained between theoretical and experimental results.

2.8.2 THERMODYNAMIC MODELS OF SECONDARY ION EMISSION

2.8.2.1 ANDERSEN AND HINTHORNE MODEL

An analytical method for the quantitative interpretation of sputtered ion intensities based on the theory of local thermodynamic equilibrium has been developed by *Andersen and Hinthorne (1973)*. The theory assumes that the majority of sputtered ions, atoms, molecules and electrons are in thermal equilibrium with each other and that equilibrium concentrations can be predicted through the use of the Saha equations.

The ionisation process is regarded as an equilibrium dissociation reaction such as -

(i) $$M^{o} \rightleftarrows M^{+} + e^{-}$$

The equilibrium constant is the concentrations of the products over the concentrations of the reactants -

(ii) $$K_{n}^{+} = \frac{Nm^{+}\, Ne^{-}}{n_{M^{o}}}$$ where Nm^{+}, Ne^{-} and $^{n}M^{o}$ are the concentrations of ions, electrons and neutral atoms respectively. Under the conditions of thermal equilibrium, the equilibrium constant is given by the Saha-Eggert ionisation equation -

(iii) $\left(\frac{2\,KT}{h^2} \cdot \frac{m_{e^-}\, m_{M^+}}{m_{M^o}}\right)^{3/2} \frac{B_{M^+}\, B_{e^-}}{B_{M^o}}\, e^{-E/KT}$

Here, m is the mass, B the partition function, E the first ionisation potential and T the absolute temperature.

The only unknown quantities in equations (ii) and (iii) are the electron density N_{e^-} and the temperature T, the remainder can be obtained from reference tables. The two unknowns may be determined by measuring the secondary ion yields of two elements of known concentration homogenously distributed throughout the sample.

The model has received some criticism from several authors, (*Slodzian 1975 and Werner 1975*), primarily on the grounds that the concept of a plasma in L.T.E. is difficult to reconcile with the actual physical process taking place under sputtering conditions: the ionisation temperatures for example are far in excess of the melting points of the solids bombarded and values range from $\sim 4000^{o}K$ to $11000^{o}K$. Furthermore, the energy distributions of secondary ions, neutrals and electrons are non-Maxwellian in nature. Nevertheless, the model has been remarkably successful in predicting concentrations of many elements on a ppm scale in a wide range of materials with an accuracy comparable to conventional analytical techniques.

2.8.2.2 JURELA MODEL

Jurela (1973), used a thermodynamic approach to secondary ion emission applying the Dobretsov equation for surface ionisation through non-equilibrium thermodynamics. The ionisation fraction was written as -

$$R^{+} = \frac{B^{+}(T)}{B^{O}(T)} \exp \frac{(-Ic - \Phi)}{KT} \qquad \text{where } Ic = I - \Delta I.$$

Here, T is the local surface temperature, ΔI the image potential energy at a critical distance from the surface and Φ the work function. Using this approach temperatures of 2000 to 5000^{O}K were obtained and considered to be more realistic than those of Andersen. However, it has been shown by *Bayly and MacDonald (1976)* that the success of the thermodynamic models rely on the strong exponential dependence of the atomic ionisation potential and that the Andersen and Jurela equations are essentially equivalent. The Jurela approach however appears to relate more closely to the physical situation since account is taken of the surface work function.

The thermodynamic model has to date been the only successful quantitative theory in secondary ion emission and therefore warrants some consideration from the point of view of photon emission. Optical techniques have long been established to measure the temperatures of plasmas particularly arc discharges (*Boumanns 1966*). Once a temperature is determined, standard spectrochemical techniques are available to calculate the concentration of the elements radiating in the discharge. As the ion-induced photon spectra from some elements resembles those of an arc it would appear feasible to apply such techniques to the ion-induced photon emission. No such attempts have been reported in the literature.

2.8.3 MOLECULAR ION EMISSION

Several models have been proposed to describe the production of molecular ions. Such ions may be produced through the breaking of bonds of chemical compounds on the surface. The process has been

termed dissociative by *Benninghoven (1969)* and chemical by Slodzian and Hennequin. *Werner (1975)* has used the idea of fingerprint secondary ion mass spectra of known compounds (such as Cr_2O, Cr_2O_2, Cr_3O etc) to predict the secondary ion yields from an unknown surface (oxidised chromium). Using this technique the oxidation of chromium was assumed to proceed through a series of phases each characterised by a specific secondary molecular ion spectrum. The oxidation of surfaces has only been studied in the case of a few transition elements by photon emission and further study would appear desirable to complement secondary ion work.

2.9 CONCLUSION

This brief survey has indicated that further information is required on the production mechanisms of secondary ions in order to form a satisfactory theory capable of predicting secondary ion yields on a quantitative basis. The successful model of Andersen and Hinthorne appears difficult to reconcile with the physical nature of ion-surface interaction. The study of photon emission from neutral and ionised particles should provide further useful data on the physical mechanisms of excitation and ionisation of target atoms during ion irradiation.

REFERENCES

ALLEN, C W, Phys. Rev., 39, 42 (1932).

ALMÉN, O and BRUCE, G, Nucl. Instr. Methods 11, 257 (1961).

ANDERSEN, C A, Microprobe Analysis, John Wiley & Sons, N.Y. (1973).

ANDERSEN, C A, and HINTHORNE, J R, Anal. Chem., 45, 1421 (1973).

ANDERSON, T, JENSEN, K A and SORENSEN, G, J.O.S.A., 59, 1197 (1969).

ANTAL, J., Phys. Lett., 35A, 493 (1976).

ARNOLD, W, Ann. Phys., 61, 326 (1897).

AUGER, P, Surface Science, 48, 1 (1975).

BAIRD, W E, ZIVITZ, M, LARSEN, J, THOMAS, E.W., Phys. Rev. A10, 2063 (1974).

BAYLY, A R, MACDONALD, R J, Proc. Australian Conf. on Nuclear Techniques of Analysis, Lucas Heights (1976).

BENNINGHOVEN, A, Z. Physik, 220, 159 (1969).

BENNINGHOVEN, A, MULLER, A, Phys. Lett., 40A, 169 (1972).

BENNINGHOVEN, A, WIEDMANN, I, Surface Science, 41, 483 (1974).

BERNHARDT, F, OECHSNER, H, STUMPE, E., Nucl. Instrum. Methods, 132, 329 (1976).

BERNHEIM, M, SLODZIAN, G., Intern. J. Mass Spectr. Ion Phys., 12, 93 (1973), 20, 295 (1976).

BOLAND, B C, IRONS, F E, MCWHIRTER, R W P, J. Phys. B1, 1180 (1968).

BOERSCH, H, DOBBERSTEIN, P et al. Z. Physik, 187, 97 (1965).

BLAISE, G, SLODZIAN, G, J. Phys. 31, 93 (1970).

BLAISE, G., Rad. Effects, 18, 235 (1973).

BÖHMER, H and LÜSCHER, E., Phys. Lett. 5, 240, (1963).

BOUMANNS, P W J M, Theory of Spectrochemical Excitation, Hilger & Watts London (1966).

BRAUN, M, EMMOTH, B, MARTINSON, I., Physica Scripta. 10, 133 (1974).

BRAUNDMEIR, A J, ARAKAWA, E T., Z. Physik, 239, 337 (1970).

BROCHARD, D, SLODZIAN, G., J. Phys., 32, 185 (1971).

CARLHEIM-GYLLENSKÖLD, V., Ark. Mat. Astron. Fys, 4, 1 (1908).

CHAUDHRI, R M et al, Nature 189, 996 (1961), 192, 646 (1961), Proc. 5th Int. Conf. on Ionisation Phenomena in Gases, Vol 11, 1195, Munich (1961), Proc. 7th Int. Conf. on Ionisation Phenomena in Gases, Vol I, 186, Belgrade (1967).

CINI, M., Surface Science, 54, 71 (1976).

COBAS, A, and LAMB, W E, Phys. Rev., 65, 327 (1944).

DATZ, S, SNOEK, C., Phys. Rev, 347A, 134 (1964).

DUNN, G H, GEBALLE, R, PRETZER, D., Phys. Rev, 128, 2200 (1962).

FANO, U, LICHTEN, W., Phys. Rev. Lett, 14, 627 (1965).

FERRELL, R A, Phys. Rev, 111, 1214 (1954).

FIRSOV,O B, J.E.T.P., 36, 1517 (1959).

FLUIT, J M, FRIEDMAN, L, VAN ECK, J, SNOEK, C, KISTEMAKER, J., Proc. 5th Int. Conf. on Ionisation Phenomena in Gases, Munich (1961).

GABLA, L, SZYMONSKI, M, SZULKIN, M., Physica 81C, 193 (1976).

GRITSYNA, V V et al, Phys. Lett, 27A, 292 (1968), Izv. An. SSSR, Ser. Fiz. 35, 578 (1971). Rad. Effects, 14, 77 (1972).

GUENOT, D, D.E.S. Orsay (1966).

HAGSTRUM, H D, Phys. Rev. 96, 336 (1954).

HAGSTRUM, H D, and BECKER, G E, Phys. Rev B, 8, 107 (1973).

HENNEQUIN, J F and VIARIS DE LESEGNO, P, Surface Science, 42, 50 (1974).

HIPPLER, R, KURGER, W, SCHARMANN, A, SCHARTNER, K H., Nucl. Instr. Meth., 132, 439 (1976).

JANEV, R K, TERZIC, I V, DAVIDOVIC, D M, Surface Science, 26, 142, (1971).

JANEV, R K, J. Phys. B., 12, 1506 (1974).

JENSEN, K, VEJE, E., Z. Physik, 269, 293 (1974).

JOYES, P., J. Phys., 29, 774 (1968), 30, 224 (1969), 30, 365 (1969), Rad. Effects, 19, 235 (1973).

JURELA, Z, PEROVIC, B., Can. J. Phys., 46, 773 (1968).

JURELA, Z, Atomic Collision Phenomena in Solids. North Holland Amsterdam (1970).

JURELA, Z, Intern. J. Mass Spectrom. Ion. Phys., 12, 33 (1973).

KELLY, R, KERKDIJK, C B., Surface Science, 46, 537 (1974).

KERKDIJK, C B and THOMAS, E W., Physica, 63, 577 (1973).

KERKDIJK, C B, KELLY, R., Surface Science, 47, 297 (1975).

KERKDIJK, C B, SMITS, C M, OLANDER, D R, SARIS, F W., Surface Science, 49, 45 (1975).

KERKDIJK, C B, Thesis, F.O.M. Laboratories, Netherlands (1975).

KERKDIJK, C B, SCHARTNER, K H, KELLY, R, and SARIS, F W, Nucl. Instr. Meth., 132, 427 (1976).

KERKOW, H., Phys. Status Solidi, 7A, 451 (1971).

KHAN, J M, POTTER, D L, WORLEY, R D, SALEM, S I, SMITH, H P., Phys. Rev. Lett. 19, 950 (1967).

KIM, K S, WINOGRAD, N., Surface Science, 43, 625 (1974).

KISTEMAKER, J, et al, Le Bombardment Ionique, C.N.R.S., Paris (1962).

KIYAN, T S, GRITSYNA, V V, LOGACHEV, Yu E, FOGEL, Ya M, J.E.T.P. Lett. 21, 35 (1975). Nucl. Instrum. Meth., 132, (1976).

KREYE, W C., J. Appl. Phys., 35, 3575 (1964).

LINDHARD, J, SCHARFF, M, KGL. Danske Videnskab. Selskab, Mat. Fys.Medd., 27, 15 (1953).

MARTEL, J G, OLSEN, N T., Nucl. Instrum. Meth. 105, 269 (1972).

MARTINSON, I., Physica Scripta, 9, 281 (1974).

MASSEY, H S W, Proc. Cambridge Phil. Soc., 26, 386 (1930).

MAYER, H, Phil. Mag., 7, 594 (1933).

McCRACKEN, G M, ERENTS, S K, Phys. Lett., 31A, 429 (1970).

McCRACKEN, G M, FREEMAN, N J, J. Phys. B 2, 662 (1969).

MERIAUX, J P, GOUTTE, R, GUILLAND, C., Appl. Phys. 7, 313 (1975).

MÜLLER, A, BENNINGHOVEN, A., Surface Science, 39, 427 (1974).

OLANDER, D R, KERKDIJK, C B, SMITS, C., Surface Science, 49, 28 (1975).

OLIPHANT, M L E, MOON, P B., Proc. Roy. Soc. (London) A127, 388 (1930).

ONDERDELINDEN, D., Appl. Phys. Lett., 8, 189 (1966), Can. J. Phys. 46, 739 (1967).

PARYLIS, E S, Proc. 7th Int. Conf. on Ionisation Phenomena in Gases, Belgrade (1967).

PEARCE, R W B, GAYDON, A G., The Identification of Molecular Spectra. London, Chapman & Hall Ltd. (1965).

REID, I, FARMERY, B W, THOMPSON, M W., Nucl. Instrum. Meth. 132, 317 (1976).

SAWATZKY, E, KAY, E, Rev. Sci. Inst., 47, 1324 (1966).

SCHROEER, J M, RHODIN, T N, BRADLEY, R C., Surface Science, 34, 571 (1973).

SHEKHTER, S S., Zh. Eksper. Teor. Fiz., 7, 750 (1937).

SHENSTONE, A G., Phys. Rev., 28, 449 (1926), 34, 1623 (1929).

SLODZIAN, G., Surface Science, 48, 161 (1975).

SNOEK, C, VAN DER WEG, W F, ROL, P K,, Physica 30, 341 (1964).

SROUBEK, Z., Surface Science, 44, 47 (1974).

STARK, J, WENDT, G., Ann. Phys., 38, 669 (1912)

STEINMANN, W., Phys. Rev. Lett., 5, 470 (1960).

STERNBERG, D., Cited in BÖHMER and LÜSCHER (1963)

STERK, A A, MARKS, C L, SAYLOR, W P,. Phys. Rev. Lett, 17, 1001 (1966).

STUART, R V, WEHNER, G K, ANDERSON, G S., J. Appl.Phys. 35, 1819 (1964).

TERZIC, I, PEROVIC, B., Surface Science, 21, 86 (1970).

THOMAS, G E, DE KLUIZENAAR, E E, Le Vide, 167, 191 (1973), Int. J. Mass. Spectry. Ion. Phys. 15, 165 (1974), Chem. Phys. 7, 303 (1975), Nucl. Instrum. Meth. 132, 449 (1976).

THOMPSON, M W., Phil. Mag, 18, 377 (1968).

TOLK, N H, SIMMS, D L, FOLEY, E B, WHITE, C W, Rad. Effects. 18, 221 (1973).

TSONG, I S T., Phys. Stat. Sol. 7, 451 (1971).

TSONG, I S T, McLAREN, A C, Spect. Act. 30B, 343 (1975).

VAN DER WEG, W F, LUGUJJO, E, 5th Int. Conf. on Atomic Collisions in Solids, Gatlinberg (1975).

VAN DER WEG, W F, ROL, P K, Nucl. Instrum. Meth. 274 (1965).

VAN DER WEG, W F, BIERMAN, D J, Physica, 44, 206 (1969).

VAN DER WEG, W F, TOLK, N H, WHITE, C W, KRAUS, J M., Nucl. Instrum. Meth. 132, 405 (1976).

VARNERIN, L J., Phys. Rev., 91, 859 (1953).

WERNER, H W, DE GREFTE, H A M, VAN DEN BERG, J., Adv. Mass. Spect., 6, 673, (1974).

WERNER, H W., Vacuum, 24, 493 (1975).

WERNER, H W, Surface Science, 47, 301 (1975).

WARCZAK, A, BROZDOWSKA-WARCZAK B, PEDRYS, R, GABLA, L., Acta. Phys. Pol. A47, 543 (1975).

WARCZAK, A., Acta. Phys. Pol. A48, 579 (1975).

WHITE, C W, TOLK, N H., Phys. Rev. Lett., 26, 486 (1971).

WHITE, C W, SIMMS, D L, TOLK, N H., Science, 177, 481 (1972).

WHITE, C W, SIMMS, D L, TOLK, N H, McCAUGHAN, D V., Surface Science, 49, 657 (1975).

WHITE, C W, TOLK, N H, KRAUS, J, VAN DER WEG, W F., Nucl. Instr. Meth., 132, 419 (1976).

WINDAWI, H M, Surface Science, 55, 593 (1976).

ZWANGOBANI, E, MACDONALD, R J, Radiation Effects. 20, 81 (1973).

CHAPTER THREE

EXPERIMENTAL METHOD

3.1 GENERAL DESCRIPTION OF THE EXPERIMENTAL APPARATUS

A schematic diagram of the accelerator and target chambers is given in Fig 3.1. The ion source provided a beam of ions which could be accelerated to a maximum energy of 100 KeV. The ion beam was mass-analysed and switched to one of either two analysed beam lines. A quadrupole lens was used to focus the beam and deflector plates used to steer it through an aperture into the target chamber.

3.2 EXPERIMENTAL DETAILS

3.2.1 ION SOURCE AND SWITCHING MAGNET

Ions were produced by an Ortec 350 duoplasmatron ion source. The Von Ardenne duoplasmatron source is widely used in ion beam technology and has been extensively studied (*Moak et al, 1959, Lêjeune 1974*). This type of ion source offers a number of advantages over other types such as large ion beam intensity of singly charged ions and high gas efficiency. The source was easily dismantled and filament replacement relatively simple. Filaments were fabricated from platinum gauze 80 mesh, 0.003 inch diameter wire,coated with a standard emission solution of barium carbonate. Using a filament current of 20 amps., typical filament lifetimes were of the order of 1000 hours.

Matheson research grade inert gas was bled into the ion source through a control valve. The magnetic separator also enabled industrial grade gases to be used in the ion source.

The ion beam once extracted from the ion source was accelerated to the required energy using a 100 KeV power supply.

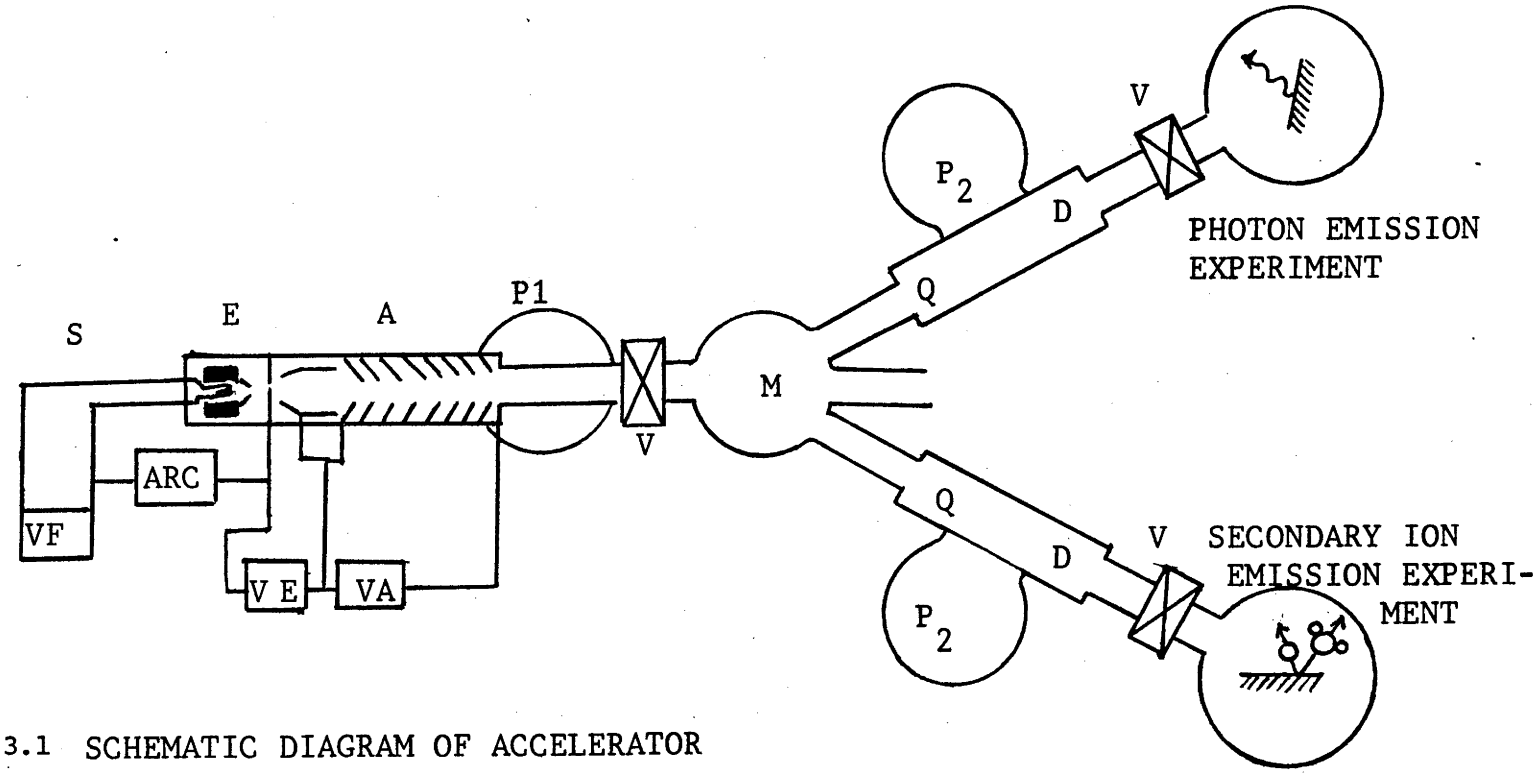

FIG 3.1 SCHEMATIC DIAGRAM OF ACCELERATOR

S - SOURCE, E - EXTRACTOR, A - ACCELERATION TUBE, VF - FILAMENT VOLTAGE SUPPLY, M - SEPARATOR MAGNET, Q - QUADRUPOLE LENS, D - X,Y DEFLECTOR, V - U.H.V. VALVE, P - 1200 LS^{-1} DIFFUSION PUMP, P_2 - 500 LS^{-1} DIFFUSION PUMP.

The beam was then mass-analysed and switched into the selected beam line by a magnetic separator. The maximum field capabability of the magnet was approximately 7.5 KG with a 3 cm gap between the poles and a 100 KeV Ar^+ beam could be easily switched through the required angle of 30 degrees into either of the analysed beam lines. The magnetic field was calibrated using a nuclear resonance fluxmeter.

3.2.2 ION OPTICS

An existing electrostatic triplet quadrupole lens was used to focus the ion beam. The lens was originally designed for operation with proton beams but was satisfactory in focusing inert gas ions and molecular ions. The theoretical aspects of this type of lens have been discussed by *Enge (1960)* and the properties of the particular lens used has been discussed by *Zwangobani (1972)* obviating the need for a detailed discussion here. The lens was modified by the addition of an isolated aperture mounted on the lens entrance to facilitate convenient monitoring of the ion beam.

A simple beam steering system was situated between the quadrupole lens and target chamber. The beam steerer provided some deflection of the ion beam in the X and Y directions and was primarily used for final alignment of the beam with the target in the target chamber. The beam steering plates were each 5 cms long and 2 cms wide with a plate separation of 2 cms.

3.2.3 ACCELERATOR VACUUM SYSTEM

The duoplasmatron ion source section, magnetic separator region and beam lines were evacuated by oil diffusion pumps fitted with water cooled baffles. The pumps were backed by a common rotary pump and a reservoir system such that the ion source and beam

lines could be continuously pumped but exposed to the rotary pump for the minimum amount of time. This reduced oil vapour back-streaming from the rotary pump into the beam lines. A further precaution against rotary pump oil was provided by the addition of a chemically activated copper mesh foreline trap to the backing line. The oil diffusion pumps were charged with Santovac 5 diffusion pump oil because of its resiliance to 'cracking'. The accelerator vacuum system pressure was continuously monitored and safeguards built into the control system against power failure or rotary pump breakdown.

Typical background pressures in the ion source section and beam lines were 5.10^{-8}Torr. and 5.10^{-7} Torr. respectively, rising to 4.10^{-6} Torr. and 1.10^{-6} Torr. during ion source operation. The pressure rise was due to the higher gas load of the source gas and ion beam.

3.2.4 TARGET CHAMBER

An existing 12 inch diameter 304 stainless steel chamber was modified by the addition of several two inch diameter ports fitted with 4 inch flanges. These ports were used for mounting an observation window, ionisation gauge and target holder. Two existing 6 inch ports were used for feedthroughs and the quartz vacuum window. The essential features of the system are illustrated in Fig 3.2.

3.2.4.1 VACUUM SYSTEM

The target chamber was pumped by a 650 litres per second oil vapour diffusion pump charged with Santovac 5 oil and backed by a rotary oil pump. The rotary pump was trapped by a chemically activated copper mesh sieve and a liquid-nitrogen-cooled glass

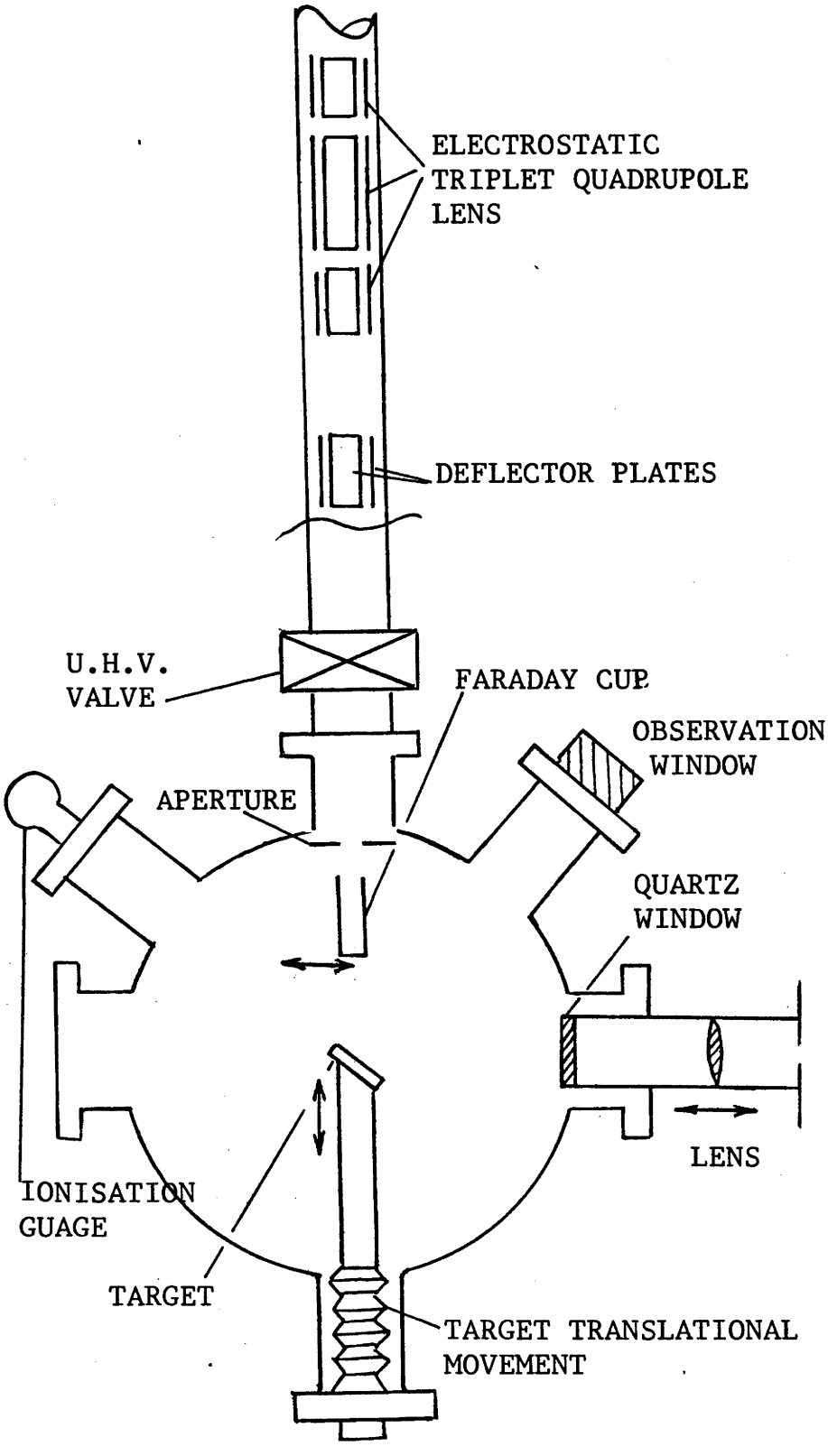

FIG 3.2 SCHEMATIC DIAGRAM OF THE TARGET CHAMBER

foreline trap. The diffusion pump was trapped by a water-cooled chevron baffle and a 6 inch liquid nitrogen trap.

The target chamber assembly had seven Viton A 0-ring seals, the remainder being UHV copper seals and aluminium wire seals. The main flanges of the chamber were sealed by double 1/8 inch Viton A 0-rings with the space in between evacuated to backing line pressure. The use of this guard vacuum system reduced leakage through the main flange seals. The target chamber could only be baked to a maximum temperature of 100^{o}C because of the Viton 0-rings and a bake out at this temperature with a trapped system led to a minimum background pressure of about 5.10^{-8} Torr. measured on an ionisation gauge. Measurements of the background gas constituents were made with an E.A.I. model 250 residual gas analyser. Identification of the mass spectra indicated that the principal component in the residual gas was water vapour. The absence of an oxygen peak and the lack of response of the gas analyser to the presence of helium when used as a test gas indicated that the system was free from major leaks.

3.2.5 DETECTION SYSTEM

The detection system comprised of a quartz vacuum window, focusing lens, grating monochromator and photon counting system.

The quartz window used in the detection system was obtained from Ceramaseal Incorporated. The window used was high quality,2.88 inch in diameter and polished to within 0.0004 inch per inch with parallelism of the polished faces of 0.005 inch. The window was bonded with a high melting point lead alloy onto a sleeve of 304 stainless steel. This assembly was welded onto a stainless steel re-entrant port designed to mate with the 6 inch

side port of the target chamber.

A 2 inch diameter 13 cms focal length quartz lens was used to focus light emitted from the target through the vacuum window onto the entrance slit of the monochromator. The lens was designed to utilise the maximum aperture of the vacuum window and to match the aperture of the monochromator at a magnification of unity. The lens was mounted inside a simple sliding tube assembly for fine focusing adjustments.

3.2.5.1 GRATING MONOCHROMATOR

The majority of the photon measurements were made using a Bausch and Lomb 0.5 metre scanning monochromator model 33-86-45. This instrument had an effective aperture of f/4.4 and was fitted with a 1200 lines per mm plain diffraction grating of blaze angle 10^{0} 22' (blaze wavelength 3000 Å in first order).

Light from the entrance slit at the front of the instrument was directed onto the right hand side of a concave collimating and condensing mirror of diameter 18.5 cms at the rear of the instrument. The collimated beam was directed to the grating situated at the front of the monochromator 11.6 cms above the centre of the slits, where it was dispersed by the grating and reflected to the left hand side of the same concave mirror. The beam was then refocused and reflected off a plane mirror situated at an angle of 45^{o} to the exit slit. This particular optical system had the advantage of a large aperture but had a limiting resolution of 3 Å , caused by the off axis angle in the two directions of the collimating mirror (*Manson, 1966, Bausch and Lomb, 1974).*

The grating mount was rotatable about an axis inclined at an angle of 14 degrees and adjustment was made by revolving a graduated drum. This activated a sine bar linkage in the instrument providing a strictly linear wavelength presentation. The wavelength drive system was modified by the attachment of a precision stepper motor (Calderon Limited, size 15) and gearbox (Weyers Limited). The stepper motor was driven by pulses furnished by a Macleans stepper-motor control box. The control box had constant stepping rates of 2, 4, 10, 20, 40, 100, 200 and 400 pulses per second. The stepper-motor required 12 pulses per revolution which was further reduced by 1000:1 in the precision gearbox such that 20 steps per second corresponded to a wavelength scanning speed of 100 Å per minute. The scanner could alternatively be operated in the single pulse mode (a single pulse equivalent to 1/12 Å) such that an external timer or scalar could be used to increase the signal to noise ratio for low intensity photon levels or offset the ion beam fluctuation by integrating over a fixed ion dosage.

The modest resolution of the Bausch and Lomb monochromator precluded precision wavelength measurement and the determination of emission line profiles. The shape and width of strong emission lines of particular interest were studied using a Jarrell-Ash 82-010, 0.5 metre Ebert scanning spectrometer. This instrument had an effective aperture ratio of f/8.6 and was fitted with a 1180 groove mm^{-1} grating and supplied with fixed slits of width 10μ, 25μ and 50μ. The wavelength drive was modified by the addition of a precision stepping motor and gearbox as with the Bausch and Lomb system. The instrument had a resolution of approximately 0.2 Å using the 10μ entrance and exit slits.

3.2.5.2 PHOTON COUNTING SYSTEM

3.2.5.2.1 PHOTOMULTIPLIERS

An E.M.I. 9789 QB photomultiplier was used as the photon detector on the scanning monochromators. The tube had a 13 stage dynode chain and was a 2 inch diameter end-on model. The K-Cs photocathode was sensitive to ultraviolet radiation, the lower limit of 2000 Å determined by the transmission of the photomultiplier quartz window. The tube used had an exceptionally low dark current.

Photomultipliers are ultimately limited in their sensitivity to low light levels by the presence of a thermionic current from the photocathode (dark current). There have been many studies of the thermionic dark current and methods of reducing it, (*Sharpe, 1964, Gadsden, 1965)*, the most common method being to reduce the temperature of the photomultiplier. The 9789 QB photomultiplier used in these experiments was a special 'A' tube selected for its low dark current of 0.02 nA at a voltage of 1070 volts at room temperature. This level of dark current was considered to be acceptable and no attempt was made to cool the photomultiplier.

The signal to noise ratio from a photomultiplier may be enhanced by operating in the single photon counting mode. Photon counting permits discrimination against the d.c. component of dark current associated with surface leakage as well as low amplitude pulses not arising from photocathode emission. Photon counting provides a capability to perform accurate measurements at very low light levels where the signal is statistically or quantum limited. The advantages of photon counting over conventional d.c. operation have been discussed in detail by many researchers (*Arecchi et al, 1966, Morton, 1968, Oliver et al, 1968, Foord et al, 1969, Zatzick, 1970.)* Since it was necessary to operate in the single photon

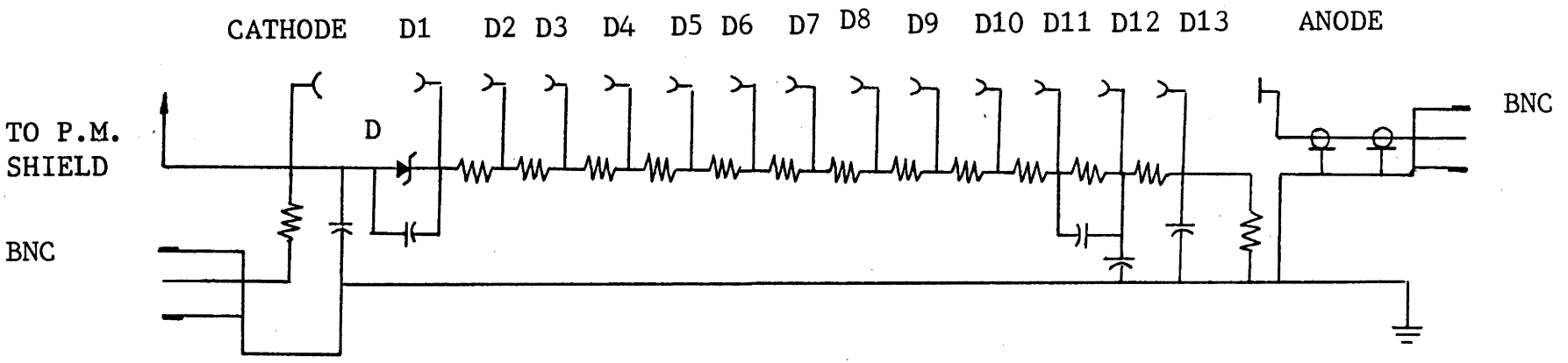

ALL RESISTANCES 1M, ½W 2%
ALL CAPACITORS 0.01, 3KV
DIODE 200V ZENER

FIG 3.3 WIRING DIAGRAM OF 9789 QB PHOTOMULTIPLIER TUBE BASE (ZATZICK)

counting mode some attention was paid to the photomultiplier dynode chain and electrical screening.

The photomultiplier dynode chain illustrated in Fig 3.3 was wired according to *Zatzick, (1970)*. The input high voltage line was filtered with a 1 MΩ resistor and 0.01 μF capacitor which gave an attenuation of 10^{-4} - 10^{-6} at 1 MHZ. A zener diode was used to maintain a constant voltage of 200 volts potential between the cathode and first dynode. The use of 1 MΩ resistors per dynode stage assured a divider current of 100μA maximum to reduce any possible Joule heating effects. The final three dynodes were by-passed to ground with high frequency 0.01μF disc ceramic capacitors to reduce R.F.I. pick up via the dynode to anode capacitance. The dynode chain was shielded from electrical and magnetic interference by a cylindrical mu-metal shield secured around the photomultiplier tube.

The photomultiplier was mounted inside an aluminium housing on the exit slit of the monochromator. A simple camera shutter was mounted immediately in front of the photocathode inside the housing to elliminate any input signal and enable an estimate of the background photon leakage and dark current to be made.

3.2.5.2.2 COUNTING CIRCUIT

The photon counting circuit used is shown in Fig 3.4. Pulses from the photomultiplier were fed into a pre-amplifier (Ortec 9301) and then to the main amplifier (Ortec 451). The output from the main amplifier was fed into two counting systems. The first system consisted of a single channel analyser, which acted as a discriminator (Ortec 406A), a monitor pulse counter (Ortec 715), a ratemeter (Ortec 441), and a two pen recorder. This system enabled rapid and easy signal optimisation when tuning the monochromator to

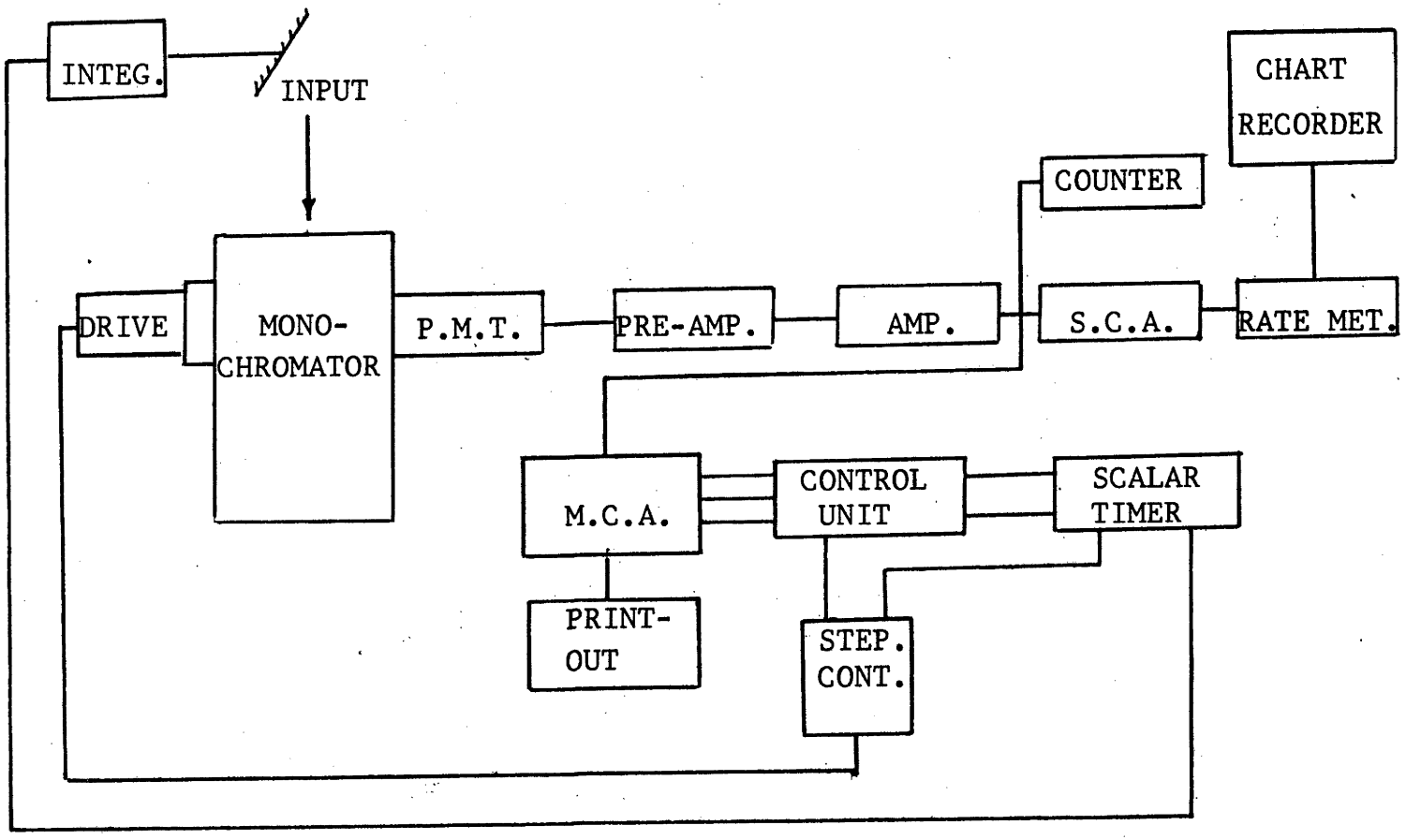

FIG 3.4 BLOCK DIAGRAM OF DATA ACQUISITION ELECTRONICS

to a particular emission line and was particularly suitable for obtaining wavelength scans over the region 2000 to 6000 Å when the wavelength stepping-motor was operated in the continuous stepping mode.

The second counting circuit employed a multi channel analyser (Ortec 6240, 4096 channel M.C.A), operated in the multi-scaling mode and could fully exploit the single stepping capabilities of the wavelength drive system. The pulses from the amplifier were fed through the internal discriminator of the M.C.A. and gated on and off by a scalar-timer system for a pre-selected time interval or accumulated ion dose on the target, measured by a beam current integrator. The circuit was used to step the wavelength drive system such that pulses from the photomultiplier could be accumulated in the M.C.A. for a pre-set time (or ion dosage) per pre-selected wavelength interval.

The M.C.A. system provided a very sensitive method of low level photon detection, the lower limit being limited by the background count rate from the photomultiplier of approximately 1 cps. The system also enabled data to be collected in digital form for computer analysis and plotting. In the case of precision line-profile measurements using the Jarrell-Ash spectrometer and M.C.A. counting circuit, a maximum wavelength resolution of 8.10^{-4} Å per channel could be achieved.

3.3 CALIBRATION OF THE DETECTOR SYSTEM

In order to compare the relative intensity of emission lines produced by ion irradiation of the target, the relative detection efficiency of the complete detection system was determined. The relative detection efficiency of the monochromator and detection system was found by comparison with a calibrated tungsten strip lamp, over the spectral region of 2000 Å to 6000 Å. The absolute wavelength

calibration was checked using the 6328 Å line of a He-Ne laser and the 3274 Å and 3247 Å CuI resonance lines from a hollow cathode lamp.

The relative intensity calibration was performed using a Philips W2 KGV 221 tungsten ribbon lamp fitted with a silica window. The lamp was calibrated for effective spectral radiance at a temperature of 2700°K by the C.S.I.R.O. National Standards Laboratory. The calibration was performed at a current of 14.39 Amps, and voltage of 8.51 volts. The conditions used to calibrate the tungsten ribbon lamp were reproduced for the purpose of the relative detection efficiency measurements. The filament current was measured by monitoring the voltage across a standard 0.1Ω resistance.

The intensity of the tungsten lamp at the calibration temperature was such that the lamp could not be placed directly in the target chamber without saturating the counting system. To overcome this difficulty the lamp was placed outside the chamber and the light reflected off a standard reflector of barium sulphate. The reflectance of $BaSO_4$ was taken from the data of *Grum and Luckey (1968)*. The measured intensity distribution over the wavelength region of 2000 Å to 6000 Å is shown in Fig 3.5 and is to be compared with the intensity distribution of the standard lamp corrected for reflectance from the $BaSO_4$ reflector. The relative intensity or detection sensitivity was calculated as the ratio of the measured and calibrated distributions.

The emissivity of the tungsten lamp decreased very rapidly at shorter wavelengths to such an extent that stray light in the monochromator from longer wavelengths may have contributed to the short wavelength calibration. Correction of the short wavelength calibration was made using the method described by *Van Den Bos et al (1968)*. The signal $S(\lambda)$ was measured with and without a glass filter

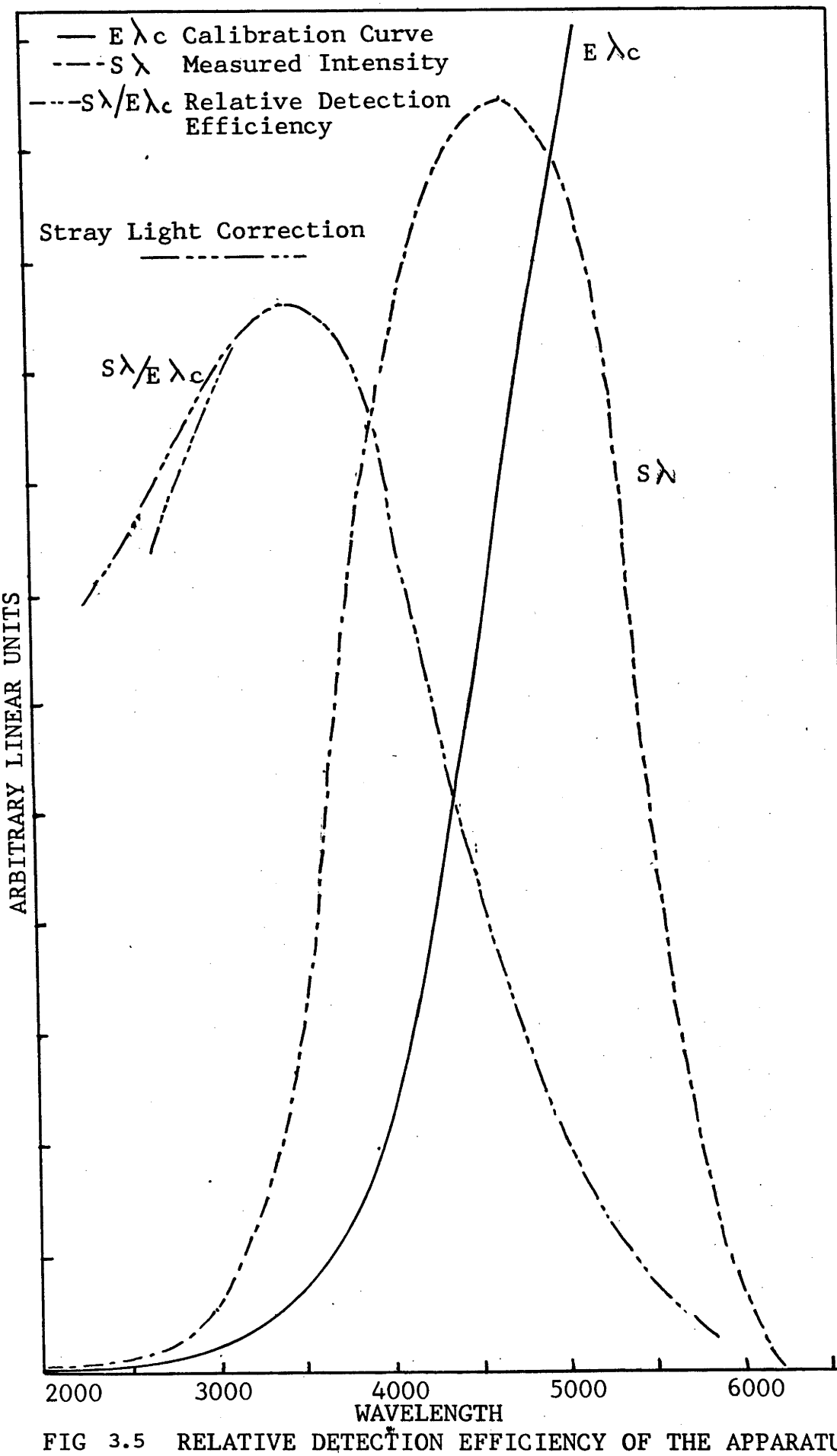

FIG 3.5 RELATIVE DETECTION EFFICIENCY OF THE APPARATUS.

interposed between the monochromator and tungsten lamp. It was assumed that the glass absorbed radiation below 3300 Å and transmitted approximately 85 per cent of the light above 4000 Å. The signal measured with the glass filter in place was specified as S(glass) and the signal strength measured without the glass filter as Sλ total. The signal measured below 3300 Å was then calculated from -

$$S(\lambda) = S\lambda(\text{Total}) - S(\text{glass})/0.85$$

For longer wavelengths the sensitivity of the photomultiplier decreased and straylight may have had some influence but this contribution was not considered to be as important as in the ultraviolet region.

The relative detection efficiency of the detector system was found to peak at a wavelength of approximately 3500 Å . On the basis of the calibration curves the detection system was considered sensitive enough to study optical emission over the wavelength region 2000 to 6000 Å. The region of maximum sensitivity from 2000 Å to 4000 Å corresponded to region of the spectrum which contained a large number of strong resonance emission lines of most elements.

3.4 EXPERIMENTAL TECHNIQUE

3.4.1 TARGETS

Polycrystalline targets were prepared from high purity (99.999 per cent), 1/4 inch and 3/8 inch diameter rods supplied by Materials Research Corporation. A slow speed diamond saw was used to cut discs typically 2 mm in thickness. The discs were polished to a mirror finish using a diamond polishing compound and degreased in solvents.

The targets were mounted on a copper target holder at an angle of 45 degrees to the primary beam. The use of a copper target holder assembly ensured that any beam misalignment could be detected

by identification of the CuI resonance lines at 3247 Å and 3247 Å. The geometry shown in Fig 3.2 was selected because of its use by a large number of other researchers and to enable comparisons to be made with published data. The target holder was supported by a 1 inch Edwards U.H.V. linear translational movement. The linear translation was used to align the ion bombarded region of the target with the optical axis of the detection system.

3.4.2 PRIMARY ION CURRENT MEASUREMENT

With a 5 mm entrance aperture mounted inside the target chamber typical beam current densities were of the order of 75 to 100μA cm^{-2}. The primary ion current was measured by interposing a simple Faraday cup between the entrance aperture and target. The Faraday cup was fabricated from an aluminium cylinder 8 mm in diameter and 80 mm in length. The ratio of the length to diameter for the Faraday cup was approximately 10:1 to reduce secondary electron emission. *(Kuyatt 1968)*. During an experimental run the stability of the primary ion current was continuously monitored by measuring the total current on the entrance aperture with a beam current integrator and the total current on the target under study. The primary ion beam was found to be stable to within ± 5 per cent at 100 μA cm^{-2}.

REFERENCES

ARECCHI, F T, GATTI, E, SONA, A., Rev. Sci. Inst., 37, 942 (1966).

BAUSCH and LOMB, Private Communication (1974).

ENGE, H A., Rev. Sci. Instr., 32, 662 (1961).

FOORD, R, JONES, R, OLIVER, C J, PIKE, E R., Appl. Optics, 8, 1975 (1969).

GADSEN, M., Appl. Optics, 2, 1446 (1965).

GRUM, F, LUCKEY, G W., Appl. Optics, 7, 2289 (1968).

KUYATT, C E., Methods of Experimental Physics, 7, 18 (1968).

LEJEUNE, C., Nucl. Instr. Methods, 116, 417 (1974).

LEJEUNE, C., Nucl. Instr. Methods, 116, 429 (1974).

MANSON, N., Thesis, Aberdeen University (1966).

MOAK, C D, BANTA, H F, THURSTON, J N, JOHNSON, J W, KING, R F., Rev. Sci. Instr. 30, 694 (1959).

MORTON, G A., Appl. Optics, 7, 1, (1968).

OLIVER, C J, PIKE, E R., J. Phys. D. 1, 1459 (1968).

SHARPE, J., E.M.I. Symposium (1964).

VAN DEN BOS, J, WINTER, G J, DE HEER, F J., Physica, 40, 357 (1968).

ZATZICK, M R., Application Note 71021 SSR Instruments Co.

ZWANGOBANI, E., Thesis, A.N.U., (1972).

CHAPTER FOUR

PHOTON EMISSION FROM ION-BOMBARDED METALS, SEMICONDUCTORS, AND INSULATORS

4.1 INTRODUCTION

Experiments were conducted on a wide variety of metals, semiconductors and insulating targets to obtain photon emission spectra characteristic of a large number of elements, produced by inert and reactive ions. The influence of the band structure of the target on the photon emission has also been investigated for a variety of wide band-gap semiconductors. The results of this survey study have indicated several areas for subsequent detailed study which are discussed further in the following chapters.

4.2 EXPERIMENTAL CONDITIONS

The initial survey of photon emission from metals, semiconductors and insulators was conducted under background gas pressures of approximately 5.10^{-8} Torr., the major background gas component being water vapour. A primary ion energy of 50 KeV was typically employed and a maximum beam current density of 100 μA cm^{-2} was used. All metal targets were high purity materials obtained from Materials Research Corporation and were either polycrystalline or single crystal targets randomly orientated to minimise any possible crystal orientation effects. Samples were polished to a mirror finish with diamond polishing compound and degreased in solvents. The Bausch and Lomb low resolution high aperture monochromator was used for maximum sensitivity.

Photon data was taken after prolonged bombardment of the target (typically 2 hours at 100 μA cm^{-2}). This enabled the bulk

of surface contaminants and oxides to be removed and gave a constant photon signal. It was found necessary to remove the quartz vacuum window periodically and clean off sputter deposits which otherwise attenuated the photon emission.

4.3 PHOTON EMISSION FROM METALS

4.3.1 MAGNESIUM AND ALUMINIUM Mg, Al

These elements yielded strong photon signals when bombarded with 50 KeV Ar^+ ions and in both cases emission lines from neutral and charged particles were detected, the highest charge state being Al III (Al^{++}). An example of the type of spectrum obtained from 50 KeV Ar^+, N_2^+ and O_2^+ bombardment of Al is given in Fig 4.1. The neutral lines are unmarked and the second and third spectra are indicated by the conventional spectroscopic roman numerals II and III respectively.

The Mg spectrum gave very strong emission of the 2795.5, 2798 and 2802 Å Mg II lines arising from the resonance doublet $3s^2S - 3p^2P^o$ and the multiplet $3p^2P^o - 3d^2D$. The strongest MgI emission was the $3s^2\,{}^1S - 3p^1\,P^o$ resonance transition at 2852 Å. The Al spectrum was characterised by four strong neutral resonance lines at 3082 Å, 3092 Å, 3944 Å and 3961.5 Å. Strong emission lines identified as type II and III were also observed. The ratio of the population of the $3d^2D_{5/2}$ to the $3d^2D_{3/2}$ level (levels responsible for the 3082 Å and 3092 Å emission lines) was estimated to be 1.7. This value compares reasonably well with those estimated for the $nd^2D_{5/2}$: $nd^2D_{3/2}$ ratio (n = 3, 4, 5) of 1.5, 1.4, 1.7 by *Jensen and Veje (1974)*, (50 KeV Xe^+ bombardment) and the ratio of 2 estimated by *Thomas and De-Kluizenaar (1974)*, using 10 KeV Kr^+ bombardment under both 'clean' and contaminated conditions.

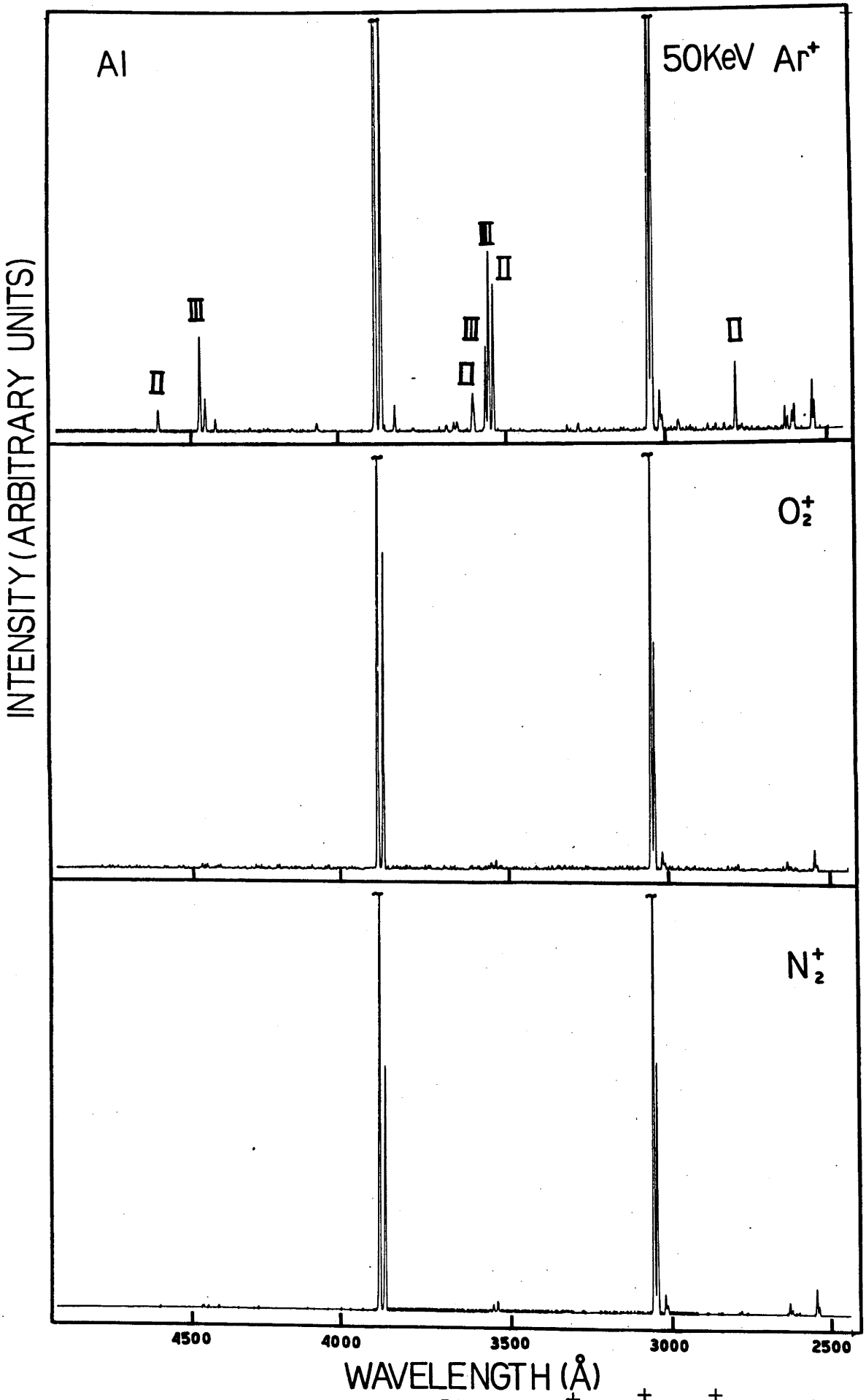

FIG 4.1 PHOTON SPECTRA FROM 50 KeV Ar^+, O_2^+, N_2^+ → Al

These values are close to the ratio of the statistical weights (2J + 1) of 1.5 for the levels in question, assuming that Russell-Saunders coupling is applicable (*Herzberg, 1934*). Molecular radiation has been reported by some reseachers from the MgO Green System in the region 4900-5200 Å, however, no such radiation was detected in this study. Furthermore the spectra were all found to be free of CH radiation which is known to result from hydrocarbon contamination of the target surface by diffusion pump oil (*White et al 1972*). This indicated that the experimental conditions here were such that the target surfaces were free of oil contamination and oxides.

It has been reported by *Terzic´and Perovic´(1970)* that ArII emission at 4879 Å was produced by 40 KeV Ar^+ bombardment of Al. The experimental conditions were almost identical to those of this study, but no ArII radiation was detected. The identification of this line was however not confirmed by the presence of any other ArII emission lines known to occur in the same wavelength region (*Striganov and Sventiskii, 1968*) which are of equal intensity. The half width of optical emission lines originating from back scattered primary ions are also known to be exceptionally large compared to those from sputtered atoms (section 2.4), but the spectra shown by the authors indicate a similar half width for the ArII and AlIII emission lines.

Bombardment of both Mg and Al with N_2^+ and O_2^+ beams resulted in a change of the relative intensities of the neutral and ion lines. A comparison of the N_2^+ and O_2^+ induced spectra with that produced by Ar^+ (all at 50 KeV) is shown in Fig 4.1 for the Al target. The reactive ions substantially increased the photon yield of the neutral atoms relative to the ion spectra. A similar result was obtained in the case of the MgI and MgII emission. The reactive ion bombardment also gave rise to a discolouration of the

bombarded region. An enhancement of the photon yield from the neutral species has been previously reported (section 2.5) for targets bombarded with inert gas ions in a background of oxygen or water vapour. The enhancement can be qualitatively understood on the basis of the transfer electron model and energy band diagrams such as that of Fig 2.13A. The evidence here then further suggests that the target surface is altered by reactive ion bombardment to such an extent that its electronic structure can be considered to assume the properties of an oxide and possibly a nitride. The relative position of the excited atomic or ionic level to the electronic energy band structure of the target surface then determines whether or not a particular emission line is enhanced through the blocking of electronic exchange with the surface.

4.3.2 Sc, Ti, V, Cr, Mn, Fe, Ni, Cu, Zn.

These metals can be divided according to their electron configuration into two groups. From Sc through to Ni (the transition metals) the electron arrangement is of the form $3d^n\ s^m$ where n = 1,2, 3, 5,5, 6, 7, 8 for the respective metals and m = 2 in all cases with the exception of Cr where m = 1. The second group which contains Cu and Zn have a filled d shell of 10 electrons and a single s electron for Cu and a filled 4s shell for Zn. Since the outer shell valence electrons are responsible for the optical spectra, the large number of valence electrons present in the first group give rise to very rich spectra not only in arc excitation but also under ion irradiation. A typical example of the rich complex spectra produced by ionic bombardment of Cr with 50 KeV Ar^+, N_2^+ and O_2^+ is shown in Fig 4.2.

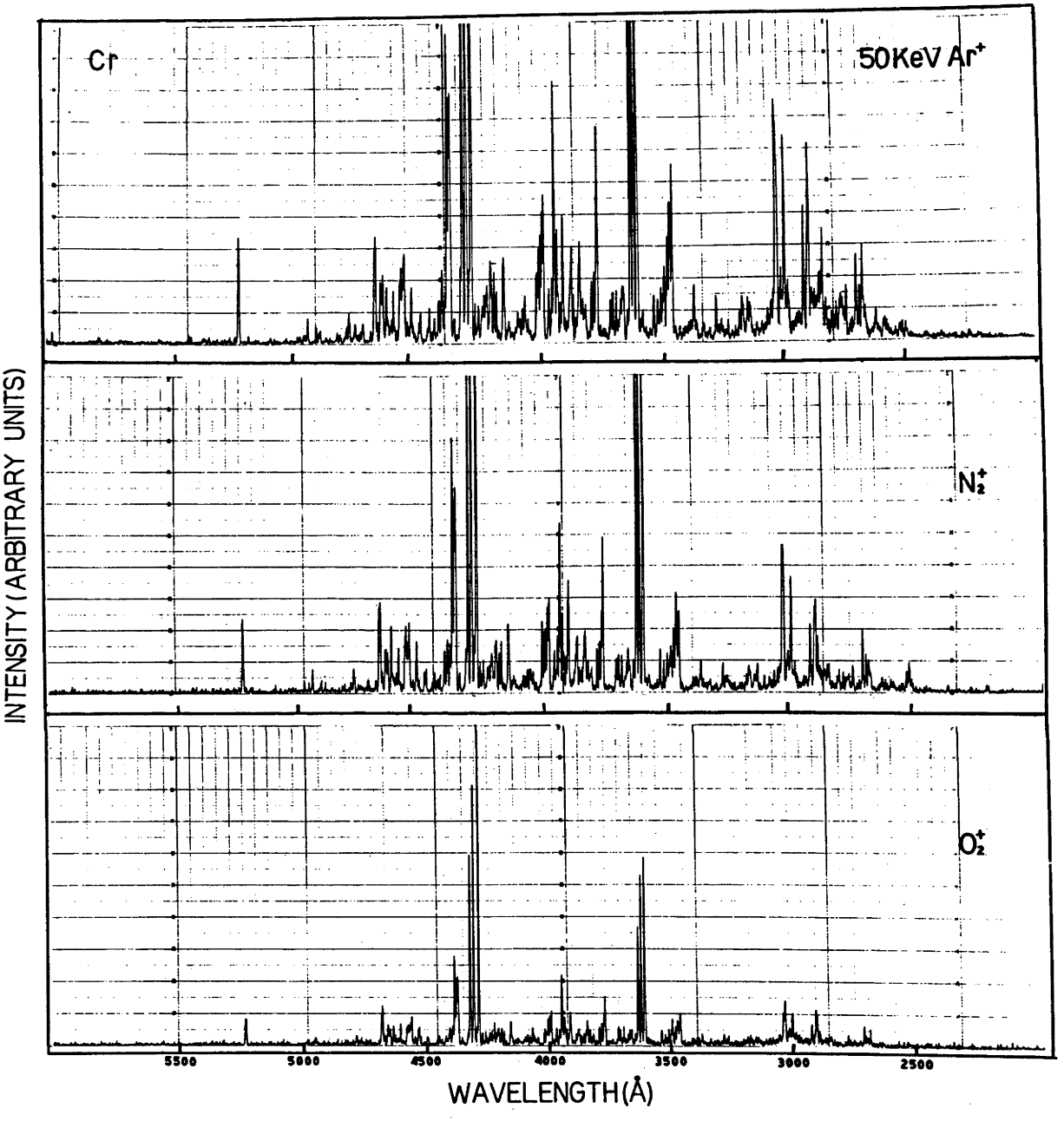

FIG 4.2 PHOTON SPECTRA OF Cr PRODUCED BY INERT AND REACTIVE ION BOMBARDMENT.

The spectra although complex, can readily be identified from standard wavelength reference tables. In the case of Cr the spectrum is characterised by two groups of three neutral emission lines of wavelengths 3605, 3594, 3579 Å and 4290, 4275, 4254 Å.

Reactive ion bombardment of the transition metals did not drastically alter the detected spectra in the same manner as the lighter elements. In most cases very little emission from ionised species was detected, but some weak CrII emission was observed between 2790 Å and 2843 Å (N.B.S. Tables). Energy levels of excitation values as high as 6.9 eV were excited in the CrI spectra. In this first group of transition metals a weak continuum or broad band radiation was detected over the region 2500 to 5500 Å. This continuum emission will be discussed further in section 4.3.3.

Spectra from the second group of transition metals were found to be much simpler, particularly in the case of Cu where the dominating feature was the CuI resonance doublet at 3247 Å and 3274 Å. It is interesting to compare ratios of the population of the $4p^2P^o_{3/2}$ and $4p^2P^o_{1/2}$ levels responsible for the resonance transitions. Published values available to date are compared with the present study, the values obtained in arc discharges and a value measured in the experimental apparatus using a Varian hollow cathode lamp operated at 3 mA, in Table 4.1A, B, C.

TABLE 4.1A

CuI Resonance Doublet

λ	Transition	J
3247.5	$4s^2S - 4p^2P^o$	1/2 - 3/2
3274	$4s^2S - 4p^2P^o$	1/2 - 1/2

TABLE 4.1B

Ion-Induced Data

Author	Fluit	Thomas & De Kluizenaar		Present Study		
Ion	Ar^+	Kr^+	Kr^+	Ar^+	Ar^+	N_2^+
Energy (Kev)	15	10	10	50	80	50
Angle of Incidence(^{o})	?	0	0	45	45	45
Vacuum (Torr)	?	8.10^{-8}	$5.10^{-5}0_2$	5.10^{-8}	1.10^{-7}	1.10^{-7}
I 3247.5	4500	160	220	3880	8550	670
I 3274	2500	87	120	2150	4780	360
Ratio	1.8	1.84	1.84	1.8	1.8	1.85

TABLE 4.1C

Arc Excitation Values

Reference	NBS	Striganov	Moore	Zaidel	MIT	Kayser
3247.5	5000	10000	1000	500R	5000R	1000R
3274	2500	10000	600	300R	3000R	500R
Ratio	2.0	1.0	1.7	1.7	1.7	2.0

Hollow Cathode Ratio - 1.75

It can be seen from the tabulated data that for the ion induced optical spectra a result of mean value 1.82 is obtained for the ratio of the intensities. This value appears to be consistently obtained irrespective of ion energy, ion type, angle of incidence or vacuum conditions. Conversely a significant variation in arc excitation data is observed. This is most certainly due to the difficulty in obtaining stable arc conditions and the difficulty of analysing

photographic plates. The CuI resonance emission in an arc discharge is also subject to self reversal due to absorption and in Table 4.1C the measurements subject to line reversal are indicated by the letter R. The hollow cathode lamp gave a value of 1.75, again very close to the ion induced data. These values are also close to the ratio of the statistical weights of 2.0.

Almost all of the lines listed by Striganov and Sventiskii for the region 2000 to 6000 Å in the CuI spectrum were detected. The lines identified are shown on the energy level diagram of Fig 4.3. A small number of transitions from the CuII spectrum were also detected, the strongest being the $4p^3F^o - 4s^2\ ^1G$ and $4p^3D^o - 4s^2\ ^1G$ transitions at 3687 Å and 4044 Å respectively.

Of particular interest in the CuI spectrum were the presence of transitions between the ^4D and ^4F terms. The ^4D term arises from the electron configuration $3d^9 4s5s$ and lies above the series limit of the normal doublets (0.64 eV above the ionisation potential, *Striganov and Sventiskii, 1968*). In combination with the lower $^4F^o$ term ($3d^9 4s4p$), sharp and diffuse emission lines are known to occur in arc spectra (*Allen, 1932*) depending upon the J value of the upper state. Whenever the upper state is a $^4D_{5/2}$ or $^4D_{3/2}$ the emission lines are broad and diffuse, an example being the $4F_{7/2} - {}^4D_{5/2}$ at 4586.97 Å. The reason for this broadening was put forward by *Wentzel and Shenstone (1926-1931)*, and is due to the atomic process of autoionisation. An atom excited to an energy state above the series limit is in such a condition that a spontaneous transition, resulting in the effective ejection of an electron, will occur and the atom will return to the series limit usually as a ground state ion (*Foster, 1964*). If the probability of the electron

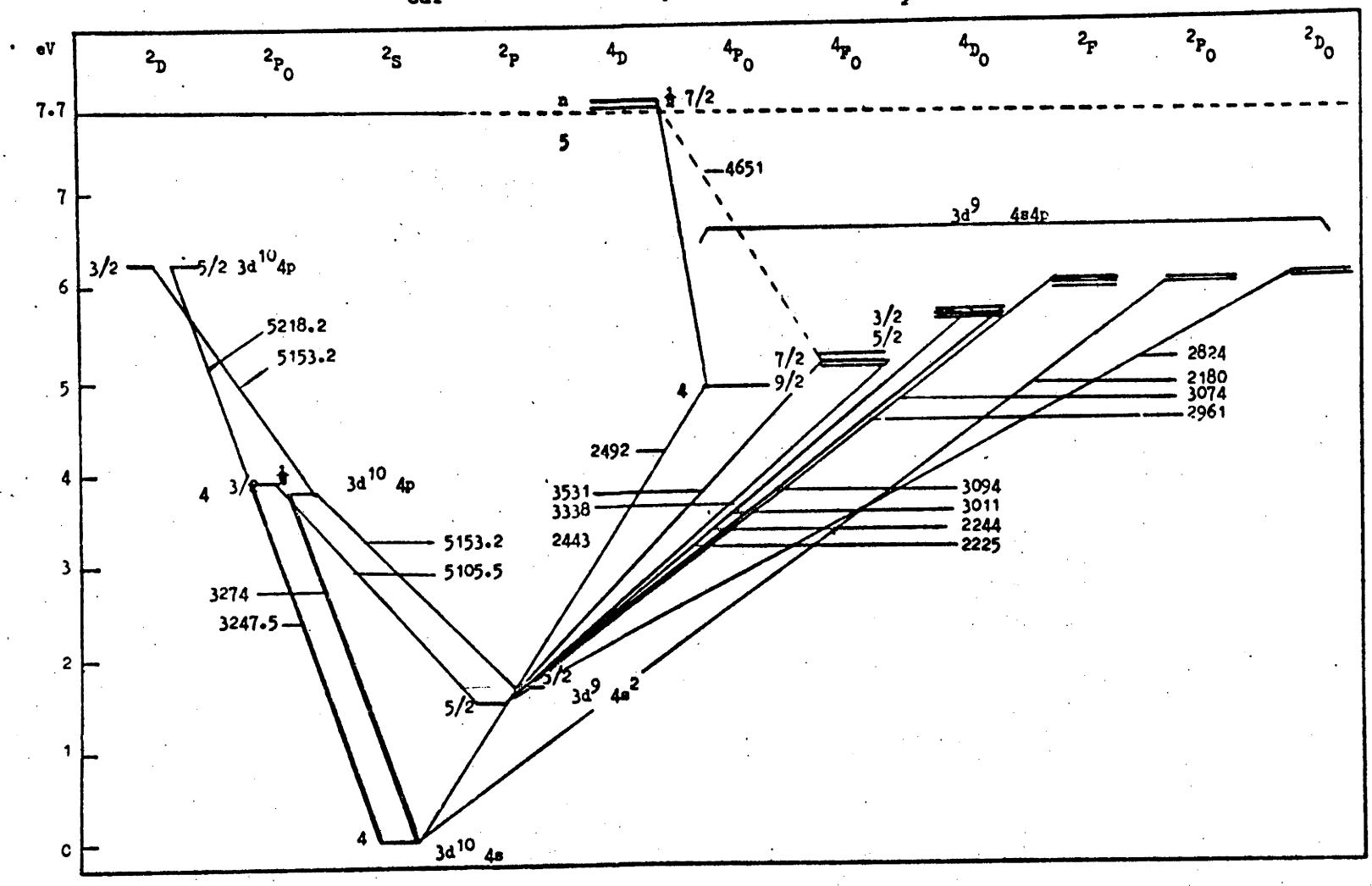

FIG 4.3 ENERGY LEVEL DIAGRAM OF CuI

transition into the continuum state is large the lifetime of the autoionising state becomes very small 10^{-13} sec to 10^{-15} sec and therefore according to the uncertainty principle $\Delta E \Delta \tau \simeq \hbar/2\pi$, any emission line involving this state becomes broadened.

The autoionisation process is of importance to the *Blaise and Slodzian (1970)* theory of secondary ionisation. Briefly, it has been suggested by the authors that secondary ion emission from copper proceeds via an excited autoionising state of the atom M* ($3d^9 4s5s$ configuration of Cu). The atom subsequently decays by an autoionising or Auger process of the type $M^* \rightarrow M^+ + e^-$. In the experiments discussed here the sharp transition $4F_{9/2} - 4D_{7/2}$ at 4651 Å and the very weak transition $4F_{7/2} - 4D_{5/2}$ at 4587 Å, were in fact detected but poor counting statistics prevented any measurements of the relative half widths of these emission lines. The 4587 Å line has also been observed during 8 KeV He^+ bombardment of Cu (*Gabla et al, 1974*). The detection of these emission lines further illustrates the similarity between the ion-induced and arc-excited spectra and provides some evidence in support of the Blaise and Slodzian model.

4.3.3 Zr, Nb, Mo, Hf, Ta, W

The heavy element group listed above all gave rich spectra under inert and reactive ion bombardment, but the most prominent feature was a strong broad-band emission extending over the region 2500 Å to 5500 Å. A comparison of the continuum from V, Ti and W under a variety of conditions is shown in Fig 4.4. The continuum is far more pronounced for certain elements in the heavy atom group and the effect is strikingly shown in the logarithmic intensity versus wavelength plots of Fig 4.5. In this figure the overall shape of the continuum for 45 KeV Ar^+ bombardment of Zr, Nb and Mo

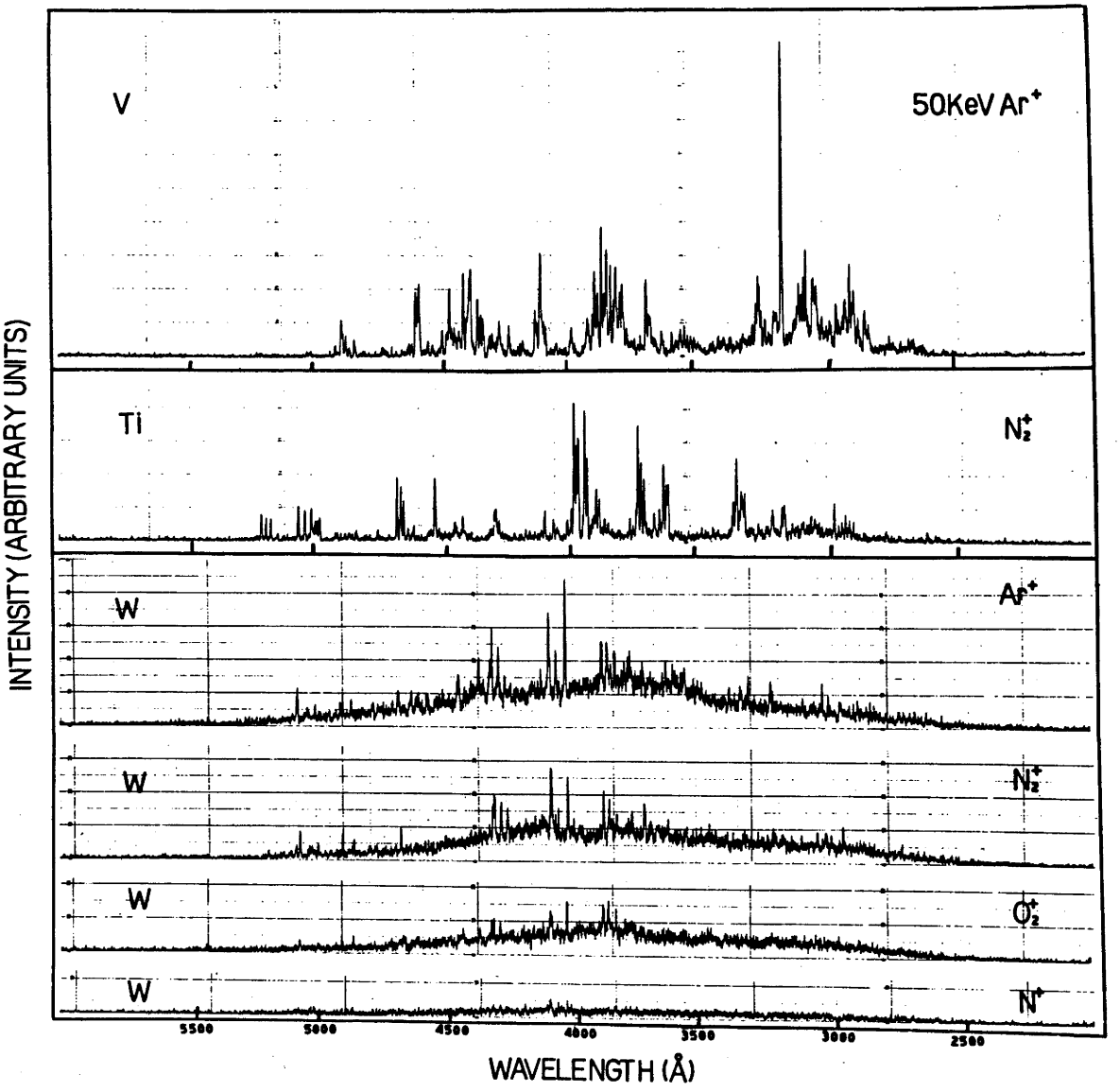

FIG 4.4 PHOTON SPECTRA FROM WEAK AND STRONG CONTINUUM EMITTERS.

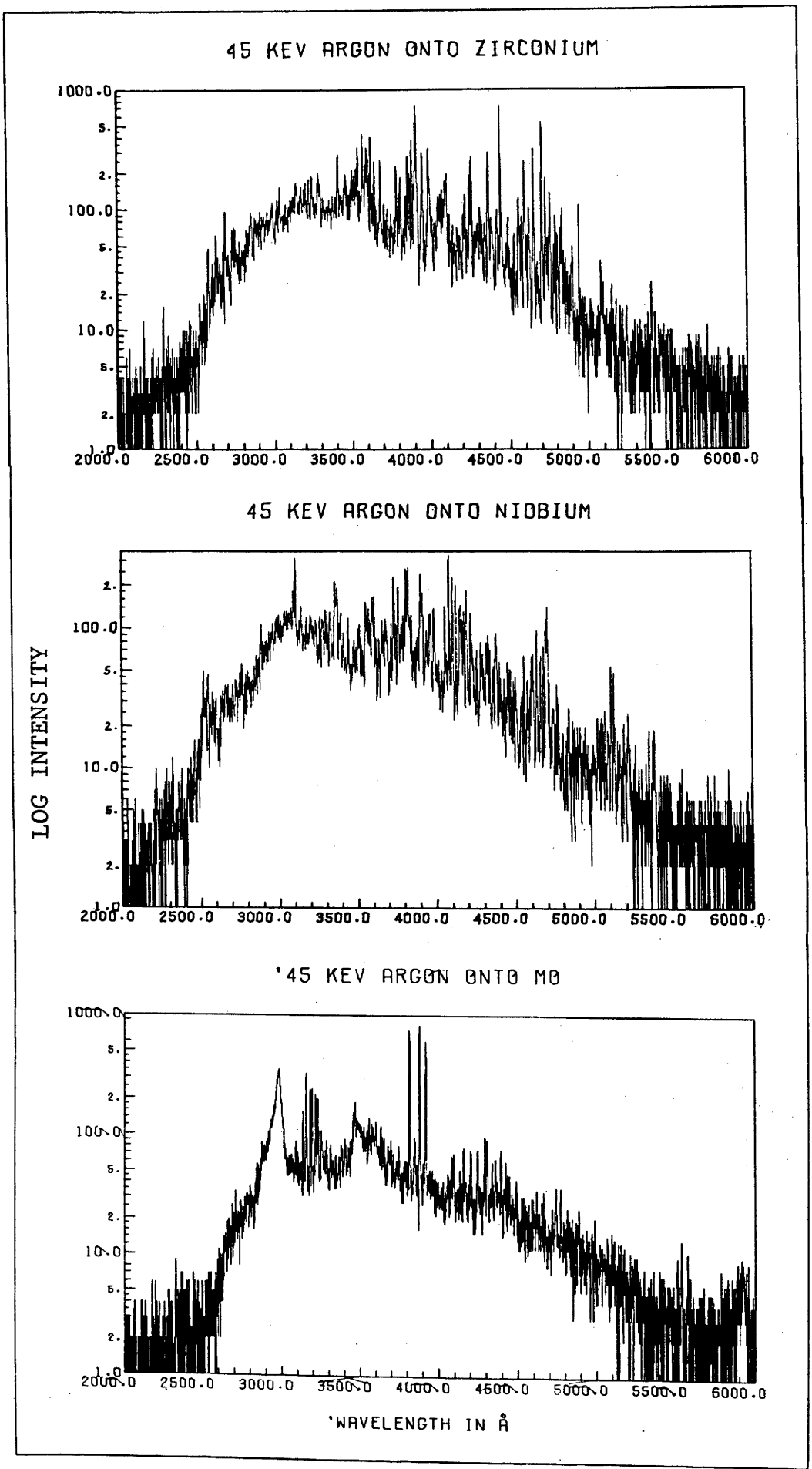

FIG 4.5 PHOTON SPECTRA FROM CONTINUUM EMITTERS.

is seen to be very similar. When corrections were made for the transmission function of the detection system, the shape of the continuum was only marginally intensified at the long wavelength end. As reported by a few researchers (*White et al, 1976, Kerkdijk et al 1976)*, some structure was detected in the Mo continuum (Fig 4.5). A broad peak at 2960 Å, 3465 Å and 3560 Å was evident as well as strong MoI emission lines.

In order to determine whether or not the continuum radiation was produced inside or outside of the target a simple experiment was performed. The target was bombarded at a slightly negative angle with respect to the monochromator such that only radiation produced in front of the target was detected. The target was then moved backwards using the translational movement and the decay of the photon signal measured. A typical result for 80 KeV Ar^+ bombardment of Mo is shown in Fig 4.6 for two MoI emission lines (3798 Å and 3864 Å) and a continuum region at 2957 Å for a decay distance of 2.5 mm in front of the target surface. The result is very similar to that published by White and Kerkdijk and indicated that the lifetime of the excited state of the continuum radiation was somewhat longer than that of the atomic emission lines.

(Kerkdijk et al 1976)

It is currently thought that the continuum is produced by excited neutral clusters, most probably dimers, sputtered from the target by the ion beam. Confirmation of this hypothesis should be provided by the study of the sputtered atoms and molecules, but since the radiating species appear to be neutral *(Kerkdijk et al 1976)* post-ionisation techniques must be employed.

Oechsner and Gerhard, 1974, have studied the mass spectra of neutrals sputtered by 1 KeV Ar^+ from 11 different metals, using a hf plasma technique. Among the targets studied were Zr, Mo, Hf, Ta and W, all strong continuum emitters. However, the results

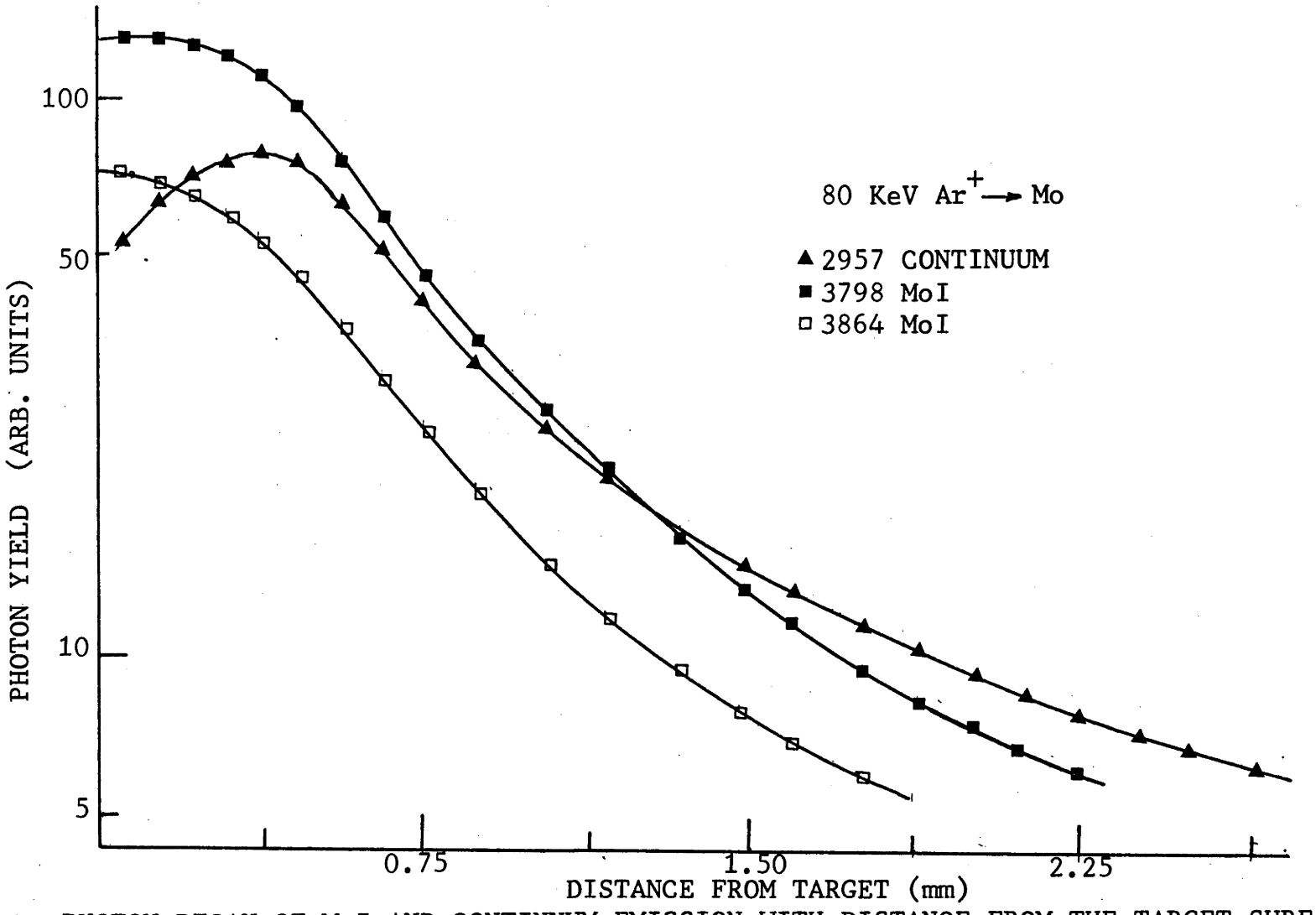

FIG 4.6 PHOTON DECAY OF MoI AND CONTINUUM EMISSION WITH DISTANCE FROM THE TARGET SURFACE.

indicated that the ratios of diatomic species Me_2 and neutral triatomic complexes Me_3 to monatomic atoms R_{21} and R_{31}, were of the order of 1.5 to 3×10^2 for R_{21} and 2.4 to 10×10^4 for R_{31} for the continuum emitters, and ranged from 3.8 to 11.7×10^2 and 6.3 to 11.3×10^4 for other metals. The greatest number of molecular species were found to originate from Au, which does not emit a broad-band continuum. There have been no other published values of these ratios to date and further work is necessary to confirm these results, particularly at higher bombarding energies, (since the intensity of the continuum is known to increase with incident energy, *Tolk et al 1973*). The measurement of neutral atom complexes is also further complicated by cluster formation mechanisms and stability of the molecules during post-ionisation.

A correlation does exist between the targets which give rise to continuum emission and the particular electronic structure of the free atoms. Elements of the fourth period of the periodic table in which the free atom possesses incomplete d shells are known to be broad band emitters. The valence electrons are responsible for the bonding of elements and more specifically the cohesive energy of the solid. The cohesive energy (energy required to dissociate 1 g - at. of a solid substance into free atoms at $0^{\circ}K$) is directly related to the occurrence of continuum radiation. The cohesive energy varies from a minimum of 15.41 K cal/g - at. for mercury to a maximum of 199.7 K cal/g - at. for tungsten, throughout the periodic table (*Gschneidner, 1974*). Table 4.2 shows the correlation between the cohesive energy and the continuum emitters observed by *Gritsyna, 1976, White, 1976, Van der Weg, 1975, Kerkdijk, 1976* and the present study. The maximum in the cohesive energy occurs at the configurations d^3s^2 (vanadium) and d^4s^2 (tungsten). Above a value of 135 Kcal/g - at.,

(5.9 eV per atom), the continuum is very pronounced, whereas elements with cohesive energy below 80 K cal/g - at. (3.5 eV per atom) do not produce any continuum radiation.

TABLE 4.2

The Relationship between Continuum Emitters and Cohesive Energy

Target Element	Electron Conf.	Cohesive Energy	Gritsyna (1975)	White (1976)	Kerkdijk (1976)	V.D.Weg (1975)	Present Study
Mg	$2p^6 3s^1$	35	-		-		-
Al	$3s^2 3p^1$	77	-		-		-
Sc	$3d^1 s^2$	80					W
Ti	$3d^2 s^2$	112			+	+	W
V	$3d^3 s^2$	122	+		+		W
Cr	$3d^5 s^1$	95	+				W
Fe	$3d^6 s^2$	99				+	W
Ni	$3d^8 s^2$	102	+			-	W
Cu	$3d^{10} s^1$	81	-	-		-	-
Zn	$3d^{10} s^2$	31	-				-
Zr	$4d^2 5s^2$	146	+		+	+	S
Mb	$4d^4 5s^1$	174	+		+		S
Mo	$4d^5 5s^1$	157		+	+	+	S
Hf	$5d^2 6s^2$	146	+				S
Ta	$5d^3 6s^2$	187	+	+	+	+	S
W	$5d^4 6s^2$	200	+	+		+	S
Pt	$5d^9 6s^1$	135	+				W

Key: + continuum reported
- no continuum
W weak
S strong

4.3.4 Ag, Pt, Au, Pb

The noble metals when bombarded with either inert or reactive molecular ions gave very simple spectra characterised by only a few intense neutral lines. The spectra for 45 KeV Ar^+ bombardment of Ag Au and Pb are shown in Fig 4.7. The most interesting feature of each spectrum is the presence of a number of weak, broad emission lines in the wavelength interval 3500 to 4500 Å. These emission lines can be attributed to ArI and ArII. Some 23 lines of Ar were detected in this region from a Pb target by *Gabla (Private communication, 1975)*. These were the only spectra in which optical emission from the primary ion was detected although some emission may have been present in spectra from other elements but was not resolved from the target atom lines. The width of the Ar lines were approximately 5- 10 Å broad as compared to the target atomic emission lines of ~3 Å (limit of the monochromator resolution).

The most intense emission lines arising from the de-excitation of sputtered Ag target atoms were the $5^2S_{1/2}$ - $5p^2P^o_{3/2}$ and $5^2S_{1/2}$ - $5p^2P_{1/2}$ transitions at 3281 Å and 3383 Å respectively. The intensity ratio of these lines at 80 KeV Ar^+ bombardment and 45 degrees incidence was measured as 2.1 to be compared with the statistical weight ratio of 2.

4.4 PHOTON EMISSION FROM SEMICONDUCTORS

4.4.1 Si

The bombardment of Si with reactive and inert ions of energy 50 KeV gave results very similar to those of Mg and Al under the same conditions. A region of the spectrum containing most of the emission produced under 50 KeV Ar^+ bombardment is shown in Fig 4.8A. As in the case of Mg and Al, intense emission lines belonging to the II and

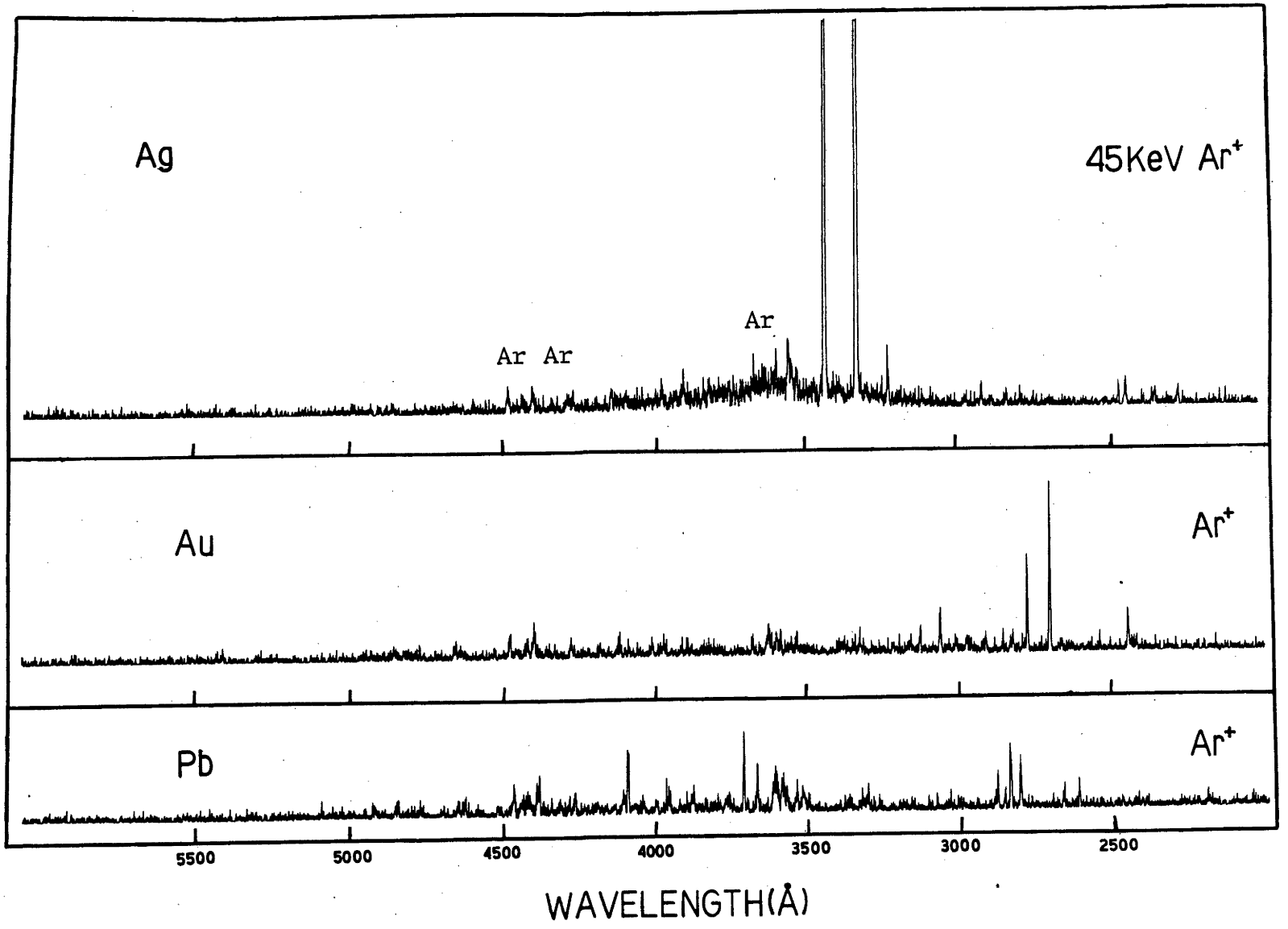

FIG 4.7 PHOTON SPECTRA FROM NOBLE METALS.

III spectra were observed. The strongest emission line was identified as the $3p\,^1P^o - 3p^2\,^1D$ SiIII transition at 2542 Å. To confirm that the emission originated from charged particles, a grid was mounted approximately 1 mm in front of the bombarded region and a positive potential of several KV applied. The neutral emission at 2882 Å was unaltered whereas the SiIII emission was decreased by approximately 40 per cent. The absence of any effect for the neutral emission was taken as evidence that the primary beam was not defocusing and causing the observed changes in the ionised emission.

Under reactive ion bombardment the relative intensities of the SiIII and SiI emission lines were considerably altered (Fig 4.8C,D). Further observations were made of the relative intensities of the SiIII to SiI emission lines as a function of current density in a background pressure of 5.10^{-7} Torr. using 45 KeV Ar^+ bombardment. At a current density of 15 μA cm^{-2} the ratio of the SiI 2882 Å and SiIII 2542 Å lines was near unity. However, at a density of 60 μA cm^{-2} the ratio of SiIII/SiI was 2/1 as in Fig 4.8A. The intensity of the SiI line increased by a factor of two and the SiIII line by a factor of 4, i.e. linearly with beam current. These results can be understood on the basis of the sensitivity of the SiI emission to target surface conditions.

In Fig 4.9 the energy levels of the SiI and SiIII emission lines are correlated with the band structure of Si and SiO_2. The values of the energy levels in Si were taken from the 50th edition of the Handbook of Chemistry and Physics. The energy levels of Si in Si and O (SiO_2) were taken from the work of *Ershov and Lukirskii (1967)*. In the diagram it is seen that the upper level of the 2882 Å transition of SiI, the $4s\,^1P^o$ state, lies opposite the energy gap of SiO_2 and opposite the conduction band of Si. If the

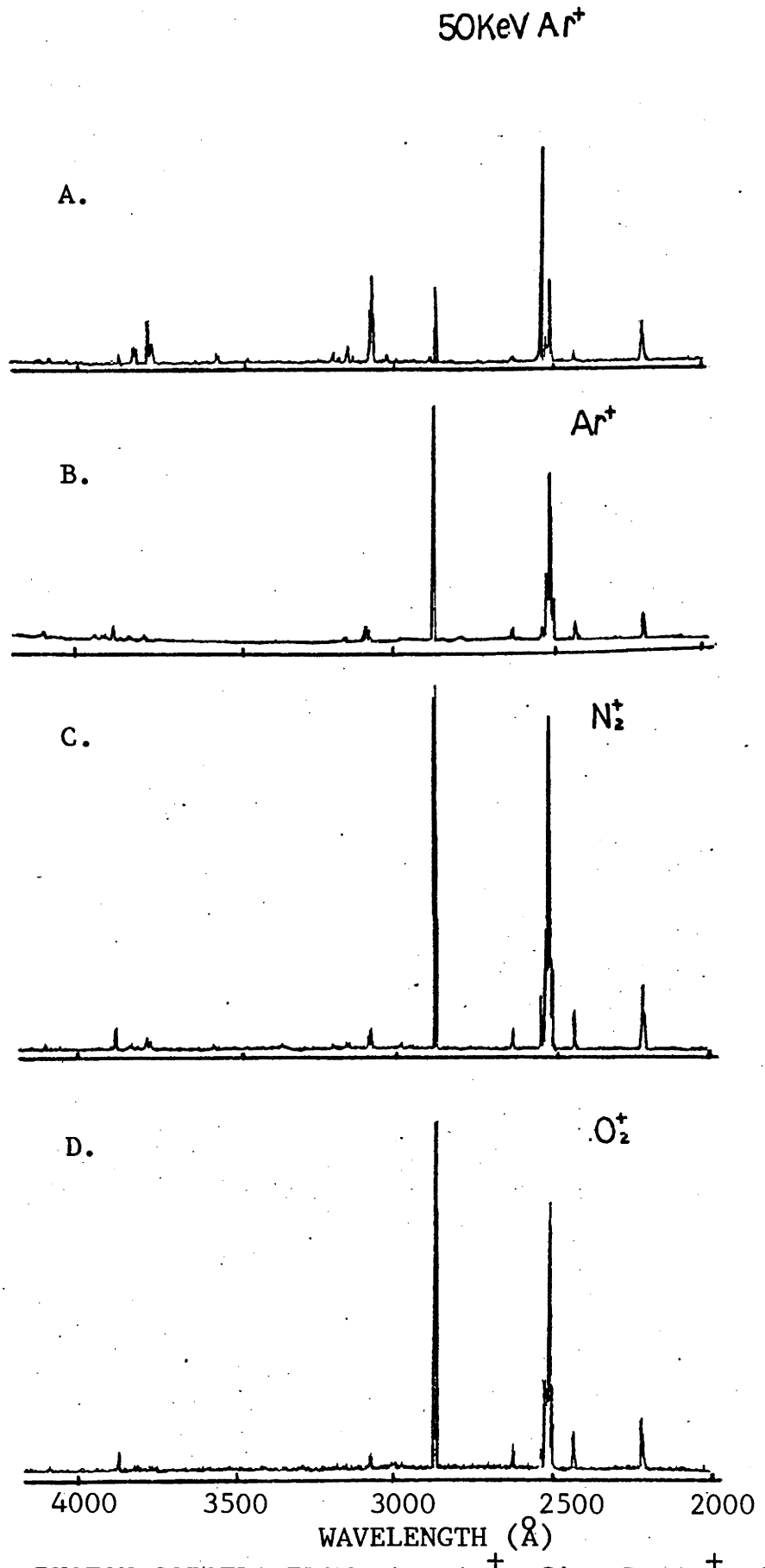

FIG 4.8 PHOTON SPECTRA FROM A. $Ar^+ \rightarrow Si$, B. $Ar^+ \rightarrow SiO_2$
C. $N_2^+ \rightarrow Si$, D. $O_2^+ \rightarrow Si$

assumption is made that the target surface takes on an oxide-like band structure when the primary ion current is insufficient to clean the surface of adsorbed background gas (mainly water vapour), then the SiI behaviour can be understood from Fig 4.9. The $4s^1P^o$ level cannot de-populate by electron exchange with the contaminated (oxide) surface but under clean conditions can de-excite by non-radiative electron exchange of the type discussed in section 2.2 with the Si surface. The SiIII level however, lies below the bottom of the valence band of Si and opposite the valence band of SiO_2. A change is therefore not expected as the surface changes from Si to SiO_2 since the electron in the excited state is unable to undergo a resonance exchange with either Si or SiO_2, and the intensity of the SiIII emission is only dependent upon the number of sputtered Si atoms.

In the case of O_2^+ and N_2^+ bombardment (Fig 4.8C,D) the ratios of the SiIII/SiI lines were identical to those from Ar^+ bombarded silica target (Fig 4.8B). The evidence obtained therefore strongly suggests that a pure silicon target rapidly takes on an oxide like structure whilst under oxygen bombardment, and it may be inferred that the same mechanisms occur for nitride formation when Si is bombarded with N_2^+ ions.

These results indicate a possible means of distinguishing between the two de-excitation mechanisms responsible for de-populating the $4s^1P^o$ level non-radiatively. As discussed in section 2.2, the excited electron can tunnel through the potential barrier by a resonance ionisation mechanism into the vacant electron states in the pure Si (transition A Fig 4.9). Alternatively, an Auger process may occur in which the atom retains its neutrality and an electron is emitted by the target (transition $\acute{B}$ $\acute{B}$) or the excited atom (B,B).

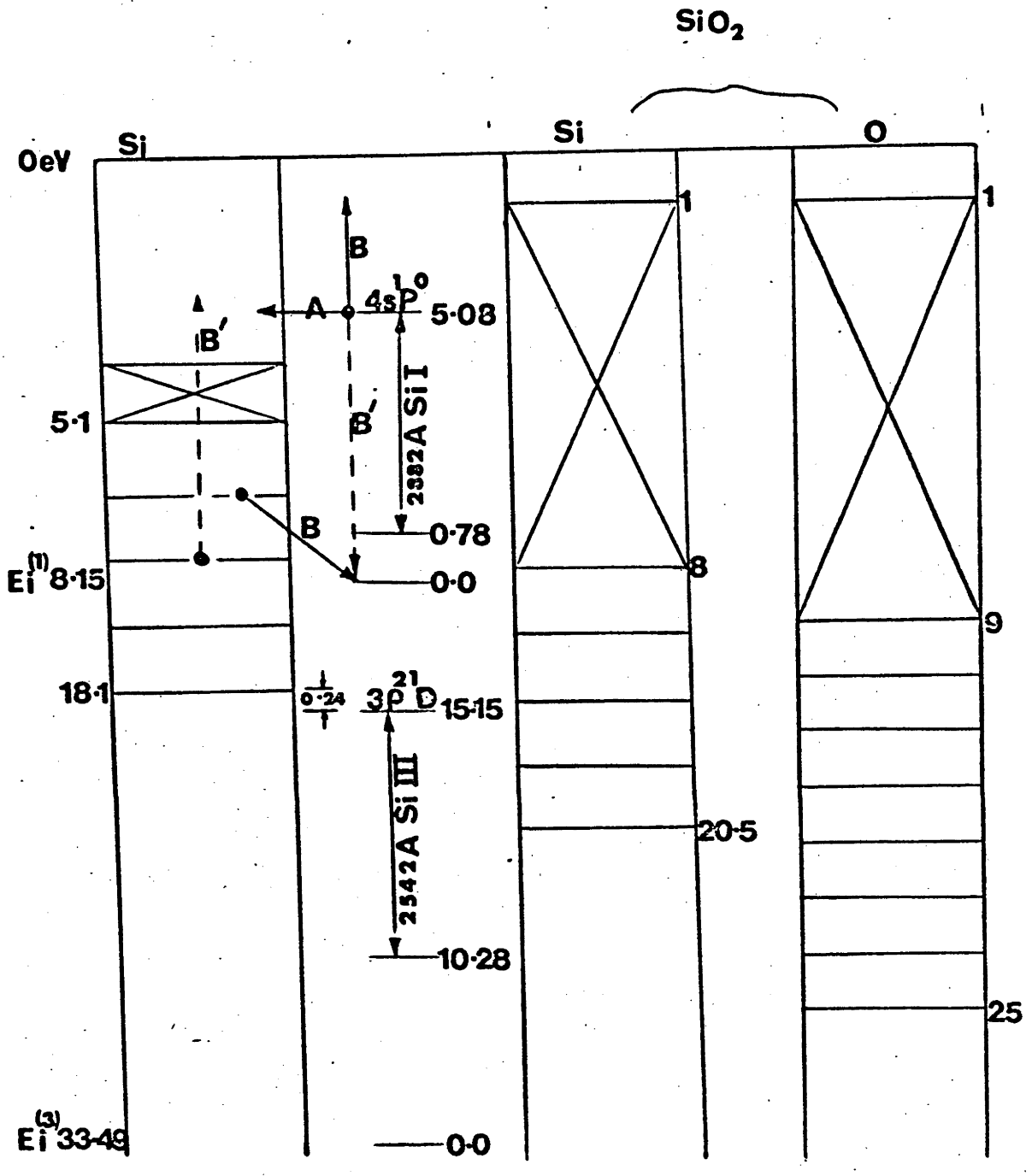

FIG 4.9 ENERGY BAND DIAGRAM OF Si AND SiO_2

AND EXCITED LEVELS OF SiI AND SiIII

An experiment based on optical and secondary ion measurements was performed to illucidate the predominant de-excitation mechanism and is discussed in Chapter Five.

4.4.2 Ge

The GeI spectrum was very pronounced under inert and reactive bombardment. The stronger emission lines occurred at 2652 Å, 2710 Å, 3039 Å and 2755 Å from the GeI spectrum. An emission line was observed at 2845 Å and was identified as the $4p^2\ ^2D_{5/2} - 4f^2F$ transition of GeII (*Lang, 1929*), the strongest transition listed for GeII in the 2000 to 6000 Å region. The only other emission identified from charged species was the $4d^2D_{3/2} - 5p^2P_{1/2}$ transition of GeIV at 2788.61 Å. (*Lang, 1929*). The Ge target appeared to be relatively unaffected under N_2^+ and O_2^+ bombardment and only slight changes in the relative intensities of the emission lines were observed.

4.4.3 III-V SEMICONDUCTORS

A series of measurements were made on a range of In and Ga III-V semiconducting compounds to determine the influence, if any, of the band gap on the ion-induced photon emission and to detect optical emission from the sputtered V elements. The materials studied were In and Ga compounds of Sb, As and P. These materials were all high purity samples obtained from R.R.E., England.

The Ga compounds all yielded strong GaI emission lines under the impact of 50 KeV Ar^+, the most intense being the transitions $4p^1P^0_{3/2} - 5s^{1\,2}S_{1/2}$ at 4172 Å and the $4p^1\ ^2P_{1/2} - 5s^1\ ^2S_{1/2}$ transition at 4033 Å. All of the weaker GaI lines listed in the N.B.S. tables were also detected. A strong emission line at about 2780 Å was also observed which could not be identified as GaI,

but was present in all Ga samples. Measurements taken on the secondary ion spectrometer (*Bayly, 1975*) indicated that there were no major contaminants in any of the samples. These results indicated that the emission line was most probably a Ga line possibly from the GaII spectrum.

The In compounds also gave strong InI emission, particularly the 4511 Å , 4102 Å, 3256 Å and 3039 Å lines. In all cases no photon emission attributable to the V elements Sb, As or P was observed, although all of these elements have strong emission lines listed in the wavelength region studied.

There has been only one reported study of ion-induced photon emission from a III-V semiconductor. *Koval and others, 1974,* studied photon emission from 25 KeV Ar^+ bombardment of (100) and (111) faces of GaAs. The authors detected the 4172 Å and 4033 Å GaI lines but could not observe any As emission since the strongest AsI lines occurred outside their detection region. However, it was proposed on the basis of the electron exchange model, that most of the GaI emission would occur only from fast Ga atoms. The slower excited Ga* atoms were assumed to be resonantly ionised. The As levels were correlated with the band gap and conduction band of GaAs, and photon emission from both slow and fast particles was expected to occur.

4.4.3.1 ENERGY BAND AND ATOMIC LEVEL CORRELATIONS

The energy of the excited levels of Ga, In and V elements are correlated with the solid state band structure of the III-V compounds in Fig 4.10. The diagrams have been drawn by assuming that the target still retains its bulk solid state structure and is not drastically altered by the crystalline to amorphous transition which is known to rapidly occur when the solid is bombarded with ions (*Naguib and Kelly, 1975*). The assignment of energies to the

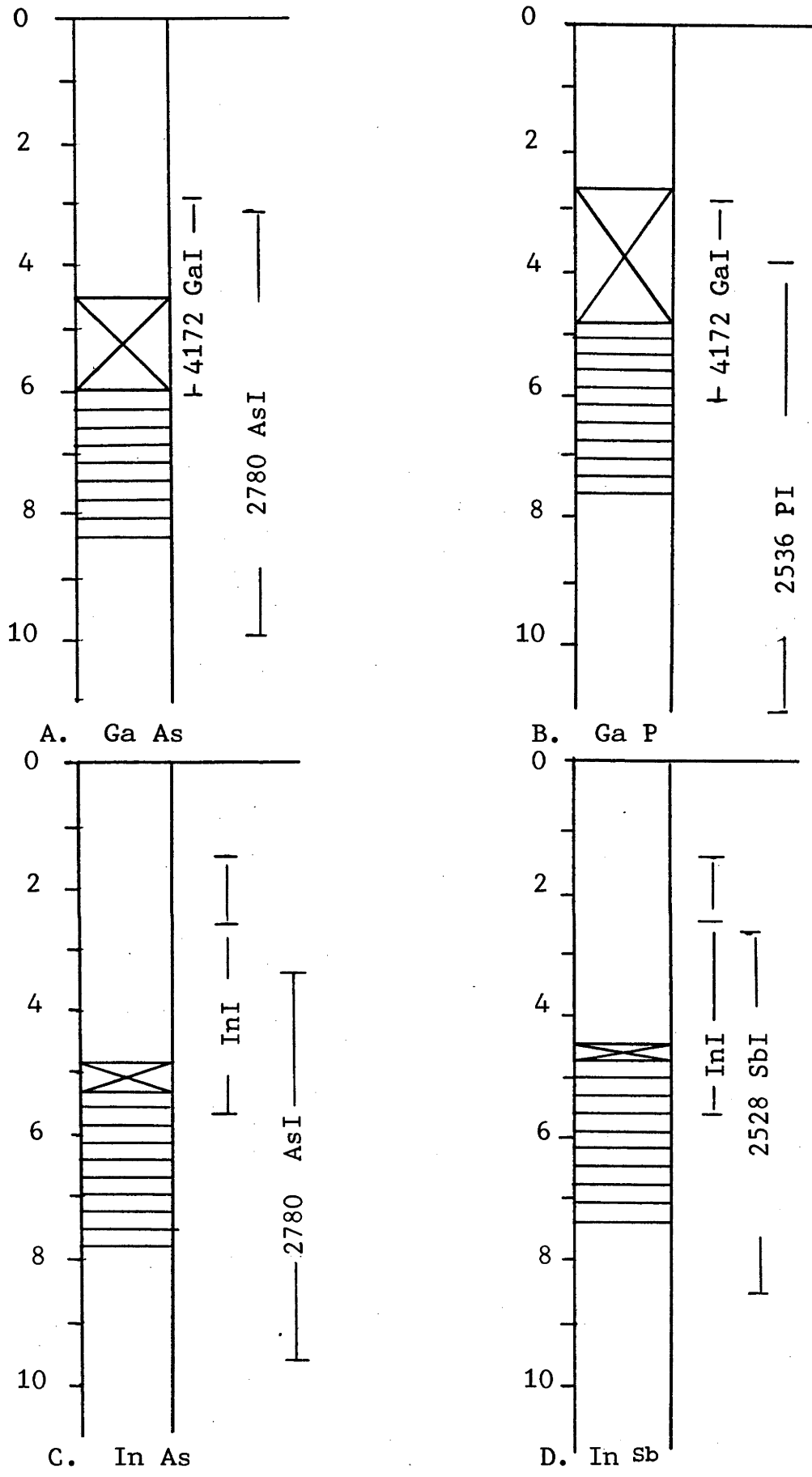

FIG 4.10 ENERGY LEVEL DIAGRAMS FOR SOME III - V SEMI-CONDUCTING COMPOUNDS.

band gaps and work functions, is based on numerous published values (*Gobelli and Allen, 1965, Sobolev and Syrbu, 1965, Wieder, 1971, Chen, 1971, Madey and Yates, 1971*).

In the case of (110) GaAs it can be seen that the upper level of both the GaI and AsI transitions, lie above the energy gap of GaAs. It therefore follows that if the simple resonant ionisation mechanism is operative in this system both Ga* and As* excited particles emitted from the solid will be de-excited and emitted as Ga^+ and As^+ ions. Fig 4.10A is slightly different to that of *Koval et al* where the authors used a work function of 3 eV and not a value of 4.7 eV as suggested by many authors (*Chen, 1970, Gobelli and Allen, 1965*).

A similar situation occurs for the excited states of Ga and Sb at the surface of GaSb, where the resonance transitions are equally probable for Ga* and Sb* atoms.

For the GaP case, shown in Fig 4.10B, the energy band diagram is such that the Ga* and P* levels are adjacent to the large energy gap of 2.2 eV (*Sobolev and Syrbu, 1964*).

In the case of InSb, InAs and InP semiconducting compounds, the energy diagrams are such that the excited atomic levels of In and the V elements are all correlated with empty electronic states in the III-V conduction bands. Examples are shown in Fig 4.10C for InAs and InSb. On the basis of these energy band diagrams an enhancement of photon emission from Ga* is predicted from GaP relative to GaAs (and also GaSb), assuming that the sputtering yields for the compounds are similar. Table 4.3 compares the relative yields from the GaI 4172 Å emission line from GaAs, GaP and GaSb. It can be seen that the Ga emission from GaP is a factor of 3 and 5 greater than emission from GaAs and GaSb respectively.

TABLE 4.3

Relative Intensity of the 4172 Å GaI Emission Line from Ga Compounds

Compound	GaSb	GaAs	GaP
Intensity	700	1200	3500

In the case of the In compounds the intensities of the InI emission lines were very similar, varying from 600 to 1000 cps. In the latter case such a variation might be expected due to the slight misalignment of the target during target replacement. The large variation in GaI emission was however reproducible over a number of experimental runs.

4.4.3.2 LINE PROFILES OF GaI EMISSION

In an attempt to confirm whether or not the excited Ga atoms were composed of predominantly fast or slow excited particles (as suggested by Koval and partially substantiated by the GaI yields from Ga compounds), the low resolution monochromator was replaced by the higher resolution Jarrell Ash spectrometer. The emission line profile of the GaI 4172 Å from both GaSb and GaP was measured under 80 KeV Ar^+ bombardment and an angle of incidence of 45^o. The result obtained is shown in Fig 4.11. The instrumental resolution is indicated by the reference profile which was obtained by scanning through the AlI 3961 Å resonance line produced by a hollow cathode lamp. The peaks of all three profiles have been normalised.

The emission line profile is seen to be asymmetric in both cases, being broadened substantially on the shorter wavelength side of the central maximum. This effect is due to the Doppler shift

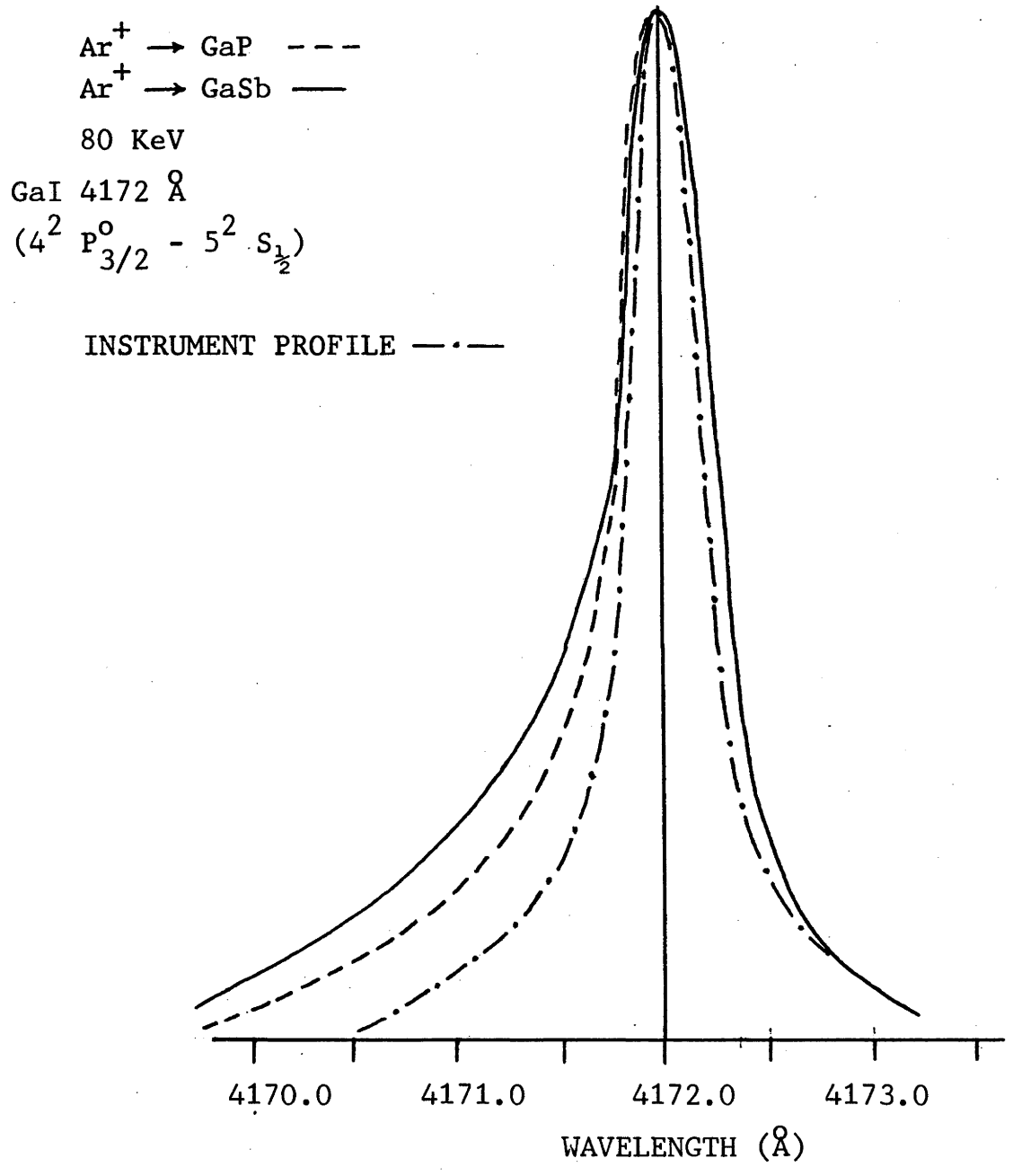

FIG 4.11 COMPARISON OF THE EXPERIMENTAL LINE PROFILES FROM GaP AND GaSb. THE RESULTS ARE NORMALISED AT THE MAXIMA.

produced by the fast sputtered particles moving towards the direction of observation, an effect observed previously by several researchers (section 2.4). However, of particular interest in these results is the difference in the intensity of the line on the short wavelength side of the peak from GaSb as compared to that from GaP. In the former the emission is marginally more intense over the 4170 Å to 4171.7 Å region relative to the central maximum. A wavelength shift of 1.6 Å corresponds to an effective energy of the emitting Ga particles of ~ 5 KeV. On the longer wavelength side of the emission line the two profiles match almost exactly. The F.W.H.M. can be estimated to give an effective energy of approximately 450 eV for the majority of the emitting particles. There is therefore evidence that the emission from GaSb is composed of relatively more faster (higher energy) particles than the emission from GaP providing confirmation of the mechanisms proposed by Koval.

4.4.3.3 PHOTON EMISSION FROM V ELEMENTS

The absence of optical emission from the elements Sb, As and P may be understood if the intensity scale for ion-induced optical emission is similar to that encountered in arc excitation. An estimate of the relative intensity of the GaI 4033 Å line to the AsI 2780 Å line can be obtained from the theoretical expression for the absolute intensity of an emission line. From standard spectrochemical relationships (*Boumanns, 1966*) the intensity Iqp of a transition between the upper state q and lower state p is given by -

(i) $$Iqp = \frac{d}{4\pi} Aqp\ h\ \nu_{qp}\ n\ g_q \exp(-E_q/KT)/Z$$

where d is the depth of the source, A_{qp} the transition probability, h Planck's constant, ν_{qp} the frequency, n the concentration or density of excited neutral atoms in the level q, g_q the statistical weight of the level, K the Boltzmann constant, T the absolute temperature and Z the partition function.

Using equation (i) and substituting the frequency for the wavelength, an expression for the relative intensity of the GaI to AsI lines is obtained in (ii) -

$$(ii)\quad \frac{I_{As}(2780\ \text{Å})}{I_{Ga}(4033\ \text{Å})} = \frac{A_{As}}{A_{Ga}} \cdot \frac{\lambda 4033}{\lambda 2780} \cdot \frac{n_{As}}{n_{Ga}} \cdot \frac{g_{2780}}{g_{4033}} \cdot \frac{\exp(-E_{2780}/KT)}{\exp(-E_{4033}/KT)} \cdot \frac{Z_{Ga}}{Z_{As}}$$

The spectroscopic data of *Penkin and Shabanova, 1963, and Lawrence 1966,* was used in the calculation, and the partition functions taken from *Drawin and Felenbok (1965).* The ratio of the concentrations of As:Ga was taken as unity (even after high doses ($\sim 10^{17}$ ions/cm^2) all of the III-V compounds studied are known to retain their stoichiometry, *Naguib and Kelly (1975).* The value chosen for the absolute temperature was 6000°K. This temperature was estimated by *Bayly (1975)* to be the temperature necessary to obtain the correct ratio of 1:1 for Ga:As using the thermodynamic Saha-Eggert equations applied to secondary ion data. The secondary ion data was taken from the same sample under similar vacuum and bombardment conditions. The value of 6000°K is also a typical 'temperature' obtained for a large number of quantitative measurements made by *Andersen et al (1973),* based on the use of the Saha-Eggert equations in secondary ion analysis.

Substitutions of the relevant values into equation (ii) gave a value of approximately 2.10^{-5} for the ratio of the AsI 2780 Å emission intensity to the GaI 4033 Å intensity. The intensity of the GaI 4033 Å line from GaAs was typically 800 cps and on the basis of equation (ii) the AsI 2780 Å line is estimated to be ~ 2.10^{-2} cps. The background count rate (dark count plus stray light) was typically 2 cps so that if the same intensity scale, predicted on the basis of equation (ii) is applicable to the ion-induced emission, the AsI emission is below or of the order of, the sensitivity of the counting system, even allowing for an error of 10^2 in the calculation.

In conclusion of this study of ion induced photon emission from III-V semiconductors, it can be stated that the experimental evidence supports the use of the transfer electron model to describe emission from the III elements. Furthermore, the failure to detect emission from V elements may be understood if it is assumed that the photon yield $\propto C \exp - E/KT$ where C is some constant such as the thermal partition function, and KT a characteristic energy describing the particular system in the L.T.E. model of *Andersen and Hinthorne (1973)*. Electronic band structure may also influence the photon emission from the V elements, but the effect could not be observed because of the photon yield which, on the basis of this model, is assumed to be very low.

4.5 PHOTON EMISSION FROM INSULATORS

4.5.1 ALKALI HALIDES - LiF, NaCl, NaBr, KCl, RbCl, CsI.

When the alkali halides were bombarded, photon emission was observed only from the cation of each compound. Low lying excited states of Li, Na, K, Rb and Cs were excited by 50 KeV Ar^+ primary ions. The strongest photon emission was produced by Ar^+ on NaCl

where some 40 Na lines were emitted. The most intense radiation was the $3s^2S - 3p^2P^o$ transition giving rise to the NaI D lines at 5889.9 and 5895.9 Å. Strong NaII emission was identified as the 3s [1 1/2]^o- 3p [2 1/2]^o transition at 3092.7 Å and the 3s [1 1/2]^o - 3p [1/2] transition at 3533 Å. In all cases no emission was detected from the adions.

In addition to the atomic line emission from the cation each halide spectrum contained broad band optical emission extending over the wavelength region 2500 - 5000 Å. The peak in the broad band emission from each compound occurred in a slightly different region of the spectrum varying from ~ 3300 Å for NaCl to 4000 Å for RbCl.

There have been very few reported results concerning photon emission from ion-bombarded ionic crystals. *White et al (1972)* have observed line and broad band emission from 5 KeV He^+ impacting CaF_2. The peak in the continuum occurred at 3000 Å and the general shape of the emission was very similar to that observed here from CsI where the peak occurred at 3500 Å. In the present study, the broad band emission was only detected when samples were bombarded at 45^o incidence. When bombarded at normal incidence or approximately 5^o negative with respect to the monochromator the continuum radiation was not observed indicating that the radiation was fluorescence from the bulk of the target.

Broad band emission has also been reported from 10-30 KeV H^+ and He^+ bombardment of aluminium by *Zivitz and Baird (1976)*, and the radiation has been explained in terms of the recombination mechanism. The authors calculated the shape of the spectral distribution expected from the electron-hole recombination model and obtained a reasonably close fit to their experimental data. Such a model may also be able to predict characteristic spectral distributions from the

alkali halides and account for the variation in the position of the peak of the intensity from crystal to crystal.

The absence of photon emission from the adion may also be interpreted using equation (i). In the case of NaCl the ratio of the ClI emission at 4526 Å and the NaI emission at 5889.9 Å is calculated to be of the order of 10^{-10}, considerably weaker than the As:Ga emission intensity ratio calculated in section 4.4.3.2.

4.5.2 POLYMERS - POLYMETHYL METHACRYLATE (PERSPEX)

$CH_2\ C(CH_3)COOCH_3$

There have been few studies of the effects of ion bombardment on polymers. *Dillon et al (1968)* have studied positive ion emission resulting from 2 KeV N_2^+ bombardment of polyethylene, polypropylene and several other polymers using a time-of-flight mass spectrometer. Large fragment ions of up to m/e 400 were detected. Photon emission from polymer films has been reported by *Gritsyna et al (1973)*. The films were produced on a substrate surface through dissociation of hydrocarbon molecules present in the residual gas in the target chamber. Emission from helium backscattered from the target surface and molecular emission from gas filled spherulites penetrated by the incident beam was observed. No emission was reported from C or H.

In the case of the perspex sample, photon emission from atomic and molecular particles was observed when bombarded with 50 KeV Ar^+ ions at a current density of 60 μA cm^{-2}. The spectrum is shown in Fig 4.12. The 2478.6 Å CI emission line was observed as well as the Hγand Hβlines. Molecular CH radiation was also identified at around 4300 Å. This emission has been reported several times by researchers and identified as CH emission resulting from

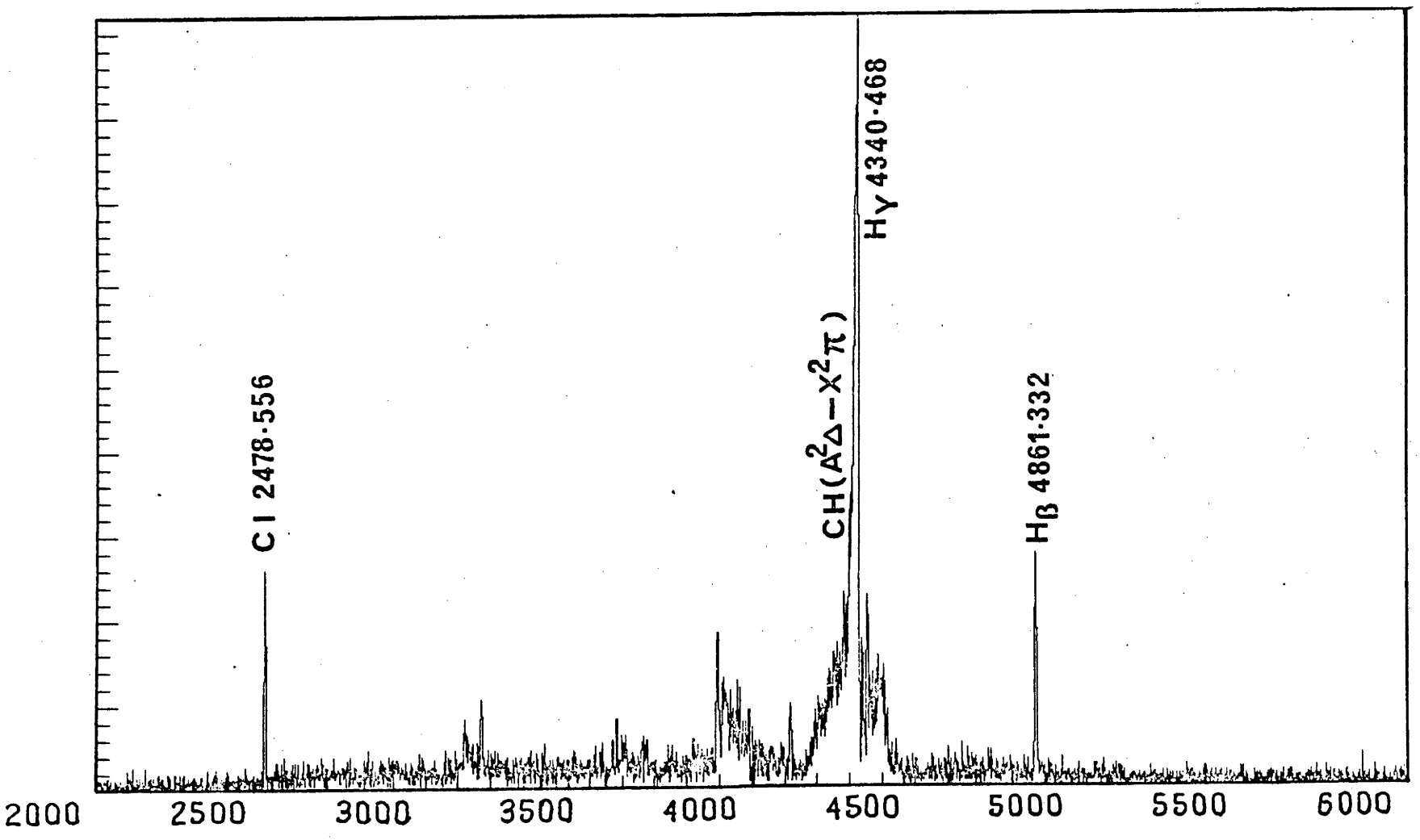

FIG 4.12 PHOTON SPECTRUM FROM AN Ar^+ BOMBARDED POLYMER

target contamination from vacuum pump oil (*Andersen et al, 1971*).

The results here then indicate that bombardment of a polymer with energetic ions leads to the sputtering of carbon, hydrogen and CH molecules in excited states in a similar manner to that produced by ion irradiation of metals, semiconductors and insulators.

4.6 SUMMARY

The survey of photon emission produced by the bombardment of a wide range of materials with inert and reactive ions has enabled certain characteristics of the emission to be recognised and indicated areas that require further study. The results can be briefly summarised by dividing the elements studied into three groups. The first group containing the light elements is characterised by strong emission from neutral particles and also charged particles. These elements are considerably influenced by reactive ion bombardment and the electronic band structure is seen to determine the relative intensities of the emission lines. The second group containing the transition elements gives rise to rich spectra similar to that produced in arc excitation, superimposed on a background continuum in certain cases. The spectra from this second group appear to be relatively unaffected by reactive ion bombardment. The third group comprising the heavier elements can be sub-divided into those that emit very strong continuum and those that give few atomic emission lines but whose spectra contain weak emission from backscattered primary particles. Again both sub-groups are relatively unaffected by reactive ion bombardment.

The detection of optical emission from secondary ions should make possible the correlation of secondary ion and photon measurements. The similarity between ion-induced photon emission and arc excitation in (a) the population of excited states, (b) the complexity of lines emitted from some elements, and (c) the intensity scale of excitation of certain elements (Cl, Br, F, I, As, P, Sb), has also enabled the anology between the two excitation mechanisms to be examined further. The following chapters are concerned with these aspects of ion-induced photon emission.

REFERENCES

ALLEN, C W, Phys. Rev., 39, 42 (1932).

ANDERSEN, C A, HINTHORNE, J R., Anal. Chem., 45, 1421 (1973).

ANDERSON, N, CARRIVEAU, G W, JENSEN, K, VEJE, E., Phys. Lett, 35A, 19 (1971).

BAYLY, A R, Unpublished data (1975).

BLAISE, G, SLODZIAN, G., J. Phys., 31, 93 (1970).

BOUMANNS, P W J M., Theory of Spectrochemical Excitation, Hilger & Watts, London (1966).

CHEN, J M., Surface Science, 25, 305 (1971).

DILLON, A F, LEHRLE, R S, ROBB, J C, THOMAS, D W., Adv. Mass. Spectry., 4, 477 (1968).

DRAWIN H W, FELENBOK, P., Data for Plasmas in Local Thermodynamic Equilibrium, Gautheir-Villars, Paris (1965).

ERSHOV, O A, LUKIRSKII, A P., Soviet Phys. Sol. Stat., 8, 1699 (1967).

FLUIT, J M, FRIEDMAN, L, VAN ECK, J, SNOEK, C, KISTEMAKER, J., Proc. 5th Int. Conf. on Ionisation Phenomena in Gases, Munich, (1961).

FOSTER, E W., Rep. Prog. Phys., 27, 469 (1964).

GABLA, L, SZYMONSKI, M, SZULKIN, M., Physica 81C, 193 (1976).

GOBELLI, G W, ALLEN, F G., Phys. Rev., 137, 245 (1965).

GRITSYNA, V V, KIVAN, T S, KOVAL, A G, FOGEL, Ya.M., J.E.T.P., 31, 796 (1970).

GSCHNEIDNER, K A., Solid State Physics, 16, 276 (1964).

HERZBERG, G., Atomic Spectra and Atomic Structure, Dover, N.Y (1945).

JENSEN, K, VEJE, E., Z.Physik, 269, 293 (1974).

KAYSER, H, Tabelle der Hauptlinien der Linienspektra aller Elememente Springer, Berlin, (1939).

KERKDIJK, C B, SCHARTNER, K H, KELLY, R, SARIS, F W., Nucl. Instr. Methods, 132, 427 (1976).

KIYAN, T S, GRITSYNA, V V, LOGACHEV, Yu.E, FOGEL, Ya.M., J.E.T.P. Lett, 21, 35 (1975).

KOVAL, A G, VYAGIN, GI, BOBKOV, V V, KLIMOVSKII, Yu.A., STREL'CHENKO, S S, FOGEL, Ya.M., Soviet Phys. Tech. Phys., 18, 1105 (1974).

LANG, R L., Phys. Rev., 34, 697 (1929).

LAWRENCE, G M., Astrophys. J., 148, 261 (1967).

MADEY, T E, YATES, J T., J.Vac. Sci. Tech., 8, 39 (1971).

MARTIN, P J, MACDONALD, R J., Phys. Lett. 55A, 483 (1976).

M.I.T. Wavelength Tables (G.R. Harrison, M.I.T. Press, N.Y.) (1939).

MOORE, C E., A Multiplet Table of Astrophysical Interest, Washington, (1945).

NAGUIB, H M, KELLY, R., Rad. Effects, 25, 1 (1975).

N.B.S. Tables of Spectral Line Intensities, Parts I, II, (1961).

OECHSNER, H, GERHARD, W., Surface Science, 44, 480 (1974).

PENKIN, N P, SHABANOVA, L N., Opt. I. Spektroskopiya, 14, 12 (1963).

SHENSTONE, A G., Phys. Rev., 28, 449 (1926).

SHENSTONE, A G., Phys. Rev., 34, 1623 (1929).

SHENSTONE, A G., Phys. Rev., 38, 873 (1931).

SOBOLEV V V, SYRBU, N N., Soviet Phys. Sol. Stat., 6, 2018 (1965).

SOBOLEV, V V., Soviet Phys. Sol. Stat., 6, 2488 (1965).

STRIGANOV, A R, SVENTITSKII, N S., Tables of Spectral Lines of Neutral and Ionised Atoms, Plenum, (1968).

TERZIC, I, PEROVIC, B., Surface Science, 21, 86 (1970).

THOMAS, G E, DE KLUIZENAAR, E E., Int. J. Mass. Spectry. Ion Phys., 15, 165 (1974).

TOLK, N H, WHITE, C W, SIGMUND, P., Bull. A M., Phys. Soc. 18, 686, (1973).

VAN DER WEG, W F, LUGUJJO, E., Atomic Collisions in Solids, two eds., S. Datz, B.R. Appleton and C.D. Moak (Plenum 1974).

WENTZEL, G., Z. Physik, 43, 524 (1927).

WHITE, C W, SIMMS, D L, TOLK, N H., Science, 177, 481 (1972).

WHITE, C W, TOLK, N H, KRAUS, J, VAN DER WEG, W F., Nucl. Instr. Methods, 132, 419 (1976).

WIEDER, H H, J. Vac. Sci. Tech., 8, 211 (1971).

ZAIDEL, A N, PROKOF'EV, V K, RAISKII, S M, Tables of Spectrum Lines, Pergamon, (1961).

ZIVITZ, M, THOMAS, E W., Nucl. Instr. Methods., 132, 411 (1976).

CHAPTER FIVE

PHOTON EMISSION FROM NEUTRAL AND CHARGED PARTICLES SPUTTERED FROM LIGHT ELEMENTS

5.1 INTRODUCTION

The study of photon and secondary ion emission from ion bombarded solids may be used to obtain information on the excitation and de-excitation processes which result from atomic collisions in solids. The theoretical aspects of these mechanisms and the experimental evidence available at the present time has been reviewed in Chapter Two. In particular the electron transfer processes (section 2.2) have been discussed in some detail since there is some confirmation that these processes are responsible for the neutralisation and ionisation of excited sputtered particles produced by ionic bombardment of some elements. No information however is available on the specific type of non-radiative electron transfer processes which occur between the sputtered particles and the target surface. In this chapter these processes are examined in detail for the specific case of the light elements Mg, Al and Si. In Chapter Four the survey study of these elements under various types of bombardment has shown that the photon emission from neutral emitters is strongly enhanced by reactive ion bombardment and the composition of the background gas (section 2.5.7). Furthermore, the photon emission can be attributed to the charged second and third spectra. The presence of charged particle emission has enabled correlations to be made with data obtained from secondary ion measurements taken on the secondary ion mass spectrometer of *Bayly and MacDonald (1976)*, from ion bombarded Si and SiO_2. In this manner more information on the processes which affect ion and photon emission from pure and

oxidised targets has been obtained.

In sections 2.4 and 2.5.3, it has been shown that the study of emission line profiles from backscattered primary ions and also sputtered neutral atoms provides a means of obtaining a value of the survival coefficient. This coefficient is an important factor in that it characterises the type of non-radiative mechanism that is responsible for de-exciting the backscattered or sputtered particles. The measurement of this coefficient is therefore expected to indicate the predominant de-excitation mechanism for the target under study. The failure to detect strong photon emission from backscattered primary particles has precluded the study of line profiles from these particles but the strong emission of sputtered neutral and ionised particles from the light elements and their oxides has enabled further information to be obtained on the shape of neutral and ion emission line profiles. The biparticle model of Van der Weg and Biermann, which has been discussed in section 2.5.3, has been applied to these measurements in an attempt to obtain values of the survival coefficients.

5.2 DE-EXCITATION PROCESSES NEAR THE SURFACE OF ION BOMBARDED SiO_2 AND Si

The results discussed earlier in section 4.4.1 concerning the changes observed in the photon emission due to Ar^+ bombardment of Si, O_2^+ bombardment of Si and Ar^+ bombardment of silica, indicated that the relative changes observed in the charged and neutral particle photon emission may be interpreted on the basis of the electron transfer model. This model has been considered in more detail for the specific case of Ar^+ bombardment of an oxide layer on a Si substrate where both secondary ion and photon emission yields have been correlated.

Specifically, the yield and energy spectra of Si^{+} and Si^{++} were compared with the yield of several emission lines in the SiI, SiII and SiIII spectra as the ion beam eroded through the oxide to the Si substrate.

5.2.1 TARGET PREPARATION

Silicon wafers (high purity transistor grade from Monsanto), were polished to a mirror finish with 6 μm diamond paste, and degreased in solvents. Oxide layers were prepared by placing several wafers in a quartz furnance tube, maintained at 950°C to 1000°C and passing wet oxygen over the silicon crystals. This method, described by *Deal (1963)*, proved to be a satisfactory technique for producing oxide films free from pin hole discontinuities. The oxide thickness was estimated from the interference colour charts of *Pilskin and Conrad (1964)* and by multiple beam interferometry. In general the oxide thickness was of the order of 3000 Å.

5.2.2 EXPERIMENTAL MEASUREMENTS

5.2.2.1 PHOTON MEASUREMENTS

The photon measurements were made using the same experimental arrangement as described in section 3.2.4 and a 45 KeV Ar^{+} beam at an angle of 45° to the target normal. Measurements were made using the Bausch and Lomb monochromator. To reduce edge effects from the non-uniform beam profile, the slit height and width was reduced to view an area of approximately 100 μm wide by 1 mm in height located in the centre of the 5 mm diameter bombarded region on the target surface. The alignment was achieved by means of a He-Ne laser. Using the data acquisition system of Fig 3.4 , two types of measurements were performed. In one the monochromator was

tuned to a given line and its intensity as a function of time was monitored during the erosion of the oxide layer with the ion beam. In the second type of experiment, sequential measurements of the intensity of the lines listed in Table 5.1 were taken as a function of time, again as the oxide layer was eroded away.

TABLE 5.1

Emission Lines of the SiI, SiII and SiIII Spectra monitored.

Spectral Type	Wavelength (Å)	Transition Lower	Transition Upper	Energy of the Levels Lower	Energy of the Levels Upper (ev)
SiI	2211	$3p^2\ ^2P_1$	$3p^3D^o_2$	0.00	5.61
SiI	2516	$3p^2\ ^3P_2$	$4s^3P^o_2$	0.03	4.95
SiI	2882	$3p^2\ ^1D_2$	$4s^1P^o_1$	0.78	5.08
SiII	3856	$3p^2\ ^2D_{5/2}$	$4p^2P^o_{3/2}$	6.86	10.07
SiIII	2542	$3p^1P^o_1$	$3p^2\ ^1D_2$	10.28	15.15
SiIII	3086*	$3d^3D_3$	$4p^3P^o_2$	17.72	21.72
SiIII	3093*	$3d^3D_2$	$4p^3P^o_1$	17.72	21.73

* line not fully resolved from neighbouring line of the same type of atom or ion.

(References, Striganov and Sventiskii; Zaidel, Prokof'ev, Raiskii).

5.2.2.2 SECONDARY ION MEASUREMENTS

Secondary ion measurements were performed on the system shown schematically in Fig 5.1. *(Bayly and MacDonald, 1976).* The target was fixed such that the ion beam was incident at 45° to the surface, and ion measurements were made normal to the surface. The target and collimator were surrounded by a cooled (-20°C) copper shield to define an electrostatic field free region and to reduce

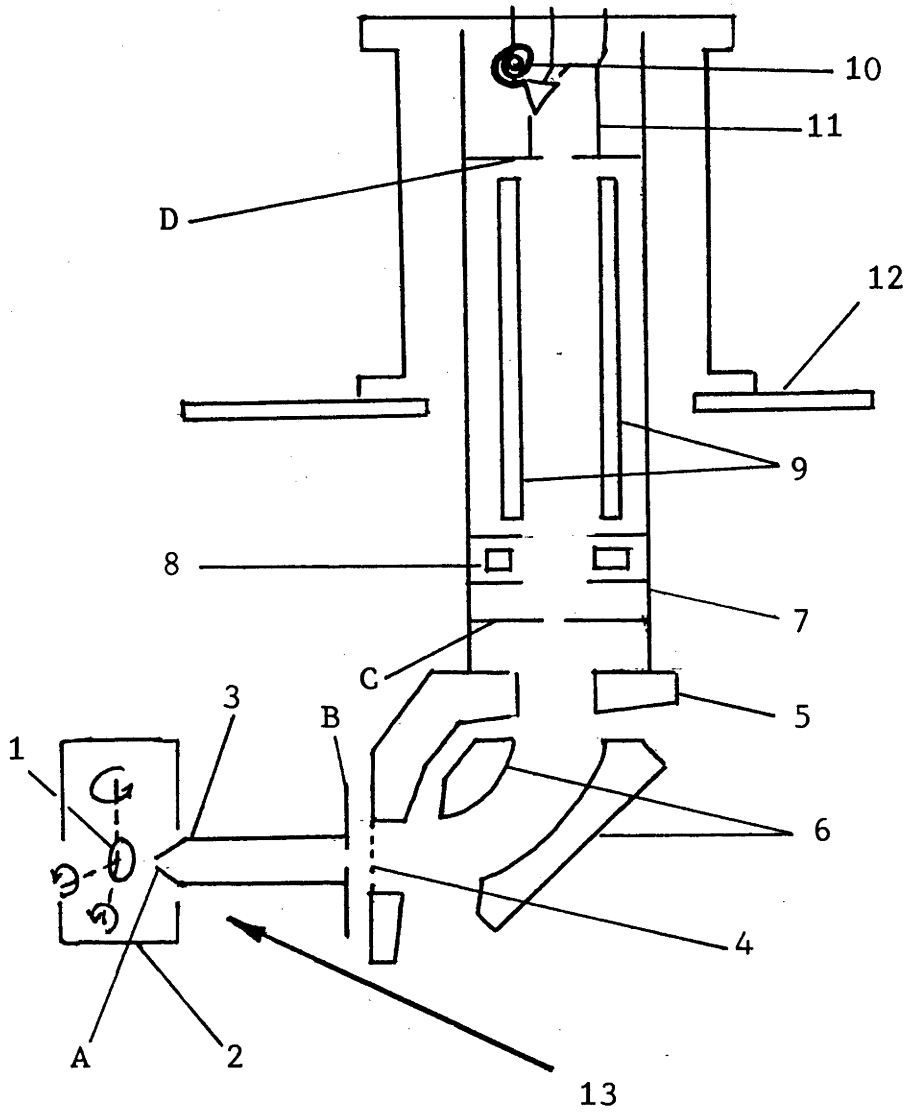

FIG 5.1 SCHEMATIC DIAGRAM OF THE SYSTEM FOR THE STUDY OF SECONDARY ION EMISSION.

(1) TARGET, (2) ELECTROSTATIC SHIELD, (3) DRIFT TUBE, (4) EXIT GRID TO DRIFT TUBE, (5) HERTZOG PLATES, (6) SPHERICAL ELECTROSTATIC ANALYSER ELECTRODES, (7) EXIT DRIFT TUBE, (8) EINZEL LENS, (9) QUADRUPOLE MASS FILTER, (10) CHANNELTRON, (11) ION DEFLECTOR FOR OFF AXIS CHANNELTRON, (12) MOUNTING FLANGE, (13) INCIDENT ION BEAM.

A, B, C, D ARE DEFINING APERTURES AFFECTING COLLIMATION, ENERGY RESOLUTION AND MASS RESOLUTION.

(Bayly and MacDonald (1976))

the water vapour pressure in the vicinity of the target surface. The target was masked with a Mo disc with a 1.7 mm aperture. The beam diameter was 3 mm and the geometrical spot, as observed by the collimator of the spectrometer was 1 mm. Using this arrangement effects from the edge of the bombarded area were minimised. To reduce surface charging, a simple electron gun capable of producing up to 100 μA of electrons, was pointed at the surface.

The system shown in Fig 5.1 consists basically of a collimator, an electrostatic energy analysing system and a quadrupole mass spectrometer. Ions were detected by an ion counting system employing a 4000 channel multichannel analyser operated in the multichannel scaling mode. The system enabled mass spectra or a sequential series of energy spectra to be measured.

In these experiments Si^{+} and Si^{++} ions were monitored continuously in a sequence of 32 consecutive energy scans, each from 0 to 200 eV, recorded in 128 channels at the rate of 1 second per channel, while the target was being continuously sputtered.

In both photon and ion experiments the same target was used, the bombarded areas separated by only a few millimetres.

5.2.3 PHOTON EMISSION RESULTS

A typical result obtained by scanning through the SiI lines studied in a single run are shown in Fig 5.2A. The lines from the excited atom show a marked drop in intensity from the oxide to the substrate. Typically these lines were found to decrease by a factor of 30, in agreement with a previous study by *White et al (1975)*. In some runs the rate of photon decay was quite rapid while in others it took somewhat longer. The broadened transition from the oxide to clean surface state is most probably a result of

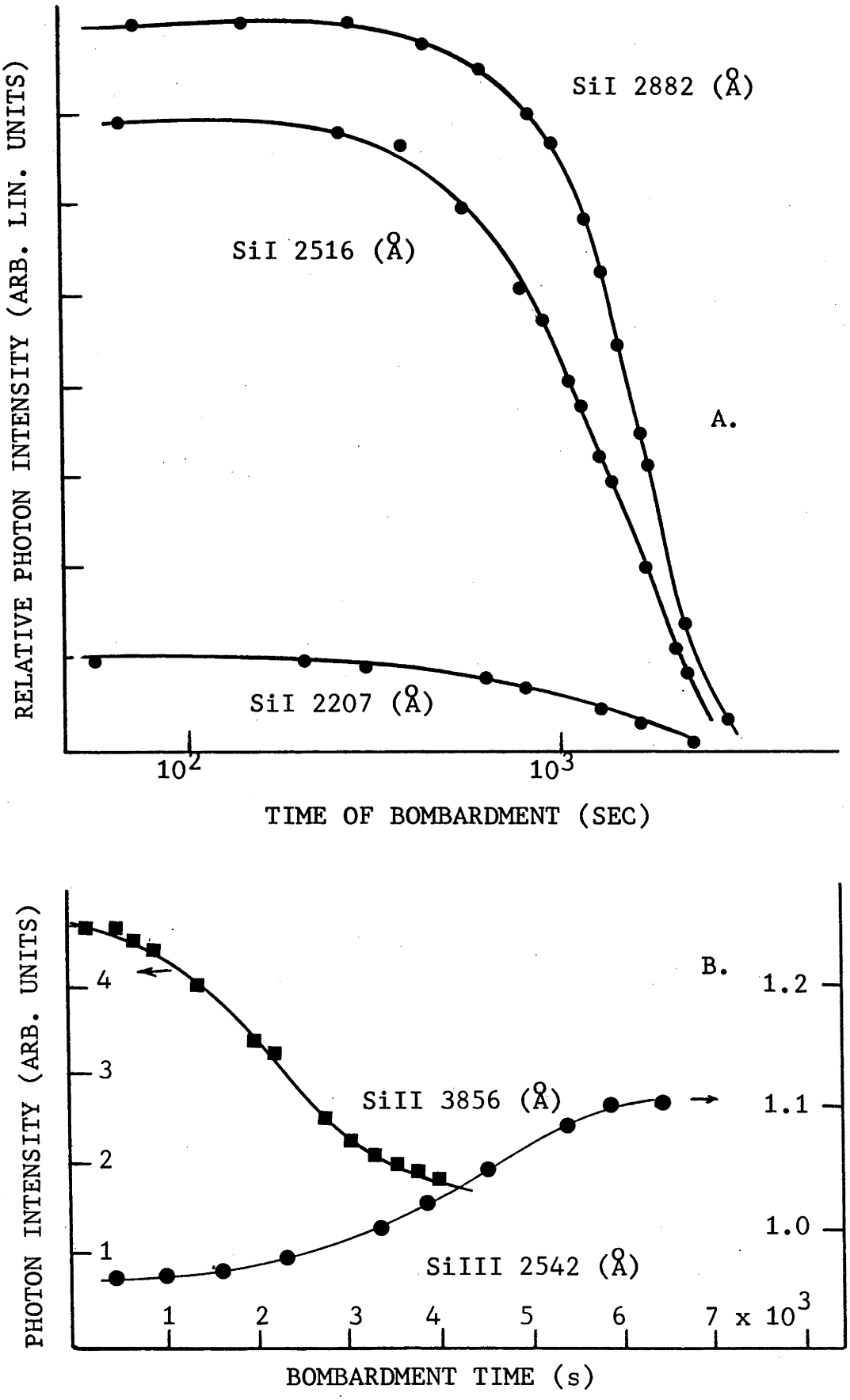

FIG 5.2 PHOTON DECAY OF SiI, SiII AND SiIII EMISSION LINES.

persisting edge effects due to the non-uniform beam intensity profile contributing to the observed photon yield and also partly due to recoil implantation effects. Such problems have been encountered elsewhere *(Kelly and Kerkdijk, 1974)*. For a detailed study of the interface, the beam must be made more uniform but this problem does not affect the present interpretation. Interference colour observations indicate that the transition through the interface corresponds to the interval of changing photon intensity.

The 3856 Å SiII emission also showed a decrease in intensity by a smaller factor of approximately 2. The SiIII lines however all showed a slight increase in intensity as the oxide layer was removed from the semiconductor. The increase was approximately 10 per cent and was reproducible in experiments where the intensity change of a single line was monitored. The changes in the photon yields of the 3856 Å SiII and 2542 Å SiIII lines are shown in Fig 5.2B.

5.2.4 SECONDARY ION EMISSION RESULTS

Fig 5.3 shows representative energy spectra from the 32 individual spectra obtained in each experiment. In this figure the change with Ar^+ ion dose of selected regions of the energy spectrum and of the total integrated yield obtained from each spectrum is shown. The change in yield from selected parts of the spectrum is the result likely to be obtained with an ion microprobe, operating with a fixed secondary ion energy pass band.

In Fig 5.3 it is seen that the Si^+ spectra change from an approximate E^{-2} energy dependence on the high energy side of the peak for emission from SiO_2, to a much less pronounced energy dependence from Si. The total yield is seen to decrease by a factor

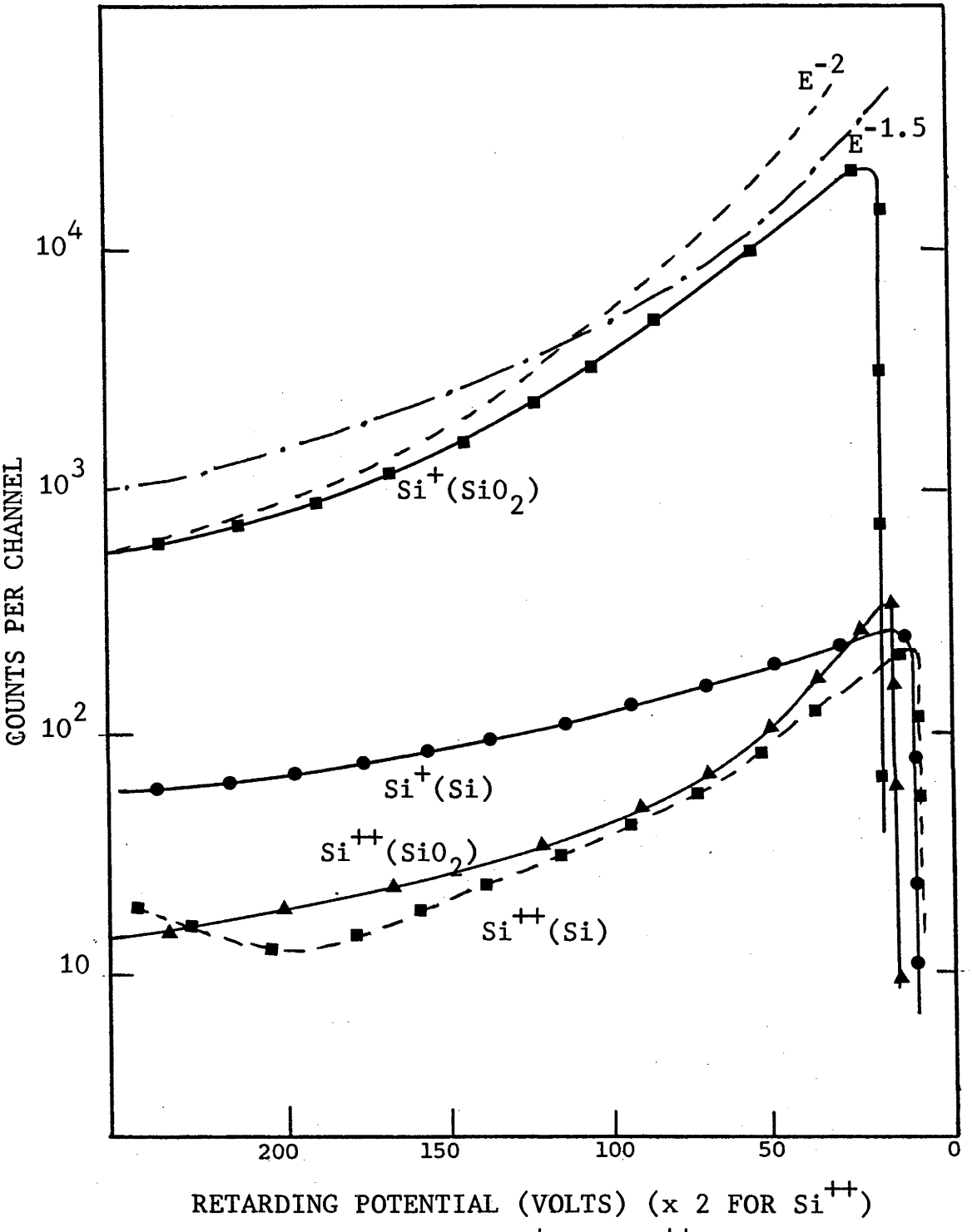

FIG 5.3 ENERGY SPECTRA OF Si^+ AND Si^{++} IONS EMITTED FROM Si AND SiO_2 DURING 43 KeV Ar^+ BOMBARDMENT OF AN SiO_2 LAYER ON Si. ENERGY DEPENDENCES OF THE FORM $E^{-1.5}$ AND E^{-2} ARE SHOWN FOR COMPARISON.

of 50, while the yield in the peak decreases by a factor of 100. The shift in peak position in going from the oxide to the Si is possibly due to a small surface charging, the equilibrium charge-up resulting in a potential of 14 eV in these experiments. The peak in the energy spectrum after correction for surface charging remained constant at approximately 12 eV.

The Si^{++} energy spectra from the oxide and clean surface were essentially the same with the exception of the high energy region, where a second high energy peak appeared to emerge. The integrated counts, low energy peak and high energy tail all showed a slow fall in yield throughout the experiment except for a sharp rise in yield at the oxide-semiconductor interface by a factor of almost 3. The Si^{+} and Si^{++} yields are shown in Fig 5.4.

The sharper transitions observed at the Si/SiO_2 interface in the secondary ion experiments compared to the broader transitions observed in the photon measurements were most probably due to the fine collimation and the use of a small aperture mask minimising the effects of inhomogeneity in the primary beam intensity profile. A calculation of the oxide thickness assuming that the interface was located as indicated in Fig 5.4, and assuming a density of 2.2 gm cc^{-1} and a sputtering rate of 4 atoms per ion at 45^{o} incidence *(Edwin, 1973)* gave a value of 2500 Å which was comparable to the interferometric value of 3000 Å. The 500 Å difference can be accounted for by the error in the ion dose measurements which were probably too low for two reasons. Firstly, the beam density at the centre of the beam spot may have been higher than the average density, and secondly, the secondary electron emission from the beam defining aperture resulted in a 10-20 per cent reduction in current measurements.

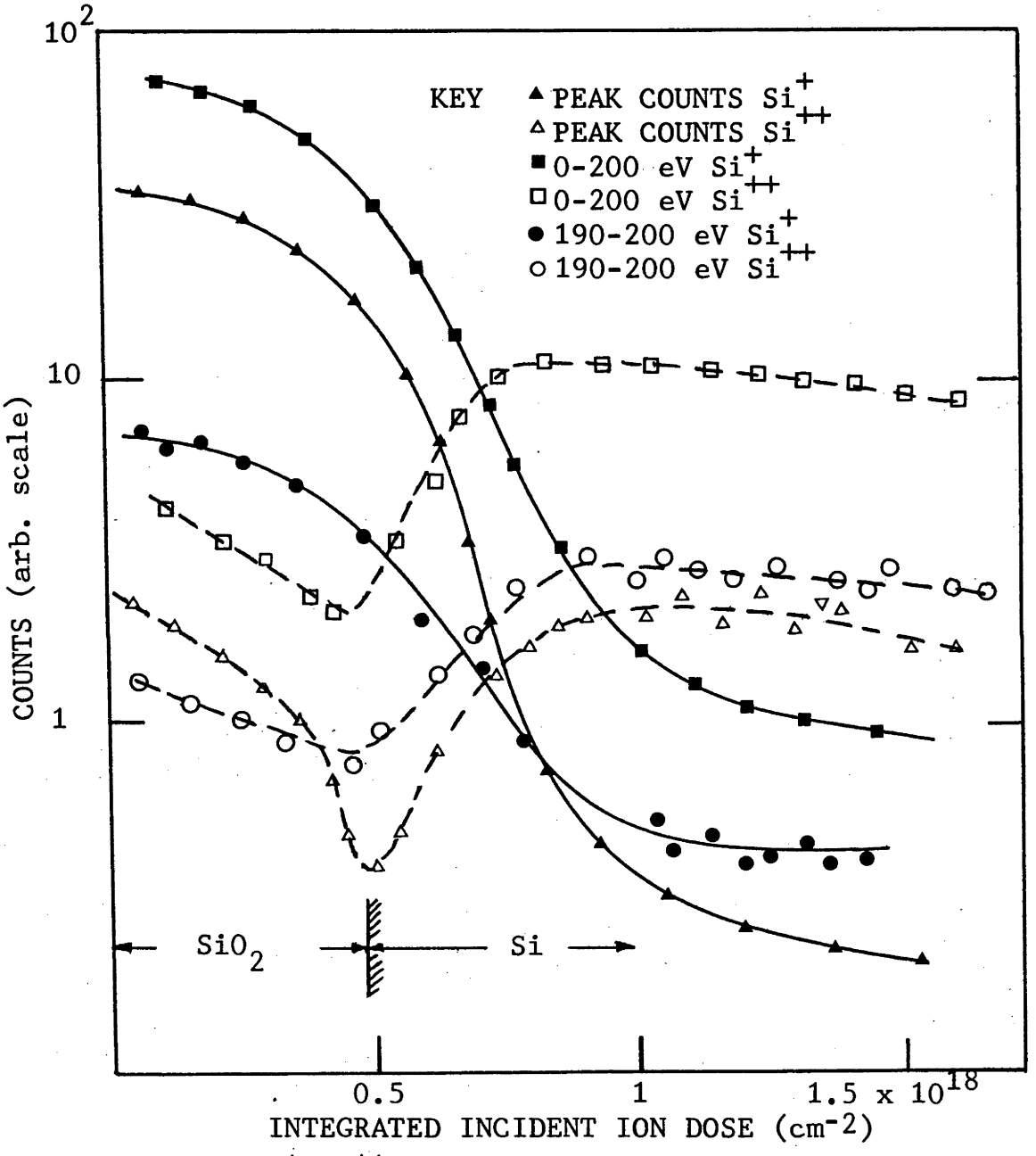

FIG 5.4 Si^+ Si^{++} YIELDS AS A FUNCTION OF ION DOSE

5.2.5 DISCUSSION OF RESULTS

The diagram shown in Fig 4.9 has been extended to take into account the energy levels of SiI, II, III emission lines and Si^{+}, Si^{++} secondary ions. The relevant electronic energy level diagram for the experiment is shown in Fig 5.5. Implicit in the interpretation of the results is the assumption that the creation of excited atoms and ions of silicon relative to the total sputtered silicon atom yield is essentially independent of whether the Si is emitted from an oxide or a semiconductor. It is also assumed that the observed changes in yield are the result of different de-excitation mechanisms occurring at the two types of surface, and that the oxide layer is in fact SiO_2 (at least away from the interface). Recent results published by *Harrington et al (1975)* (using Auger electron spectroscopy measurements) appear to confirm this assumption. Furthermore, it is also assumed that the bulk band structure of Si holds at the surface and is not significantly altered by the effect of amorphisation due to ion irradiation.

The work of White et al suggested that observed decay of the SiI emission following the transition from the oxide to the semiconductor was due to an enhanced probability of non-radiative decay of the excited state when the atom is near the clean semiconductor surface over that near the oxide. The non-radiative process was suggested to be either a resonance ionisation of the atom by transfer of the excited electron to the empty silicon conduction band states of the type A in Fig 5.5, or alternatively, an Auger de-excitation involving an electron transition of the type BB or $\overset{\prime\prime}{BB}$. These processes have been discussed in detail earlier in Chapter Two.

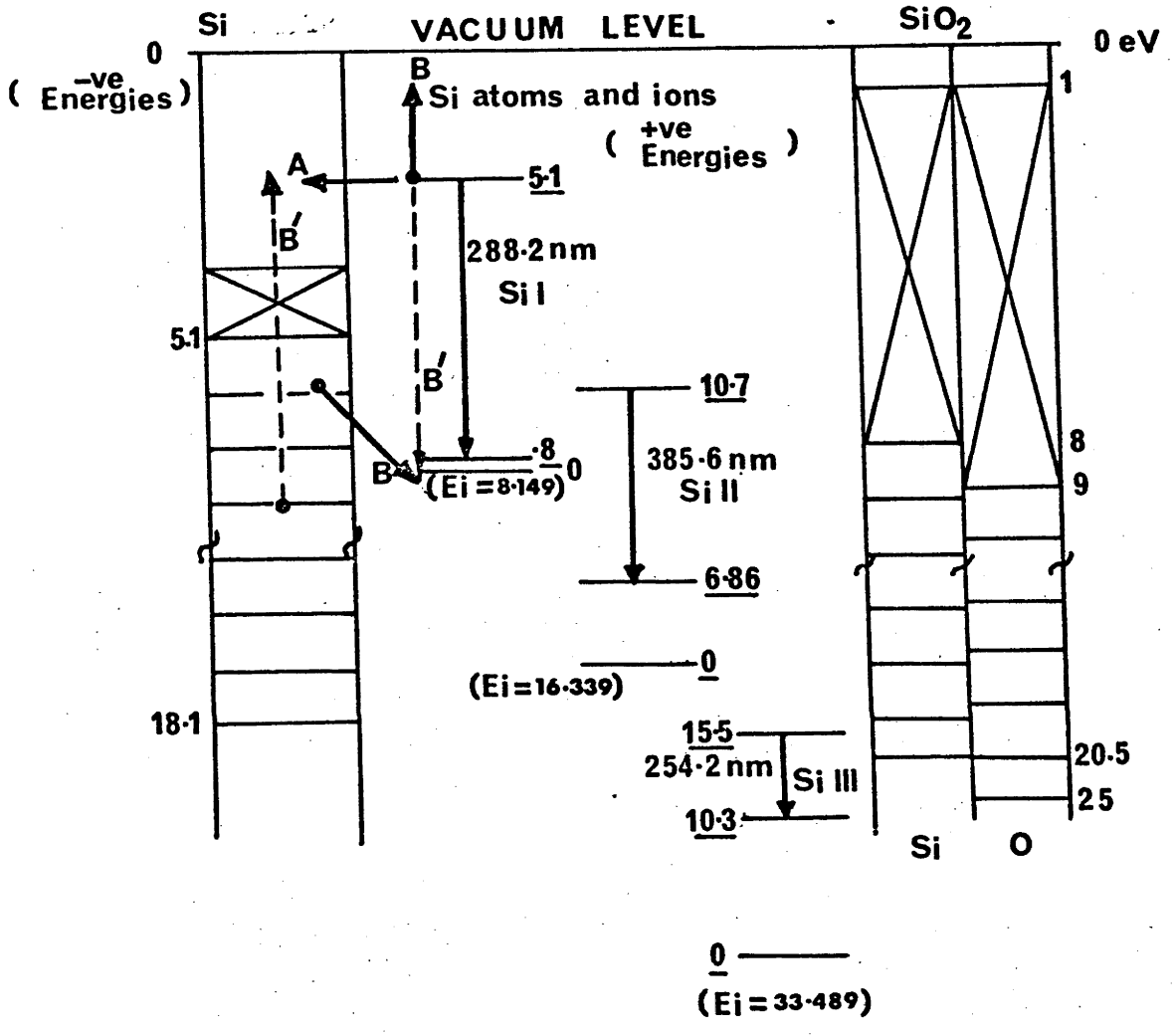

FIG 5.5 ENERGY BAND DIAGRAMS OF Si AND SiO_2 CORRELATED WITH THE EXCITED LEVELS OF ATOMS AND IONS

The Si^+ ion yield showed a very similar decay to the SiI line, both decreasing in intensity by almost the same factor. From these results some estimate can be made of the proportion of sputtered Si atoms emitted as ions (Si^+/Si) or as excited atoms ($\Sigma SiI/Si$). Assuming cosine distributions of the emitted particles, and including such factors as transmission of the secondary ion system, collection efficiency of the optical system etc. and using the data of *Andersen and Bay (1975)* for the Si sputtering yield, the proportion of ions and excited atoms emitted from the oxide are of a similar magnitude. The same is true for the semiconductor, though the proportions change, e.g. from the oxide, Si^+/Si is about 10 per cent but from the semiconductor it is more like 0.01 per cent. The simple resonance ionisation model for the decay of the SiI lines then cannot be true, since it would lead to an increase in the Si^+ yield. The decays of the SiI and Si^+ yields are so similar they must be considered closely related. The transition rates for the processes giving rise to the neutralisation and de-excitation must be very nearly equal, and this would be satisfied if both neutralisation and de-excitation involved an electron transition from the Si semiconductor valence band to the ground state of the free atom. The SiI de-excitation would then involve the emission of an Auger electron from the atom while the Si^+ neutralisation would involve excitation of an electron into the conduction band of the Si.

Alternatively, for the SiI de-excitation a resonance transfer of the excited electron of the neutral atom to the empty conduction band followed by a resonance neutralisation from the full valence band is energetically possible. The equivalent mechanism for neutralisation of the Si^+ ion would simply be the latter resonance neutralisation to the ground state or possibly the lower

excited states of the neutral atom. To account for the high ion emission from the oxide the ground state of the neutral atom must then lie opposite the forbidden gap of SiO_2. This may or may not be so since the width of the conduction band of SiO_2 is not accurately known. To distinguish between the Auger process and the double resonance process would require observation of the characteristic Auger electrons. Unfortunately the Auger electron energy from the SiI de-excitation would be ~ 0.1 eV and therefore indistinguishable from the bulk secondary electron yield.

The variation of the Si^{++} is very different to that of the Si^{+}. The behaviour in the interface region cannot be ignored. The results can be interpreted as showing a slow decay of Si^{++} yield with time, but with a rapid rise in Si^{++} yield at the interface due to rise in sputtering yield of the Si atoms. *Edwin (1973) and Andersen and Bay (1975)* have measured the sputtering yields of SiO_2 and Si and their results give yields of 1.6 atoms per ion and 1.75 atoms per ion from the oxide and the semiconductor respectively. The incident ions were 32 KeV Ar^{+} and 45 KeV Ar^{+} incident normal to the surface. Assuming the yields increase at the same rate if the incident direction is changed to 45°, the yield of Si atoms will increase by a factor of 3 in going from the oxide to the semiconductor. This is very close to the factor by which the Si^{++} yield increased sharply at the interface. The slow decrease of the Si^{++} yield could be a result of Ar build-up in the surface layer altering the cascade energy spectrum and resulting in a slight decrease of Si^{++} ions.

Consider the possible non-radiative processes involving the Si^{++} ion. The Si^{+} ground state lies opposite the filled valence bands of both semiconductor and oxide, and hence the neutralisation

probability for Si^{++} by resonant electron transfer to the ground state should only differ according to the respective density of states in these valence bands. It is possible to obtain resonance transfer of electrons from the Si valence band to an excited state of the Si^{+} ion. For example, the $4p^2$ level lies opposite the Si valence band but opposite the energy gap of SiO_2. In fact, this level is the upper level of the observed SiII transition and therefore, neutralisation of Si^{++} by this means would lead to an increase in the 3856 Å SiII emission. Rough estimates of the yields of Si^{++} and SiII photons (this SiII line was the only line from Si^{+} identifiable in the range 2000 to 6000 Å), indicate that much of the emission of SiII in this range from the Si substrate would then be due to neutralisation of Si^{++} by electron transfer to an excited state of Si^{+}.

The SiII line showed only moderate decay. From Fig 5.5 the Auger de-excitation process of the general type B,B or $\acute{B}\acute{B}$ is possible for the relevant levels of the Si^{+}, with electron transfer from near the top of the valence bands of both oxide and semiconductor to the ion ground state. This would result in Auger electrons with energies of about 5 eV from Si and 2 eV from SiO_2. Thus the change in the SiII yield would depend only on the change in the transition probabilities and consequently would be much less than in the case of the decay of Si^{+}, where the neutralisation process is blocked from SiO_2. However, the SiII emission is from an excited Si^{+}, so that Auger neutralisation similar to that postulated to account for the change in the Si^{+} yield observed in the secondary ion measurements is possible, with the excitation energy of the SiII upper level being transferred to the valence band electron from Si, in the neutralisation process. This would produce a decay in the SiII emission similar to that in the Si^{+} (and SiI) but the competing process of neutralisation

of the Si^{++} leads to an enhancement of the SiII photon yield. The combination could result in the small decrease observed in the SiII photon emission.

Estimates of yields also suggests that most of the Si^{++} emission may be in an excited state. This would aid the Si^{++} neutralisation mechanism suggested above. The behaviour of the SiIII emission was similar to that of Si^{++} in that both exhibited a net increase in emission after penetration of the oxide, but the SiIII emission does not show an increase related to the sputtering yield.

Two further points relevant to this discussion are worth consideration. Firstly, it has been suggested that the origin of ions from insulators, particularly ionic solids, lies in the breaking of the chemical bond (section 2.8). The present study of SiO_2 indicates a high proportion of particles emitted from the oxide are in a non-ionised state and this is difficult to reconcile with the chemical bond rupture model, which implies a high degree of ionisation. Secondly, the Si^{++} energy spectrum obtained from a clean surface showed some evidence of a high energy peak occurring above 400 eV. This may support the kinetic ionisation model of Joyes (section 2.8.1.1) of formation of doubly ionised ions in light elements since the model involves the formation of deep holes in the atom and the persistance of these holes to decay by Auger transitions to the ion outside the metal. This would firstly involve high collision energies and secondly fast excited atoms if the decay is to occur outside the solid. This contribution to the ionisation would therefore appear at high energies from the clean surface. *Joyes (1972)*, has discussed this mechanism in relation to the $Al\text{-}Al_2O_3$ system and some experimental evidence has been obtained which appears

to substantiate the Joyes model. *Brochard and Slodzian (1971)* measured a decrease in the Al^{++} yield from Al when exposed to background oxygen pressure of 1.10^{-6} Torr. to 6.10^{-5} Torr. *Hennequin and Viaris de Lesegno (1971)* detected the Auger electrons predicted by Joyes from Al and also found the Auger yield to decrease with oxygen partial pressure. In both cases the decrease was rapid (the Auger and Al^{++} yields), dropping by a factor of 3.

The Joyes model is worth considering in the results of the present experiment on Si. The model has been outlined earlier in Chapter Two. The kinetic emission mechanism proposed by Joyes is based on the creation of a hole on a bound level of one of two atoms involved in a collision inside a solid and the subsequent escape and de-excitation by Auger electron emission of the excited metastable to form an ion outside the solid.

The probability of hole formation may be estimated using the *Fano and Lichten (1965)* promotion model for gases. As the distance between the nuclei of the collision partners is reduced the electronic levels become molecular levels. When two levels cross it is possible for electronic exchange to occur between them such that higher levels empty before the collision can be partly filled. In the Si-SiO_2 system the collision partners of interest are Si → Si and Si → O. The correlation diagram for gaseous Si → Si (Fig 5.6A) and Si → O (Fig 5.6B) collisions show the type of molecular levels likely to be promoted during the collisions of atoms in Si and SiO_2. The diagrams have been drawn using the data of *Slater (1955)* under the same assumptions as used by Joyes for the Al → Al and Al → O cases. The correlation diagram for Si → Si shows the energy levels of Si ($R = \infty$) joined to those of the united atom (Ni) at R = 0. The initial 2p Si level gives rise to 4 molecular levels (in an identical

manner to the Al → Al case), the 4 fσ receiving the greatest promotion. According to the Joyes model the 4 fσ level, once it crosses the conduction band, may become a virtual bound state, i.e. no longer well defined but broadened such that the upper energies of the level interact with free states above the Fermi energy (Fig 2.15B) enabling electrons to escape (Section 2.8.1.1). In the Si → O situation the level receiving the largest promotion is of the 3 dσ type which joins at R = 0 at an energy of nearly -10 eV in the united atom (Ti), compared to only -0.9 eV for the 4fσ level in the Si → Si collision. The assumption is therefore, on the basis of this model, that 2p hole creation is unlikely in a Si → O collision as in an Al → O collision. The Si-SiO_2 system is more difficult to interpret than the Al-Al_2O_3 system because of the existence of the forbidden band gaps. Furthermore, the exact evolution of the 4 fσ level is not given by the correlation diagrams. As with the Al-Al_2O_3 system however, the model does indicate that the creation of a 2p hole is less likely in a Si → O collision than a Si → Si collision.

From the experimental point of view, if such a mechanism is in operation, the presence of oxygen in silicon should lead to a rapid decrease in ions which are of a kinetic nature. In this particular experiment an increase is expected in the yield of high energy ions as the SiO_2 layer is sputtered from the substrate. It might also be expected that some of these high energy ions will be in excited states and capable of emitting photons during de-excitation. The experimental results indicated a high energy peak at around 400 eV in the Si^{++} energy spectrum from the clean silicon surface and the emission from SiIII, (Si^{++}), line monitored at 2542 Å indicated a rise of only 10 per cent when the oxide was penetrated by the ion beam. However, the most intense and lowest excited state of SiIII

A.

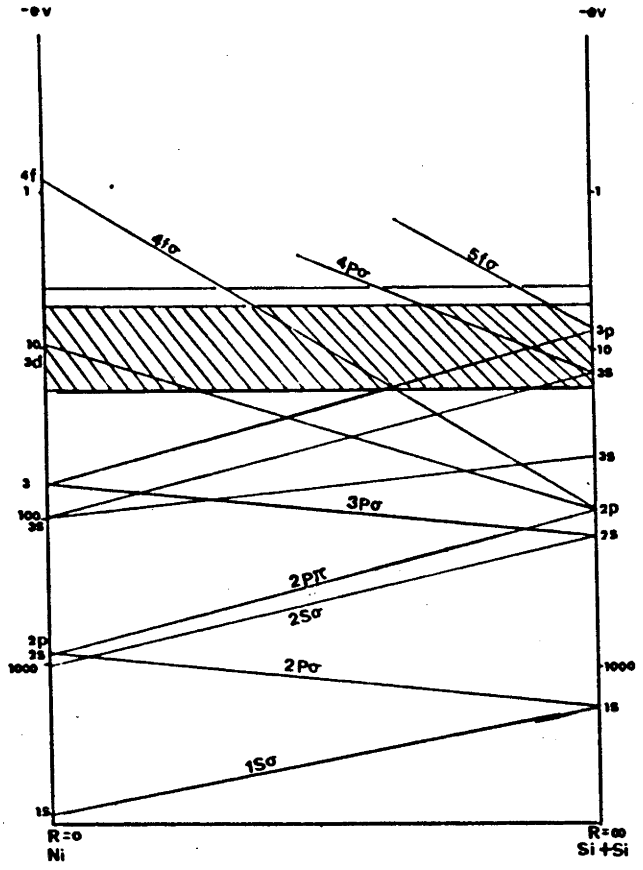

B.

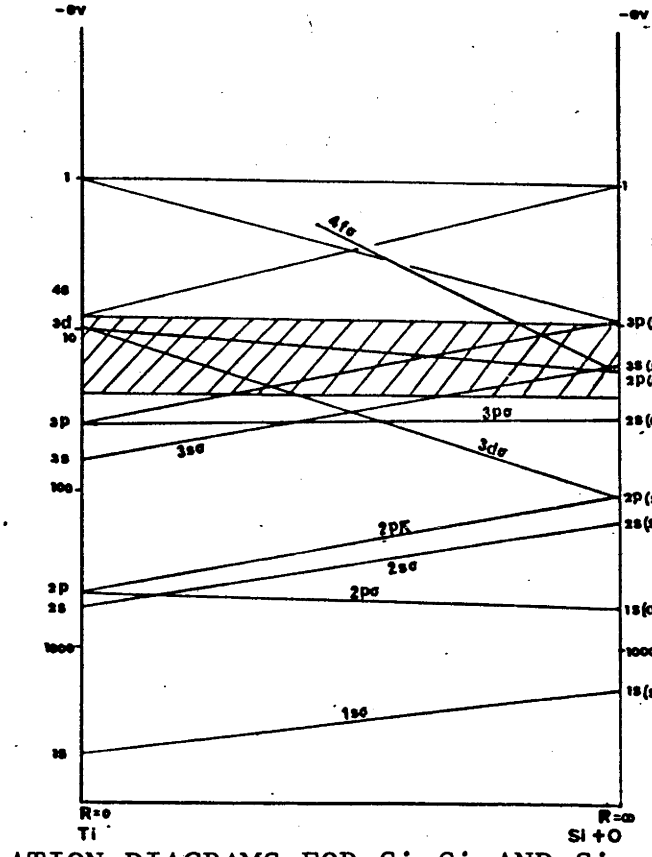

FIG 5.6 CORRELATION DIAGRAMS FOR Si→Si AND Si→O

occurs at 1206.5 Å at an excitation energy of 10.27 eV and is outside the range of detection.

5.2.6 SUMMARY OF THE SiO_2 - Si DATA

The differences between photon or secondary ion emission due to ion bombardment of SiO_2 and Si can be accounted for by electron transitions between the solid and the ejected atom or ion. The most likely transitions are double resonance transitions, or Auger transitions, involving neutralisation or de-excitation of the ejected ion or atom near the target surface. Much of the present argument relies on correlating the absolute yields of photons and ions and these yields can only be estimated very crudely. However, these experiments have shown that with accurate yield estimates, the correlation of photon emission and secondary ion emission provides a valuable means of evaluating some of the models of excitation and ionisation during ion-surface interaction.

5.3 EMISSION LINE PROFILES FROM SPUTTERED PARTICLES

There have been only a few studies of the shape and shifts of emission lines from neutral particles sputtered by an ion beam from a target surface, the most recent being the study of *Hippler and others (1976)*. There have been no studies made of the emission line profiles from excited sputtered ions. The present study was undertaken to examine the effect of the target electronic band structure on the emission lines produced by Ar^+ bombardment of Mg, Al, and Si and their respective oxides.

The apparatus used is described in section 3.2.4, the only modification being the addition of the Jarrell Ash 0.5 metre scanning spectrometer. This instrument when fitted with 10 μm slits

had an instrumental resolution of approximately 0.2 Å ± 0.03 Å measured using the AlI 3961 Å line of a hollow cathode lamp. The instrument aperture of f/8 and slit widths of 10 μm required long photon counting times for low signal strengths. Typical run times took up to 2 hours to obtain a complete line profile. During this time the primary ion beam current was continuously monitored and found to be stable within ± 5 per cent. A primary beam of 80 KeV Ar^+ at an angle of incidence of 45° to the target normal was used in all the measurements. A list of the lines studied and their experimentally measured line widths from clean and oxide surfaces is given in Table 5.2.

TABLE 5.2

Estimated values of F.W.H.M. for Mg, Al and Si.

Emmission Line (Å)		F.W.H.M. ± 0.03 Å	
	Type	Mg	MgO
2852	I	0.4	0.34
2975	II	0.8	0.7
2977	II	0.8	0.65
2803	II	0.9	0.65
		Al	Al_2O_3
3082	I	0.65	0.37
3092	I	0.50	0.38
3944	I	0.60	0.42
3961	I	0.50	0.42
3587	II	0.85	0.8
3601	III	1.3	1.3
		Si	SiO_2
2882	I	0.5	0.44
2542	III	0.8	0.7

In the case of Al an attempt was made to estimate the Doppler shift of the neutral lines from reference lines provided by a hollow cathode discharge lamp. However no measurable shift was observed. Hippler et al have studied the 3093 AlI profile from clean and oxidised targets using 300 KeV Ar^+ ions and observed a shift of only 0.1 Å. The measurements were made with an instrument of resolution 0.5 Å as compared to the present study in which the instrumental resolution was 0.2 Å. The poorer resolution of Hippler et al must raise some doubt about their ability to resolve a 0.1 Å shift from the reference line. On the basis of the present results it may be stated that the shift of the neutral Al line is not sufficient to be measured under the present conditions and is less than the instrumental resolution of 0.2 Å.

5.3.1 RESULTS

Fig 5.7 shows the emission line profiles obtained from Mg and MgO at an angle of incidence of 45°. The instrumental resolution is indicated by the inner dashed line. All the emission line profiles have been normalised at their maxima. In this figure several features are evident. The lines all exhibit broadening on the short wavelength side of the central maxima. This effect is a result of the emitting particles having velocity components in the direction of observation giving rise to the Doppler 'blue' shift. The most prominent feature is the much larger line width observed for the MgII line compared to the MgI emission lines. The 2802 Å MgII line from pure Mg was estimated to be 0.85 Å compared to 0.4 Å for the 2852 Å MgI line. In the case of the MgO crystal the width was reduced to 0.6 Å for MgII and 0.35 Å for MgI. A considerable blue shift in the MgII emission was however still observed from MgO with some intensity

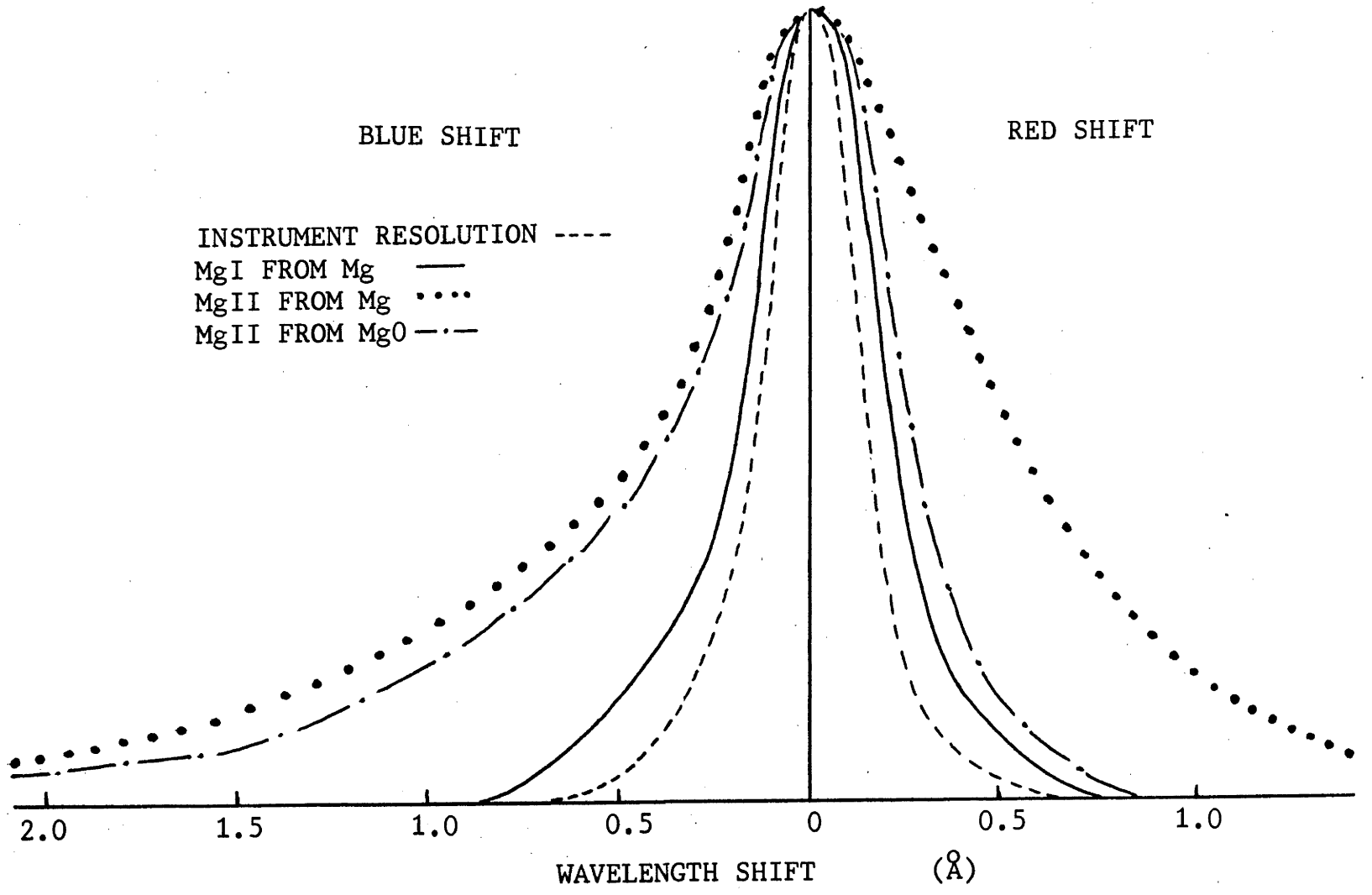

FIG 5.7 LINE SHAPES OF MgI AND MgII FROM Mg AND MgO

in the line occurring approximately 2 Å from the central maximum.

The red shift of the MgII line from the Mg target is not observed in the case of the MgO target. An explanation of this effect is difficult but may be due to the surface reflectance. In studies of the emission line profiles of backscattered radiating primary ions it has been shown that considerable red shifts are present (section 2.4). Theoretical line profiles can be fitted to the experimental results by assuming that the red shift is produced by the reflectance of the radiation emitted by the particles scattered off the surface towards the monochromator. This may also be the case for fast sputtered emitting ions. The absence of the large red shift in the case of the MgO target is possibly due to the weaker reflectivity of the MgO surface compared to that of Mg, in the ultraviolet region of the spectrum.

The results shown in Fig 5.7 were typical of those obtained from Al, Al_2O_3, Si and SiO_2 under the same conditions, in that the charged particle emission line profiles were always considerably broader than the neutral line profiles. Table 5.2 shows the emission lines studied and their estimated F.W.H.M. (full width half maximum). The line with the largest half-width was found to be that of the Al III 3601 Å transition, estimated to be 1.3 Å wide. This value was obtained from both the metal and oxide targets. The neutral AlI widths were found to be reasonably reproducible for all the resonance lines and measured as 0.5 - 0.6 from Al and 0.4 from Al_2O_3. The SiI emission line at 2882 Å was found to be approximately 0.5 Å from Si and 0.44 Å from SiO_2. This result is somewhat different to that reported by *White et al (1975)*, who measured the width of the SiI 2882 Å produced by 80 KeV Ar^+ of Si and SiO_2 to be 5.1 Å and 1.1 Å respectively for the same geometry. The authors

interpreted the difference in half widths as being an effect of the band structure of the target influencing the emission. In the case of Si the 2882 Å excitation level ($4s^1P^o$ of Fig 5.5) lies opposite the empty conduction band of Si. Slow particles are therefore expected to de-excite by non-radiative electronic transitions involving the target leaving only fast particles to escape and radiate. In the case of SiO_2 the relevant level is opposite the oxide band gap prohibiting non-radiative processes and a larger proportion of slow excited particles are expected to contribute to the emission line. Since the spectrometer integrates over the angular distribution of the emitting particles a broader line is expected from Si than SiO_2. This was in fact observed. The degree of broadening is however suprising if one considers the half width to represent the average velocity of the emitters in the direction of observation. Equating the average velocity to an effective energy, the result of White et al of 5.1 Å would correspond to approximately 40 KeV particles. The present value of 0.5 Å corresponds to an effective energy of about 400 eV and is consistent with other published results for other targets *(Van der Weg and Bierman, 1965)*. The present half-width value for the 2882 Å SiI is also consistent with those measured for the AlI and MgI profiles for which the above theory also applies. The effective energy of AlI and MgI emitters also correspond to about 400 eV.

5.3.2 DISCUSSION

The large half widths of the emission line profiles of the ionised particles indicate that these particles possess much higher energies than the neutral emitters. In some instances the ionised emission produces half widths larger than that of the neutral emission

by more than a factor of 2. Furthermore, all the neutral emission lines were found to be influenced by the nature of the target whereas only a few of the ionised lines indicated any significant change when moving from a clean surface to an oxide surface.

The larger velocities of the ionised emitters, inferred from their half-widths, may be assumed to result from biparticle collisions of incident ions and surface atoms. To examine this further, the theoretical model of *Van der Weg and Biermann (1965)*, recently applied to a number of neutral emission lines by *Hippler et al (1976)*, has been applied to the emission line profiles from MgI, MgII and AlII and AlIII. This model has been reviewed in section 2.5.3, but for the purpose of this discussion will be briefly outlined. The number of particles contibuting to radiation with wavelength $(\lambda + \Delta\lambda)$ which result from binary collisions at the target surface is given by -

$$N(\lambda+\Delta\lambda)\, d\lambda = \int\int [P \text{ exc } (\phi)\,] \, [\sigma(\phi)\,] \, [R(\phi,\alpha)\,] \left[\delta\left(\frac{V\beta}{C} - \frac{\Delta\lambda}{\lambda}\right)\right] \times 2\pi \, \text{Sin}\phi \, d\phi \, d\gamma \, d\lambda$$

In this expression the probability of excitation is given by the first term, the scattering cross section by the second, the probability for escape in an excited state by the third and finally the δ function denotes the condition for a Doppler shift $\Delta\lambda$ from the wavelength λ for a particle of velocity $V\beta$. The angles ϕ,α,β and γ represent the scattering angle, the angle of incidence of the primary ion, the direction of observation and the azimuthal angle respectively. In order to evaluate this expression a number of simplifying assumptions are made. The probability of excitation is assumed to be ~ Cos ϕ (this simplifying assumption is made by Van der Weg and Bierman since

the exact form is not known for ion-solid interaction), the differential cross section $\sim 1/\cos^2\phi$ and the probability for escape in an excited state is given by -

$R(\infty) = \exp - (A/a\ V\ 1)$ (section 2.3) where V 1 is the velocity of the emitting particle perpendicular to the target surface and A/a the survival coefficient. The perpendicular velocity component is given by -

$$V\ 1 = \frac{2M_1}{(M_1 + M_2)} \sqrt{\frac{2E_o}{M_1}} \cos\phi\ (\sin\phi \cos\gamma \cos\alpha - \cos\phi \sin\alpha)$$

where E_o is the primary energy and M_1, M_2 the masses of the incident ion and target atom respectively. The A/a coefficient was estimated by Van der Weg and Bierman to be $\sim 2.10^6$ cm sec^{-1} for the CuI 3247 Å line produced by 80 KeV Ar^+ on Cu. Hippler et al estimated the value to be 3.10^6 cm sec^{-1} for 300 KeV Ar^+ on Cu for the same line and also obtained a value of 5.10^5 cm sec^{-1} for the AlI 3092.8 Å line from 300 KeV Ar^+ on Al.

The expression for $N(\lambda+\Delta\lambda)$ was evaluated for the system of 80 KeV $Ar^+ \rightarrow$ Cu for the CuI 3247.5 Å line, as a check against the theoretical result of Van der Weg. The expression was evaluated using the values for α and β for the Van der Weg and Bierman experiment and the A/a coefficient was varied from 2.10^6 cm sec^{-1} to 4.10^6 cm sec^{-1}. This produced a shift in the maximum of the line of 0.2 Å as predicted by the authors.

As a further test a polycrystalline Cu target was bombarded with 80 KeV Ar^+ ions and the 3247.5 Å CuI line profile was measured at an angle of 45° incidence and observation angle of 90° (the only angle available on the present system). The result is reproduced

in Fig 5.8A and compared with a theoretical calculation using a value of 2.10^6 cm sec^{-1} for A/a and an azimuthal angle γ of zero. Because the band width of the monochromator cannot be neglected in comparison to the line profiles, the theorectical curve has been convoluted with the instrument function which is a Gaussian curve of half-width 0.2 Å. Only a limited agreement was obtained between the theoretical and experimental curves, the better fit being given when a value of A/a of 2.10^6 cm sec^{-1} was used as in the case of the Van der Weg and Bierman experiment. The theoretical Doppler shift of 0.3 Å under these conditions could not be detected when a Cu hollow cathode lamp was used as a reference, therefore the curves in Fig 5.8A have been normalised at their maximum intensity at zero wavelength shift.

Theoretical curves were calculated for the neutral and ion lines and compared with experimental results. Fig 5.8B shows some typical results for Mg. In the case of the 2802.7 MgII line resonable agreement was obtained using a value of 5.10^5 cm sec^{-1} for the A/a coefficient, but only a value of zero gave any reasonable fit for the neutral lines. The previous study of Hippler et al obtained reasonable fits for the AlI line using a value of 5.10^5 cm sec^{-1}, their experimental half widths being of the order of 1.2 Å from the metal surface, (estimated from Fig 10 of Hippler et al 1976), and 0.8 Å from Al_2O_3, i.e. comparable to the AlII and AlIII emission profile measured here.

5.3.3 SUMMARY

The measurement of line profiles from neutral and ion emission has shown that the ions possess considerably more energy than the neutrals which is reflected in their widths. The emission lines from neutral particles are narrower by a factor of nearly 2

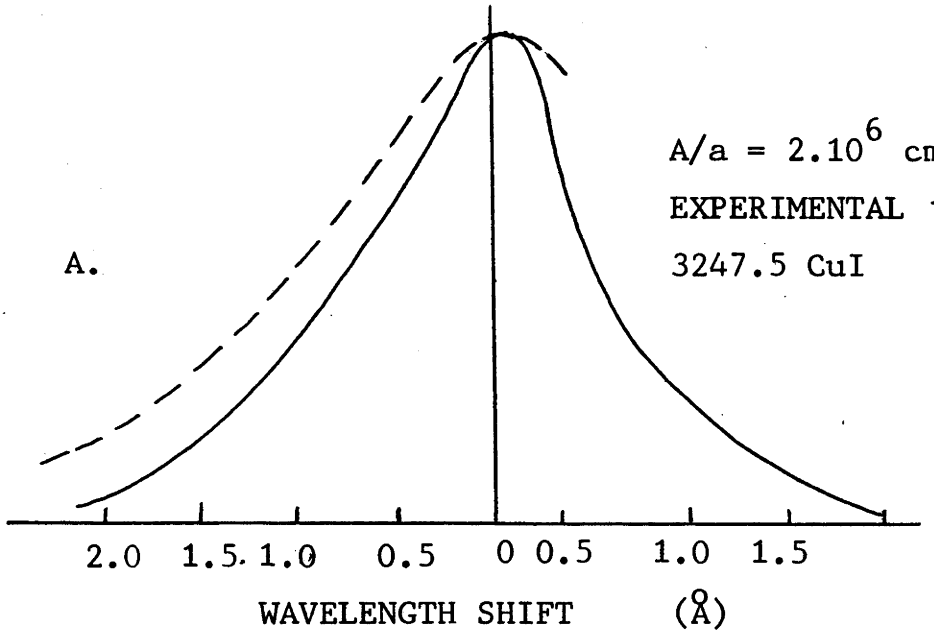

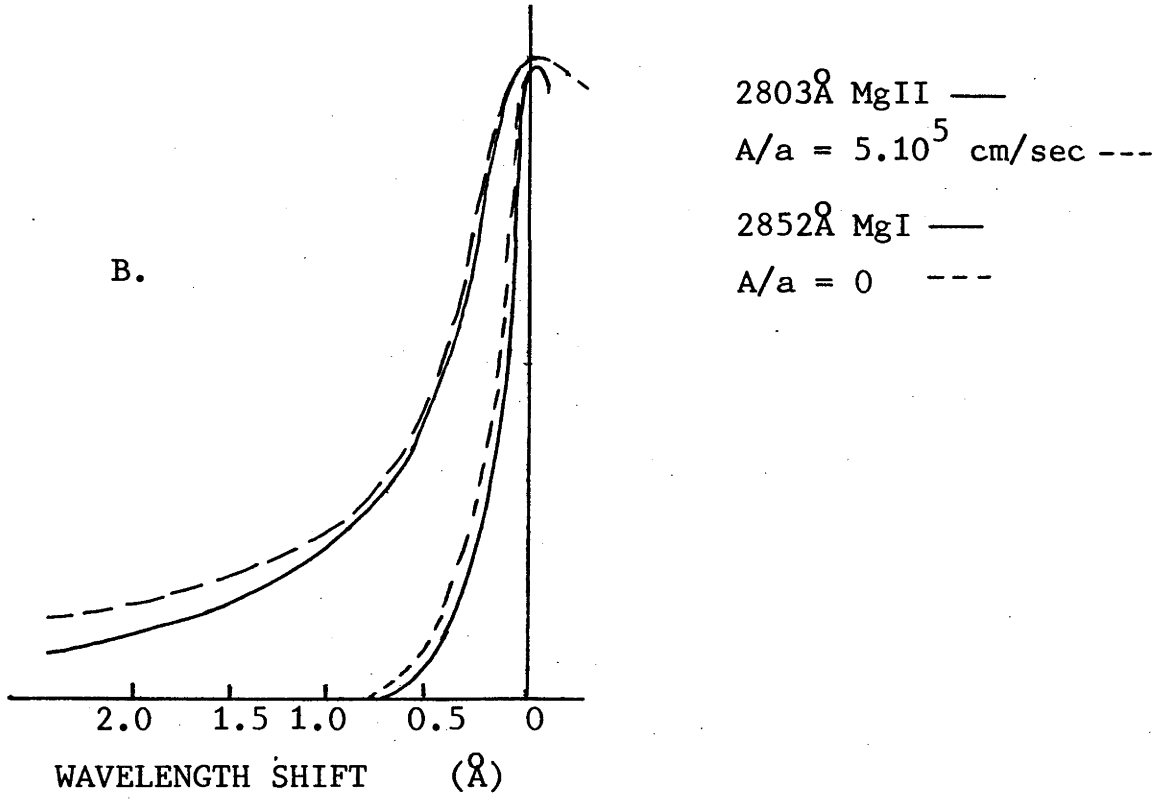

FIG 5.8 THEORETICAL AND EXPERIMENTAL LINE SHAPES FOR (A) 80 KeV $Ar^+ \rightarrow$ Cu AND (B) 80 KeV $Ar^+ \rightarrow$ Mg. ALL PEAKS ARE NORMALISED AT THEIR MAXIMA.

in some instances, but are seen to be influenced by the chemical nature of the target. The neutral lines from the oxides were 0.05 to 0.1 Å narrower than the emission lines from the metals. This variation between the metal and oxide can be explained in terms of the position of the excited level with respect to the band structure of the target as suggested by *White et al (1975)*. The effect observed by these authors for the SiI 2882 Å line from a Si target has been found to be much less marked in the present study and this discrepancy is difficult to understand since the experiments were performed under similar conditions. The present results also indicate a much narrower line width for the AlI emission lines than observed by Hippler et al. This discrepancy is however, reconcilable with the variation in experimental conditions. The data of these authors was taken with a spectrometer of resolution 0.5 Å at an observation angle normal to the target surface and using a primary beam of 300 KeV Ar^+ ions, as compared to the present resolution of 0.2 Å, observation angle of 90^o and primary energy of 80 KeV.

The binary collision model of Van der Weg and Bierman gave moderate agreement with the Cu results but could only be fitted to the Si, Al and MgI emission assuming a survival coefficient of zero. The probability for survival of an excited state is given by $R = \exp(-A/a\ V\ 1)$ (section 2.3), therefore for the case of a survival coefficient of zero the implication is that all slow sputtered particles may escape and radiate. The emission line profiles from ionised particles were in reasonable agreement with theoretical calculations if a survival coefficient of 5.10^{-5} cm sec^{-1} was assumed. If the majority of slow ions are assumed to have energies of the order of 10 eV to 20 eV (*Bayly and MacDonald, 1976*) a survival probability of 0.7 may be estimated for the MgII emitters. This compares to a value

of 0.027 estimated by Van der Weg and Bierman from the neutral CuI emission line for slow neutral copper atoms.

In conclusion therefore the present study has shown, in agreement with that of Hippler et al, that the present form of the biparticle collision model does not accurately predict the shape of emission line profiles from neutral particles and further theoretical investigations are necessary. Refinements may be required in the simple expressions used to describe the excitation probability, and account taken of the cascade contribution to the emission. The simple model of binary collisions between incident ions and surface target atoms does not explain the behaviour of the photon emission produced under channeling conditions, from an oxidised aluminium target. This particular experiment is described in the following chapter.

REFERENCES

ANDERSEN, H H, BAY, H L., J. Appl. Phys. 46, 1919 (1975).

BAYLY, A R, MACDONALD, R J., J. Phys. E. Sci. Inst. In press.

BAYLY, A R, MACDONALD, R J., Unpublished data.

BROCHARD, D, SLODZIAN, G., J. Phys., 32, 185 (1971).

DEAL, B F, J. Electrochem. Soc., 110, 527 (1963).

EDWIN, R P, J. Phys. D: Appl. Phys. 6, 833 (1973).

FANO, V, LICHTEN, W., Phys. Rev. Lett., 14, 627 (1965).

HARRINGTON, W L, HONIG, R E, GOODMAN, A M., WILLIAMS, R., App. Phys. Letts. 27, 644 (1975).

HENNEQUIN, J F, VIARIS DE LESEGNO, P., C.R. Acad. Sci., 272B, 1259 (1971).

HIPPLER, R, KRUGER, W, SCHARMANN, A, SCHARTNER, K H., Nucl. Instr. Meth., 132, 439 (1976).

JOYES, P., J. Phys. C. 5, 2192 (1972).

KELLY, R, KERKDIJK, C B., Surface Science, 46, 537 (1974).

PILSKIN, W V, CONRAD, E E., I.B.M. Journ. 43, Jan. (1964).

SLATER, J C., Phys. Rev., 98, 1039 (1955).

STRIGANOV, A R, SVENTITSKII, N S., Tables of Spectral Lines of Neutral and Ionised Atoms, Plenum (1968).

VAN DER WEG, W F, BIERMAN, D J., Physica, 44, 206 (1969).

WHITE, C W, SIMMS, D L, TOLK, N H, McCAUGHAN, D V., Surface Science 49, 657 (1975).

ZAIDEL, A N, PROKOF'EV, V R, RAISKII, S M., Tables of Spectrum Lines, Pergamon (1961).

CHAPTER SIX

SINGLE CRYSTAL EFFECTS IN THE PHOTON AND SECONDARY ION YIELDS FROM ION BOMBARDED ALUMINIUM

6.1 INTRODUCTION

The results discussed in earlier chapters have been obtained primarily from polycrystalline targets, single crystal targets randomly orientated or single crystal targets which are known to rapidly become amorphous during ionic bombardment. The work described here deals with the effect of single crystal structure on the secondary processes of photon and ion emission from aluminium bombarded with 50 KeV Ar^+ ions. There have been several reports of channeling effects on secondary ion yields by the French group at Orsay, from both transition metal alloys and aluminium *(Bernheim and Slodzian, 1973, 1976, Slodzian, 1976)* and the effects of oxygen on the ion yields. The effect of channeling on the sputtering yields from Ge and InSb has also been investigated by *Zwangobani and MacDonald (1973)*, using secondary ion analysis of the sputtered particles. The sputtering yields were compared with those predicted by the channeling model of *Onderdelinden (1968)*, and it was concluded that the overall features of the variation of yield with angle of ion incidence could be predicted using this model. Channeling effects on the photon emission from ion bombarded targets were first detected by *Fluit et al (1961)* from Ar^+ and Ne^+ bombardment of Cu. A more detailed study of optical excitation during ion bombardment of copper under channeling conditions has recently been made by *Van der Weg et al (1976)*, who used both 50 KeV and 100 KeV Ar^+ primary ions. (Section 2.5.6). The emission intensity of lines emitted by backscattered He atoms and ions during

bombardment with 100 and 200 KeV He^+ ions was also investigated. In both the backscattered helium and recoil sputtered copper particles it was found that atomic excited states were created in particles originating from deeper inside the crystal compared to particles that were ionised.

In the present work a single crystal aluminium target has been studied since it is known (section 4.3.1.) that the light elements emit strong emission lines from the charged II and III spectra. The presence of charged particle photon emission has enabled correlations to be made with secondary ion analysis performed simultaneously on the same target. In this manner more information is provided on the behaviour of secondary processes under channeling conditions.

6.2 EXPERIMENTAL

The target was a high purity single crystal of aluminium cut and orientated such that the <100> axis was normal to the target surface. The crystal was polished using successively finer grades of metallurgical diamond polishing compound to a minimum of 0.25μm grain size. The alignment was checked using the Laue X-ray diffraction technique and found to be within 1/2 degree of the (100) face, i.e. within the limits of the back diffraction alignment procedure. Once degreased in solvents the target was not treated further, but experimental data was taken only after ~ 5 hours preliminary bombardment to remove any surface oxides and crystal damage introduced through the polishing procedure. The crystal, although damaged by the primary ions, gave stable and reproducible results after this period.

The primary beam used was a 50 KeV Ar^+ beam with a current density of 75 μa cm^{-2} at the target surface. The target was mounted in a 20 inch diameter vacuum chamber which could be evacuated to a background pressure of 5.10^{-7} Torr. A precision goniometer enabled the target to be rotated about the surface normal in steps of 0.01 degrees. Two experiments were performed, one using an angle of incidence of 45^{o} to investigate the <110> channels and a second at 54.7^{o} to the (100) face to investigate the <111> direction. The secondary ions were collected normal to the target and photons detected perpendicular to the beam axis in all cases. Secondary ion measurements were taken on the secondary ion mass spectrometer of *Bayly and MacDonald (1976)*. The instrument had facilities for mass scans and energy scans of secondary ions up to mass 400 AMU and energies 0-500 eV. Photon emission was analysed with the Bausch and Lomb high aperture (f/4.4) medium resolution monochromator over the wavelength region 2000 Å to 6000 Å. The data acquisition system is shown in schematic form in Fig 6.1. Essentially the monochromator was tuned to a selected emission line and the mass spectrometer to a selected ion of a given energy. The photon data and secondary ion data was then accumulated in pulse form in two multichannel analysers for a preselected time interval and given crystal orientation. The crystal was then stepped by a preselected amount of rotation (minimum of 0.01 degrees) and the counting procedure repeated. Using this system it was possible to simultaneously collect secondary ion and photon data for a given rotation angle of the target. The system was also provided with a two pen chart recorder for continuous monitoring of the ion and photon signals. The primary ion current was monitored on an insulated aperture mounted on the entrance to the target chamber and also periodically measured by inserting a moveable

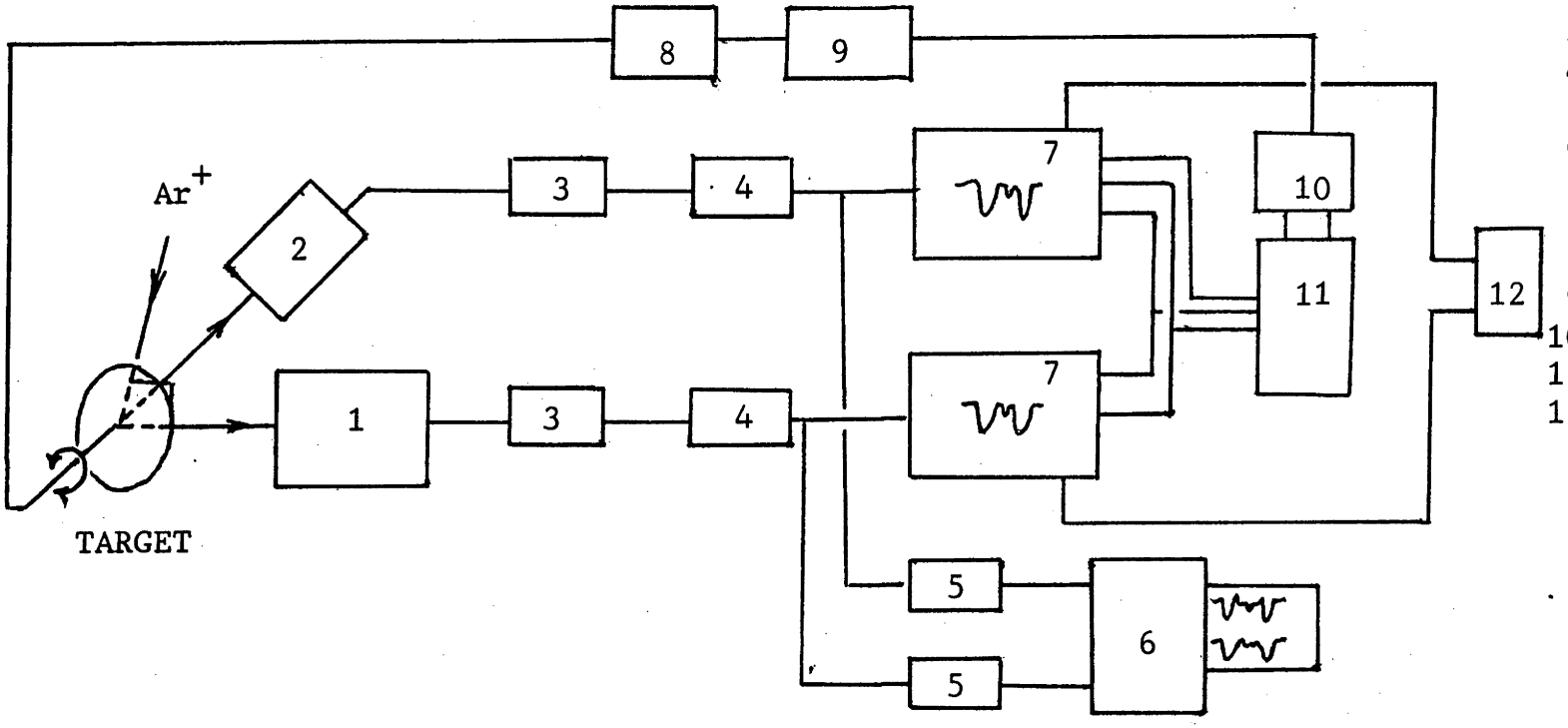

1. PHOTON ANALYSIS
2. ION ANALYSIS
3. PRE-AMP
4. AMPLIFIER
5. RATE METER
6. CHART RECORDER
7. M.C.A.
8. GONIOMETER CONTROLLER
9. STEP MONITOR
10. TIMER
11. CONTROL
12. DIGITAL OUTPUT

FIG 6.1 SCHEMATIC OF DATA ACQUISITION ELECTRONICS FOR SIMULTANEOUS PHOTON AND ION DETECTION.

faraday cup into the beam again at the entrance to the experimental chamber. The primary beam was found to be stable within ± 5 per cent over a period of many hours.

A list of the wavelengths and transitions measured and also the secondary ions monitored is given in Table 6.1.

TABLE 6.1

Wavelengths, Transitions and Secondary Ions Monitored.

Wavelength (Å)	Transition	Energy (eV)	J
3082	$3p^2P^o$ - $3d^2D$ Al I	0.00- 4.02	1/2 - 3/2
3093*	$3p^2P^o$ - $3d^2D$ Al I	0.01- 4.02	3/2- 5/2, 3/2
3944	$3p^2P^o$ - $4s^2S$ Al I	0.00- 3.14	1/2 - 1/2
3962	$3p^2P^o$ - $4s^2S$ Al I	0.01- 3.14	3/2 - 1/2
2816	$3p^1P^o$ - $4s^1S$ Al II	7.42-11.82	1 - 0
3587*	$3d^3D$ - $4f^3F^o$ Al II	11.85-15.30	2 - 4
3655*	$4p^3P^o$ - $5d^3D$ Al II	13.08-16.47	2 - 3
3901	$3p^1P^o$ - $3p^{21}D$ Al II	7.42-10.60	1 - 2
4667*	$5p^1P^o$ - $11s^1S$ Al II	15.6 -18.26	1 - 0
3602	$3d^2D$ - $4p^2P^o$ Al III	14.37-17.81	5/2 - 3/2
3612	$3d^2D$ - $4p^2P^o$ Al III	14.37-17.80	3/2 - 1/2
4480*	$4f^2F^o$ - $5g^2G$ Al III	20.78-23.54	5/2, 7/2-7/2
4512	$4p^2P^o$ - $4d^2D$ Al III	17.80-20.55	3/2 - 5/2
4529*	$4p^2P^o$ - $4d^2D$ Al III	17.81-20.55	3/2-5/2, 3/2

* line not fully resolved from neighbouring line of the same spectrum.
Wavelength reference *(Stirganov and Sventitskii, 1968)*.

Ion	Energy (eV)
Al^+	20,50,100,150,200
Al^{++}	100,200.

6.3 RESULTS

6.3.1 PHOTON DATA

Fig 6.2 shows the result obtained when the primary beam was set at 45 degrees to the target surface normal and the target rotated some 140 degrees. Results are shown for the 3602 Å AlIII and 3962 Å AlI transitions. It can be seen that in both cases very pronounced minima occur which are separated by an angle of 90°. These minima occur whenever the primary argon beam is directed along a <110> direction. A smaller minimum also is seen midway between the major channeling dips and this can be interpreted as a prominent <111> planar channeling effect. The dips are more pronounced for the AlI emission than the AlIII emission and far more detail is resolved in the former. These results were typical of the channeling effects observed from all of the neutral and charged particle photon emission. In order to estimate the difference in photon yields when the primary ion beam was directed along a channeling and a random direction, a photon spectrum was taken at a minimum and maximum yield position. The minimum case is shown in Fig 6.3. The ratio of the yields at the two points is given in Table 6.2 for the strongest AlI, II and III emission lines. The CuI lines indicated in Fig 6.3 were a result of the primary beam striking the copper target holder. The ratio of the 3247 Å CuI line at the minimum and maximum positions was found to be unity and provided a useful check of the beam stability during these measurements.

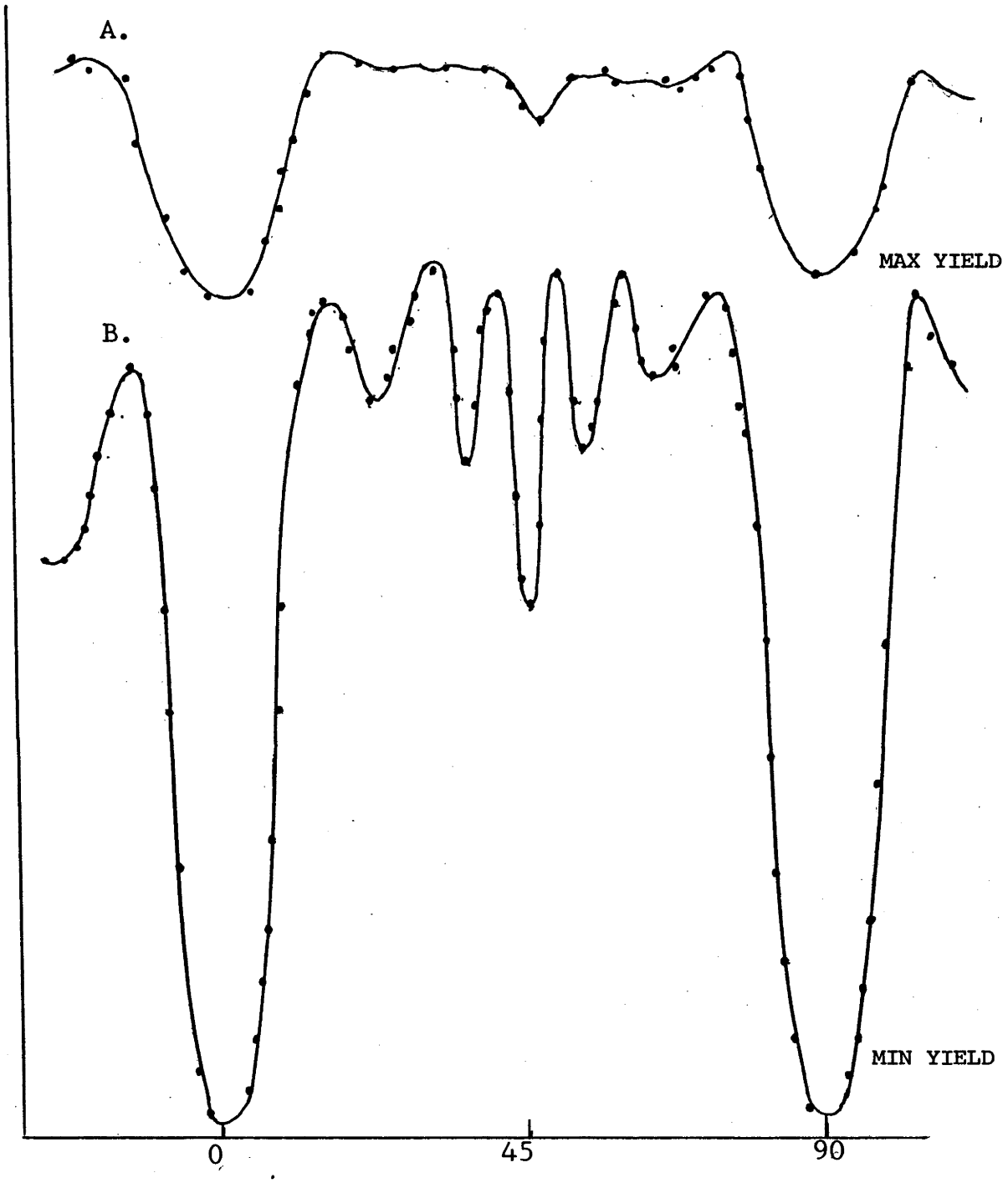

FIG 6.2 PHOTON YIELDS FROM Al AS A FUNCTION OF TARGET ROTATION. (A) 3602(Å) Al III, (B) 3962(Å) AlI.

TABLE 6.2

Ratio of the Photon Intensity at a Maximum and Minimum Yield Position

Wavelength		Ratio
Al I	3082	2.1
Al I	3093	2.5
Al I	3944	2.5
Al I	3962	2.5
Al II	2816	2.5
Al II	3587	2.4
Al II	4667	2.0
Al III	3602	1.6
Al III	4480	1.4
Al III	4512	1.3
Al III	4529	1.4
Cu I	3247	1.0

As a general observation it can be seen that the emission lines are affected in yield in the channeling and non-channeling directions by factors which appear dependent upon the charge state of the radiating particles. The neutral lines were affected the most and III lines the least. The effect is more obvious with reference to Fig 6.3 where the 3602 Å AlIII line is seen to be the third most intense emission line in the spectrum (neglecting instrument transmission corrections) and is more intense than two of the AlI resonance lines. This is to be compared to Fig 4.1 for polycrystalline Al in which all the neutral emission lines are far more intense than those from the ions.

The dependence of the particle charge state on the photon emission as a function of target position was investigated further. The target was rotated such that the primary ion beam was directed along the <110> direction and the monochromator tuned to a given emission line. The change in the photon yield was then recorded for a clockwise

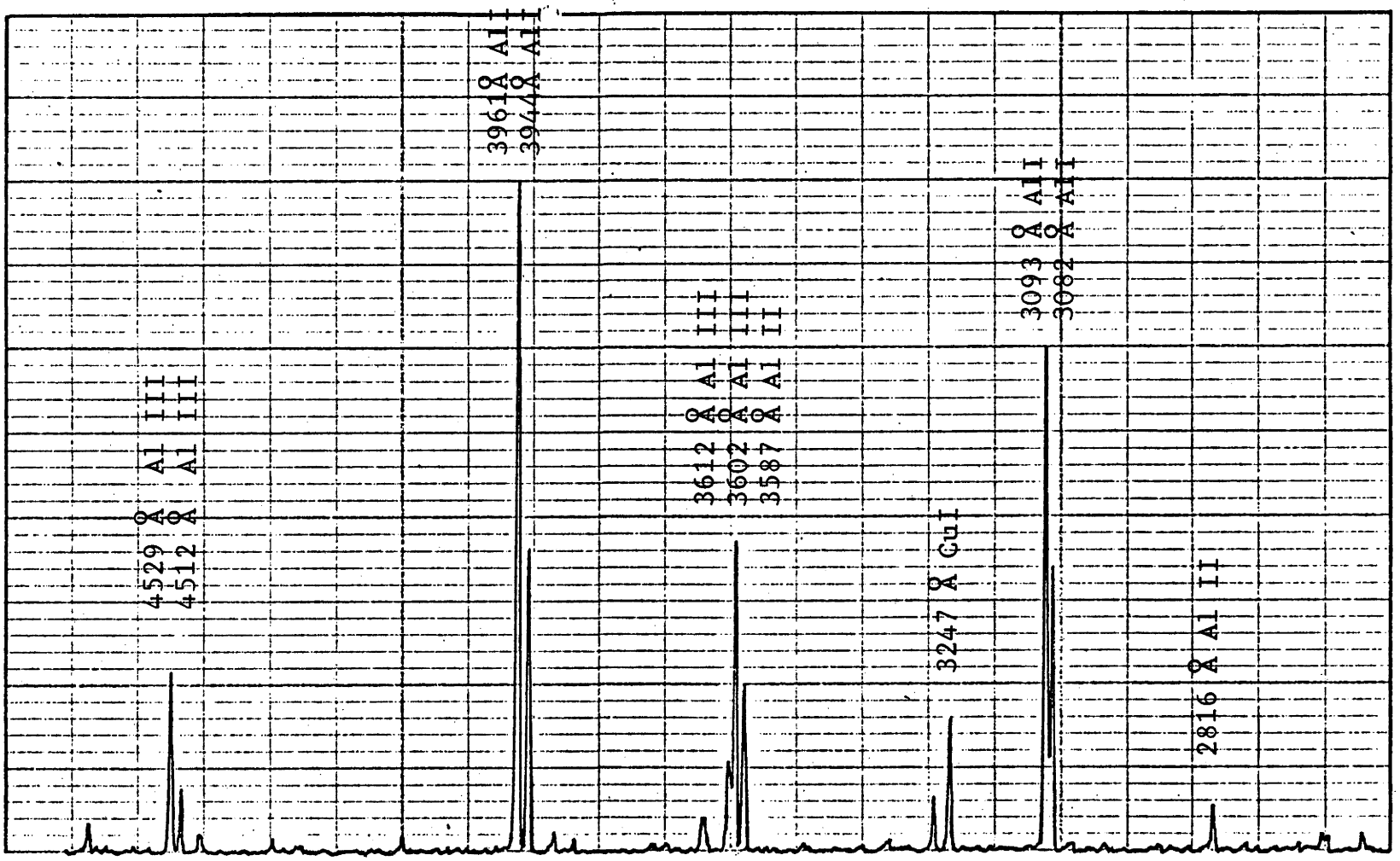

FIG 6.3 PHOTON SPECTRUM TAKEN AT A CHANNELING MINIMUM.

and counter clockwise rotation of the target. The procedure was repeated for a number of lines and the result obtained for reproducible scans of several strong emission lines is shown in Fig 6.4. The change in Al^+ ion yield (50 eV) has been included for comparison. The yields have been normalised at the shoulder of the minimum. It can be seen that the minimum in the photon yield is again dependent upon the charge state of the emitter.

6.3.2 SECONDARY ION DATA

Fig 6.5 shows the variation in secondary ion yield of 50 eV Al^+ and 100 eV Al^+ compared to the 3944 Å AlI emission. The fine structure of the photon emission yield is reproduced exactly in the 100 eV Al^+ yield although the relative changes are not equal. The lower energy Al^+ plot is however very different in the region between 0 and 90 degrees and indicates a relative increase in yield where a decrease is indicated by the 100 eV Al^+ and photon yields. The dependence of the yield of secondary ions on the ion energy was investigated in the same manner as the photon yields. The mass spectrometer was tuned to the Al ion of interest (both Al^+ and Al^{++} were studied) and energy scans taken at minimum and maximum yield positions. The exact positioning of the target was achieved both by observation of the goniometer step-counter reading and the variation of the photon yield monitored on the chart recorder. The energy spectra of Al^+ and Al^{++} at a channeling minimum A and maximum B and the ratio of these two energy spectra is shown in Fig 6.6. It can be seen that for both the Al^+ and Al^{++} yields that the ratio of secondary ions from a channeled direction is essentially constant over the energy range 50 - 200 eV but significantly increased at low energies (<50 eV). The ratio A/B effectively represents the minimum yield χ_{min}

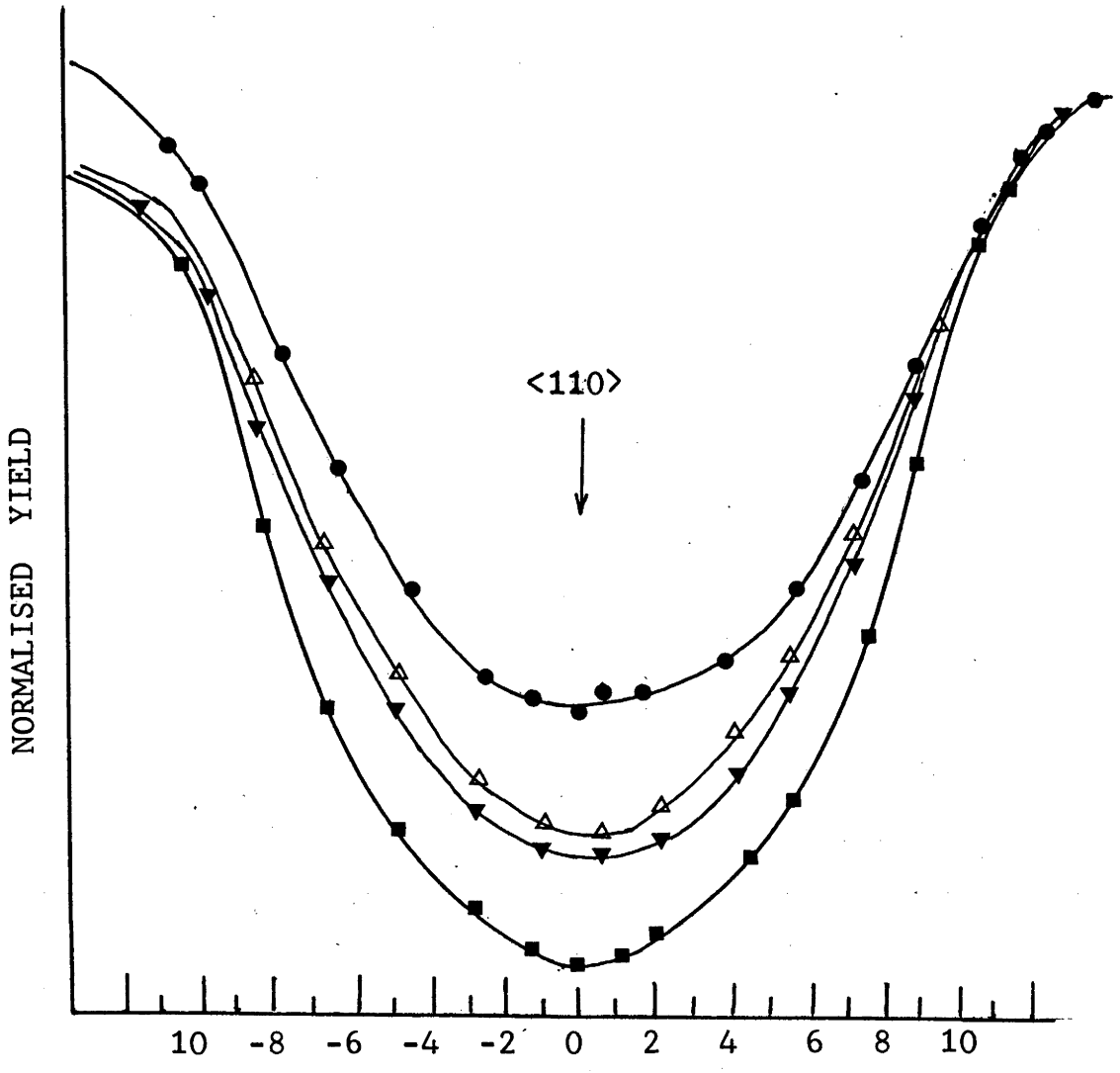

FIG 6.4THE VARIATION IN PHOTON AND ION YIELDS WITH TARGET ROTATION ABOUT THE SURFACE NORMAL

- ● Al III 3602 Å
- △ Al^+ (50 eV)
- ▲ Al II 3587 Å
- ■ Al I 3962 Å

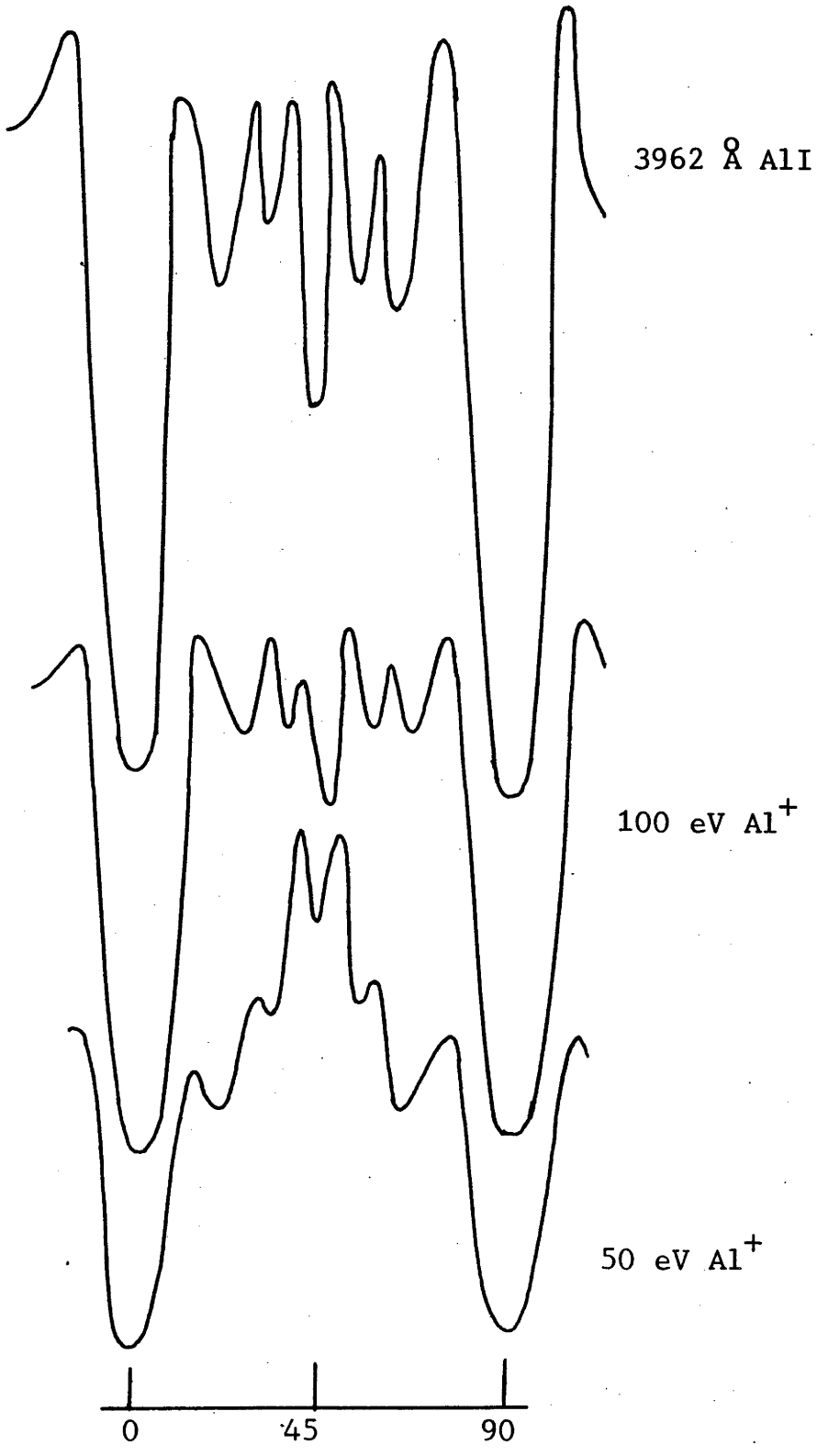

FIG 6.5 SECONDARY ION YIELD VARIATION WITH TARGET ROTATION FOR DIFFERENT ION ENERGIES.

for the secondary ions. The energy dependence of the secondary ions was further studied by rotating the crystal through a channeling minimum and monitoring the variation of aluminium ions of various energies.

6.4 DATA ANALYSIS AND DISCUSSION

It is evident from the results obtained that the overall features of the yield variation with target rotation are reproduced in both the photon and secondary ion measurements. There are however, differences in the minima and relative yields which appear to be dependent upon both the energy of the detected particle in the secondary ion results and the charge state of the emitter in the photon results. In order to investigate any possible correlation with sputtering yield changes, the model of Onderdelinden may be applied to the specific case of 50 KeV Ar^+ incident on the (100) face of Al.

Whenever an incident beam is aligned within a critical angle for channeling $C\psi_c (1<C<2)$ the primary beam, according to the Onderdelinden model, may be divided inside the target crystal into two beams. The aligned beam experiences low energy loss and the non-aligned or random beam behaves as a beam in a random solid. The critical angle ψ_c is given by -

(i) $\psi_c = (3a^2 Z_1 Z_2 e^2/4\pi\varepsilon_o E d^3)^{1/4}$, where Z_1 and Z_2 are the atomic numbers of the ion and target atom, E the ion energy, d the distance between the atoms in the row and -

(ii) $a = a_o 0.8853 (Z_1^{2/3} + Z_2^{2/3})^{-1/2}$ where a_o is the Bohr radius. The equation is considered valid only for energies smaller than -

(iii) $$E < E' = \frac{2 Z_1 Z_2 e^2 d}{4\pi \varepsilon_o a^2}$$

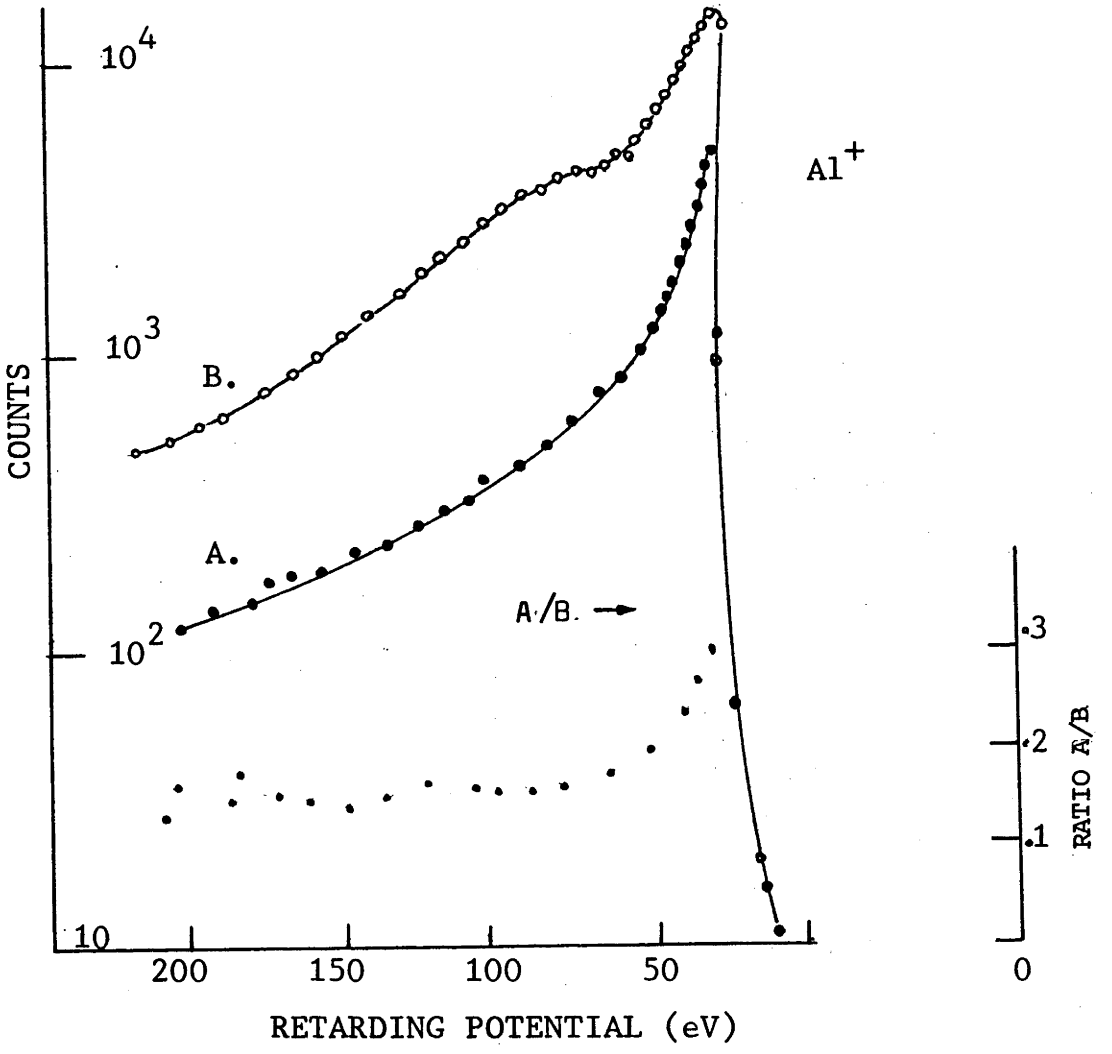

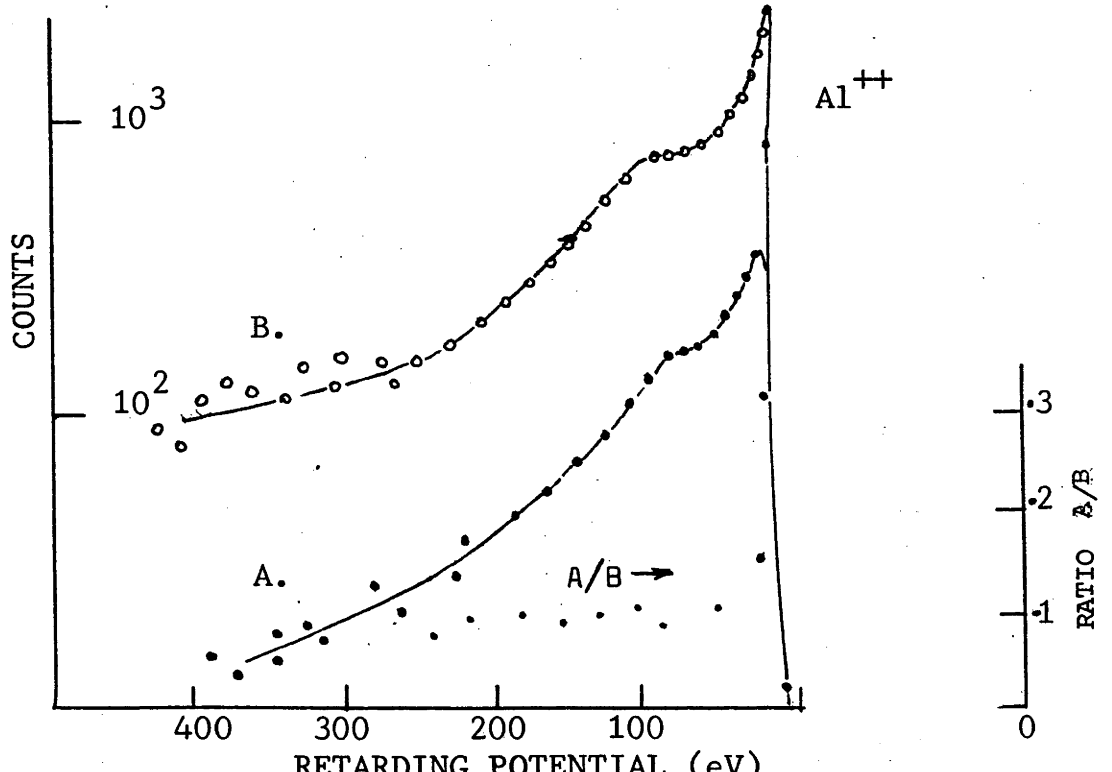

FIG 6.6 ENERGY SPECTRA OF Al^+ AND Al^{++} AT CHANNELING MINIMUM A AND MAXIMUM B.

The value of ψ_c for 50 KeV Ar^+ onto (100) Al using equation (i) is found to be 5^o. The sputtering yield is found from the random component to be given by -

(iv) $N_c = \pi \psi_c^2 d^3 N$, where N is the target atom density. If the incident beam has an angle ψ with a string direction, i.e. $\psi < C\psi_2$, the random fraction is given by -

(v) $N_{nc} = [P_o^2 (P_{max}(0))^{-2} + (1 - P_o^2 (P_{max}(0))^{-2}) \psi^2 (C\psi_2)^{-2}]^{-1}$

where $P_{max}(0) = \psi_c d$ and $P_o = (Nd)^{-1}$.

Table 6.3 shows ψ_W the measured values of the full width at half minimum yield (for the <110> direction) for the strongest AlI, AlII and AlIII emission yields and the Al ions monitored.

TABLE 6.3

Values of ψ_W(Full width at half minimum) for Photon and Ion Yields

Emission	Line/Energy	ψ_W	$\psi_c/0.5\ \psi_W$
Al I	3093 Å	16.6	0.6
Al I	3962 Å	16.0	0.63
Al II	3587 Å	16.0	0.63
Al III	3603 Å	16.4	0.61
Al^+	20 eV	16.4	0.61
Al^+	50 eV	16.4	0.61
Al^+	100 eV	16.4	0.61
Al^+	150 eV	16.4	0.61
Al^+	200 eV	16.8	0.60
Al^{++}	20 eV	16.4	0.61

The measured values of ψ_W were found to be greater than the theoretical ψ_c in all cases. The mean value of 1/2 ψ_W can be estimated to be 8.2 degrees. The dependence of the sputtering yield on ψ has been calculated using equation (v) and the results for C = 1, 1.2, 1.4 and 1.6 have been compared with the experimental result for the AlI 3961 Å emission in Fig 6.7A. It can be seen that the agreement between the calculated and experimental yields is reasonable for small angles, the better agreement occurring for the case C = 1.6.

The dependence of the minimum photon yield on the emitting particle has been observed for the case of Ar^+ on copper by *Van der Weg et al (1976)*. It was observed that the minimum yield χ_{min}, defined as the ratio of the intensities at the channeled and a non-channeled direction, was related to the excitation energy E_{exc} of the particular line. E_{exc} was defined as the energy of the upper level relative to the ground state.

In the present study the χ_{min} values for the AlI, II and III emission as a function of the excitation energy E_{exc} have been plotted in Fig 6.7B for two sets of data. It is evident that the χ_{min} value increases with increasing excitation energy, in agreement with the observations of Van der Weg et al for Ar^+ bombarded Cu. It is possible from Fig 6.6 to estimate the χ_{min} values for secondary ions of various energies from the ratio A/B. The χ_{min} for Al^+ varies from approximately 30 per cent for low energy ions to 18 per cent for particles of energy greater than 50 eV. In the case of Al^{++} the χ_{min} value remains nearly constant at 10 per cent for energies above 20 eV (~50 eV Al^+). The χ_{min} value for ions less than 20 eV in energy is estimated to be about 16 per cent. The evidence suggests therefore that the χ_{min} value depends not only on the excitation energy but also on the kinetic energy or alternatively, the velocity of the detected particles.

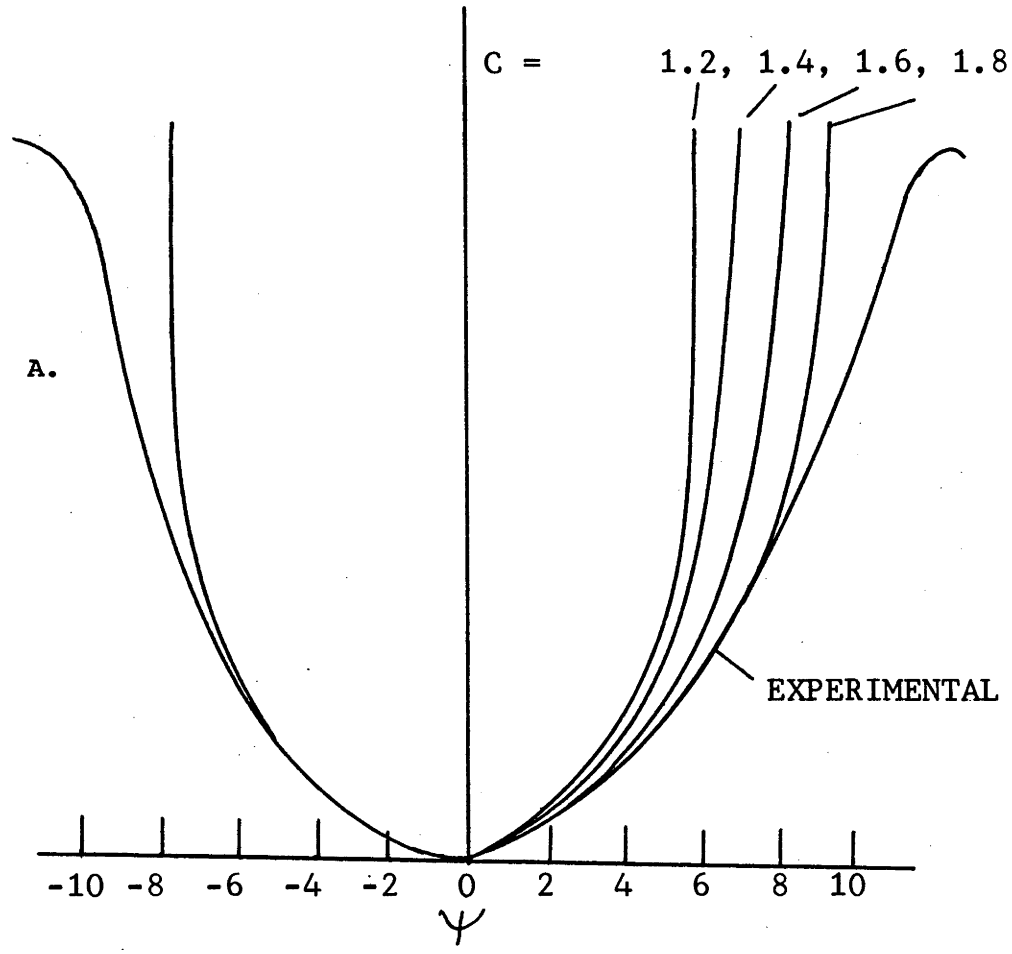

FIG 6.7 COMPARISON OF EXPERIMENTAL AND CALCULATED YIELDS

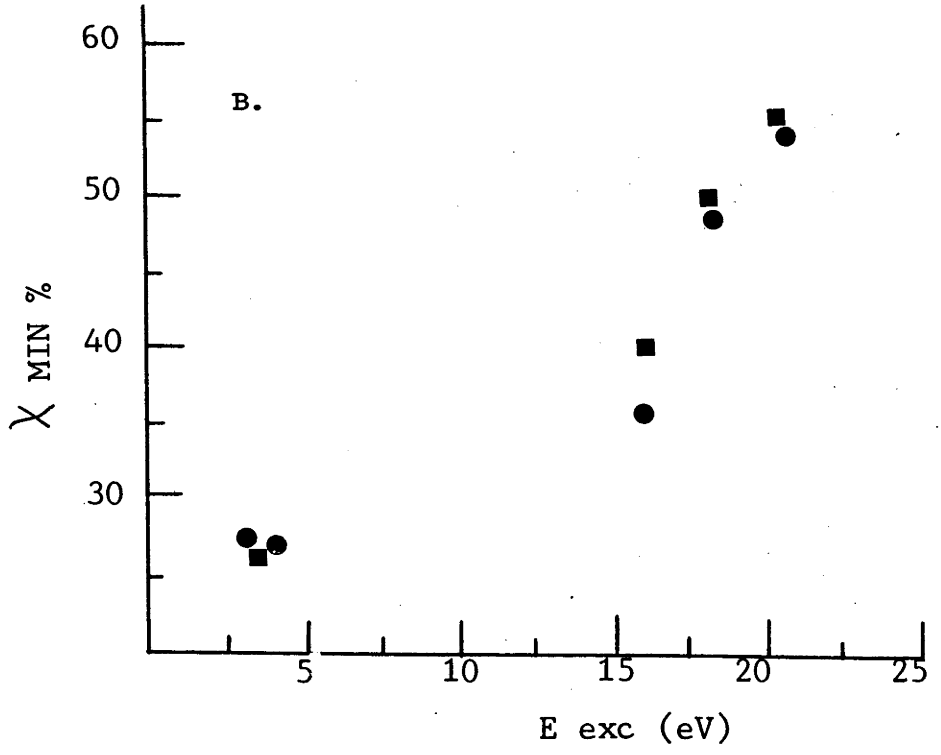

FIG 6.7 DEPENDENCE OF χ MIN ON EXCITATION ENERGY.

The present experiments have shown that there is no significant difference in the angular width of the channeling dips from either atomic or ionic emission lines or secondary ions of energies of (0-200) eV. The width of the channeling dip, according to Van der Weg et al, is related to the depth from which the emitted particles originate, the narrower the dip the greater the depth. If this assumption is justified the conclusion must be that the ions and excited neutrals all originate from the same depth in the crystal. However, the authors assumed ionic lines were emitted from a region very close to the surface giving higher photon yields than neutrals and therefore different minimum yields. It was proposed that recoil copper particles were created in biparticle collisions with argon atoms. Lower excited states were considered more likely to be retained by the particles during their passage from the excitation region in the target to the vacuum than high excited states. The conclusion reached was that high excited states and ions were created only from very close to the surface and gave rise to high minimum yields

The biparticle collision model discussed in section 5.2.2 has been shown to give only moderate agreement with experimental data from copper and a reasonable fit to experimental data from the lighter elements, only if a survival coefficient of zero was assumed for neutral lines and 5.10^3 m sec^{-1} for ion lines. In addition measurements of emission line profiles have indicated that the half-widths of ion lines and hence the velocity of radiating charged particles is much greater than those of emission lines from neutral particles. There is also evidence that suggests that the minimum yields observed in the channeling experiments are related not only to the excitation energy of the upper level of the transition, but also the velocity of the emitters. This is also indicated in the secondary ion yields. In Fig 6.5 the low energy ion yield behaves in a different manner to that

of the higher energy ion and the photon yields. The increase in yield between the two <110> minima is possibly related to low energy focusing effects (*Dennis and MacDonald, 1972*), arising from focused collision sequences and preferential ion ejection from the bombarded crystal. The effect is not seen in the photon or higher energy ion yields and further work is necessary to examine these effects. The correlation between the photon and ion yields at higher energies is strikingly illustrated in Fig 6.8. In this case the target was bombarded at 54.7° to the (100) surface normal, i.e. along <111> direction) and the target rotated through 360° such that planar channels were investigated. The results shown in Fig 6.8 are for 200 eV Al^+ ions and the 3962 Å AlI photon yield. It can be seen that the channeling dips correspond almost identically in both plots with similar variations in relative yields.

To investigate the effect of surface conditions on the channeling effects, oxygen was leaked into the experimental chamber. The partial pressure was varied from the minimum background pressure of 5.10^{-7} Torr. to a maximum of 9.10^{-5} Torr. measured on the target chamber ionisation gauge. During the slow pressure change, the target was rotated and the 3961 Å photon and 50 eV Al^+ yields monitored. The result for the 3961 Å AlI yield shown in Fig 6.9, is surprising in that channeling dips are observed in the photon yield over the entire pressure range. At low pressures the emission appears insensitive to oxygen, the intensity and directional effects remaining constant when a pressure of ~ 2.10^{-6} Torr. is reached. After this point the photon yield increases but the directional effects are still evident. Some of the finer structure is not resolved but the major minima are still very pronounced. In addition an increase with oxygen pressure is seen in the yield of the trailing shoulder of each channeling dip. A similar

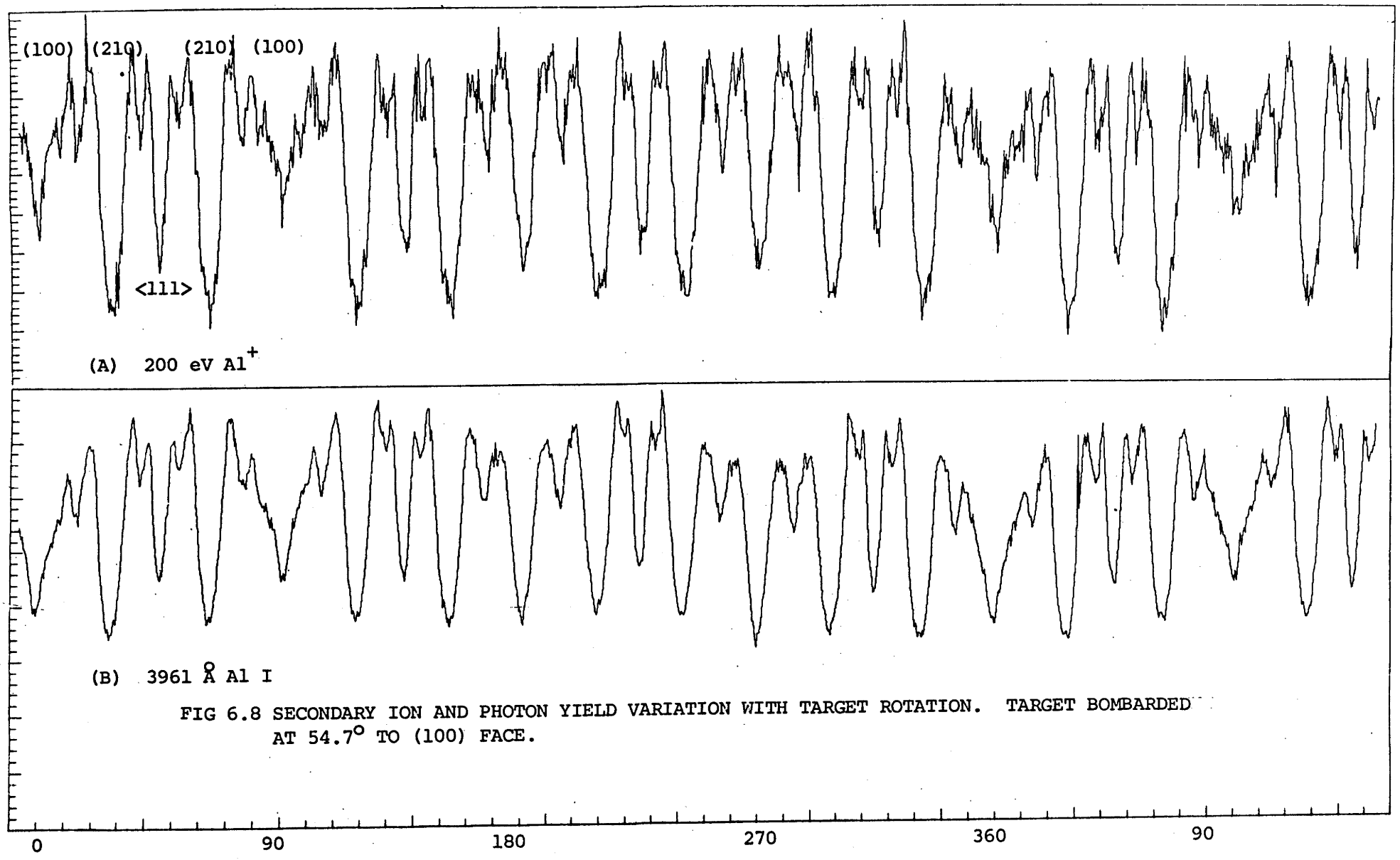

FIG 6.8 SECONDARY ION AND PHOTON YIELD VARIATION WITH TARGET ROTATION. TARGET BOMBARDED AT 54.7° TO (100) FACE.

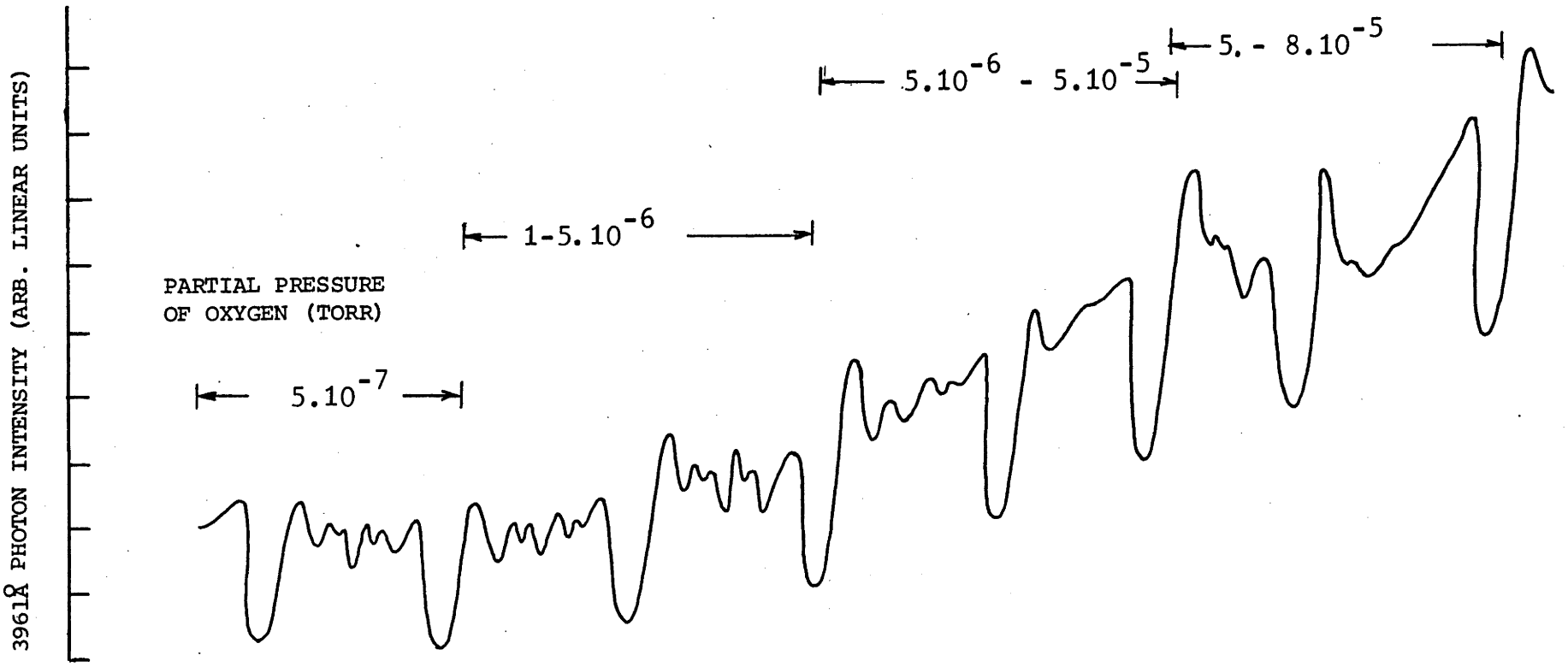

FIG 6.9 THE EFFECT OF OXYGEN ON THE PHOTON YIELD FROM Al UNDER CHANNELING CONDITIONS

result was observed for the 50 eV Al^+ ions. *Bernheim and Slodzian (1973)* have performed a similar experiment on an aluminium single crystal using 6.2 KeV Ar^+ ions and a current density of 600 μa cm^{-2}. The authors detected secondary ions of energy 0-15 eV and observed the effect of oxygen on the yield. At a pressure of 8.10^{-8} Torr. directional effects were observed but at 5.10^{-5} Torr. these effects disappeared and the ion yield enhanced by a factor of 100, saturated. Under the present conditions it is assumed that the crystal surface was covered with an oxide monolayer. According to *Dushman (1964)* an approximate estimation of the arrival rate of gas molecules at the target surface is given by -

$$\nu = \frac{3.5 \cdot 10^{22} P}{(MT)^{1/2}} \quad \text{molecules cm}^{-2} \text{ sec}^{-1}$$

where M is the molecular weight, T the temperature and P the pressure in Torr.

For the case of oxygen at ~10^{-4} Torr, the arrival rate of oxygen molecules may be estimated to be about 4.10^{16}, that is a sorption rate which is a factor of 10^2 higher than the arrival rate of primary ions at a current density of 75 $\mu A cm^{-2}$.

Jona (1967), using low energy electron diffraction has shown that chemisorption of dry and wet oxygen at temperatures below 500°C on clean {111},{100} and {110}Al surfaces occurs in a disordered fashion and gives rise to amorphous layers. In the case of {100} Al the L.E.E.D. pattern from crystalline Al was obliterated at an exposure of 700L (1 L = 10^{-6} Torr. sec). It is therefore expected that if photon excitation occurs by biparticle collisions between primary ions and surface target atoms, that at the oxygen exposures used here all directional effects should be reduced considerably if not totally. However, the persistance of channeling effects at high

background gas pressures indicate that the collision cascade in the solid beneath the amorphous oxide surface layer is the major mechanism affecting secondary ions and photon yields. The apparent discrepancy between this result and that of Bernheim and Slodzian may be explained as follows. Firstly, the authors stress that oxygen was admitted into the vacuum system through a tube directly on to the target surface such that the true oxygen partial pressure at the surface was most probably much higher than that indicated on the vacuum chamber pressure gauge. Secondly, the authors used a primary beam of energy 6.2 KeV. A high surface oxide coverage and a low primary energy would lead to the elimination of directional effects more rapidly than observed here since the lower energy beam would have a shorter range and be less likely to penetrate the growing oxide monolayer thus reducing the collision cascade effects of the underlying crystal substrate.

6.5 CONCLUSION

For the first time both secondary ion and photon yields have been simultaneously measured from aluminium under channeling conditions of the primary beam of argon. Pronounced directional effects have been observed in both measurements. The angular widths of the channeling minima has been measured for ions and photons and found to be 8 degrees half-width at half minimum compared to a theoretical estimate of 5 degrees. The Onderdelinden sputtering model appears to give agreement with experimental data for the overall shape of the channeling dips only for small angles and a C value of 1.6. The width of the channeling dips has indicated that both ions and photon emitting particles originate from the same depth in the crystal. The measurement of χ_{min} values has indicated a dependence upon the energy of the secondary ions and also the excitation energy of the upper levels of the optical transitions.

Oxygen adsorption on the target surface was found to increase both photon and ion yields but not to eliminate directional effects in the yield variations with target rotation. This observation has indicated that the concept of simple biparticle collisions between the primary ion and surface atoms does not provide a satisfactory explanation for photon emission under these conditions and that cascade effects must also be considered.

REFERENCES

BAYLY, A R, MACDONALD, R J., J.Sci. Inst. E. (in press).

BERNHEIM, M, SLODZIAN, G., Surface Science, 40, 169 (1973).

BERNHEIM, M, SLODZIAN, G., Int. J. Mass. Spect. Ion Phys., 12, 95 (1973).

BERNHEIM, M, SLODZIAN, G., Int. J. Mass. Spect. Ion Phys., 20, 295 (1976).

DENNIS E, MACDONALD, R J., Rad. Effects., 13, 243 (1972).

DUSHMAN, S., Foundations of Vacuum Science Technology, John Wiley & Co Ltd. (1964).

FLUIT, J M, FRIEDMAN, L, VAN ECK, J, SNOEK, C, KISTEMAKER, J., Proc. 5th Int. Conf. on Ionisation Phenomena in Gases, Munich (1961).

JONA, E., J. Phys. Chem. Sol., 28, 2155 (1967).

ONDERDELINDEN, D., Appl. Phys. Lett., 8, 189 (1966).

SLODZIAN, G., Surface Science, 48, 161 (1975).

VAN DER WEG, W F, TOLK, N H, WHITE, C W, KRAUS, J M,, Nucl. Instr. Meth., 132, 405 (1976).

ZWANGOBANI, E, MACDONALD, R J., Rad. Effects, 20, 81 (1973).

CHAPTER SEVEN

THE SPECTROSCOPY OF ION-INDUCED PHOTON EMISSION AND ITS APPLICATION TO QUANTITATIVE SURFACE ANALYSIS

7.1 INTRODUCTION

There are many techniques available for the analysis of the surface of materials which employ the use of ion beams, the more common of which have been described previously (section 1.3). Some techniques offer element detection in the parts per million region (particularly secondary ion mass spectrometry or SIMS), with depth resolutions in the monolayer region. The SIMS method uses an ion beam to sputter the surface atoms of the target. A fraction of these sputtered particles are electrically charged and can be collected and analysed according to their charge to mass ratio in a mass spectrometer. In quantitative analysis using SIMS, a relationship is required between the sputtered ion intensities and the elemental concentration in the bombarded target. There have been numerous attempts to obtain a theoretical relationship between the two (section 2.8), but perhaps the most successful of these attempts has been the local thermodynamic equilibrium (L.T.E.) model developed by *Andersen and Hinthorne (1973)*.

Ionic bombardment of solids also leads to the emission of photons. The emission is composed of sharp atomic emission lines and arises from sputtered particles de-exciting free from the influence of the target surface. The analysed spectra closely resemble those of an arc discharge and characteristic emission lines of the elements can easily be identified from standard wavelength reference tables. In the following the possibility of describing the photon emission in terms of a plasma, i.e. an arc discharge, in L.T.E. is examined.

Standard spectrochemical techniques are then used in an attempt to obtain quantitative analysis using ion beam excited photon emission. This is a much different approach to that of *Tsong et al (1975)* in which quantitative analysis (of insulators only to date) is based on the use of standards and an accurate knowledge of sputtering yields.

7.2 LOCAL THERMODYNAMIC EQUILIBRIUM IN A PLASMA

The temperature of a plasma can be defined in a number of ways (*Boumanns, 1966*):

(1) The electron temperature, which arises from the kinetic energy of the electrons,

(2) The gas temperature, due to the kinetic energy of the neutral atoms,

(3) The ionisation temperature, which governs ionisation equilibria, and

(4) The excitation temperature, which describes the population of various energy levels.

In molecular gases temperatures can also be assigned to dissociation equilibria and to the rotational and vibrational states of the molecules. When the system is in thermal equilibrium, all definitions lead to the same numerical value. In thermal equilibrium, the velocity distribution of free molecules, atoms, ions and electrons is given by the Maxwell-Boltzmann distribution function. Further, each separate kind of particle populates the available excited energy levels according to the Boltzmann distribution law and the degree of ionisation of atoms, molecules and radicals is governed by the equations of Saha.

7.3 L.T.E. AND SECONDARY ION ANALYSIS

The quantitative model developed by Andersen and Hinthorne to describe secondary ion emission is based on the formation of a plasma in L.T.E. in the target during ion irradiation. The validity of the use of this model is based on the agreement obtained by the authors of their experimental data with other established analytical techniques, when their data was corrected using the plasma equations describing L.T.E. The concentration of a given element in the target is calculated using the Saha-Eggert equation -

$$\text{(i)} \quad \frac{n^+ n_e}{n_o} = \frac{Z^+(T)}{Z^o(T)} \cdot 2 \cdot \frac{(2\pi mKT)^{3/2}}{h^3} \exp - (E_r - \Delta E_r)/KT$$

where n^+, n_e and n_o represent the concentration of ions, electrons and neutrals, Z^+,2, Z^o their respective partition functions, K is Boltzmann's constant, h, Planck's constant, E_r the ionisation potential and T the temperature. ΔE_r is a correction arising from the depression of the ionisation potential in the plasma. The only unknown parameters in equation (i) are the electron concentration, n_e and the temperature, T which can be determined from the measured ion currents of two elements of known concentration in the target. The method takes advantage of the presence of oxygen either as a background gas or a primary ion to improve secondary ion yields, apparently by reducing ion neutralisation or by changing the work function of the target (*Andersen, 1961*).

This model has received some attention in recent years with regard to the analysis of stainless steels (*Morgan and Werner, 1976 , Rüdenauer et al, 1976, Tsunoyama et al, 1976*). One of the principal objections to its use is the temperature used to fit the data and to determine elemental concentrations from the secondary ion yields. The temperature values usually range from 4000°K to 11000°K, much higher

than the melting point of the target and difficult to relate to the physical process involved. The energy distributions of secondary particles (ions, atoms and electrons) are also non-Maxwellian and usually characterised by a low energy peak (of ~ 20 eV for ions and 3-10 eV for neutrals and electrons) followed by a high energy tail. (Figs 1.1, 1.1A, 1.1B).

7.4 L.T.E. AND ION INDUCED PHOTON EMISSION

There have been only two reported measurements of the temperature of a sputtering photon source. The first was by *Mayer (1933)* who studied photon emission from metals bombarded with alkali primary ions. A temperature of the source of emission of Na lines from sodium ions striking platinum was estimated to be 30,000^{o}K. *Kato, Shimizu and Ishitani (1974)* have also estimated the temperatures of metallic and oxidised targets sputtered with 14 KeV Ar^{+}. The temperature determined from the sputtered excited neutral atoms was around 4000^{o}K from Al and 5000^{o}K to 8000^{o}K from Al_2O_3. A similar result was obtained when the temperatures were calculated using the data of *Kerkow (1972)*, and generally it was found that the oxidised targets gave higher temperatures than metallic targets. These temperatures were similar to those determined purely from SIMS experiments (*Shimizu et al 1974*).

7.5 THE CALCULATION OF TEMPERATURES USING SPECTROCHEMICAL METHODS

The intensity of an emission line in a plasma is given, according to Boumans by -

(i) $$I_{qp} = A_{qp}\ h\ \nu_{qp}\ n\ g_q\ Z^{-1} \exp(-E_q/KT)$$

where A_{qp} = transition probability from an upper limit q to a lower level p

ν_{qp} = frequency

n = density of excited particles

g_q = statistical weight of the upper level q

E_q = energy of excitation

Z = partition function

T = excitation temperature

Re-arranging and using the relative intensity I'_{qp} and the relative transition probability A'_{qp} -

(ii) $$\ln \frac{I'_{qp}}{g_q A'_{qp} \nu_{qp}} = \ln \frac{n}{Z} - \frac{E_q}{KT}$$

For a given group of emission lines from atoms of the same type, $f(\ln I')$ is a linear function of E_q since n and Z will remain constant. The temperature of excitation is determined from the slope of the $f(\ln I')$ versus E_q plot. This method has been employed by many authors to determine temperatures of various types of discharges (for example *Golightly and Harris (1975)* - argon plasma jet source, *Corliss (1962)* - arc discharge).

An alternative method of temperature determination is to measure the relative intensity of two emission lines of a particular neutral atom or two lines emitted by an ion. Equation (i) then becomes -

(iii) $\frac{I_a}{I_b} = \frac{(gA)_a}{(gA)_b} \frac{\nu_a}{\nu_b} \exp [- (Ea-Eb)/KT]$ which can

be re-written as -

(iv) $$T = \frac{5040\ (Va-Vb)}{\log\ (gA)_a / (gA)_b - \log \lambda_a/\lambda_b - \log I_a/I_b}$$

where V is the excitation potential in eV of the upper levels of the transitions of lines a and b of wavelength λa and λb.

According to Boumans this approach is subject to large errors unless the difference between Va and Vb is large. The relative error (dT/T) is given as -

(v) $$\frac{dT}{T} = \frac{T}{5040\,(Va-Vb)} \cdot 0.434 \frac{dI}{I}$$

This two line method was used by *Kato et al (1974)* and errors in their temperature values were estimated to be of the order of $\pm\ 500^{o}K$ to $\pm\ 1800^{o}K$.

Implicit in either technique is an accurate knowledge of the relative transition probabilities. The method based upon the use of equation (ii) requires a large range of values of E_q and the measurement of the intensities of a number of emission lines contained within a narrow band of wavelengths in order to avoid large errors being introduced from variations in the detector sensitivity. Iron is a particularly suitable element for investigation since the relative transition probabilities are well known and a fairly wide range of values of E_q are also contained within a narrow wavelength range of the spectrum. In the present study, the first technique, based on equation (ii) is used. The second method, using equation (iv) is not universally applicable because the error condition requires

two lines close together in wavelength but far apart in excitation potential. In the measurement of arc temperatures, thermometric species are usually introduced, the two most commonly used being Cu and Zn. The ZnI 3076/3072, ZnI 3076/3282 or alternatively the CuI 5219/5106, 5153/5106, 5219/5782 emission line intensity ratios are then used in equation (iv) *(Boumans 1966)*.

7.6 EXPERIMENTAL

7.6.1 TARGETS SUITABLE FOR TEMPERATURE DETERMINATION

In the determination of a temperature from an ion induced photon spectrum, the results of the photon emission survey discussed in Chapter Four have indicated targets most suitable for study. The light elements Mg, Al and Si all emit strong lines of the neutral atom and ion which are considerably enhanced (in the case of neutral line emission), by both O_2^+ and N_2^+ primary ion bombardment. The result obtained by introducing oxygen into the target environment during Ar^+ bombardment is very similar to that observed with O_2^+ bombardment. The neutral emission is intensified and the emission from the first and second charge states is largely unaffected.

The transition models Sc, Ti, V, Cr, Fe and Ni as well as Cu and Zn, emit rich spectra very similar to an arc discharge with very little change to the relative intensity of lines within the spectrum when reactive gas is introduced or reactive ion bombardment is used.

Certain elements such as Zr, Nb, Mo, Hf and W emit strong lines superimposed upon a particularly strong background continuum, under inert and reactive gas ion bombardment. The final group of elements considered were the heavy elements Pt, Au and Pb which gave few characteristic lines and were largely unaffected by reactive gas bombardment. These results indicate that the most appropriate group

for study under the assumption of L.T.E. are the transition metals and Cu and Zn.

7.6.2 EXPERIMENTAL METHOD

The apparatus used for studying the photon emission has been described in Chapter Three. In these experiments primary ions of 50 KeV energy were used to bombard polycrystalline targets of 99.999 per cent purity under high vacuum conditions (~ 1.10^{-7} Torr.). The targets were irradiated at an angle of 45^{o} to the normal and the photon emission observed perpendicular to the ion beam axis with a monochromator. Beam current densities of the order of 100 μa cm^{-2} maximum were used. A UHV Granville-Phillips valve was fitted to the experimental chamber in order to leak in oxygen to a pressure of ~ 5.10^{-5}Torr. measured on an ionisation gauge.

7.7 RESULTS

A typical ion bombardment excited spectrum obtained from Fe is shown in Fig 7.1 and the FeI lines used for temperature determination have been indicated. Figs 7.2A and 7.2B show the plots obtained from Fe and Zn according to equation (ii). The vertical axis is plotted in terms of the oscillator strengths since these are more commonly tabulated than transition probabilities. The horizontal axis is plotted in the conventional units of kilokayers (KK) where 1K = 1 cm^{-1}. The temperature is given by -

(vi) $$T = \frac{-625\,Eq}{\log I\,\lambda^3/gf - c}$$ where f is the oscillator strength and c a constant. The oscillator strengths of *Valters (1964)* were used for the Fe plot and those of *Schuttevaer (1943)* for Zn. The equivalent arc temperatures of the photon source for 50 KeV Ar^{+}

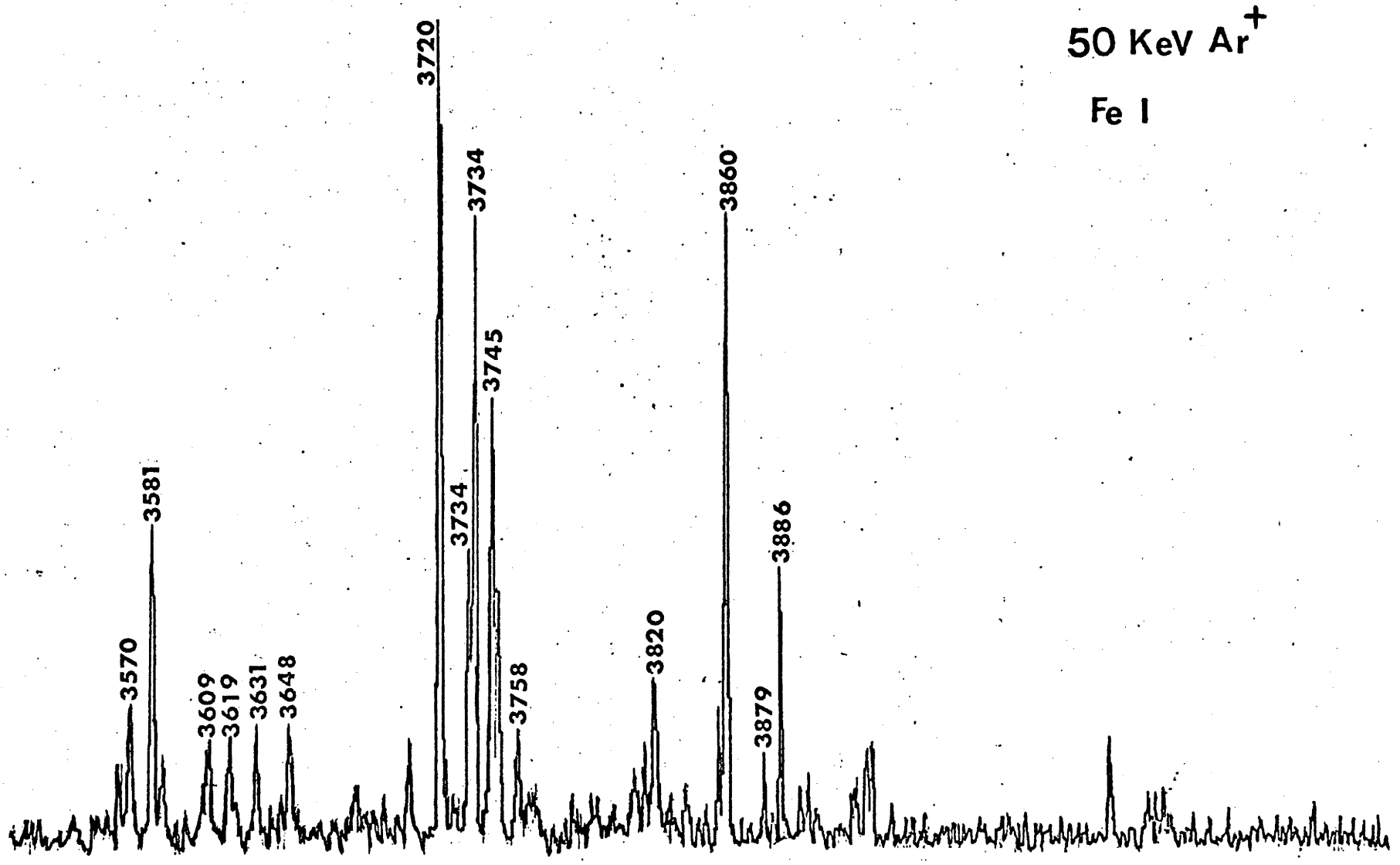

FIG 7.1 FeI SPECTRUM PRODUCED BY 50 KeV Ar^+ BOMBARDMENT OF A PURE IRON TARGET.

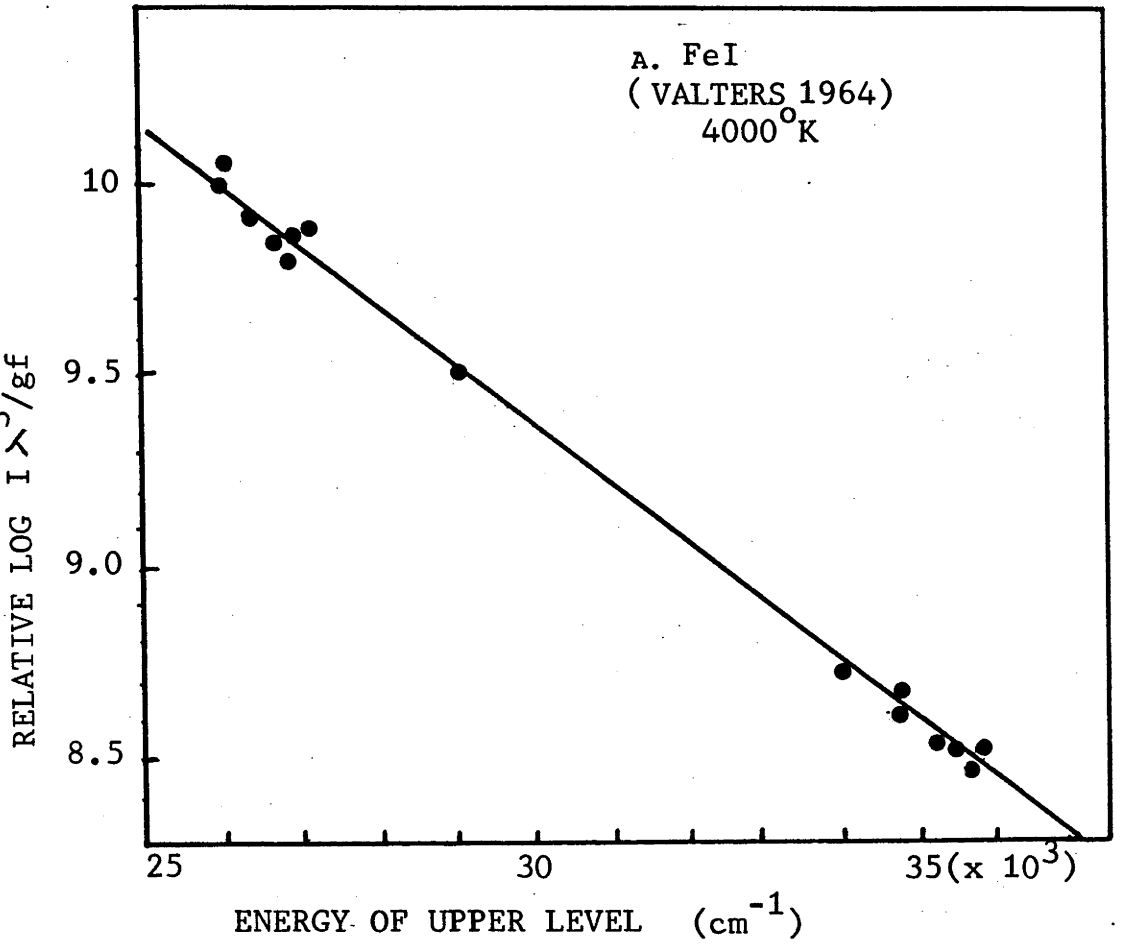

FIG 7.2 TEMPERATURE DETERMINATION FROM ION BOMBARDMENT OF Fe AND Zn.

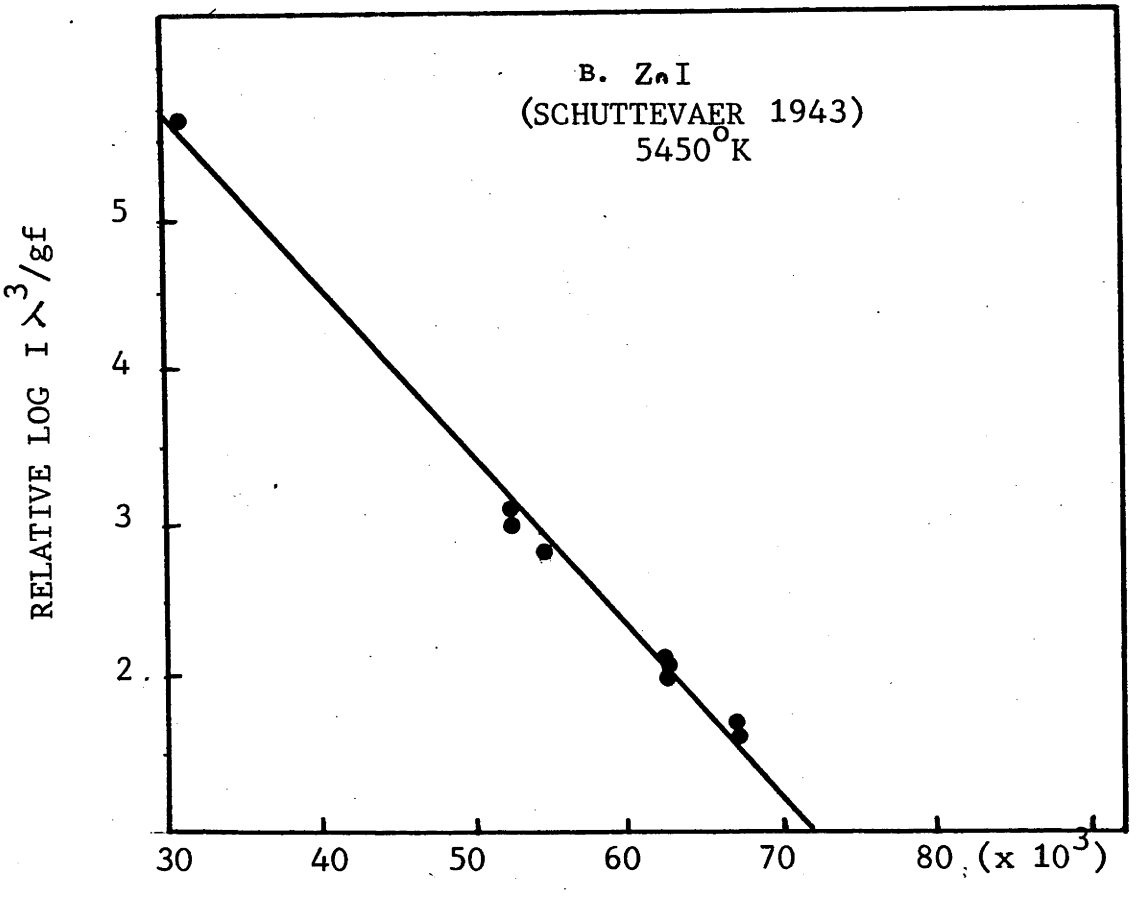

bombardment of Fe and Zn were 4000°K and 5450°K respectively. The results obtained by *Corliss(1962)* for Fe and Zn seeded Cu arcs using the published intensities of the N.B.S. Tables of Spectral-Line Intensities are shown in Fig 7.3. The linear fits of the ion-induced spectra and copper arc spectra are seen to be comparable. Temperatures determined for Ar^+ bombardment of Cr, Fe, Ni, Cu, Zn and also a heavier Sn target are given in Table 7.1.

TABLE 7.1

Experimentally Determined Excitation Temperatures

Target	T°K (±50)
Cr	3300
Fe	4000
Ni	4700
Cu	4000
Zn	5450
Sn	4700

7.8 DISCUSSION

7.8.1 QUANTITATIVE ANALYSIS USING PHOTON EMISSION

On the basis of the results obtained from the temperature plots, an attempt was made to determine the concentration of Cr present in a sample of stainless steel (supplied by A.I.S. Pty.Ltd, Port Kembla). The temperature was determined from the Fe emission lines since the large majority of Cr lines were blended with certain Fe lines. The intensities of an FeI line and a CrI line were then measured and corrected for the instrument transmission function. The relative concentration of Cr to Fe was calculated using equation (vii).

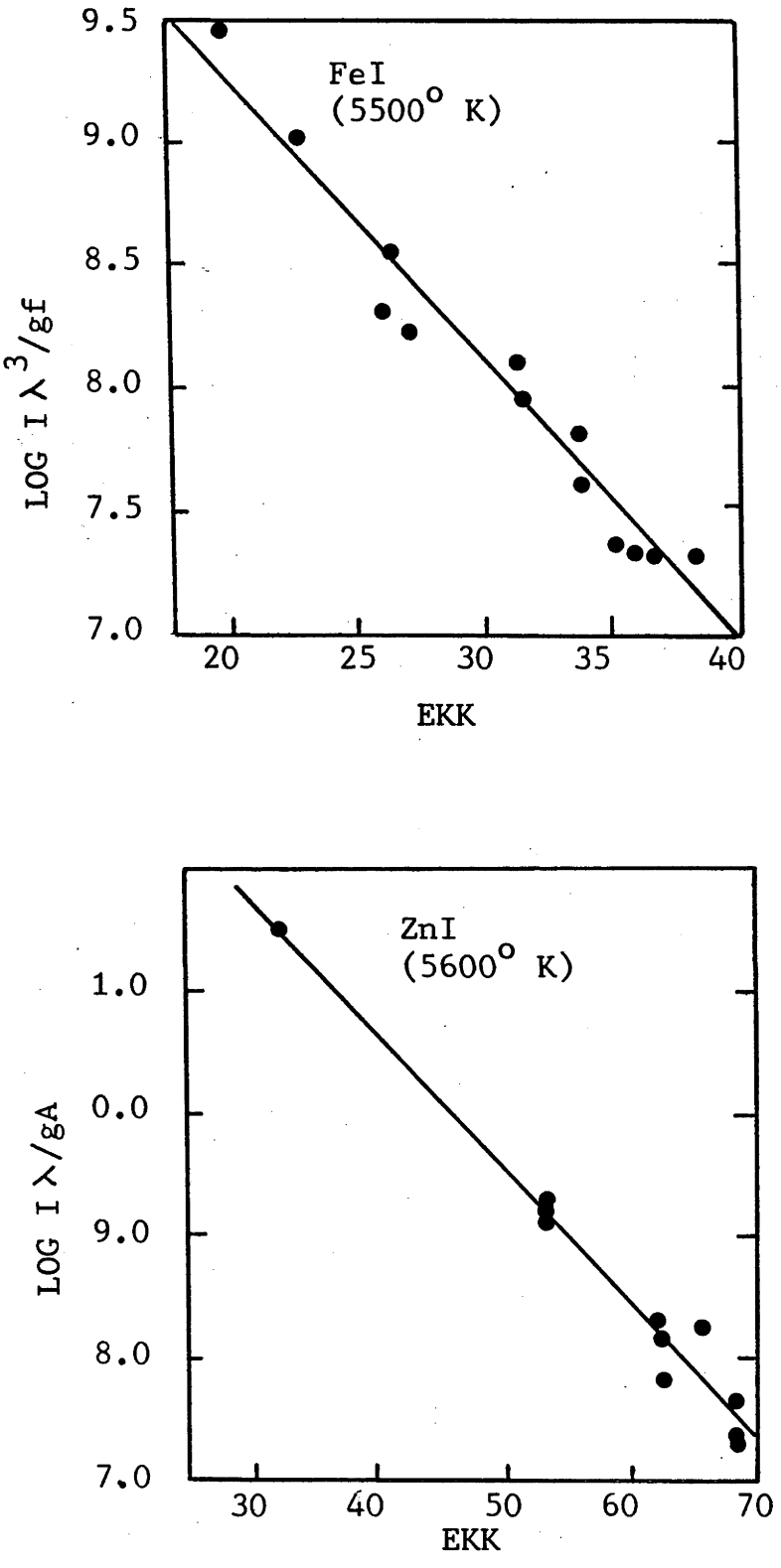

FIG 7.3 TEMPERATURE PLOTS OF THE N.B.S. ARC (CORLISS 1962)

$$\text{(vii)}\quad \frac{I_{Cr}}{I_{Fe}} = \frac{A_{Cr}}{A_{Fe}} \cdot \frac{\lambda_{Fe}}{\lambda_{Cr}} \cdot \frac{n_{Cr}}{n_{Fe}} \cdot \frac{g_{Cr}}{g_{Fe}} \cdot \frac{10^{(-5040.V_{Cr}/T)}}{10^{(-5040.V_{Fe}/T)}} \cdot \frac{Z_{Fe}}{Z_{Cr}}$$

where n_{Cr}/n_{Fe} represents the relative concentrations of Cr:Fe. The equivalent arc temperature, for 50 KeV Ar^+ bombardment of the steel at a pressure of 1.10^{-7} Torr, was 3800°K. From the ratio of the FeI 3719.9 Å and CrI 4254.4 Å lines the percentage concentration of Cr was calculated to be 15 per cent, using the standard spectrochemical analysis for Fe, shown in Table 7.2.

TABLE 7.2

Standard Spectrochemical Analysis of Stainless Steel Sample

Element	C	P	Mn	Si	S	Ni	Cr	Mo	Cu
Concentration	.070	.018	.82	.52	.021	6.95	17.35	.08	.015

N.B. Fe ~ 100 - Σ C+P+Mn+Si+S+Ni+Cr+Mo+Cu ~ 74 per cent.

Other elemental concentrations measured by standard spectrochemical techniques are also given in Table 7.2. The partition functions for Fe and Cr used in equation (vii) were taken from *Drawin and Felenbok (1965)*. The value of 15 per cent Cr is in reasonable agreement with the standard technique value of 17 per cent as shown in Table 7.2.

The experiment was repeated in an oxygen atmosphere in order to enhance the intensity and possibly improve the accuracy under these conditions. The intensity of the FeI and CrI emission lines used above was measured as a function of the partial pressure of oxygen over the range of $< 5.10^{-7}$ Torr. to 5.10^{-5} Torr. The result obtained is shown in Fig 7.4. It can be seen that the photon yield in both

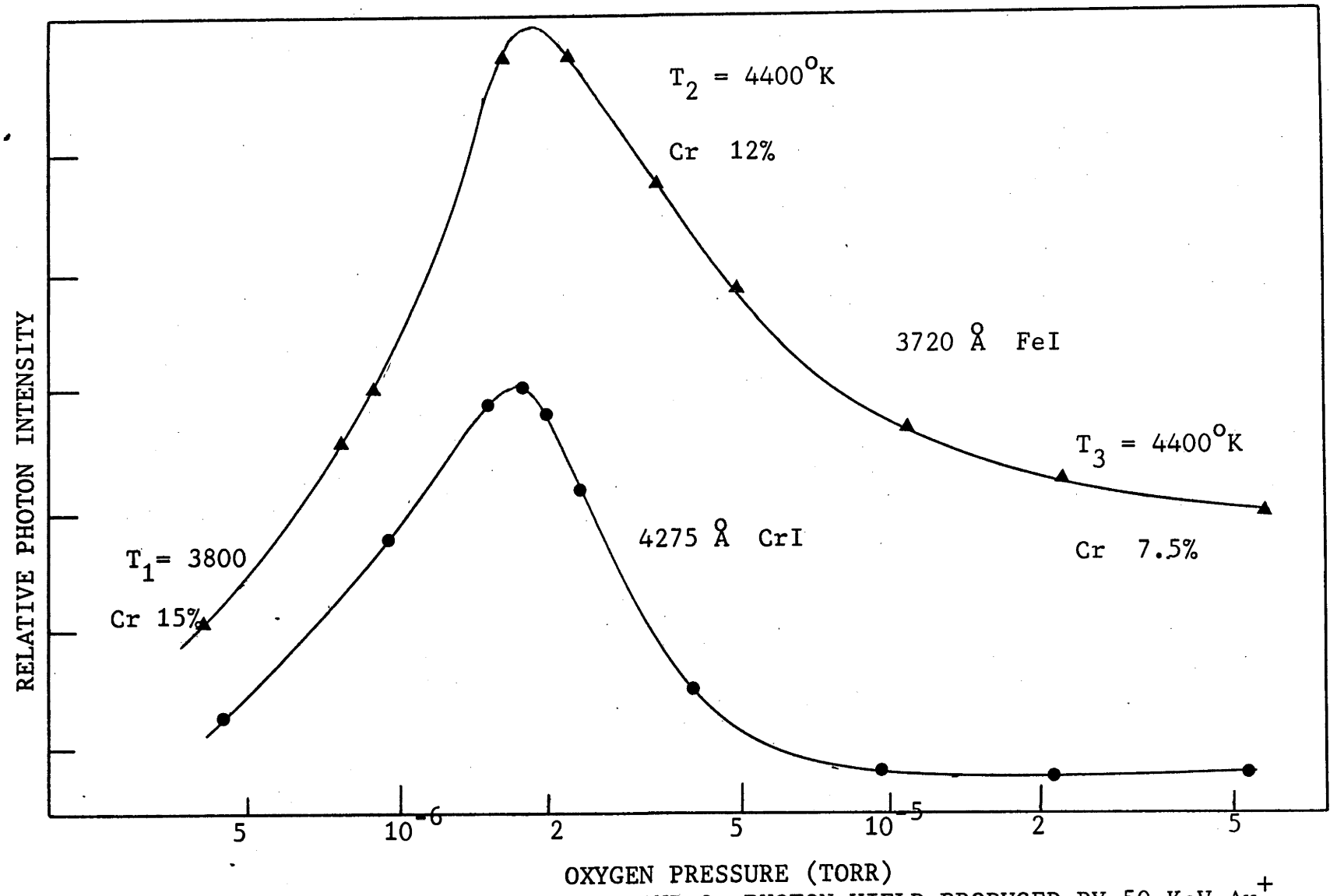

FIG 7.4 THE OXYGEN DEPENDENCE OF THE Fe AND Cr PHOTON YIELD PRODUCED BY 50 KeV Ar^+ BOMBARDMENT OF STAINLESS STEEL.

cases is changed in a non-uniform fashion and also to a different extent for the Fe and Cr lines.

The photon yields peak at approximately the same pressure value but the FeI line is intensified by a factor of about 3 whereas the CrI line is only increased by a factor of about 2. At pressures exceeding that corresponding to the peak yield of photons, the emission is seen to decay until at the maximum pressure value reached, the FeI yield has dropped to ~ 50 per cent of the peak value and the CrI yield to a value slightly below the initial 'clean' yield and a factor of 4 down on its peak value. The effective excitation temperature and Cr concentration have been calculated at the 3 points shown in Fig 7.4.

The oxygen dependent effect was investigated further by substituting a pure Cr target and monitoring the intensity of several CrI lines and a CrII (Cr^+) emission line. The transitions, wavelengths and energy values of the upper states of the lines monitored are given in Table 7.3.

TABLE 7.3

CrI and CrII Emission Lines Monitored

Wavelength (Å)	Spectrum	Transition	Energy of Upper Level (eV)
4254	CrI	$4s'a^7S_3 - 4_p1z^7P^o_4$	3.0
4049	CrI		6.9
3021	CrI	$4s^2a^5D_4 - 4_p1Y^5F^o_5$	5.1
2836	CrII	$4s^1a^6D_{4,1/2} - 4_p{}^1Z^6F^o_{5,1/2}$	5.9

1st ionisation potential = 6.76 eV.

It can be seen from Fig 7.5 that the behaviour of all the CrI emission lines is very similar and each plot exhibits a peak in the photon yield

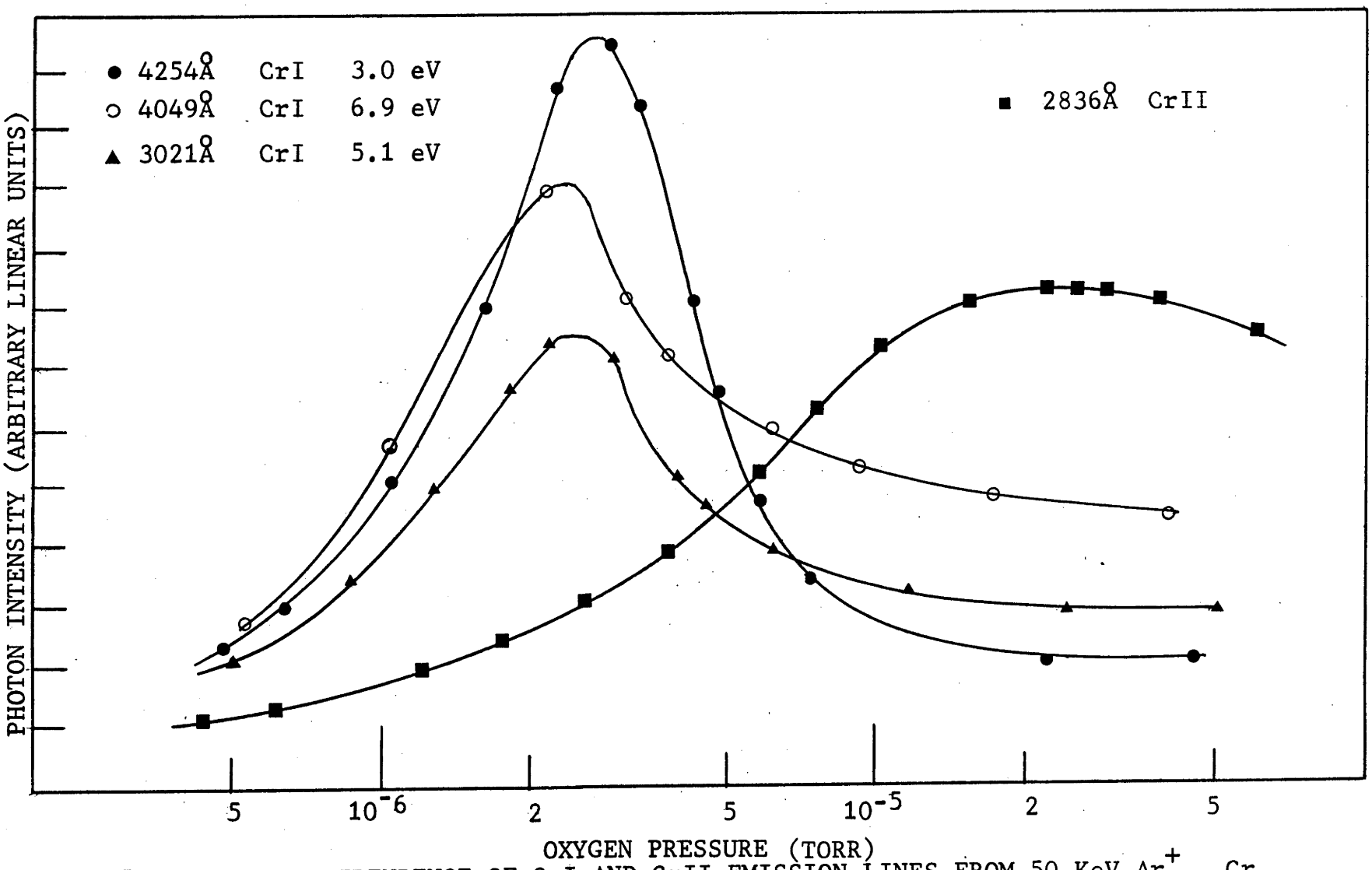

FIG 7.5 THE OXYGEN DEPENDENCE OF CrI AND CrII EMISSION LINES FROM 50 KeV Ar^+ Cr
THE CrI EMISSION LINES ARE NORMALISED AT 5 x 10^{-7} TORR.

at approximately the same pressure value. The CrII emission line however, has a very different behaviour. There is a gradual rise in photon intensity to the point where the CrI emission peaks. At this point the CrII emission appears to increase more rapidly until an apparent saturation is reached.

An experiment was conducted to investigate the behaviour of the CrI photon peak with primary beam density. The beam current was varied over the range 10-40 μa cm^{-2} and the results are shown in Fig 7.6A,B. It was found that there existed a linear relationship between the beam current density and the partial pressure of oxygen at which a peak in the 4555 Å CrI photon yield occurs.

There have been only few reports in the literature on the oxygen dependence of photon emission from ion bombarded transition metals. *Thomas and De Kluizenaar (1975)* have shown that the photon emission of CuI increases with oxygen partial pressure but does not peak and decay in the same manner as the CrI lines. The absence of a peaking effect in this instance may be explained on the basis of the current density ~ 50μa cm^{-2} used by the authors. The behaviour of CuI emission (3247 Å) with oxygen partial pressure has been examined using a current density of 55 μA cm^{-2} and 20 μA cm^{-2}. The Cu behaviour, as shown in Fig 7.7 is however different to the CrI behaviour of Fig 7.5, but it is evident that the lower current density does in fact lead to a peak in the CuI photon yield.

The temperature plots obtained from the transition metals investigated are in reasonable agreement with the data of Corliss for the seeded Cu arc and emphasise the degree to which the ion induced optical spectra resemble those of an arc discharge. The results indicate that the population of the excited states can, within the limits

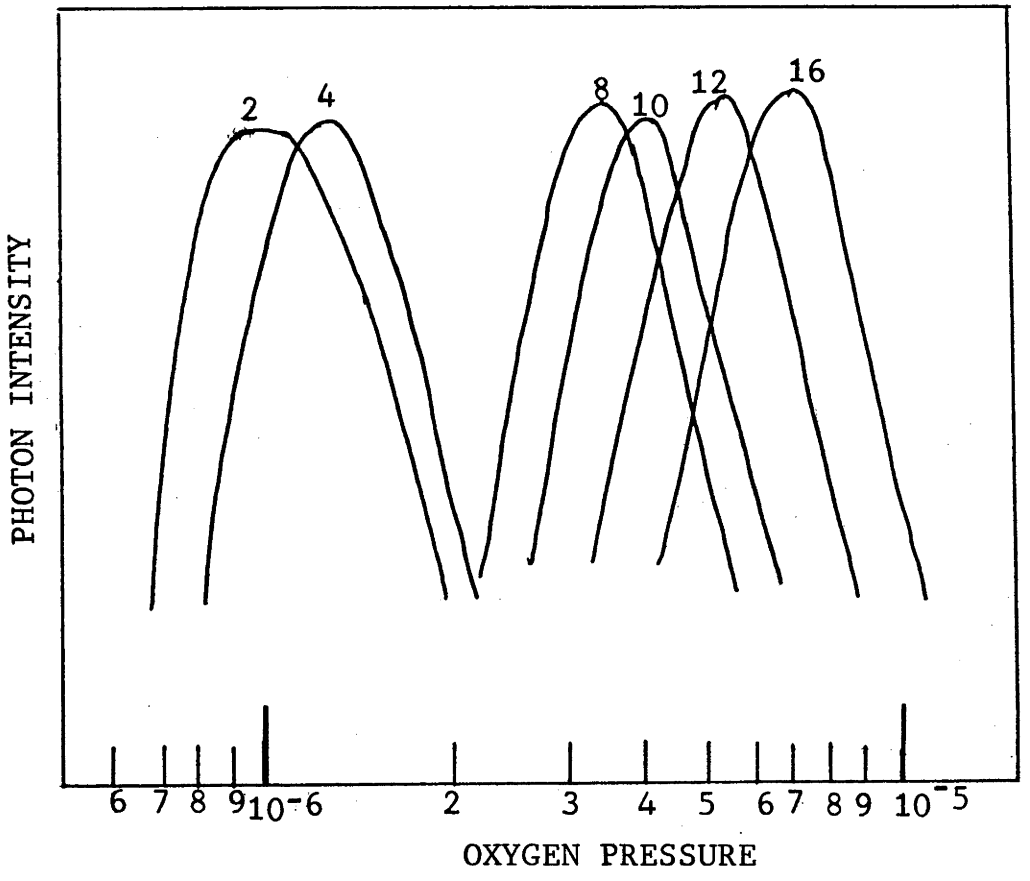

A. THE SHIFT IN THE MAXIMUM PHOTON YIELD OF THE 4254Å CrI EMISSION LINE TOWARDS HIGHER OXYGEN PRESSURES AS THE PRIMARY ION CURRENT IS INCREASED FROM 2 TO 16 μa (x 5 cm^{-2})

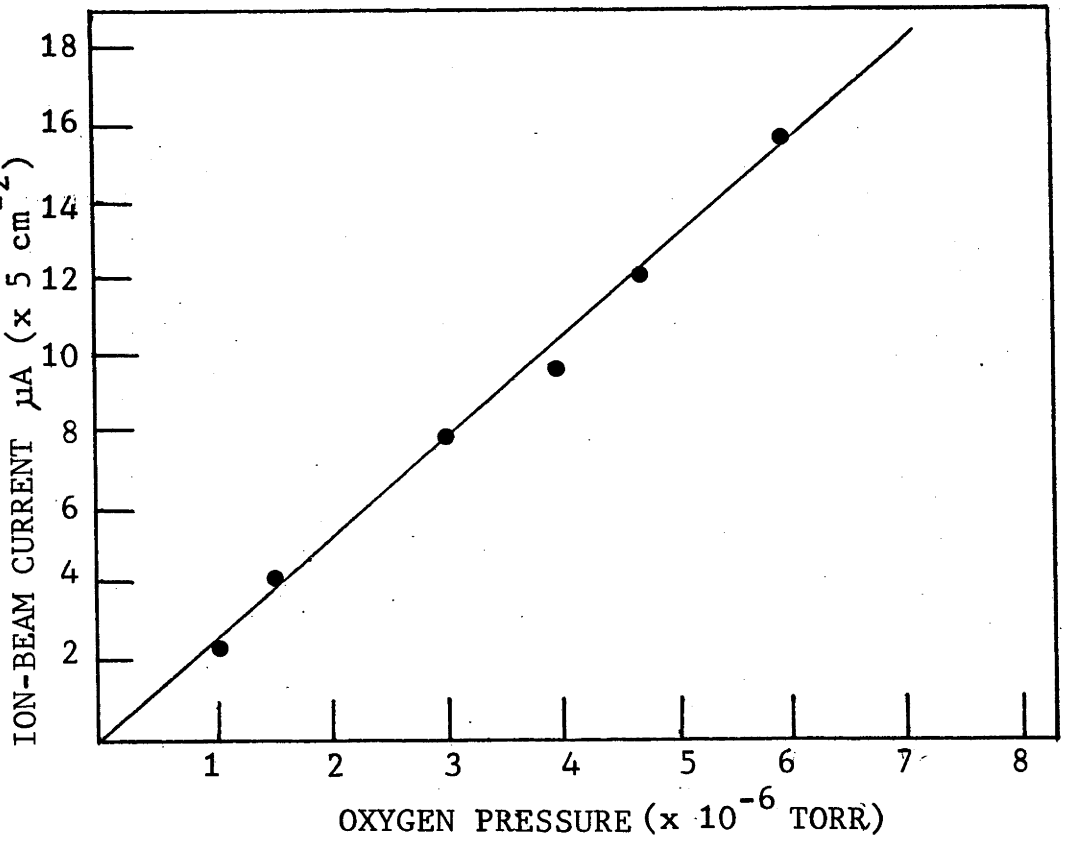

B. THE RELATIONSHIP BETWEEN BEAM CURRENT AND OXYGEN PRESSURE AT WHICH THE MAXIMUM PHOTON YIELD OCCURS.

FIG 7.6

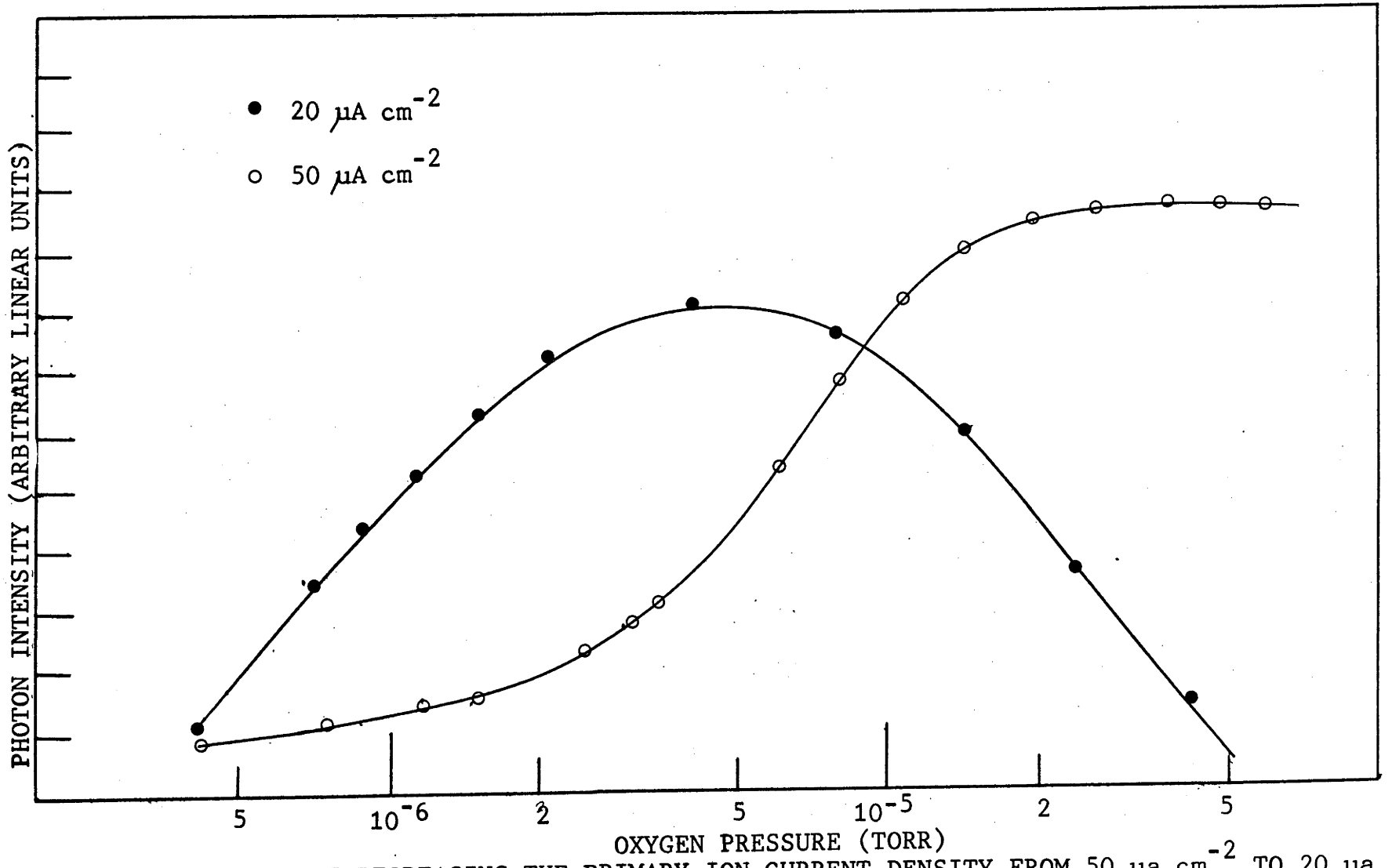

FIG 7.7 THE EFFECT OF DECREASING THE PRIMARY ION CURRENT DENSITY FROM 50 ua cm^{-2} TO 20 ua cm^{-2} ON THE OXYGEN DEPENDENCE OF THE 3247Å CuI PHOTON YIELD.

of this investigation, be described by a Boltzman distribution function.

Rudenauer et al (1976) have calculated emission temperatures for stainless steel bombarded with 5.5 KeV Ar^+, using the Andersen and Hinthorne treatment of secondary ion emission. They obtained values of 3600^oK and 5400^oK for clean and oxygenated surfaces, which agree with the spectroscopic values given here. However, the authors were unable to definitely state whether or not the concept of a plasma near the surface is correct. The equations which are derived from the plasma concept do however happen to provide a suitable means of fitting data, but the temperature T and electron density n_e could be merely fitting parameters without physical meaning. Further SIMS work by *Morgan and Werner (1976)* on an NBS 461 low alloy steel revealed that for saturation oxygen conditions the value of T was around 6300^oK using either 5.5 KeV Ar^+ or O_2^+ primary ions. A temperature value could not be determined for Ar^+ bombardment under clean conditions due to the effects of trace amounts of oxygen present. However their results indicated that the temperature increased from around 3200^oK at 2.10^{-7} Torr. (O_2^+ primary ions), to 6200^oK at 8.10^{-6} Torr. of O_2. The optical data has also indicated that the effective excitation temperature is increased by the presence of oxygen. The non-uniform behaviour of the photon yield from CrI and FeI would seem to indicate one of two possibilities. Firstly, the technique employed is not applicable under certain surface conditions to quantitative surface analysis of these elements, or secondly, the variation in the CrI and FeI yields is in fact a reflection of the real concentration of Cr and Fe atoms on the target surface in the presence of oxygen. This last possibility will be discussed further in section 7.8.3.

7.8.2 PHYSICAL INTERPRETATION OF L.T.E. TEMPERATURES

The results obtained give reasonable agreement to the theory of the existence of L.T.E. at an ion bombarded surface within the limits of the investigation. The use of L.T.E. theory and the temperatures necessary to obtain quantitative analysis using secondary ion or photon data is difficult to justify in terms of the physical processes which occur when a solid is irradiated with ions. The most likely mechanism that can possibly explain the apparent L.T.E. conditions is the thermal spike model (*Seitz and Koehler, 1956*).

Andersen (1975) has discussed the possibility of thermal spikes being the origin of the L.T.E. conditions. *Jurela (1973)* has also considered thermal spikes as a possible source of the high temperatures encountered in his model of secondary ion emission (section 2.8.2.2). A discussion of the theory of thermal spikes can be found in the work of *Seitz and Koehler (1965)*. For the purposes of this discussion a brief outline only will be given. The damage region resulting from collisions of primary ions and the target surface may be left with an excess energy when all the secondary collisions have been completed after a time of about 10^{-13} sec. This leads to the creation of a local hot-spot termed a thermal spike whose lifetime is dependent upon the conductivity of the surrounding lattice. If the thermal spike intersects the target, surface atoms may be ejected through the evaporation process. The energy spectrum of ejected atoms should be described by Maxwell-Boltzmann statistics but is in fact characterised by a low energy peak and a high energy tail (Fig 1.1). This fact is a major point against the thermal spike theory. Experimental evidence for thermal spikes is hard to obtain, but some evidence is available from the work of *Nelson (1965)* on sputtering ratios. If a thermal spike

forms at the free surface of a crystal the evaporation expected to result should manifest itself as a characteristic low-energy peak in the spectrum of ejected atoms. Furthermore the sputtering rate should rise rapidly with temperature. Confirmation of a rise in the thermal sputtering ratio with temperature was found by Nelson for a range of elements and by fitting experimental and theoretical curves thermal spike parameters were determined. The temperatures calculated were low and varied from 49°K to 1060°K.

A recent theoretical study by *Sigmund (1974)*, has shown that spike effects may be important when the spike lifetime τ is larger than the duration of the initiating cascade τ_o, and that a tendency towards L.T.E. exists in the spike which is dependent upon the excess of τ over τ_o. The Sigmund model also allows estimates of the spike temperature to be made and order of magnitude estimates for spike temperatures arising from 50 KeV Ar^+ bombardment of Cr, Fe, Ni, Cu Zn and Sn are given in Table 7.4.

TABLE 7.4

Theoretical Estimates of thermal Spike Time Constants and Temperatures

50 KeV Ar^+ Target	Time Constant	θ(eV)	Temperature K°
Cr	1.9×10^{-11}	0.42	3200
Fe	1.8×10^{-11}	0.72	5600
Ni	1.5×10^{-11}	0.84	6500
Cu	1.8×10^{-11}	0.71	5500
Zn	3.0×10^{-11}	0.43	3300
Sn	1.0×10^{-11}	0.13	1000

(Sigmund, 1974, using m = 1/3).

Estimates of the time constant τ have also been made using the model. The model determines the mean energy deposited per target atom using the theory of gross spatial distribution of deposited energy in elastic collision cascades (*Winterbon et al, 1970*). Elastic scattering at an inverse-power potential, $V \propto r^{-1/m}$ is assumed where r is the internuclear distance and $0 \leq m < 1$. The maximum energy density Θ_o (energy per atom) is given by -

$$\Theta_o = G_2 N^2/E^2 \quad \text{for } m = 1/2$$

$$\Theta_o = G_3 N^2/E \quad \text{for } m = 1/3$$

and the time constant τ by -

$$\tau = H_2 E^3/N^2 \quad \text{for } m = 1/2$$

$$\tau = H_3 E^{11/6}/N^2 \quad \text{for } m = 1/3$$

In these expressions N is the target atom density and E the primary ion energy. The parameters G_2, G_3, H_2 and H_3 have been estimated from the theoretical contour plots of Sigmund for the ion target combinations of Table 7.1. The theoretical time constant has a value of around 10^{-11} sec, which is about 100 periods of atomic vibration and within the range of thermal equilibrium (*Andersen, 1975*). The temperature values are also of the same order as the experimentally determined values with the exception of Sn. The value of the theoretical estimate is sensitive to the choice of the exponent in the scattering potential and this has been taken as m = 1/3 for all cases. However for $Ar^+ \rightarrow$ Sn the target mass is greater than the primary ion mass by a factor of nearly 3 for which the exponent value, 1/3, may not apply as well as for nearly equal target and ion masses. However, the theoretical results although only approximate do indicate that thermal spikes can account for the high temperatures which have been experimentally determined.

It has been pointed out by *Andersen (1975)* that the effective energy per atom in the spike, according to Sigmund's model, should decrease in a simple linear relationship with increasing bombarding ion energy. This inverse relationship has in fact been observed by Andersen in his microprobe analysis work. Further experimental work is desirable to ascertain whether or not such an effect can be observed in the temperatures obtained from photon analysis, and hence the validity of the Sigmund model to describe the ion-surface interaction process.

As mentioned by *Kato et al (1974)*, once a temperature has been established for the plasma it should be possible to also determine the electron density n_e, spectroscopically. The procedure is based on the measurement of an ion-atom line pair ratio and the use of the Saha equation -

$$\log n_e = -\log \frac{I^+_{qp}}{I_{qp}} + \log \frac{g^+_q \; A^+_{qp}}{g_q \; A_{qp}} - \log \frac{\lambda^+}{\lambda} - 5040 \; \frac{(V_{ij} + V^+_q - V_q)}{T}$$

$$+ 3/2 \log T + 15.684. \qquad \textit{(Boumans 1966)}$$

where $V_{ij} = I_p - \Delta E$, and the energy depression $\Delta E = 2.95.10^{-8} \gamma (n_e/T)^{1/2}$ ($\gamma \; \underset{\sim}{} \; 1.2$).

In this expression n_e is the electron density (cm^{-3}) and the remaining factors are as defined previously. The superscript $^+$ refers to the ion line. The method is again subject to large errors caused by an inaccurate value for the ratio of the transition probability A^+/A and errors in the temperature determination in addition to inaccurate estimates of the emission line intensity ratio I^+/I.

7.8.3 THE EFFECT OF OXYGEN ON PHOTON EMISSION

The oxygen dependence of the photon emission is generally interpreted in terms of the electron transfer model. This has been successfully applied to a number of elements, (section 2.5.7). The interpretation seems reasonable for the increase in yield from an oxygenated surface but the peaking effect observed for reduced beam intensities on Cu and all beam densities on Cr for the neutral spectra cannot be interpreted using this model. The effect is observed for all the CrI emission lines irrespective of their excitation potential (Fig 7.5) and also for reduced current densities on CuI emission.

Similar behaviour for the Cr^+ and Fe^+ secondary ion yield from a sample of 301 stainless steel has been observed by *Schubert (1974)*. A peak in the Cr^+ yield was found to occur when the sample was exposed for 10^{-5} Torr-sec and then bombarded with a 2 KeV Ar^+ beam of <50 nA. A peak also occurred for Fe^+ but at an exposure of ~ 10^{-4} Torr-sec. This behaviour is very similar to that observed in Fig 7.4. Frequently it is observed that the behaviour of the neutral atom photon spectra of ion bombarded solids in an oxygen atmosphere closely follows that of the first charged state of the secondary ion yield, particularly so in the case of light elements (Chapter Five). It is therefore worthwhile considering briefly some of the present ideas concerning the behaviour of secondary ions in the presence of oxygen.

Secondary ion emission has been used to study oxygen adsorption on metals and most of the information on the behaviour of secondary ions in the presence of oxygen comes from these experiments. Two methods are employed to study the adsorption of gases on metal surfaces: the static and the dynamic method. In the latter method the amount of gas adsorbed results from an equilibrium condition

dependent upon the residual gas pressure, primary ion current and sputtering rate. This situation is similar to the situation studied here. In the former method gas is adsorbed on the surface as a function of time and then the primary beam is used to analyse the surface monolayer. In the presence of oxygen the metal ion yield, M^+, is always increased and is generally termed M^+ chemical ion emission. Chemical emission of Cr^+ has been studied by several authors and in simple terms can be explained on the basis of the rupturing of molecular bonds between the Cr atoms and adsorbed oxygen atoms leaving the Cr in a charged state. *Benninghoven and Müller (1973)* have used the static SIMS technique to investigate the surface reaction occurring between Cr and adsorbed oxygen. They concluded that oxidation takes place by a progression through a series of phases. The first oxide phase occurs in the 50-100L, ($1L = 1.10^{-6}$ Torr 0_2 sec^{-1}), range when the molecular ion $Cr\ 0_2^-$ is formed on the surface. At higher oxygen coverage the emission of $Cr\ 0^+$ ions begins and the $Cr\ 0_2^-$ ion yield decreases. This is regarded as a second phase. *Werner et al (1975)*, have used the property of a given oxide structure to emit specific secondary ions to develop the concept of characteristic mass spectra or fingerprint spectra. Fingerprint spectra can be used to determine layer thickness and the degree of coverage of a metal oxide on its own metal.

The experimental results presented here concerning photon emission correspond to the dynamic SIMS technique with the photon emission governed by the beam current, the sputtering rate and adsorption of the residual gas atoms on the target surface. An equilibrium situation is maintained between the photon yield and the degree of oxygen adsorption which is determined by the primary ion current density. For a given current density the photon yield from the neutral excited particles is enhanced with oxygen partial pressure. A possible

explanation for this initial enhancement is that the radiationless de-excitation mechanisms are blocked, resulting in an increase in radiative transitions, until a maximum photon yield is reached. The partial pressure of oxygen at which the peak in the photon yield occurs is determined by the primary ion current and so is linked to the degree of surface coverage by the oxide. After this pressure, it is possible that a monolayer coverage of oxide has formed on the target surface. The oxide growth takes place through a series of phases in which the ratio of Cr to oxygen atoms is progressively decreased. This would result in a decrease in the photon yield from neutral Cr atoms. A similar situation is assumed to be applicable to the behaviour of the FeI emission line from the stainless steel sample. The behaviour of the CuI line is only similar under reduced beam currents whereas the CrI emission appears to behave in a similar fashion for all beam current densities tested.

The behaviour of the CrII(Cr^+) emission is more difficult to interpret. Its gradual rise after the neutral emission saturates and decays, implies that the ionisation mechanism, now assumed to be of a chemical and not of a kinetic nature, is independent of the number of Cr atoms present. The efficiency of the process would therefore seem to have increased with oxygen coverage. The optical emission from the CrII line is however not reflected in the secondary ion spectra of Cr^+ in the results of *Schubert (1974)*.

The results of Chapter Five indicated that the charged particles (from light elements) have considerably higher velocities than neutral particles and are significantly different in energy from ions detected by SIMS. If the CrII emission is also predominantly from higher energy particles, this may explain the different behaviour of the Cr^+ seen by Schubert and the photon emission of CrII here,

particularly as their instrument was optimised and highly selective for low energy ions.

7.9 CONCLUSION

The results of these experiments suggests that ionic bombardment of the metals studied leads to excited states of sputtered atoms which can be described by Maxwell-Boltzmann statistics. The effective temperatures are comparable to those of conventional arc discharges and also typical of temperatures determined by the application of the Saha-Eggert equations to secondary ion emission. from ion bombarded alloys. The origin of the apparent L.T.E. conditions is difficult to justify physically, but recent theoretical work has indicated that the thermal spike phenomenon may account for the high temperatures. The effective temperature of the bombarded area is a function of the oxygen partial pressure in the environment of the target, the temperature increasing with increasing partial pressure, an effect paralleled in SIMS analysis. The apparent L.T.E. does offer the possibility of spectroscopic element analysis but the oxygen dependence of the temperature complicates the analysis. Oxidation of the surface may be altering the elemental concentration in the way indicated in these results.

The behaviour of the photon intensity of given lines as a function of the 0_2 partial pressure can possibly be explained in terms of the growth of different oxide phases, the phase depending on the oxide film thickness. The anomolous behaviour of the CrII emission however does not fit this model and further work is required to understand this behaviour.

The effective arc temperature increases under increasing oxygen background pressure. An increase in the effective arc

temperature should lead to an increase in the intensity of the ion and neutral line and such an increase is observed initially for the CrI emission and CrII emission. It has been suggested that the presence of oxygen increases the work function of the surface, and this reduces the free electron density (*Andersen 1975*). It is difficult to see how the change in free electron density can affect the intensity of neutral atom lines, but such a change could affect the number of secondary ions detected and consequently affect the number of ions in a given excited state. This could possibly be the explanation for the observed behaviour of the CrII line.

The Fe/Cr ratios calculated are based on the bulk concentration of Fe. It is possible that real changes are observed in the Fe/Cr ratio, these changes being induced by the oxidation process. Both Fe and Cr concentrations may alter during oxidation at the surface. Some evidence is available to substantiate this idea. *Leygraf et al (1975)* using ultraviolet photoelectron spectroscopy and L.E.E.D. observed quite significant changes in the Fe/Cr ratio at the oxidised surface compared with that in the bulk in the clean crystal.

These results have shown that photon emission provides a means of determining effective L.T.E. temperatures from some elements but that under certain conditions significant changes are evident in photon yields which may be related to variations in element concentration. Such changes are not taken into account in quantitative surface analysis using secondary ion emission.

REFERENCES

ANDERSEN, C A., Int. Mass Spec. Ion. Phys., 2, 61 (1969).

ANDERSEN, C A, HINTHORNE, J R., Anal. Chem., 45, 1421 (1973).

ANDERSEN, C A., N.B.S. Special Publication, 427, 79, (1975).

BENNINGHOVEN, A., Surface Science, 34, 416 (1973).

BENNINGHOVEN, A, MÜLLER, A., Surface Science, 39, 416 (1973).

BENNINGHOVEN, A., Surface Science, 53, 596 (1975).

BOUMANS, P W J M., "Theory of Spectrochemical Excitation', Hilger & Watts, London (1966).

BLAISE, G, BERNHEIM, M, Surface Science, 47, 324 (1975).

CORLISS, C H, J. Res. Phys. Chem., 66A, 5 (1962).

DRAWIN, H W, FELENBOK, P., Data for Plasmas in Local Thermodynamic Equilibrium, Gautheir-Villors, Paris (1965).

GOLIGHTLY, D W, HARRIS, J L., Appl. Spect. 24, 233 (1975).

JOYES, P., Rad. Effects, 19, 235 (1973).

JURELA, Z., Int. J. Mass Spec. Ion. Phys., 12, 33 (1973).

KERKOW, H., Phys. Stat. Solidi. 10A, 501 (1972).

LEYGRAF, C, HULTQUIST, F, EKELUND, S., Surface Science, 51, 409 (1975).

MAYER, H., Phil. Mag., 7, 594 (1933).

MERIAUX, J P, GOUTTE, R, GUILLAND, C., Appl. Phys., 7, 313 (1975).

MORGAN, A E, WERNER, H W., Anal. Chem., 48, 699 (1976).

NELSON, R S., Phil. Mag., 11, 292 (1965).

RÜDENAUER, F G, STEIGER, W, WERNER, H W., Surface Science, 54, 583(1976).

SCHUBERT, R., J. Vac. Sci. Technol., 11, 903 (1974).

SCHUTTEVAER, J W, SMIT, J A., Physica, 10, 502 (1943).

SEITZ, F, KOEHLER J S., Sol. Stat. Phys. 2, 305 (1956).

SIGMUND, P., Appl. Phys. Lett, 25, 169 (1974).

THOMAS, G E, DE KLUIZENAAR, E E., Int. J. Mass. Spect. Ion. Phys., 15, 165 (1974).

TSONG, I S T, McLAREN, A C., Spectrochem, Acta, 30B, 343 (1975).

TSUNOYAMA, K, OHASHI, Y, SUZUKI, T., Anal. Chem, 48, 832 (1976).

VALTERS, A K, NIKONOVA, E I, STARTSEV, G P., Optics Spectrosc., 16, 393 (1964).

WERNER, H W., Surface Science, 47, 301 (1975).

WINTERBON, K B, SIGMUND, P, SAUNDERS, J B., Mat. Fys. Medd. Dan. Vid. Selsk., 37, No. 14 (1970).

CHAPTER EIGHT

CONCLUSION

This project was initiated in order to study photon emission from solids subjected to ionic bombardment, and a general survey study has shown that the photon emission is strongly affected by the electronic structure of the target surface and the type of primary ion used. The detection of photon emission from charged particles has enabled correlations to be made between photon and secondary ion data.

Using such correlations it has been shown that in the case of the Si - SiO_2 system that the principal mode of de-excitation of excited sputtered particles is an Auger mechanism. Furthermore, examination of emission line profiles from sputtered ions and neutrals has revealed that the radiating ions have substantially higher velocities than neutrals and that the simple biparticle collision model does not adequately predict the shape of the line profiles.

The similarities between photon and secondary ion emission have been further investigated by studying photon and ion yields from a single crystal of aluminium bombarded under channeling conditions. The results have shown that the fine structure and relative yield changes are very similar in the directional effects observed for both types of emission. Measurements of the minimum yields have indicated that the ion and excited particle yields are dependent upon the kinetic energy and also the excitation energy of the detected particles. The behaviour of the ion and photon emission with oxygen pressure has also provided further evidence against the simple biparticle collision process being the major mechanism of excited particle generation.

Arc excited photon emission bears a close resemblance to that produced by ionic bombardment of certain elements. The correspondence between the two modes of excitation has been examined more closely using the concept of local thermodynamic equilibrium, currently the most successful theory capable of predicting elemental concentrations from secondary ion data in quantitative surface analysis. The results have shown that the distribution of excited states produced during ionic bombardment of some metals can be described by a Maxwell-Boltzmann distribution function and that effective arc temperatures can be calculated. These temperatures are comparable to those found in arc discharges and also the temperature used to fit secondary ion data to the thermodynamic equations. The origin of these temperatures can be interpreted using the thermal spike concept for which recent theoretical work has indicated that under certain conditions local thermodynamic equilibrium may be valid. The behaviour of the photon yield with oxygen as a background gas has shown that the concentration of elements in the surface layer is substantially altered by the oxidation process, an effect which has not been anticipated in quantitative secondary ion analysis where oxygen is used to enhance the ion yield. These results have shown that photon emission is a sensitive technique for studying oxidation processes and that photon emission can be used to determine the excitation temperatures necessary for SIMS analysis.

Further experimental work is necessary to clarify and confirm the results reported here. Incorporation of photon emission analysis with a standard SIMS apparatus will enable effective plasma temperature determinations to be made without prior knowledge of any elemental target concentrations. These temperatures may then be compared with those calculated using the standard ion microprobe

technique to determine the correspondence between the two temperatures obtained under identical bombardment conditions and hence the usefulness of optical analysis in microprobe studies. Furthermore, the second unknown quantity in ion microprobe analysis, the electron density n_e, may also be determined optically from the ratio of an ion-atom line pair once a temperature has been established and this determination should also be compared to the n_e values used in microprobe work. There exists therefore a potentially powerful and simple method of spectroscopically determining the two major quantities of plasma temperature and electron density necessary for ion microprobe analysis, which will considerably simplify the ion microprobe analytical technique.

In addition to providing useful information relevant to SIMS analysis, future experimental work should also be concerned with extending the photon measurements into the vacuum ultraviolet region (VUV) where a large number of important transitions occur. Of particular interest is the strong oxygen emission known to occur around 1300 Å and the detection of which should provide a simple means of monitoring surface oxidation. Much of the multiply charged particle photon emission also occurs in the VUV region and the study of this emission will provide more information on the mechanisms of ionisation and excitation of atoms during ion bombardment.

Since the completion of this study the addition of an optical detection system to the secondary ion analysis experiment and the acquisition of a vacuum spectrometer, will enable many of the points raised here to be investigated in future experimental work.

ACKNOWLEDGEMENTS

This work has been performed under the Commonwealth Scholarship and Fellowship Plan and appreciation is extended to the Australian Government for making the scholarship available.

I wish to express my sincere thanks to my supervisor, Dr R.J. MacDonald, for his guidance, criticism and encouragement during this course of study.

Special thanks go to my two colleagues, Dr A.R. Bayly, for his assistance with technical matters and continual encouragement, and Mr J. O'Connor for his assistance with computer facilities and the use of his ALLPLOT. program.

I am indebted to Mr F. Buckley and his workshop staff for their co-operation and skill in matters concerning the construction of the experimental equipment.

Last, but by no means least, I wish to thank my wife Sheila, for her moral support throughout the duration of this study and her patience and skill in typing this thesis.